AD-A096 572 DAYTON UNIV OH RESEARCH INST F/G 1/3
STRUCTURAL FLIGHT LOADS SIMULATION CAPABILITY. VOLUME I.(U)
NOV 80 F K BOGNER F33615-76-C-3135
UNCLASSIFIED UDR-TR-80-73-VOL-1 AFWAL-TR-80-3118-VOL-1 NL

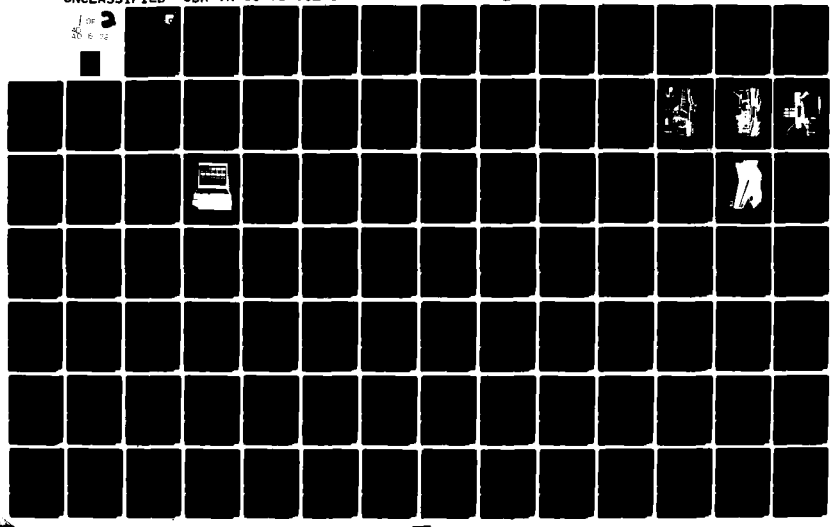

A096 594

LEVEL II

(2)

(18) AFWAL-TR-80-3118-VOL-1 (19)

(14) UDR-TR-80-93-VOL-1

(6) STRUCTURAL FLIGHT LOADS SIMULATION CAPABILITY.
VOLUME I. FINAL REPORT

AD A096572

(10) Dr. Fred K. Bogner
University of Dayton Research Institute

(11) NOV[redacted]80

(12) 190

DTIC
MAR 30 1981
E

TECHNICAL REPORT AFWAL-TR-80-3118, VOLUME I
(9) Final Report, [redacted] Jun[redacted]77 — Sep[redacted]80

Approved for public release, distribution unlimited.

(15) F33615-76-C-3135 (16) 2402 (17) 02

FLIGHT DYNAMICS LABORATORY
AIR FORCE WRIGHT AERONAUTICAL LABORATORIES
AIR FORCE SYSTEMS COMMAND
WRIGHT-PATTERSON AIR FORCE BASE, OHIO 45433

DDC FILE COPY

105400

81 3 17 030

NOTICE

When Government drawings, specifications, or other data are used for any purpose other than in connection with a definitely related Government procurement operation, the United States Government thereby incurs no responsibility nor any obligation whatsoever; and the fact that the Government may have formulated, furnished, or in any way supplied the said drawings, specifications, or other data, is not to be regarded by implication or otherwise as in any manner licensing the holder or any other person or corporation, or conveying any rights or permission to manufacture use, or sell any patented invention that may in any way be related thereto.

This report has been reviewed by the Office of Public Affairs (ASD/PA) and is releasable to the National Technical Information Service (NTIS). At NTIS, it will be available to the general public, including foreign nations.

This technical report has been reviewed and is approved for publication.

SCOTT T. DENNIS, 2Lt, USAF
Aerospace Engineer
Test and Evaluation Group
Flight Vehicle Protection Branch

THEODORE R. McLEAN, Lt Col, USAF
Chief, Flight Vehicle Protection Branch
Vehicle Equipment Division

FOR THE COMMANDER

AMBROSE B. NUTT
Director, Vehicle Equipment Division

"If your address has changed, if you wish to be removed from our mailing list, or if the addressee is no longer employed by your organization please notify AFWAL/FIES, Wright-Patterson Air Force Base, Ohio, 45433, to help us maintain a current mailing list".

Copies of this report should not be returned unless return is required by security considerations, contractual obligations, or notice on a specific document.

AIR FORCE/56780/19 February 1981 — 210

SECURITY CLASSIFICATION OF THIS PAGE (When Data Entered)

REPORT DOCUMENTATION PAGE

READ INSTRUCTIONS BEFORE COMPLETING FORM

1. REPORT NUMBER: AFWAL-TR-80-3118, Volume I
2. GOVT ACCESSION NO: AD-A096 572
3. RECIPIENT'S CATALOG NUMBER:
4. TITLE (and Subtitle): STRUCTURAL FLIGHT LOADS SIMULATION CAPABILITY VOLUME I - FINAL REPORT
5. TYPE OF REPORT & PERIOD COVERED: Final Report, June 1977 - September 1980
6. PERFORMING ORG. REPORT NUMBER: UDR-TR-80-73
7. AUTHOR(S): F. K. Bogner
8. CONTRACT OR GRANT NUMBER(S): F33615-76-C-3135
9. PERFORMING ORGANIZATION NAME AND ADDRESS: Aerospace Mechanics Division, University of Dayton Research Institute, Dayton, Ohio 45402
10. PROGRAM ELEMENT, PROJECT, TASK AREA & WORK UNIT NUMBERS: Program Element 62201F, W. U. 24020230
11. CONTROLLING OFFICE NAME AND ADDRESS: Flight Dynamics Laboratory (AFWAL/FIES), Air Force Wright Aeronautical Laboratories (AFSC)
12. REPORT DATE: November 1980
13. NUMBER OF PAGES: 176
14. MONITORING AGENCY NAME & ADDRESS (if different from Controlling Office):
15. SECURITY CLASS. (of this report): Unclassified
15a. DECLASSIFICATION DOWNGRADING SCHEDULE:
16. DISTRIBUTION STATEMENT (of this Report): Approved for public release; distribution unlimited.
17. DISTRIBUTION STATEMENT (of the abstract entered in Block 20, if different from Report):
18. SUPPLEMENTARY NOTES:
19. KEY WORDS (Continue on reverse side if necessary and identify by block number):

Aircraft Wing Structure	Stress Redistributing	Finite Element
Structural Damage	Residual Strength	Replica Specimen
Ballistic Damage	Nonlinear Analysis	Hydraulic Actuator
Flight Loads Simulation	Vertical Gunfire Facility	MAGNA

20. ABSTRACT (Continue on reverse side if necessary and identify by block number)

An experimental test facility has been developed for performing realistic simulation of flight loads on sections of aircraft wing structures. Concurrently, an analytical technique was developed for predicting the internal load distributions of ballistically damaged, multiple load path aircraft wing structures. In all, six replica wing structures and one T-38 wing structure were tested in the loads facility. The analytically predicted stresses were satisfactory, especially when the response was in the linear range. However,

DD FORM 1 JAN 73 1473 EDITION OF 1 NOV 65 IS OBSOLETE

SECURITY CLASSIFICATION OF THIS PAGE (When Data Entered)

20. (continued)

with a substantial amount of damage present and/or when the response was nonlinear, the experimental and analytical results differed substantially. This is thought to be caused by oversimplified finite element models. Further testing is forthcoming.

FOREWORD

This report describes the work performed by the University of Dayton Research Institute (UDRI) under Air Force Contract F33615-76-C-3135, Structural Flight Loads Simulation Capability. The effort was conducted for the Flight Dynamics Laboratory under the administration and technical direction of the following Air Force Project Engineers: Mr. William Hackenberger, Mr. Thomas Sabick, Mr. Charles Anderson, Capt. Paul Layte (Canadian Air Force), and Lt. Scott Dennis (AFWAL/FIESE).

Administrative project supervision at the UDRI was provided by Mr. Dale H. Whitford (Supervisor, Aerospace Mechanics Division), and technical supervision was provided by Dr. Fred K. Bogner (Group Leader, Analytical Mechanics Group). The following persons made technical contributions to the project: Mr. Ted S. Bruner, Dr. Robert A. Brockman, Mr. Robert Dominic, Ms. Susan Emery, Mr. Ira Fiscus, Mr. Carl S. King, and Mr. George J. Roth.

Accession For
NTIS GRA&I ☒
DTIC TAB ☐
Unannounced ☐
Justification
By
Distribution/
Availability Codes
Avail and/or
Dist Special
A

TABLE OF CONTENTS

SECTION		PAGE
1	INTRODUCTION	1
	1.1 OBJECTIVES	2
	1.2 GENERAL APPROACH	2
2	MAJOR DEVELOPMENT ITEMS	4
	2.1 EXPERIMENTAL FACILITY	4
	2.1.1 Concept	4
	2.1.2 Test Fixture	9
	2.1.3 Control System	13
	2.2 STRUCTURAL ANALYSIS TECHNIQUE	18
	2.2.1 Finite Element Program	18
	2.2.2 Preprocessor Program	21
	2.2.3 Postprocessor	23
	2.3 REPLICA SPECIMENS	24
3	REPLICA SPECIMEN TESTS AND ANALYSES	30
	3.1 ACTUATOR LOADS AND EQUIVALENT SECTION LOADS	30
	3.2 TEST 1 - UNDAMAGED SPECIMEN, NUMBER 1	32
	3.2.1 Instrumentation	32
	3.2.2 Load Conditions	34
	3.2.3 Load Incrementation and Data Collection	34
	3.2.4 Analysis Model	34
	3.2.5 Test/Analysis Results	45
	3.3 TEST 2 - DAMAGED SPECIMEN, NUMBER 2	47
	3.3.1 Instrumentation	47
	3.3.2 Loading	49
	3.3.3 Load Incrementation and Data Collection	49
	3.3.4 Analysis Model	49
	3.3.5 Test/Analysis Results	57
	3.4 TEST 3 - DAMAGED SPECIMEN, NUMBER 3	57
	3.4.1 Instrumentation	59
	3.4.2 Loading	59

TABLE OF CONTENTS (concluded)

SECTION			PAGE
	3.4.3	Load Incrementation and Data Collection	59
	3.4.4	Analysis Model	59
	3.4.5	Test/Analysis Results	70
3.5	TEST 4 - DAMAGED SPECIMEN, NUMBER 4		92
	3.5.1	Instrumentation	92
	3.5.2	Loading	92
	3.5.3	Load Incrementation and Data Collection	94
	3.5.4	Analysis Model	94
	3.5.5	Test/Analysis Results	94
3.6	TEST 5 - DAMAGED SPECIMEN, NUMBER 5		117
	3.6.1	Instrumentation	117
	3.6.2	Loading	123
	3.6.3	Load Incrementation and Data Collection	123
	3.6.4	Analysis Model	123
	3.6.5	Test/Analysis Results	133
4	SUMMARY, CONCLUSIONS, AND RECOMMENDATIONS		172
	REFERENCES		176

LIST OF FIGURES

NUMBER		PAGE
1.1	Program Schematic	3
2.1	Full Wing and Test Section	5
2.2	Test of Undamaged Wing Section	7
2.3	Test of Damaged Wing Specimen	8
2.4a	Test Fixture - Reaction End	10
2.4b	Test Fixture - Loading End	11
2.4c	Test Fixture - Specimen Mounted	12
2.5	Hydraulic Actuator Positions	14
2.6	Block Diagram of Load Control System	15
2.7	Control Console	16
2.8	Load Control Panel	17
2.9	Structural Analysis Technique	19
2.10	Replica Test Specimen	25
2.11	Cross Section of Replica Test Specimen	26
2.12	Planform of Replica Test Specimen	27
3.1	Positive Sign Convention	31
3.2a	Strain Gage Locations - Specimen 1	33
3.2b	Sample Experimental Data - Specimen 1, Case 1	37
3.3a	Specimen 1 Finite Element Model - Node Numbers	39
3.3b	Specimen 1 Finite Element Model - Lower Skin Membrane Elements	40
3.3c	Specimen 1 Finite Element Model - Upper Skin Membrane Elements	41
3.3d	Specimen 1 Finite Element Model - Spar Shear Panel Elements	42

LIST OF FIGURES (continued)

NUMBER		PAGE
3.3e	Specimen 1 Finite Element Model - Rib Shear Panel Elements	43
3.3f	Specimen 1 Finite Element Model - Cap Bar Elements	44
3.4	Comparison of Experimental/Analytical Results for Test 1 - Case 1	46
3.5	Strain Gage Locations - Specimen 2	48
3.6	Sample Experimental Data - Test 2	50
3.7a	Specimen 2 Finite Element Model - Node Numbers	52
3.7b	Specimen 2 Finite Element Model - Lower Skin Membrane Elements	53
3.7c	Specimen 2 Finite Element Model - Spar Shear Panel Elements	54
3.7d	Specimen 2 Finite Element Model - Rib Shear Panel Elements	55
3.7e	Specimen 2 Finite Element Model - Cap Bar Elements	56
3.8	Comparison of Experimental/Analytical Results for Test 2	58
3.9	Strain Gage Locations - Specimen 3	60
3.10	Sample Experimental Data - Specimen 3	61
3.11a	Specimen 3 Finite Element Model - Node Numbers	65
3.11b	Specimen 3 Finite Element Model - Bottom Skin Membrane Elements	66
3.11c	Specimen 3 Finite Element Model - Top Skin Membrane Elements	67
3.11d	Specimen 3 Finite Element Model - Spar and Rib Shear Panel Elements	68

LIST OF FIGURES (continued)

NUMBER		PAGE
3.11e	Specimen 3 Finite Element Model - Cap Bar Elements	69
3.12a	Equivalent Stress-Skin Element 13	71
3.12b	Equivalent Stress-Skin Element 15	72
3.12c	Equivalent Stress-Skin Element 17	73
3.12d	Equivalent Stress-Skin Element 19	74
3.12e	Equivalent Stress-Skin Element 21	75
3.12f	Equivalent Stress-Skin Element 23	76
3.12g	Equivalent Stress-Skin Element 25	77
3.12h	Equivalent Stress-Skin Element 27	78
3.12i	Equivalent Stress-Spar Web Element 53	79
3.12j	Equivalent Stress-Spar Web Element 69	80
3.12k	Equivalent Stress-Spar Cap Element 35	81
3.12l	Equivalent Stress-Spar Cap Element 37	82
3.12m	Equivalent Stress-Spar Cap Element 39	83
3.12n	Equivalent Stress-Spar Cap Element 67	84
3.12o	Equivalent Stress-Spar Cap Element 69	85
3.12p	Equivalent Stress-Spar Cap Element 71	86
3.13a	Contours of Equivalent Stress - 20% Load	87
3.13b	Contours of Equivalent Stress - 40% Load	88
3.13c	Contours of Equivalent Stress - 60% Load	89
3.13d	Contours of Equivalent Stress - 80% Load	90
3.13e	Contours of Equivalent Stress - 100% Load	91
3.14	Strain Gage Locations - Specimen 4	93

LIST OF FIGURES (continued)

NUMBER		PAGE
3.14	Sample Experimental Data - Specimen 4	95
3.16a	Specimen 4 Finite Element Model - Node Numbers	98
3.16b	Specimen 4 Finite Element Model - Bottom Skin Membrane Elements	99
3.16c	Specimen 4 Finite Element Model - Top Skin Membrane Elements	100
3.16d	Specimen 4 Finite Element Model - Spar and Rib Shear Panel Elements	101
3.16e	Specimen 4 Finite Element Model - Cap Bar Elements	102
3.17a	Equivalent Stress-Skin Element 13	103
3.17b	Equivalent Stress-Skin Element 15	104
3.17c	Equivalent Stress-Skin Element 17	105
3.17d	Equivalent Stress-Skin Element 19	106
3.17e	Equivalent Stress-Skin Element 21	107
3.17f	Equivalent Stress-Skin Element 23	108
3.17g	Equivalent Stress-Skin Element 25	109
3.17h	Equivalent Stress-Skin Element 27	110
3.17i	Equivalent Stress-Rib Web Element 38	111
3.17j	Equivalent Stress-Spar Web Element 41	112
3.17k	Equivalent Stress-Spar Web Element 52	113
3.17l	Equivalent Stress-Spar Web Element 57	114
3.17m	Equivalent Stress-Spar Web Element 70	115
3.18a	Contours of Equivalent Stress - 20% Load	117
3.18b	Contours of Equivalent Stress - 40% Load	118
3.18c	Contours of Equivalent Stress - 60% Load	119

LIST OF FIGURES (continued)

NUMBER		PAGE
3.18d	Contours of Equivalent Stress - 80% Load	120
3.18e	Contours of Equivalent Stress - 100% Load	121
3.19	Strain Gage Locations - Specimen 5	122
3.20	Sample Experimental Data - Specimen 5	124
3.21a	Specimen 5 Finite Element Model - Node Numbers	128
3.21b	Specimen 5 Finite Element Model - Bottom Skin Membrane Elements	129
3.21c	Specimen 5 Finite Element Model - Top Skin Membrane Elements	130
3.21d	Specimen 5 Finite Element Model - Spar and Rib Shear Panel Elements	131
3.21e	Specimen 5 Finite Element Model - Spar and Rib Cap Bar Elements	132
3.22a	Equivalent Stress-Skin Element 13	134
3.22b	Equivalent Stress-Skin Element 15	135
3.22c	Equivalent Stress-Skin Element 17	136
3.22d	Equivalent Stress-Skin Element 19	137
3.22e	Equivalent Stress-Skin Element 20	138
3.22f	Equivalent Stress-Skin Element 21	139
3.22g	Equivalent Stress-Skin Element 22	140
3.22h	Equivalent Stress-Skin Element 24	141
3.22i	Equivalent Stress-Skin Element 26	142
3.22j	Equivalent Stress-Skin Element 40	143
3.22k	Equivalent Stress-Rib Web Element 41	144
3.22l	Equivalent Stress-Rib Web Element 42	145
3.22m	Equivalent Stress-Rib Web Element 43	146

LIST OF FIGURES (concluded)

NUMBER		PAGE
3.22n	Equivalent Stress-Rib Web Element 44	147
3.22o	Equivalent Stress-Rib Web Element 45	148
3.22p	Equivalent Stress-Spar Web Element 51	149
3.22q	Equivalent Stress-Spar Web Element 52	150
3.22r	Equivalent Stress-Spar Web Element 53	151
3.22s	Equivalent Stress-Spar Web Element 67	152
3.22t	Equivalent Stress-Spar Web Element 68	153
3.22u	Equivalent Stress-Spar Web Element 69	154
3.22v	Axial Stress-Spar Cap Element 35	155
3.22w	Axial Stress-Spar Cap Element 36	156
3.22x	Axial Stress-Spar Cap Element 37	157
3.22y	Axial Stress-Spar Cap Element 38	158
3.22z	Axial Stress-Spar Cap Element 39	159
3.22aa	Axial Stress-Spar Cap Element 40	160
3.22bb	Axial Stress-Spar Cap Element 69	161
3.22cc	Axial Stress-Spar Cap Element 70	162
3.22dd	Axial Stress-Spar Cap Element 71	163
2.22ee	Axial Stress-Spar Cap Element 72	164
3.22ff	Axial Stress-Spar Cap Element 73	165
3.22gg	Axial Stress-Spar Cap Element 74	166
3.23a	Contours of Equivalent Stress - 20% Load	168
3.23b	Contours of Equivalent Stress - 40% Load	169
3.23c	Contours of Equivalent Stress - 60% Load	170
3.23d	Contours of Equivalent Stress - 80% Load	171

LIST OF TABLES

NUMBER		PAGE
2.1	REPLICA SPECIMENS	29
3.1	LOAD CASES	35
3.2	ACTUATOR LOADS	36

SECTION 1
INTRODUCTION

By the very nature of their reason for existence, military aircraft are susceptible to damage. The performance of a damaged aircraft can be affected in a variety of ways depending on which of the aircraft systems are affected and to what degree the damage is inflicted. Structural damage, in particular, has been responsible for the degradation of the performance of many aircraft, and in a significant number of cases, for the loss of aircraft.

It is apparent that structural vulnerability is a highly important consideration in assessing the overall vulnerability of aircraft. One way of assessing the structural survivability/vulnerability characteristics of aircraft is to perform sophisticated tests on whole aircraft and on individual components. Survivability/vulnerability test technology has received a good deal of attention in areas such as test specimen design, threat simulation, and simulation of the aircraft flow environment seen by combat aircraft. One aspect of survivability/vulnerability testing which has not been adequately treated in the past, is the simulation of actual flight loadings of aircraft structures during ballistic impact when the airflow environment is also being simulated.

Another way of assessing the survivability/vulnerability characteristics of aircraft is to perform large scale structural analyses. In the past, most structural analyses of aircraft have been restricted to linear, small deformation applications. Such analyses have not shown particularly good agreement with experimentally obtained data when applied to ballistically damaged structures, however. In order to predict load redistributions and residual strength in damaged structures, nonlinear analyses which account for elastic-plastic effects and large deformations may be necessary. These extended range

analyses have been applied, to a limited extent, to damaged aircraft structures, but they are usually very inconvenient for a survivability/vulnerability engineer to use effectively.

This report describes the results of a research project which was intended to investigate the possibility of removing some of the shortcomings in both the experimental and analytical phases of survivability/vulnerability studies. The objectives of the study are indicated below.

1.1 OBJECTIVES

The primary objective of this effort was to develop a validated experimental test capability for the realistic simulation of flight loads on aircraft wing structures during ballistic impact. In achieving this primary objective, two equally important secondary objectives were identified:

a. the development of a self-contained flight loads simulation fixture,

b. the development of a structural analysis technique for the analytical prediction of internal load distributions of damaged, multiple load path structures.

1.2 GENERAL APPROACH

The general approach to completing the program objectives is indicated in the schematic of Figure 1.1. Briefly, the total effort is split initially into parallel experimental and analytical developments. These experimental and analytical efforts coalesce into an error analysis of data obtained from experimental and analytical tests using common replica test specimens. After the error analysis shows comparable results (perhaps after several iterations as shown by the double-headed arrows), the full-scale test item is mounted in the experimental and analytical fixtures. Then reasonable agreement between the experimental and analytical test results for the full-scale item is taken to constitute a validation of the experimental test facility.

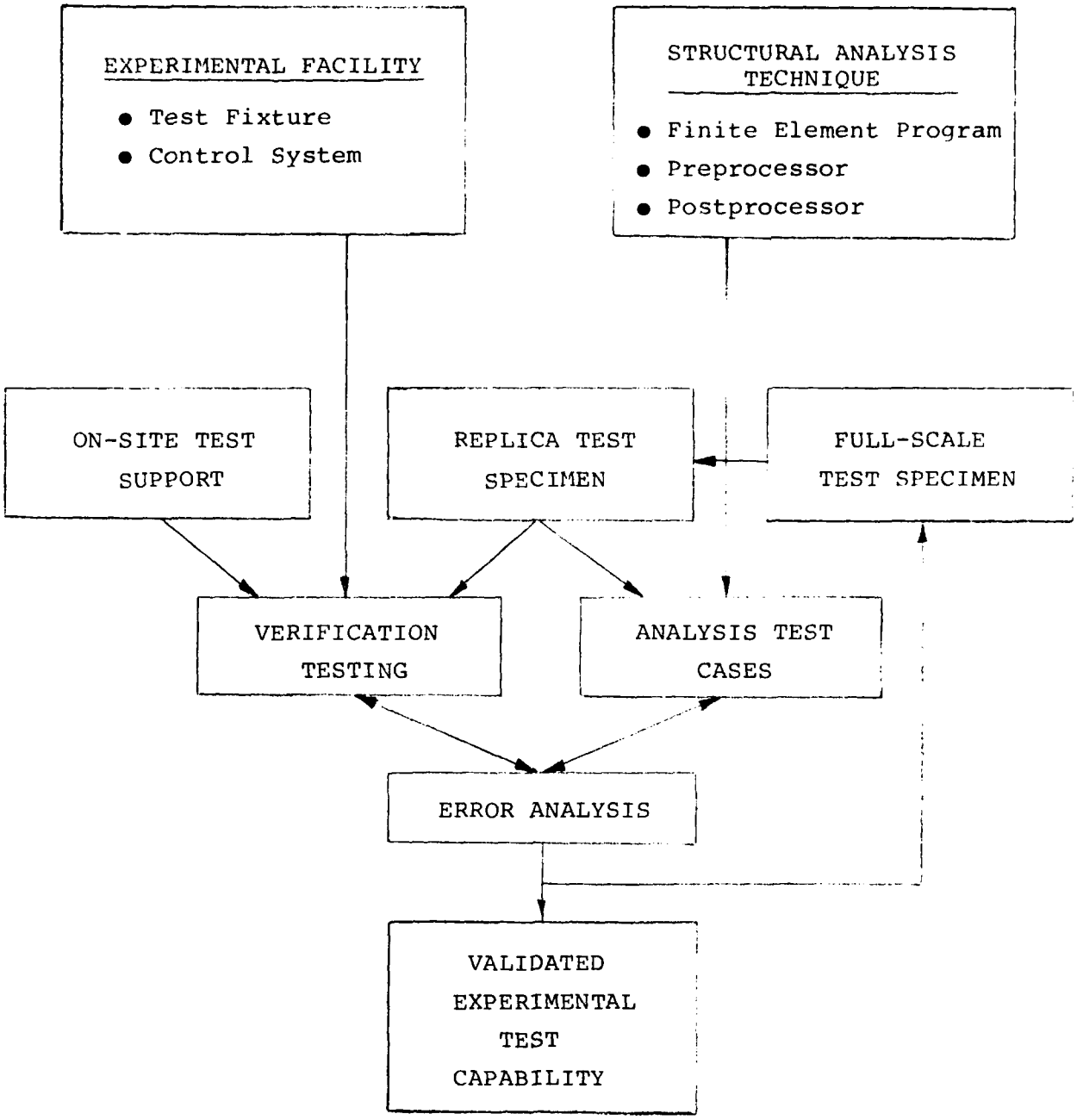

Figure 1.1. Program Schematic.

SECTION 2
MAJOR DEVELOPMENT ITEMS

This section describes the three major development items: the experimental facility, the structural analysis technique, and the replica test specimens. These items are discussed in more detail in References 1-3; the brief descriptions presented here are included for completeness.

2.1 EXPERIMENTAL FACILITY

The experimental facility[1] designed and fabricated by the University of Dayton Research Institute consists of a self-contained loading fixture and a loading control system. These systems impose realistic flight loads to aircraft wing sections. When mounted in the Vertical Gunfire Facility at Wright-Patterson Air Force Base, the test facility applies the flight loads simultaneously with ballistic impact and airflow. The following paragraphs present discussions of the basic concept of the experimental facility, the test fixture, and the control system.

2.1.1 Concept

In order to conduct tests with realistic flight loads, fixtures have been required in the past which have been large enough to mount whole aircraft wings; or tests on complete aircraft have been performed. The objective in this project was to design an experimental facility which would apply realistic flight loads to wing sections small enough so that the tests could be performed inside the Vertical Gunfire Range at Wright-Patterson Air Force Base.

Figure 2.1 shows diagrammatically a complete wing and a section cut from the wing. The isolated wing section has certain values of spanwise bending moment (M_s), spanwise shearing force (V_s) chordwise bending moment (M_c), chordwise shearing force (V_c), and torque (T), acting on the ends of the

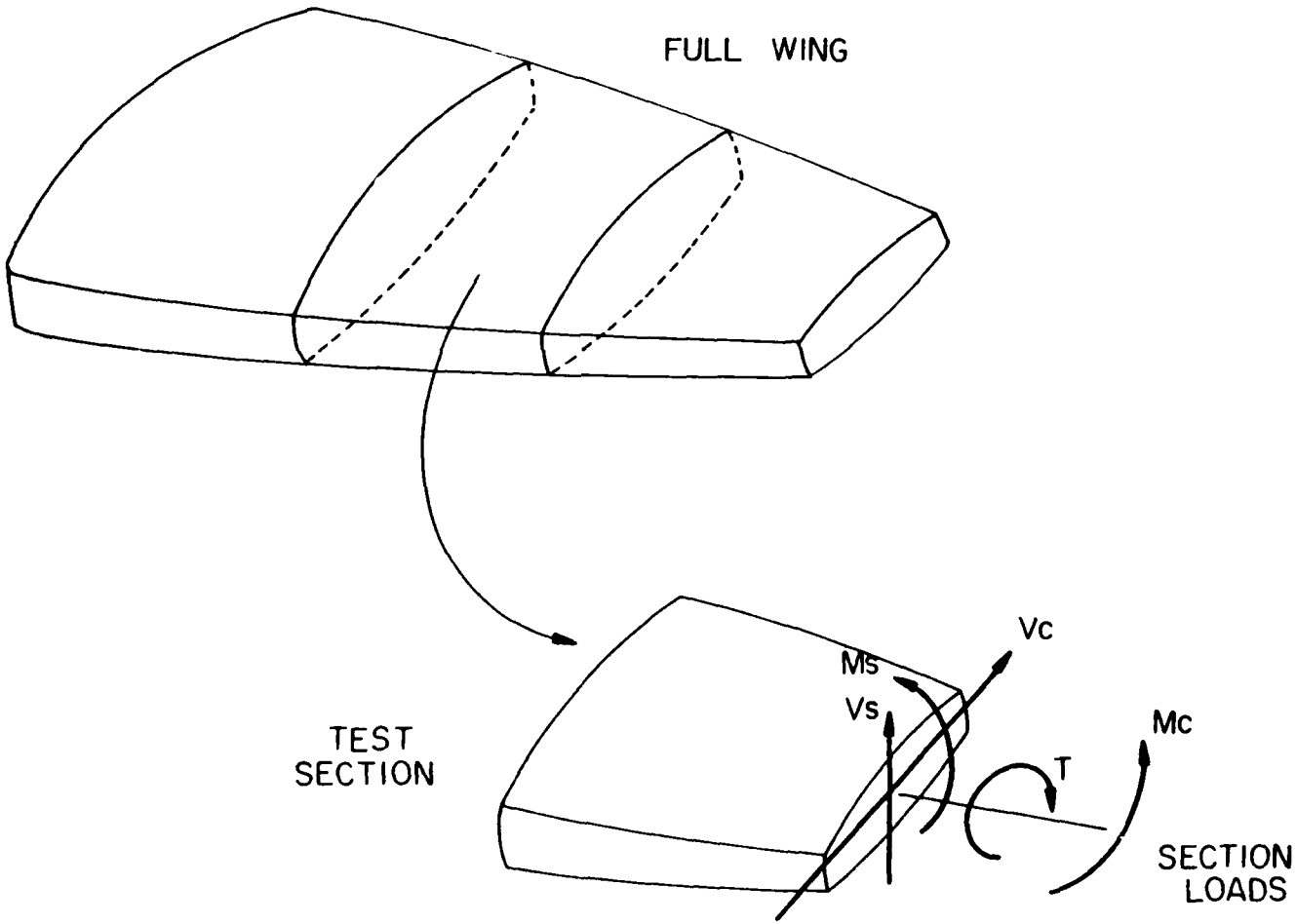

Figure 2.1. Full Wing and Test Section.

section. The values of the section loads depend on the loads applied to the wing in specific instances. The function of the experimental facility is to subject wing sections to operator specified values of the section loads, M_s, V_s, M_c, V_c, and T.

Figure 2.2 shows conceptually the experimental facility which has been designed, fabricated, and installed at Wright-Patterson Air Force Base. The facility generally consists of:

- a test fixture to apply loads to one end of a specimen and to react at the other end;
- a hydraulic system to impose on the loading frame, actuator forces which correspond to specified values of the section loads; and
- a control system to provide the test operator with a convenient means for controlling the application of the actuator loads during a test.

A test on a wing section is performed by first mounting one end of the specimen to the reaction fixture which is designed to be sufficiently massive and rigid so that negligible support movement occurs. Loads are then applied to the other end of the specimen through a rigid loading frame. Strategically placed and oriented hydraulic actuators impose forces on the loading frame which in turn imposes section loads (M_s, V_s, M_c, V_c, T) to the specimen. The loads in the actuators are controlled by varying the pressure in the hydraulic lines through a remote control console. The control console provides the capability for adjusting the relative magnitudes of the actuator loads and then to increase them proportionally. Note that the flight loads can be applied simultaneously with air flow (existing in the Air Force facility) and ballistic impact (existing in the Air Force facility).

Figure 2.3 shows a damaged wing section mounted in the experimental facility. A typical test on a damaged specimen consists of proportionally increasing the actuator

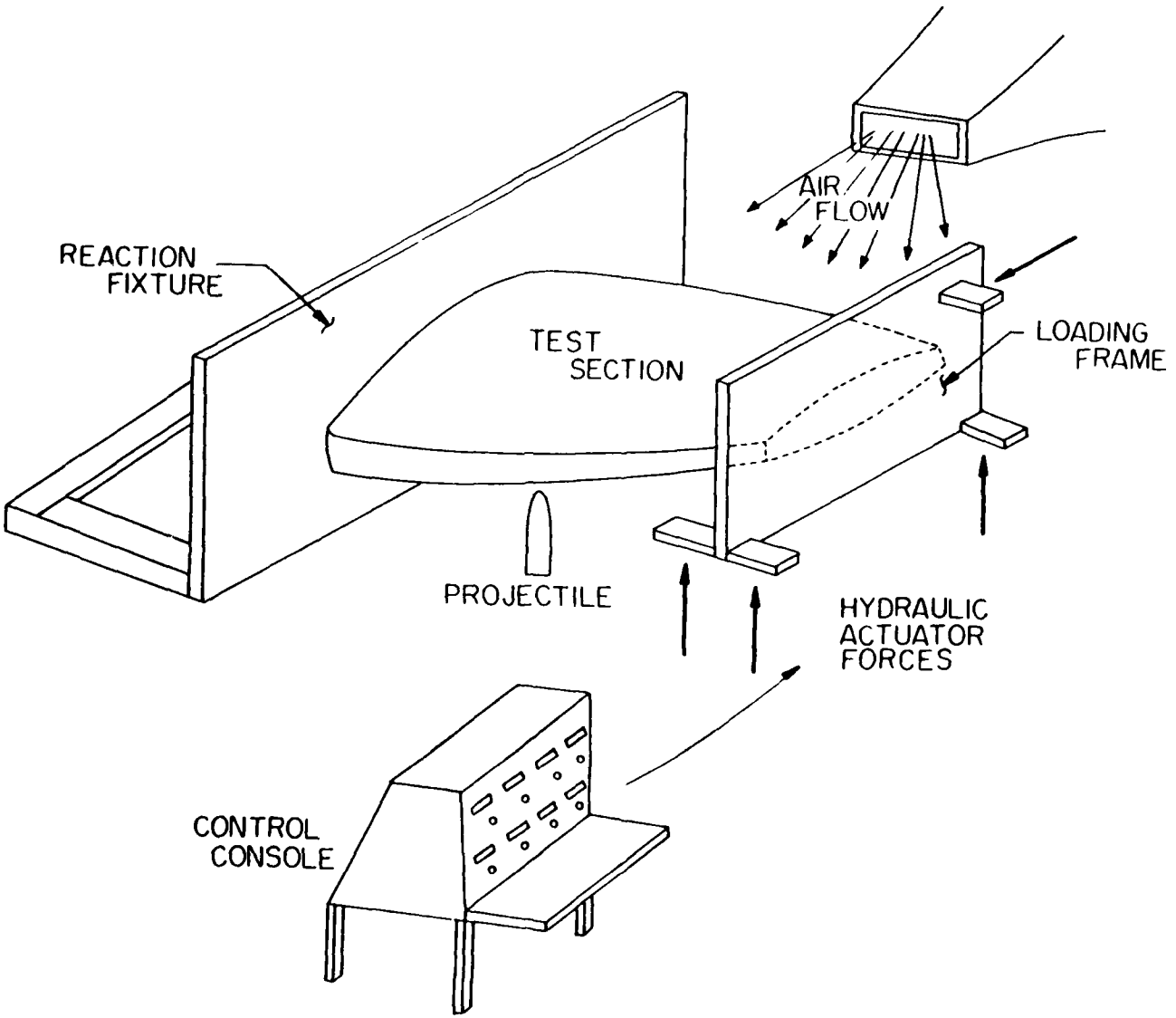

Figure 2.2. Test of Undamaged Wing Section.

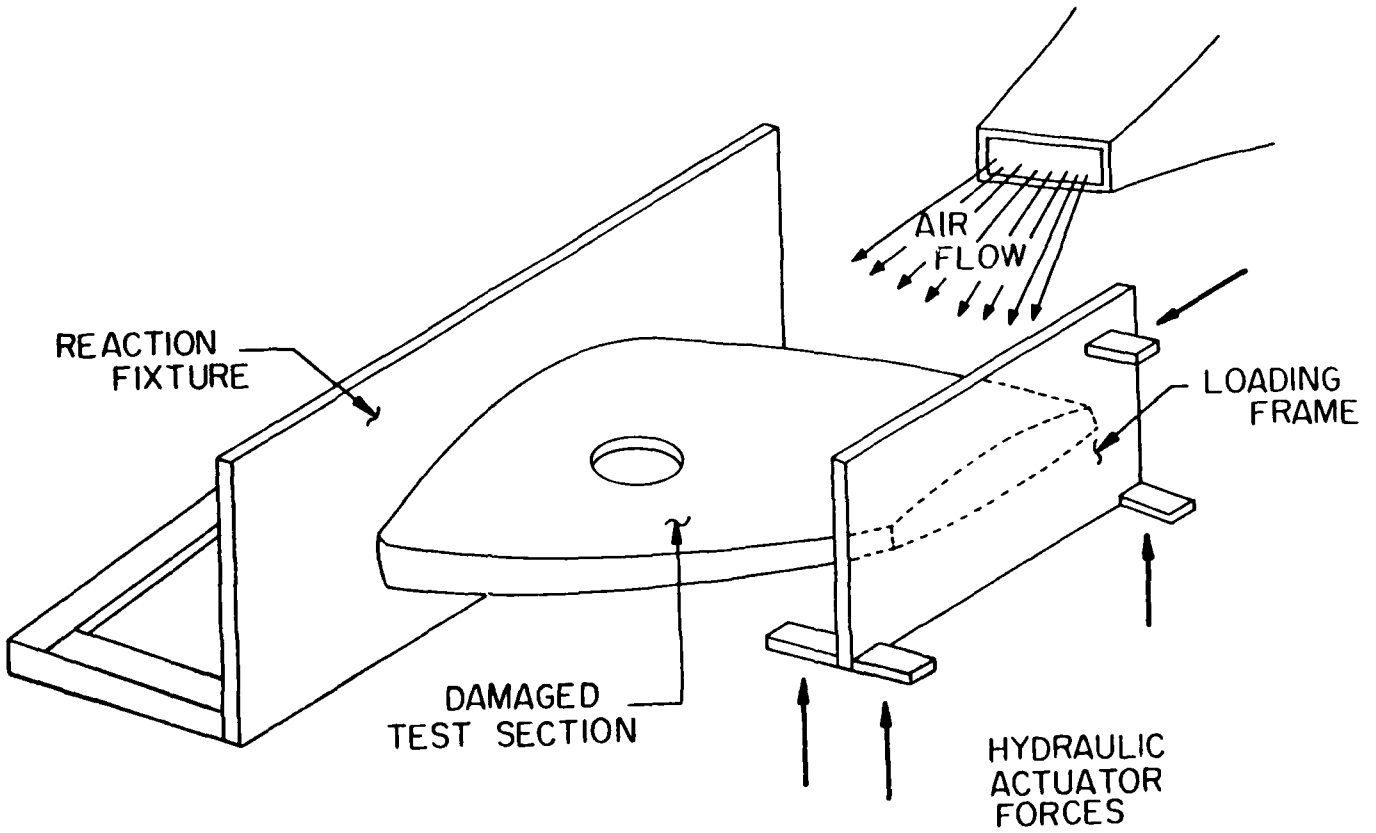

Figure 2.3. Test of Damaged Wing Specimen.

loads until failure, in order to obtain an indication of the residual strength. If the proportional loads correspond to a mix of bending moments, shears, and torque for a certain flight condition, then the failure load can be related, for example, to a certain maximum g-condition for the maneuver.

2.1.2 Test Fixture

The test fixture (Reference 1) designed to apply realistic flight loads to aircraft wing sections is a self-contained structure. The only load imposed on the structure of the Vertical Gunfire Facility during a test is the dead weight of the test fixture, specimen, and instrumentation. That is, the test fixture is free-standing; it does not have to be installed in the Vertical Gunfire Facility if airloads and/or ballistic impact are not considered during a test.

Figures 2.4a-c are photographs of the test fixture taken from various angles. The photographs show all of the major parts of the fixture:

- the reaction structure,
- the loading frame,
- the base structure,
- the hydraulic actuators.

These systems together with a test specimen form a closed structural loop.

The reaction structure consists of a thick steel plate mounted on a massive back-up structure to eliminate rigid body motion of the test specimen. One end of a test specimen is attached to the reaction structure through custom designed mounting brackets.* The reaction structure is designed to react maximum loads of M_s = 12,000,000 in. lb., V_s = 100,000 lb., M_c = 1,440,000 in. lb., V_c = 12,000 lb., and T = 2,000,000 in. lb. The reaction structure is fabricated from corrosion resistant, high-strength, low alloy (ASTMA 588) steel, having a strength of 50,000 psi.

---

*The mounting brackets proved to be a weak link in anchoring the test specimens to the back-up structure. See the discussion in Section 3.2.1, p 32.

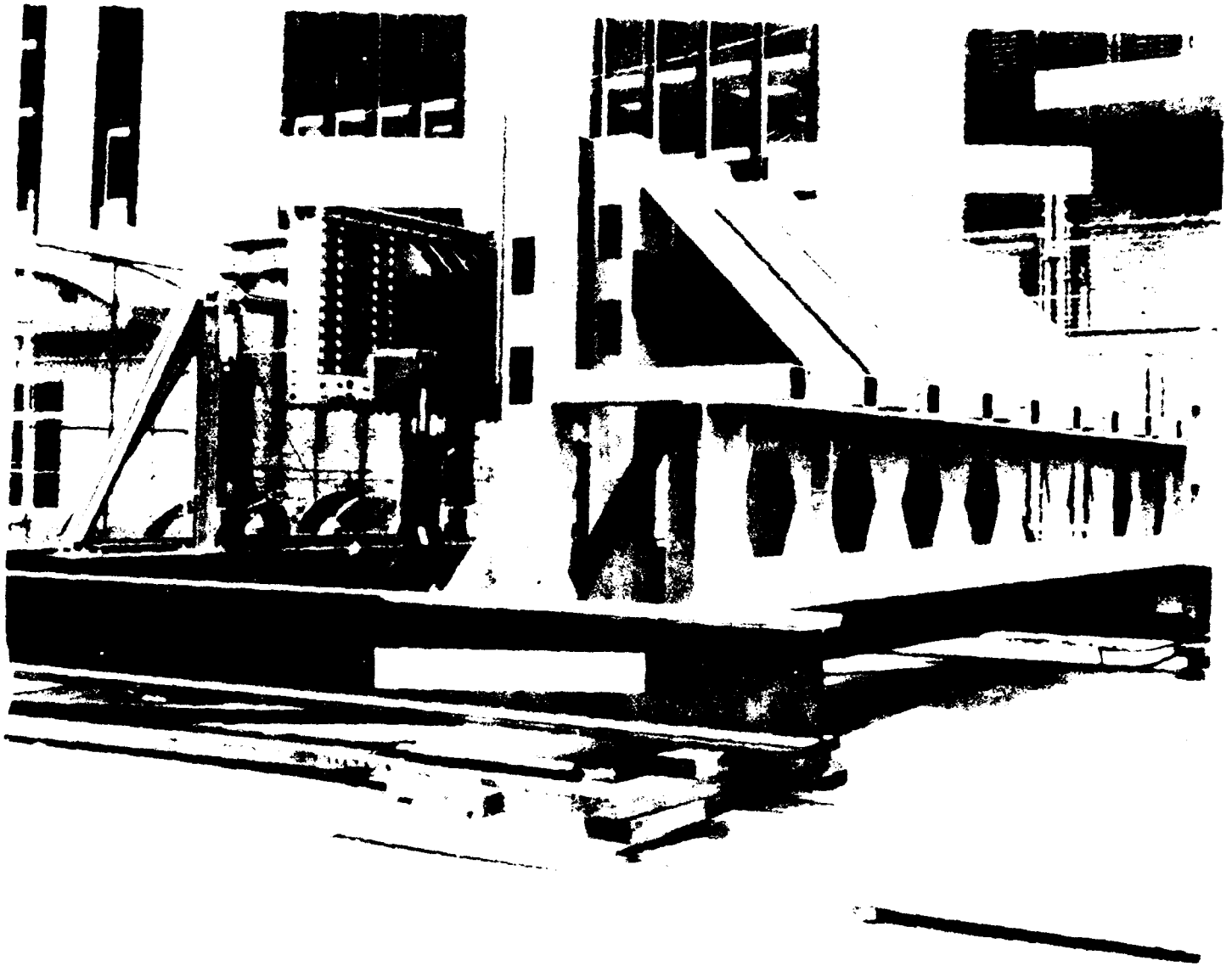

Figure 2.4a. Test Fixture - Reaction End.

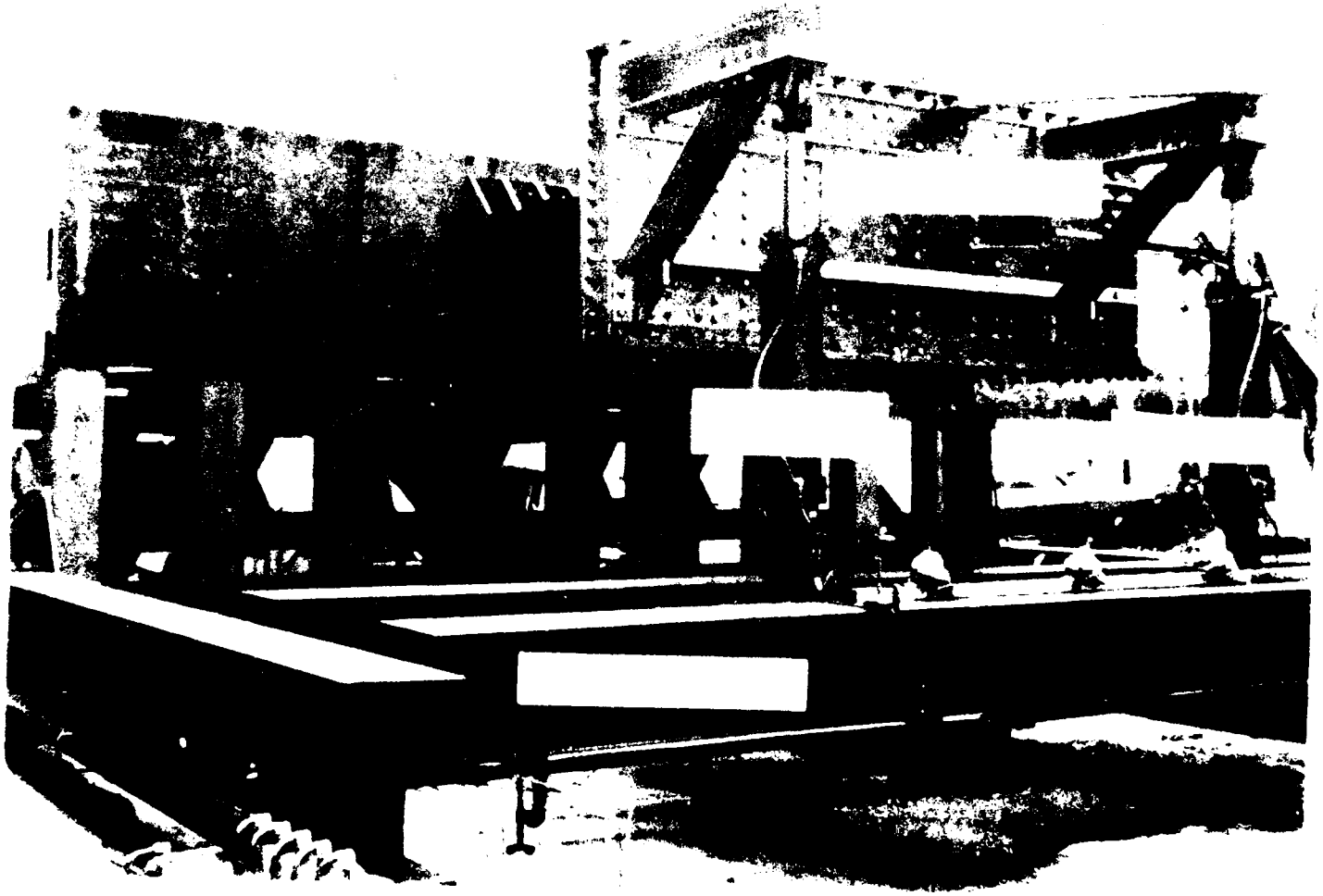

Figure 2.4b. Test Fixture - Loading End.

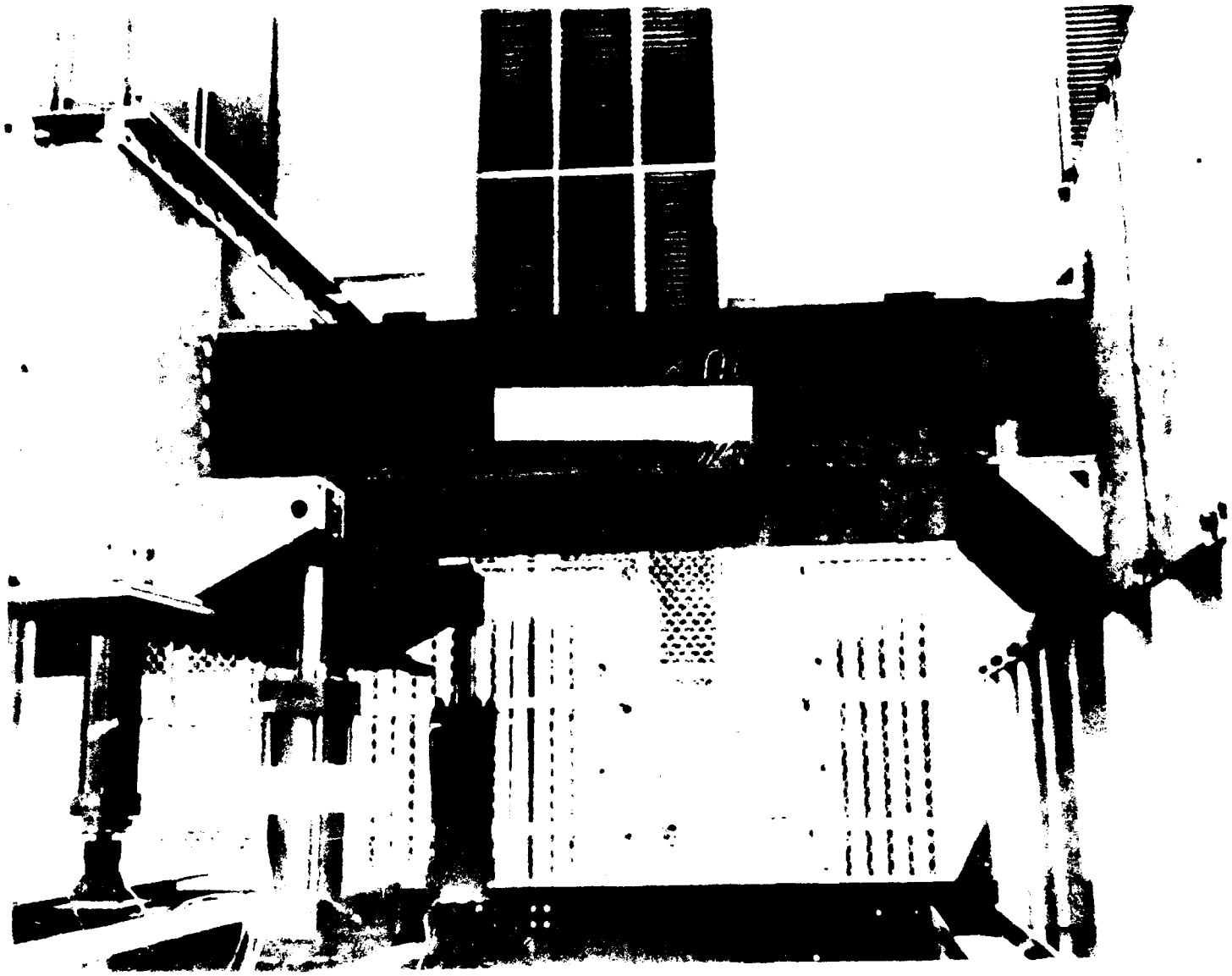

Figure 2.1c. Test Fixture - Specimen Mounted.

The loading frame is a rigid, built-up plate which transfers concentrated forces from the hydraulic actuators into the test specimen. The specimen is attached to the loading frame through custom designed mounting brackets.

The base structure is a framework of I-beams which supports the reaction structure at one end and the hydraulic actuators at the other end. The support for the actuators is moveable to allow for different length specimens. The base structure is fabricated from corrosion resistant high-strength, low alloy steel.

The hydraulic actuators are reacted by the base structure at one end and impose forces on tne loading frame at the other end. The general arrangement of the actuators is shown in Figure 2.5. Four actuators are oriented vertically and one actuator is oriented horizontally in a chordwise direction.

2.1.3 Control System

Control of the hydraulic loading system is accomplished by electrical command signals from an operator's control console. Hydraulic pressure regulators, driven by a controlled electric current, regulate the oil pressure supplied to the loading actuators. Load cells sense the resulting loads and give the console operator a positive readout of the loads being applied. The operator's console contains provisions for setting the ratios between the various actuator loads and also for controlling all loads in unison. A block diagram of the control scheme is shown in Figure 2.6.

The control console (Figure 2.7) contains all controls, readouts, and other interfaces with the operator, and all electronic equipment associated with the loading system. The console is a free standing, 50 in. high, 24 in. wide cabinet with sloping control panel (Figure 2.8). Front panel controls include the key-operated master switch, hydraulic

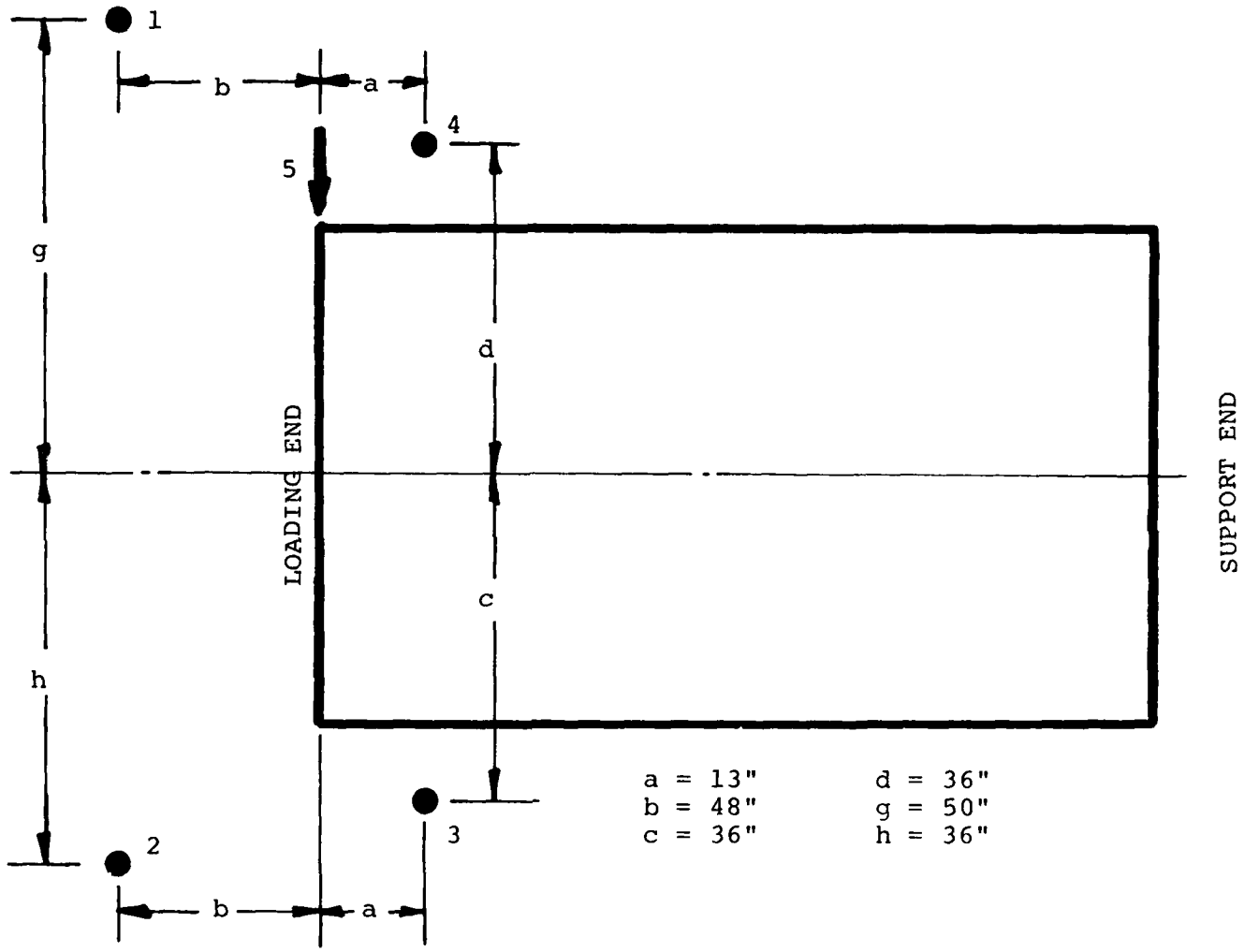

Figure 2.5. Hydraulic Actuator Positions.

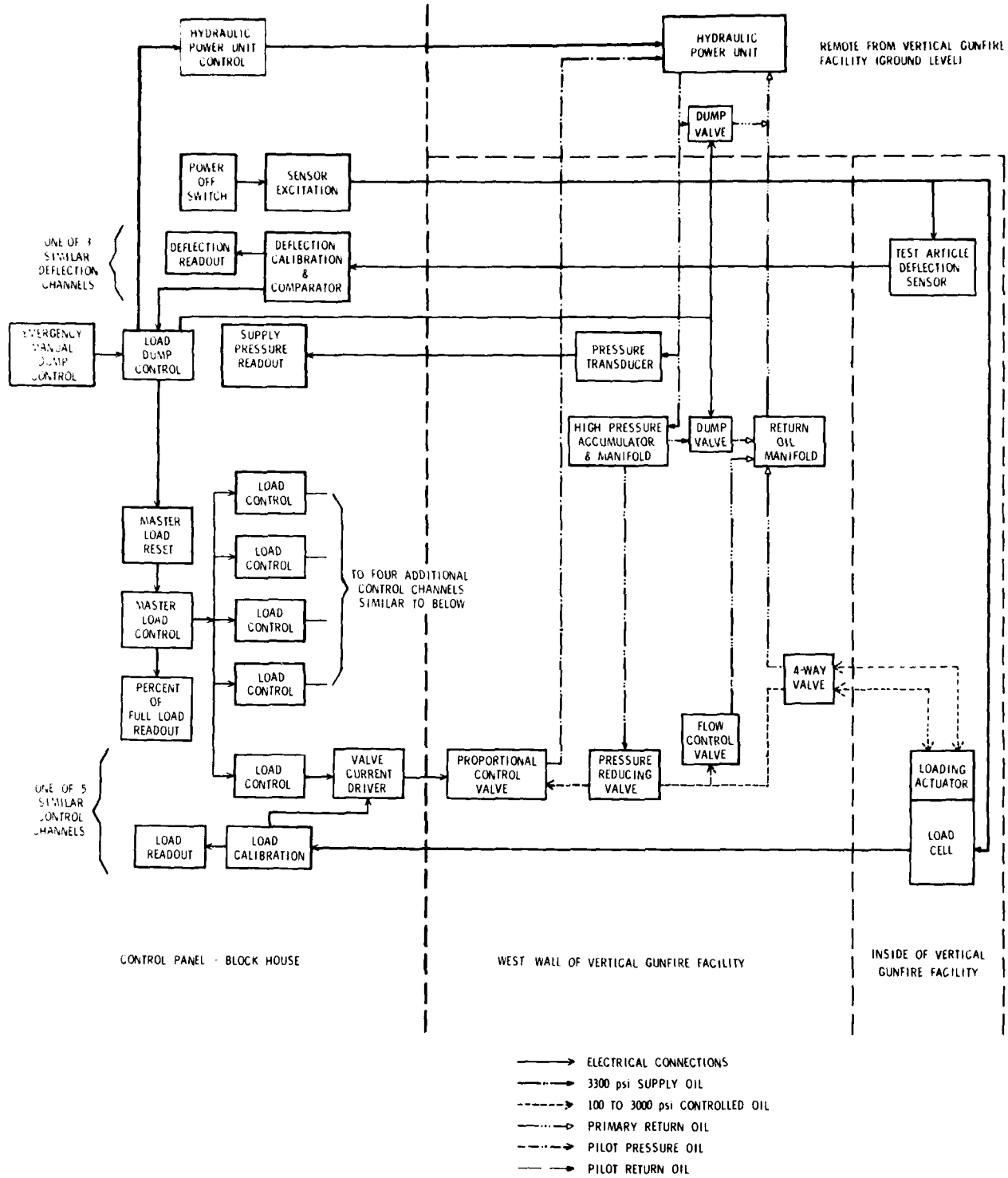

Figure 2.6. Block Diagram of Load Control System.

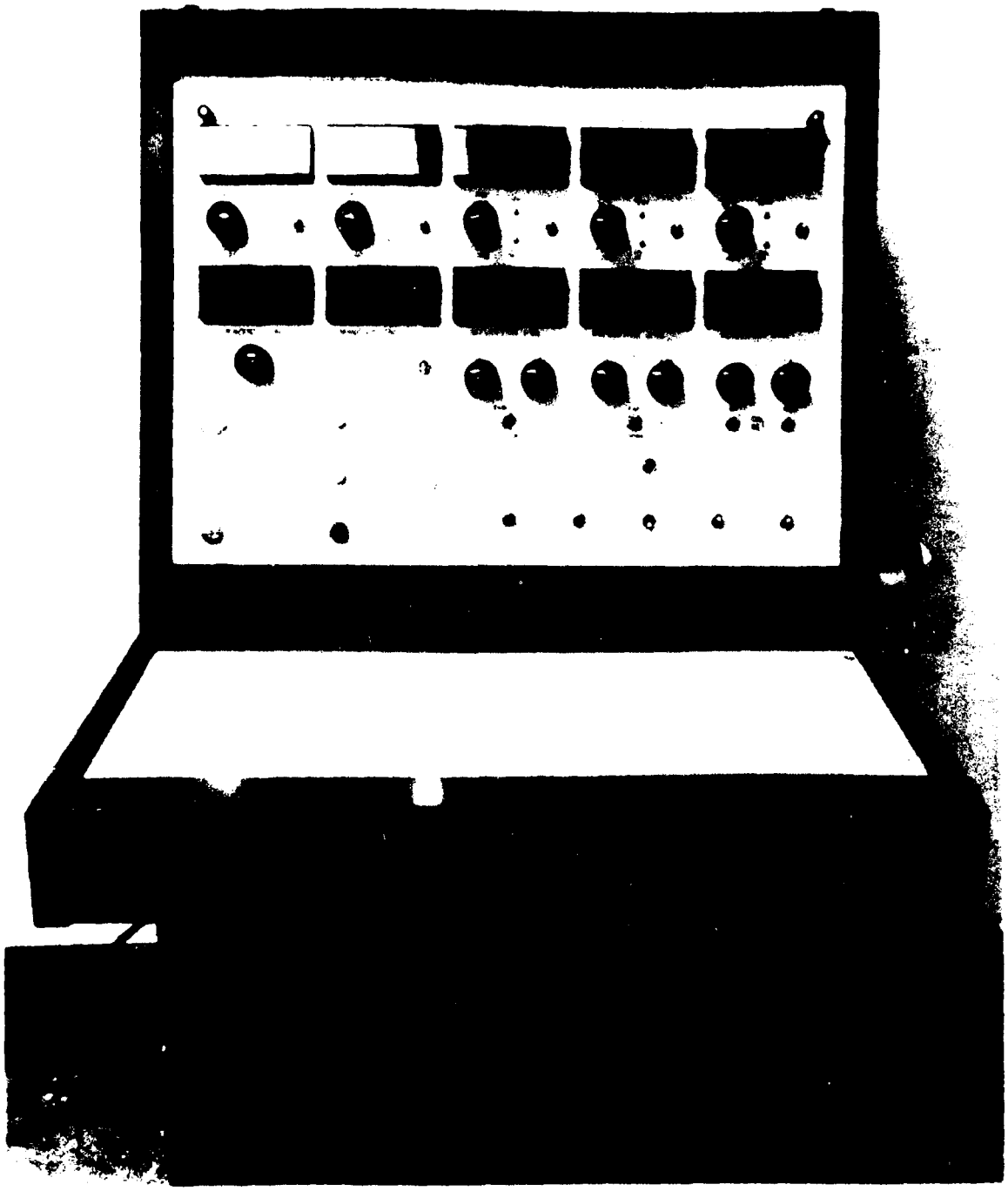

Figure 2.7. Control Console.

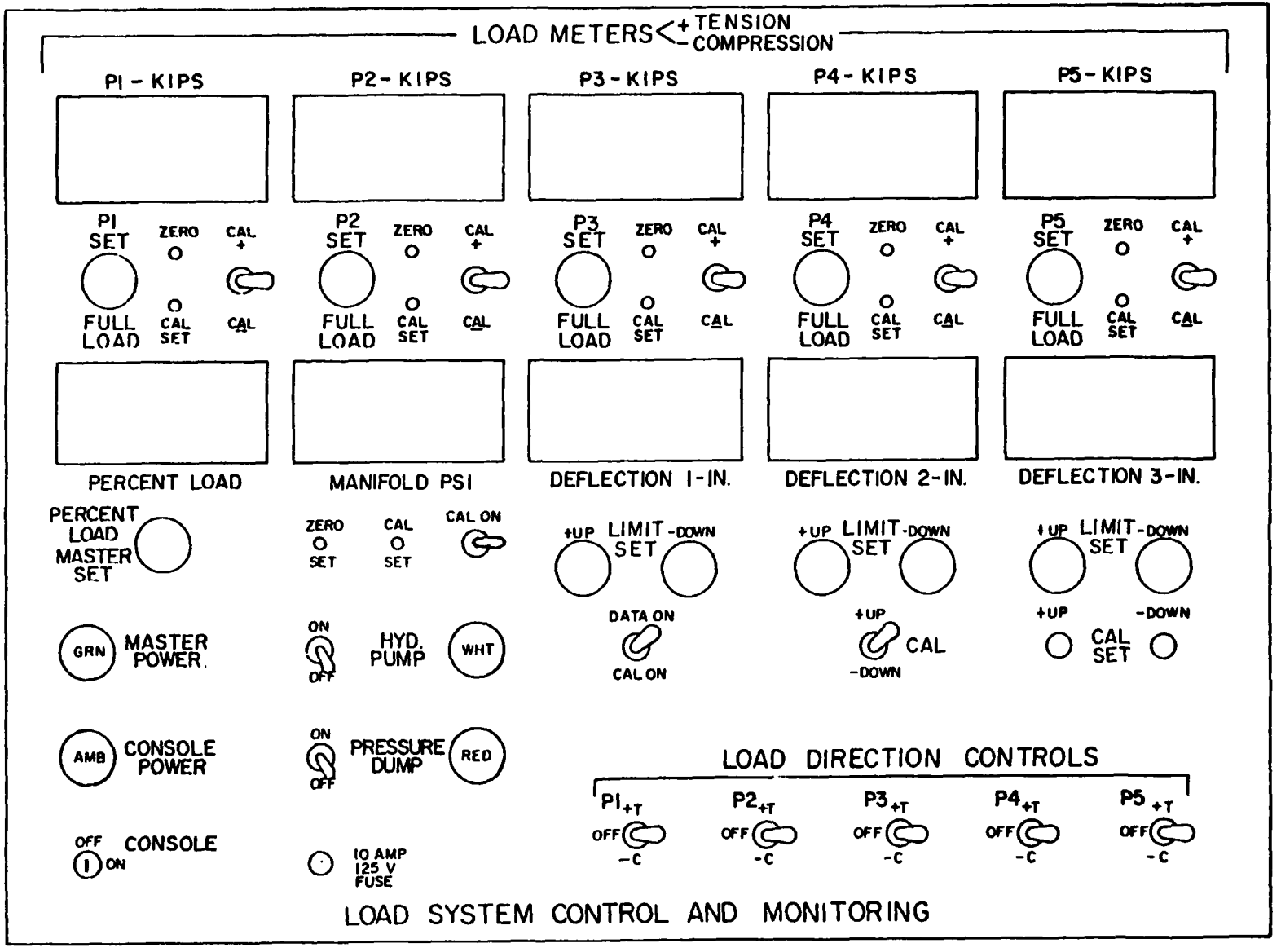

Figure 2.8. Load Control Panel.

power unit control, emergency dump, master load control, and five individual load controls. Deflection limit set dump controls, calibration span set controls, and calibration switches also are included. Digital readouts include master load control setting, five load readouts, system hydraulic pressure, and three specimen deflections.

2.2 STRUCTURAL ANALYSIS TECHNIQUE

The structural analysis technique[2] provides the survivability/vulnerability engineer with an analytical tool for predicting the static response of undamaged and damaged wing structures. The objectives of the structural analysis capability are: (a) to provide a check on experimentally obtained data, (b) to compute the internal stresses in undamaged wing structures, (c) to predict the stress redistribution in damaged wing structures, and (d) to estimate the residual strength of damaged wing structures.

The general form of the structural analysis technique is indicated in Figure 2.9. This total analysis package consists of three major blocks of computer code. The primary part of the analysis tool is a finite element structural analysis computer program, while the other two programs are a preprocessor and a postprocessor. The pre- and postprocessors essentially "straddle" the finite element program in a manner so that the composite analysis tool is convenient for the survivability/vulnerability engineer to use effectively.

The programs shown in Figure 2.9 are discussed briefly in the following paragraphs. Detailed instructions for using the structural analysis technique are contained in Reference 2.

2.2.1 Finite Element Program

The finite element program is the major part of the structural analysis technique. The particular program used is the MAGNA (Materially And Geometrically Nonlinear Analysis)

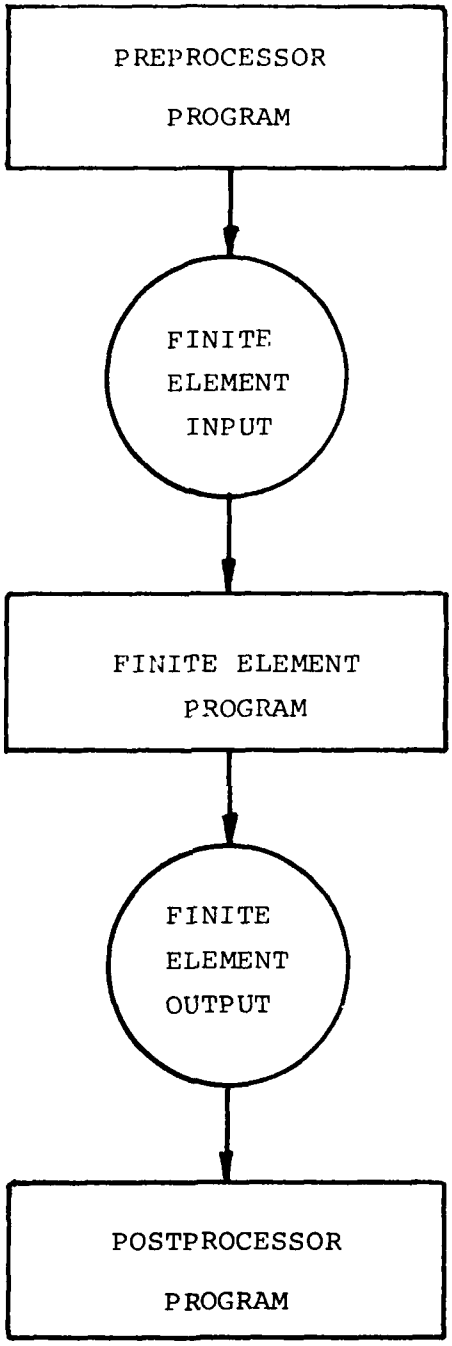

Figure 2.9. Structural Analysis Technique.

finite element program[4]. This program was initially developed by the University of Dayton Research Institute using internal funds. Therefore, MAGNA is considered proprietary, although only to a limited extent as far as the Air Force is concerned. Portions of the later stages of development of MAGNA have been funded by Air Force contracts. Therefore, the only restriction placed on the MAGNA program for the Air Force is that it not be distributed to any non-Air Force organization without permission from the University. MAGNA can be utilized on the Wright-Patterson ASD CDC computers by both Air Force personnel and by Air Force contractors. Refer to proprietary data statement included in Reference 4.

MAGNA is a large-scale computer program for the static and dynamic analysis of complex, three-dimensional engineering structures. The program is based upon the finite element method of analysis to permit the simulation of practical structures composed of many different types of elements. MAGNA combines effective isoparametric modeling techniques with state-of-the-art numerical analysis and programming methods to provide accurate and efficient solutions for large problems involving highly nonlinear response.

The modeling capabilities of MAGNA include structural elements for truss members, plane stress and plane strain sections, "shear panels," general three-dimensional solids, and thin plates and shells. All finite elements are arbitrarily oriented and are fully compatible in three-dimensional space. Degrees of freedom can be coupled to represent skewed boundary conditions, rigid regions, and complex structural joints. Uniform mass damping, as well as structural damping based upon the instantaneous stiffness, can be applied in the solution. Time history solutions are performed in MAGNA using an implicit scheme for direct integration of the equations of motion.

Each of the finite elements in MAGNA includes the effects of full geometrical nonlinearities (large displacements, large strains), using a Lagrangian (fixed reference) description of motion. In shell analysis, arbitrarily large rotations can also be treated. Material nonlinearities, in the form of elastic-plastic behavior, are analyzed using a subincremental strategy which minimizes the error in following the material stress-strain curve. Isotropic, kinematic, and combined strain-hardening rules are available for use in plastic analysis with MAGNA.

The MAGNA program includes numerous user convenience features to aid in the generation of finite element modeling data. Geometry data may be input in Cartesian, cylindrical, and spherical coordinates, or in arbitrary, user-defined systems. Incremental generation of nodal coordinates and element connections is also available to exploit repetitive patterns in the structural model. User-written subroutines, which provide for user intervention or specification of data at several stages of the analysis, can be supplied for defining mesh geometry, coordinate systems, and incremental applied loading.

Plotting utilities, in both interactive and batch forms, are also available for use in checking data, and for interpreting analysis results obtained from MAGNA. Geometry plotting, including exploded views, is currently available for all finite elements. Postprocessing functions, which are presently provided for most element types, include stress and strain contours and stress relief plots. Scaled and exploded views of close-up plots of the deformed structural model can be generated, with the undeformed geometry optionally superimposed in the display.

2.2.2 Preprocessor Program

The preprocessor program, WINGEN, is a convenient and flexible computer program designed specifically for the

generation of wing finite element models. The WINGEN program accepts data in an abbreviated format and then generates an expanded set of data which is acceptable by the finite element program.

The purpose of the pre-processor is to provide the survivability/vulnerability engineer with the capability to use a powerful, state-of-the-art, nonlinear finite element analysis computer program without having to spend the time and effort necessary for manual preparation of detailed wing finite element models and the associated data decks. Typical data which is input to WINGEN includes coordinates of key points to define the planform outline of the wing, number and spacing of spars, number and spacing of ribs, skin and rib thicknesses, bar areas and material properties. The pre-processor assumes that the input data refers to a predetermined class of structures (in particular, wing structures). The preprocessor automatically completes a finite element model of the wing, including the numbering of the nodes and the elements. Then data for the MAGNA finite element program is generated in the appropriate format; typical data generated are node coordinates, element connectivities, degree of freedom numbers, properties data, and program control parameters.

The preprocessor assumes that the wing skins are two-dimensional membrane finite elements, the spar and rib webs are two-dimensional shear panel finite elements, and the spar and rib caps are one-dimensional bar finite elements. That is, individual skin and web panels do not resist local bending forces; therefore, the resulting finite element model for some damage cases may be unrealistic. This restriction was defined, however, in a meeting with the Air Force. One area for future development on the wing preprocessor is to expand the types of finite elements which can be automatically generated in wing models. Note that the restriction of finite

element types to bars, membranes, and shear panels refers only to the preprocessor; the MAGNA program can solve more sophisticated models, but at present the data would have to be prepared manually.

The preprocessor also has the capability to create finite element models of wing structures which are damaged. The WINGEN preprocessor creates damage models in two ways:

1. The user defines a list of element numbers, and those elements are dropped from the undamaged model, and a new model is generated; and

2. The user defines the coordinates of the center of a sphere and a radius, and the preprocessor drops from the undamaged model all elements having centroids within the sphere, and generates a new model.

The output of the preprocessor is a file containing the data for the finite element program. This output file is also readable by the postprocessor so that undeformed geometry plots can be viewed before running the finite element program.

2.2.3 Postprocessor

The postprocessing capability consists of two computer programs:

1. PLOTBOB - This interactive postprocessor accepts data files from either the preprocessor or from the finite element program. Data from the preprocessor is used to present plots of undeformed finite element meshes for data checking purposes. Data from the finite element program is used to present plots of the deformed structure either singly or superimposed on top of the undeformed structure. Some of the options of this postprocessor are: plotting of lists of elements, zooming, clipping, and exploding. The model can be rotated, translated, or reflected about defined axes. Also,

either orthographic projection or perspective views can be selected. In addition, the user can selectively label nodes and elements.

2. CONTOUR - This interactive postprocessor is designed to display the results of the finite element program in various forms which the user requests selectively. Examples of the plotting options available are:

- contour plots of stress, strain, and displacement on either the undeformed or the deformed model,
- selective labeling of contours,
- relief maps of stress, strain and displacement,
- undeformed and deformed geometry,
- zooming, clipping, and exploding,
- rotation, translation, and reflection, and
- descriptive plot labeling.

2.3 REPLICA SPECIMENS

The replica specimens were designed to demonstrate and evaluate the performance of the experimental facility and the structural analysis technique. The specimens[3] are simple, rectangular construction to allow comparison of experimental and analytical results without introducing possible modeling errors due to geometrical complexity.

A photograph of a typical replica test specimen is shown in Figure 2.10. The specimens are aluminum having overall dimensions of 18 in. deep, 60 in. wide, and 94.5 in. long. The cross-section of the four-spar specimens is shown in Figure 2.11, and the planform is shown in Figure 2.12.

The total set of six replica specimens consists of two undamaged and four damaged articles. Figure 2.12 indicates a scheme for referring to individual skin panels (e.g., 2-4), spar web panels (B-5), rib web panels (d-3), spar caps (C-3), and rib caps (e-2). The two end bays are covered by the mounting brackets (see Figure 2.4c) and are not included in

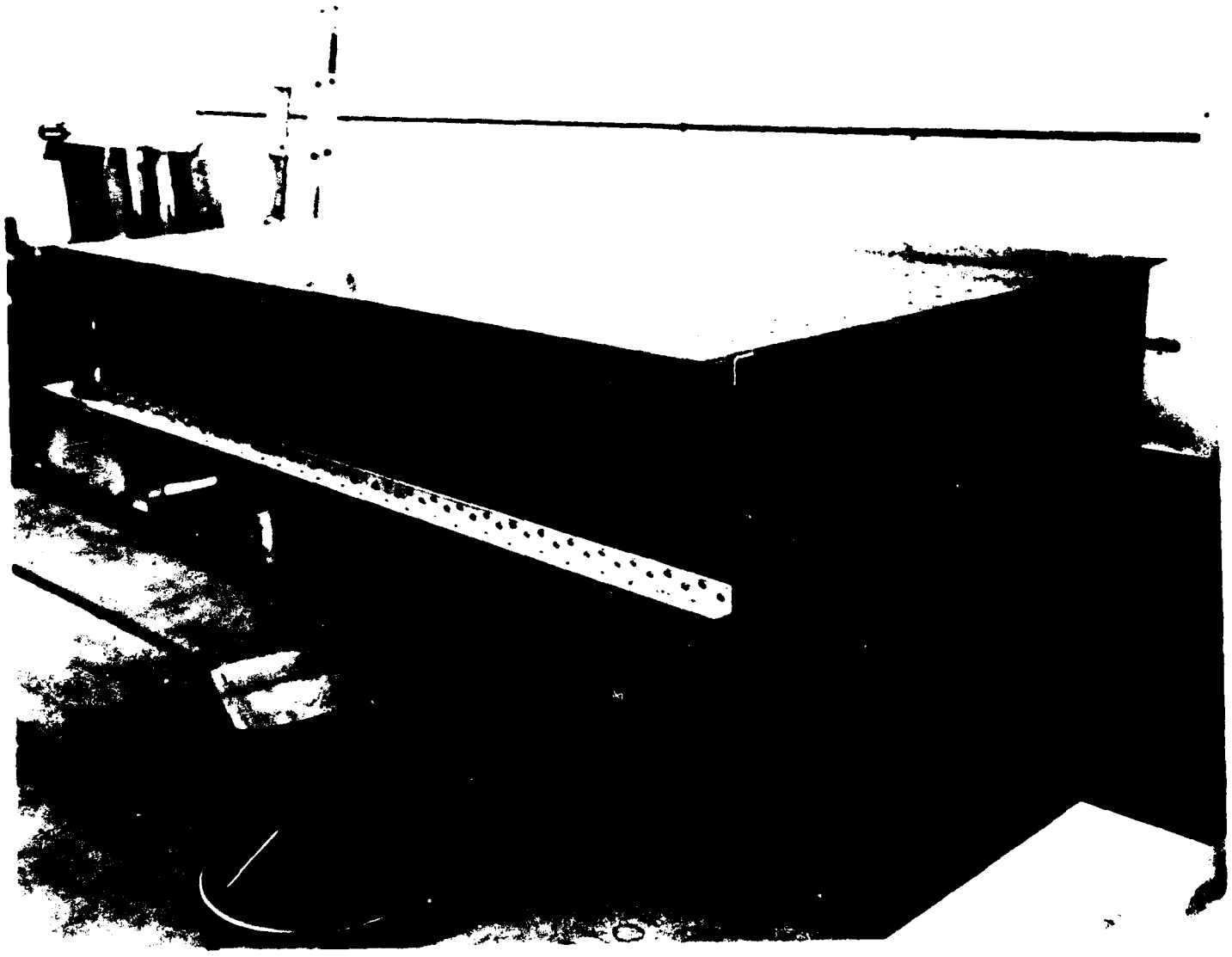

Figure 2.10. Replica Test Specimen.

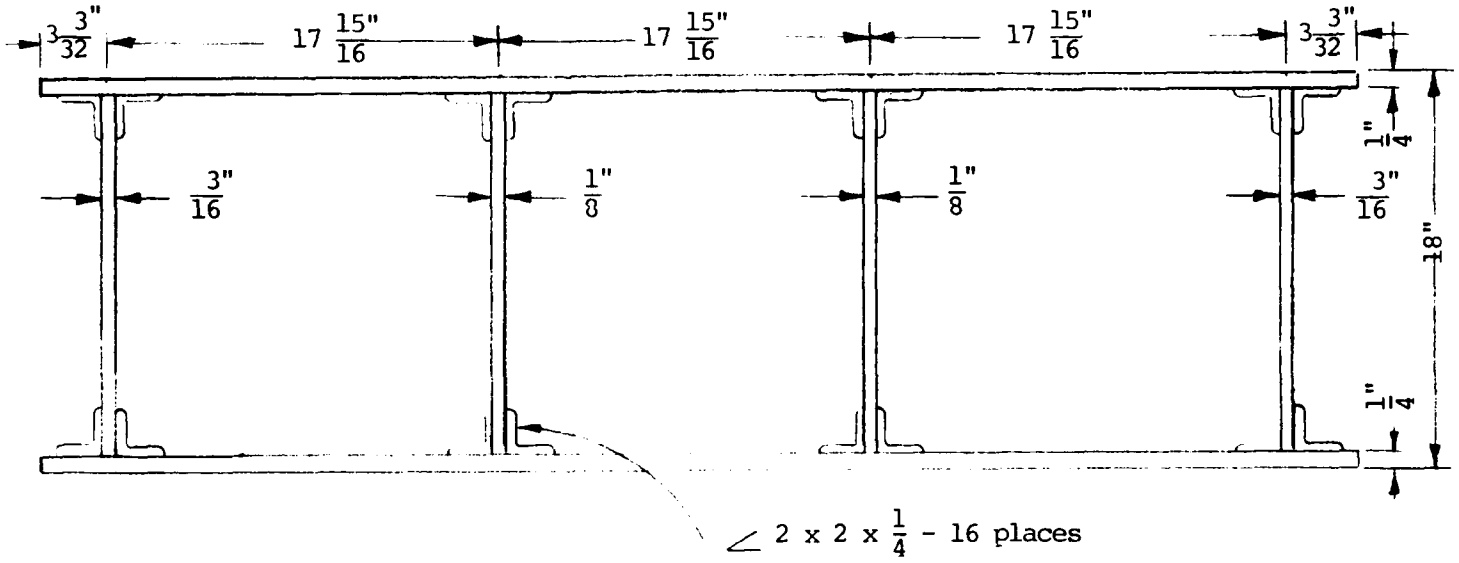

Figure 2.11. Cross Section of Replica Test Specimen.

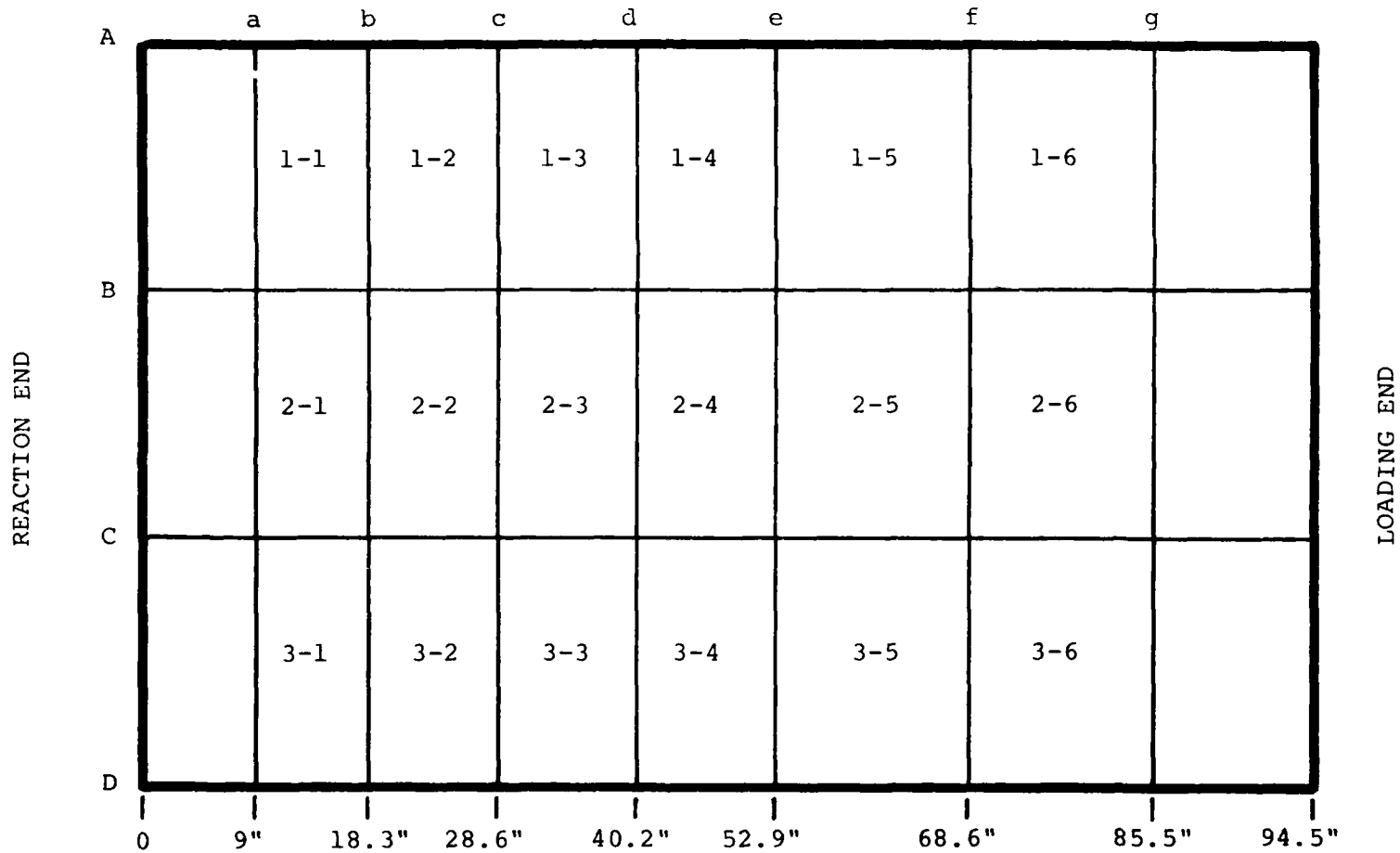

Figure 2.12. Planform of Replica Test Specimen.

the analysis model. Therefore, for convenience of the analysis, the end bays are not numbered.

The physical characteristics of the six replica specimens are listed in Table 2.1. Specimen Number 1 had no damage and was used as a control specimen to perform initial checkout of the experimental facility. Specimens 2, 3, 4, and 5 contained simulated damage as indicated in Table 2.1. Specimen 6 was a backup specimen. The damaged specimens were intended to check out the the capability of the experimental facility to apply realistic flight loads to damaged wing sections and produce failure in the test articles. The replica specimens also provided experimental results to compare with analytically determined stresses at various points of the damaged specimens.

TABLE 2.1

REPLICA SPECIMENS

Specimen Number	Damage
1	None
2	Skin, 2-4, Bottom, Removed
3	Skin, 2-4, Bottom and Top, Removed Spar Web, B-4, C-4, Removed Spar Cap, B-4, C-4, Bottom and Top, Removed
4	Skin, 1-3, Bottom and Top, Removed Spar Web, A-3, Removed Spar Cap, A-3, Bottom and Top, Removed Spar Cap, B-4, B-5, Bottom and Top, Split
5	Skin, 1-4, 2-4, 3-4, Bottom, Removed Spar Web, B-4, C-4, Removed Spar Cap, B-4, C-4, Bottom and Top, Removed
6	None

SECTION 3
REPLICA SPECIMEN TESTS AND ANALYSES

This section discusses the results of tests performed on the replica specimens using the experimental facility, and of analyses of finite element models of the replica specimens using the structural analysis technique.

3.1 ACTUATOR LOADS AND EQUIVALENT SECTION LOADS

In the tests and analyses, the section loads (spanwise bending moment $\bar{M}_s$, spanwise shear force $\bar{V}_s$, torque $\bar{T}$, and chordwise shear force $\bar{V}_c$) at the unsupported end of a test specimen, are assumed to be known. The positions of the hydraulic actuators relative to the loaded end of the replica specimens are shown schematically in Figure 2.5. Positive values of the section loads and the actuator forces (tension positive) are shown in Figure 3.1. Expressions which relate the actuator forces and the applied section loads are:

$$
\begin{aligned}
&T_1 + T_2 + T_3 + T_4 = -\bar{V}_s \\
&T_1 g - T_2 h - T_3 c + T_4 d = -\bar{T} \\
&T_1 b + T_2 b - T_3 a - T_4 a = -\bar{M}_s \\
&T_4 a - T_1 b = T_3 a - T_2 b \\
&T_5 = -\bar{V}_c
\end{aligned}
\tag{3.1}
$$

The fourth equation ensures that the actuator forces all work approximately equally; the equation forces the bending moment due to pairs of actuators on one side of the center line of a specimen to be equal to the bending moment due to pairs of actuators on the other side of the center line.

Solving Equations 3.1 for the actuator forces gives:

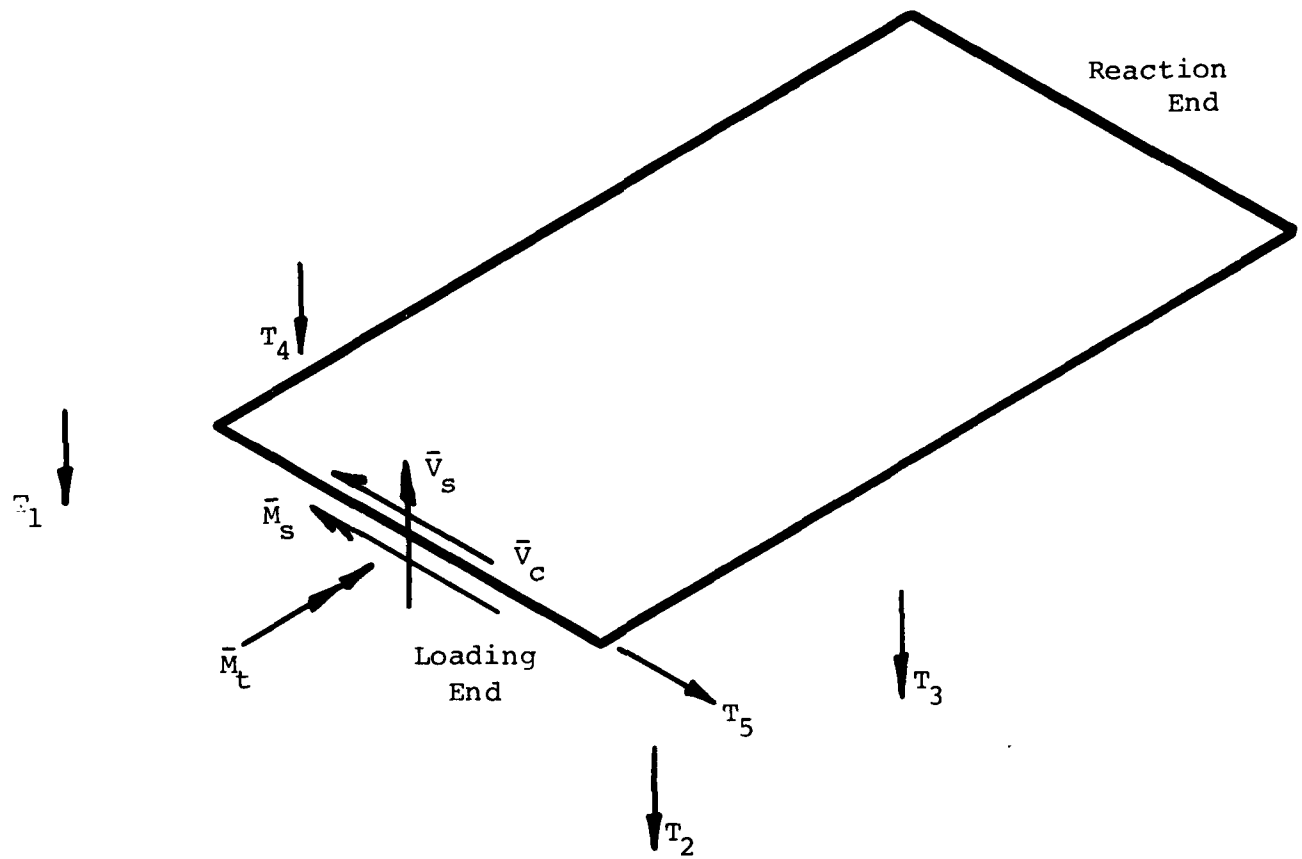

Figure 3.1. Positive Sign Convention.

$$T_1 = \frac{-(h + \frac{bc}{a})(\bar{V}_s + \frac{\bar{M}_s}{a}) - (1 + \frac{b}{a})(\bar{T} + \frac{d-c}{2a}\bar{M}_s)}{(1 + \frac{b}{a})(h + \frac{bc}{a}) + (1 + \frac{b}{a})(g + \frac{bd}{a})}$$

$$T_2 = \frac{-(g + \frac{bd}{a})(\bar{V}_s + \frac{\bar{M}_s}{a}) + (1 + \frac{b}{a})(\bar{T} + \frac{d-c}{2a}\bar{M}_s)}{(1 - \frac{b}{a})(h + \frac{bc}{a}) + (1 + \frac{b}{a})(g + \frac{bd}{a})}$$

$$T_3 = \frac{2bT_2 + \bar{M}_s}{2a} \qquad (3.2)$$

$$T_4 = \frac{2bT_1 + \bar{M}_s}{2a}$$

$$T_5 = -\bar{V}_c$$

These equations are used to determine what actuator loads the operator of the control console must impose in order to apply given values of the section loads.

3.2 TEST 1 - UNDAMAGED SPECIMEN, NUMBER 1

The first test was a series of verification tests to determine if the experimental facility was operating properly. A number of simple load cases such as pure spanwise bending, pure spanwise shear, pure torque, and combinations thereof were performed with undamaged specimen Number 1 (Table 2.1).

3.2.1 Instrumentation

Figure 3.2a shows a schematic representation of the relative locations of strain gages monitored during the tests. The numbers in circles identify strain gage rosettes while the uncircled numbers indicate individual gages.

Specimen Number 1 also was instrumented for measuring deflections at several points on the bottom surface of the specimen. No useful deflection data was obtained, however, due to excessive deformation in the support brackets which were used to mount the test specimen to the reaction fixture. The support bracket deformation resulted in erroneous deflection measurements.

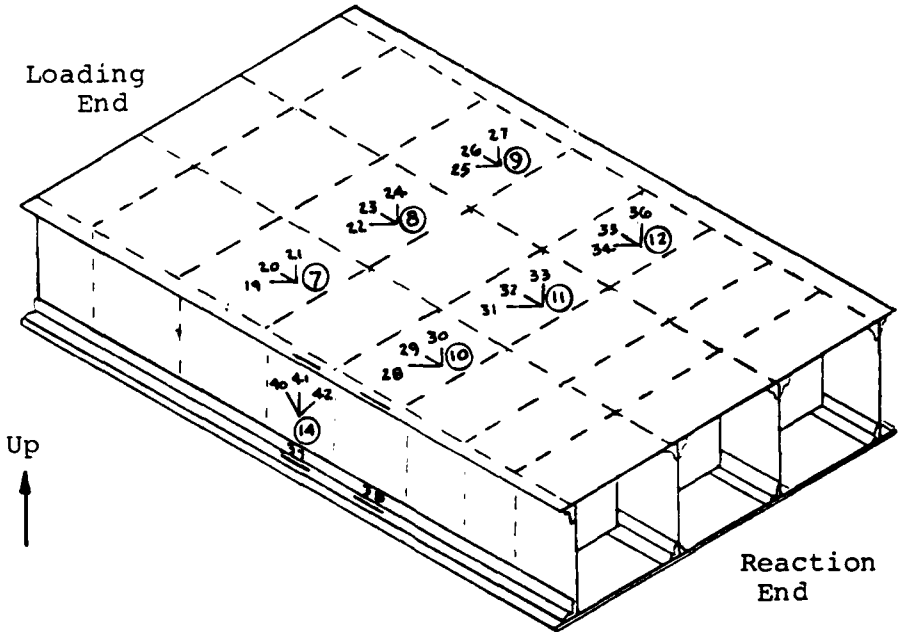

Top View

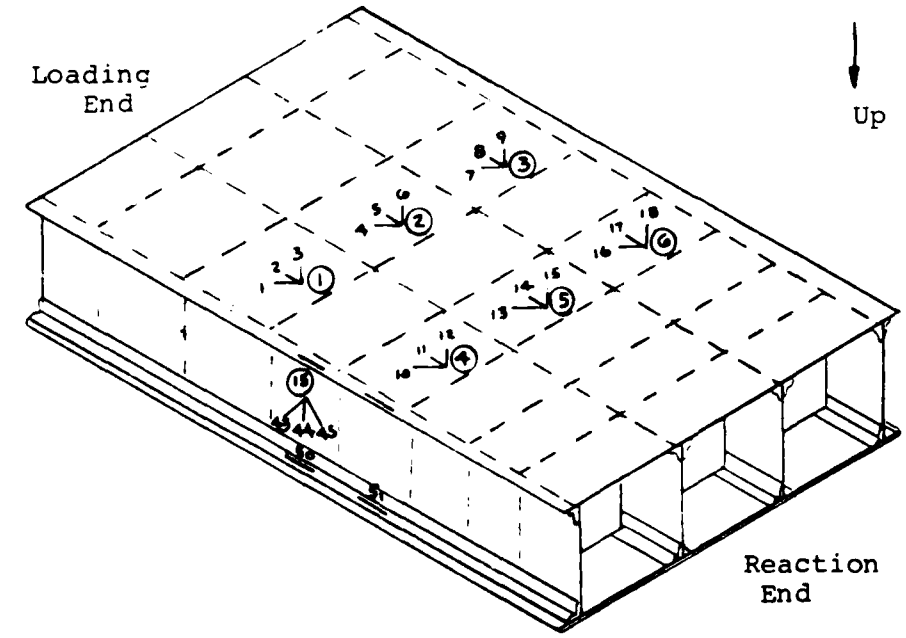

Bottom View

Figure 3.2a. Strain Gage Locations - Specimen 1.

In addition, the deflection measurements were not repeatable. Consequently, the measurement of deflections was abandoned for the remainder of the replica specimen tests.

3.2.2 Load Conditions

The particular loading conditions applied in the initial testing phase are given in Table 3.1. Using Equations 3.2, the individual actuator loads used for each of the above loading cases were calculated, these actuator loads are shown in Table 3.2.

3.2.3 Load Incrementation and Data Collection

During the five verification tests, the actuators were increased in increments of 20 percent of the maximum loads listed above until the maximum values were attained; then the actuator loads were decreased in 20 percent increments. Strain gage readings were recorded at every increment of loading and unloading by a minicomputer. A small computer program converted the gage signals into units of strain. In addition, the individual gage stresses were calculated, and in the case of the rosettes the minimum principal stress, the maximum principal stress, the maximum shear stress, and the principal angle. These calculated values were printed for each loading case for each loading increment. An example of the output of the program is shown in Figure 3.2b. The output corresponds to 40 percent of the maximum loading of case 1, pure bending.

3.2.4 Analysis Model

The undamaged replica specimen finite element model is shown in Figure 3.3a-f. The portion of the replica specimens modeled is that part of Figure 2.12 which have the bays numbered. As mentioned before, in the experimental facility the two end bays are clamped by mounting brackets and are, therefore, not considered in the analysis. The model contains 56 nodes, 36 skin membrane elements, 24 spar web shear panel elements, 15 rib web shear panel elements, 48 spar cap bar elements, and 30 rib cap bar elements. Each of the 56 nodes has three-degrees of freedom - the displacements

TABLE 3.1

LOAD CASES

Verification Case	Load Condition (maximum)
1	$\bar{M}_s = 2.7 \times 10^6$ in. lb.
2	$\bar{T} = 600{,}000$ in. lb.
3	$\bar{V}_s = 30{,}000$ lb.
4	$\bar{M}_s = 1.8 \times 10^6$ in. lb., $\bar{V}_s = 15{,}000$ lb.
5	$\bar{M}_s = 1.8 \times 10^6$ in. lb., $\bar{V}_s = 15{,}000$ lb., $\bar{T} = 600{,}000$ lb.

TABLE 3.2

ACTUATOR LOADS

Verification Case	Actuator Loads (lb)			
	T_1	T_2	T_3	T_4
1	-21,252	-23,010	+18,889	+25,380
2	- 1,704	+ 1,704	+ 6,294	- 6,294
3	- 3,069	- 3,324	-12,273	-11,334
4	-15,700	-16,998	+ 6,446	+11,253
5	-17,404	-15,294	+12,740	+ 4,959

SPECIMEN 1. TEST 1-1 12.20/78 14.44.40 READING 3

BASIC CHANNELS

CH	---MV---	VALUE--	
1	-359.716	-3.583	P1
2	-927.344	-9.251	P2
3	725.781	6.599	P3
4	1003.906	11.391	P4
5	5.469	.011	P5
6	9921.875	99.219	SL
7	-177.525	-633.135	MP
8	45.111	-.609	D1
9	72.242	-.276	D2
10	125.781	-1.327	D3

STRAIN GAGE DATA				PRINCIPAL STRESS CALCULATIONS				
CH	MV (DEG)	STRAIN	-STRESS- (PSI)	ROS-ETTE	MIN. PR STRESS	MAX. PR STRESS	MAX. SHEAR	ANGLE
1	.225	90.16	929.					
2	.656	259.71	2675.					
3	.266	104.54	1077.					
				1001	238.	2755.	1259.	46.27
4	.260	100.64	1037					
5	.717	277.13	2854					
6	.140	53.04	546					
				1002	-381.	2743.	1562.	41.61
7	.225	86.32	889					
8	.657	256.57	2643					
9	.196	76.05	783					
				1003	-111.	2607.	1359.	44.16
10	.248	94.24	971					
11	.624	239.46	2467					
12	.188	73.09	722					
				1004	41.	2485.	1222.	42.81
13	.227	87.34	900.					
14	.748	286.07	2947					
15	.249	94.59	974					
				1005	-113.	2910.	1511.	45.53
16	.208	82.21	847					
17	.744	287.27	2959					
18	.263	103.49	1066.					
				1006	-81.	2935.	1508.	46.57
19	-.205	-78.22	-806					
20	-.609	-236.06	-2431.					
21	-.196	-74.26	-765					
				1007	-2410.	66.	1238.	134.64

Figure 3.2b. Sample Experimental Data - Specimen 1, Case 1.

22	-.222	-85.07	-876.					
23	-.631	-244.24	-2516.					
24	-.176	-67.16	-692					
				1008	-2474.	134.	1304.	133.48
25	-.027	-54.62	-563.					
26	-.630	-239.97	-2472.					
27	-.219	-84.19	-867.					
28	-.174	-66.11	-681					
29	-.594	-227.38	-2342.					
30	-.192	-73.49	-757.					
				1010	-2294.	148.	1221.	-44.33
31	-.229	-87.42	-900.					
32	-.621	-238.65	-2459.					
33	.000	.00						
34	-.299	-114.76	-1182.					
35	-.683	-259.89	-2677.					
36	-.182	-69.42	-715.					
				1012	-2727.	-104.	1311.	131.15
37	.537	205.97	2120.					
38	.060	79.99	823.					
39	.001	7134.76	73488.					
40	-.038	-14.40	-148.					
41	-.003	-1.07	-11.					
42	.059	22.51	232					
				1014	-86.	211.	148.	97.77
43	.085	32.59	336.					
44	.004	1.69	17.					
45	-.078	-19875.59	-204719.					
46	-.558	-212.56	-2189.					
47	-.510	-195.02	-2009.					
48	.632	242.52	2498.					
49	.657	251.94	2595.					
50	-.625	-239.77	-2470.					
51	-.671	-257.31	-2650.					

Figure 3.2b. (concluded).

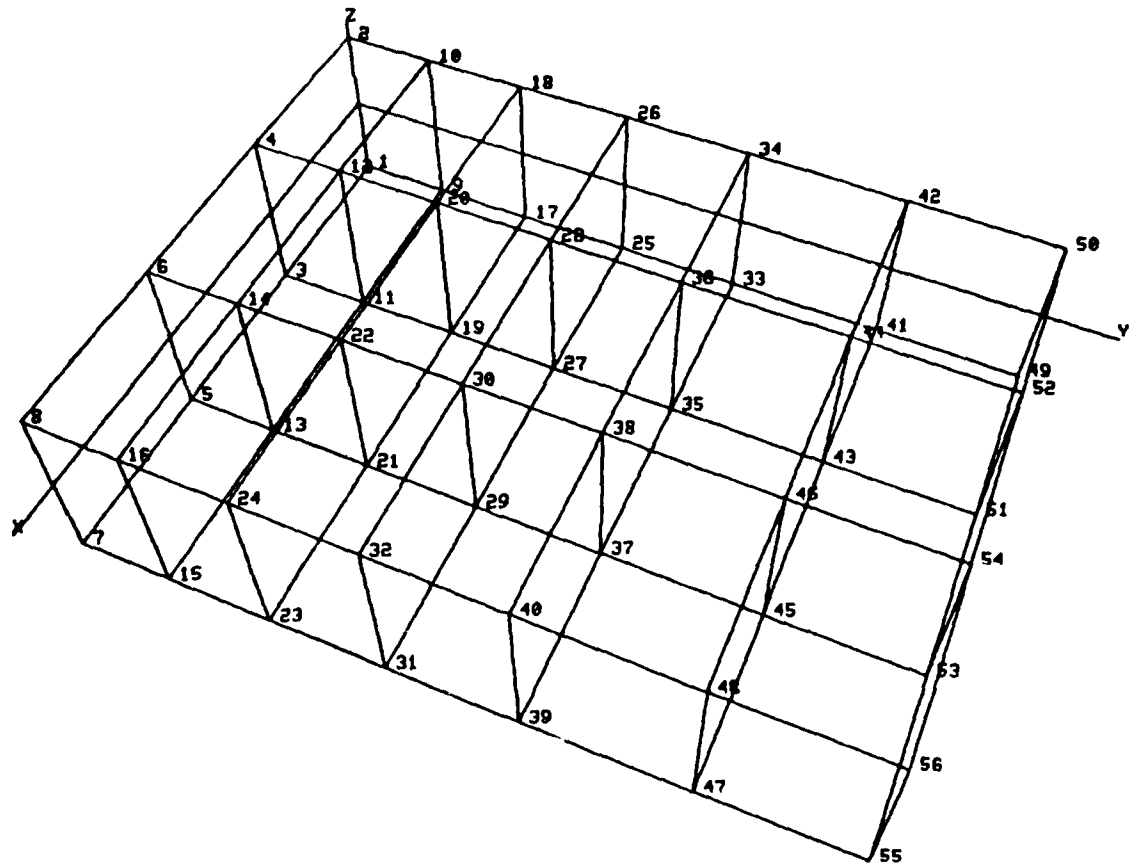

Figure 3.3a. Specimen 1 Finite Element Model - Node Numbers.

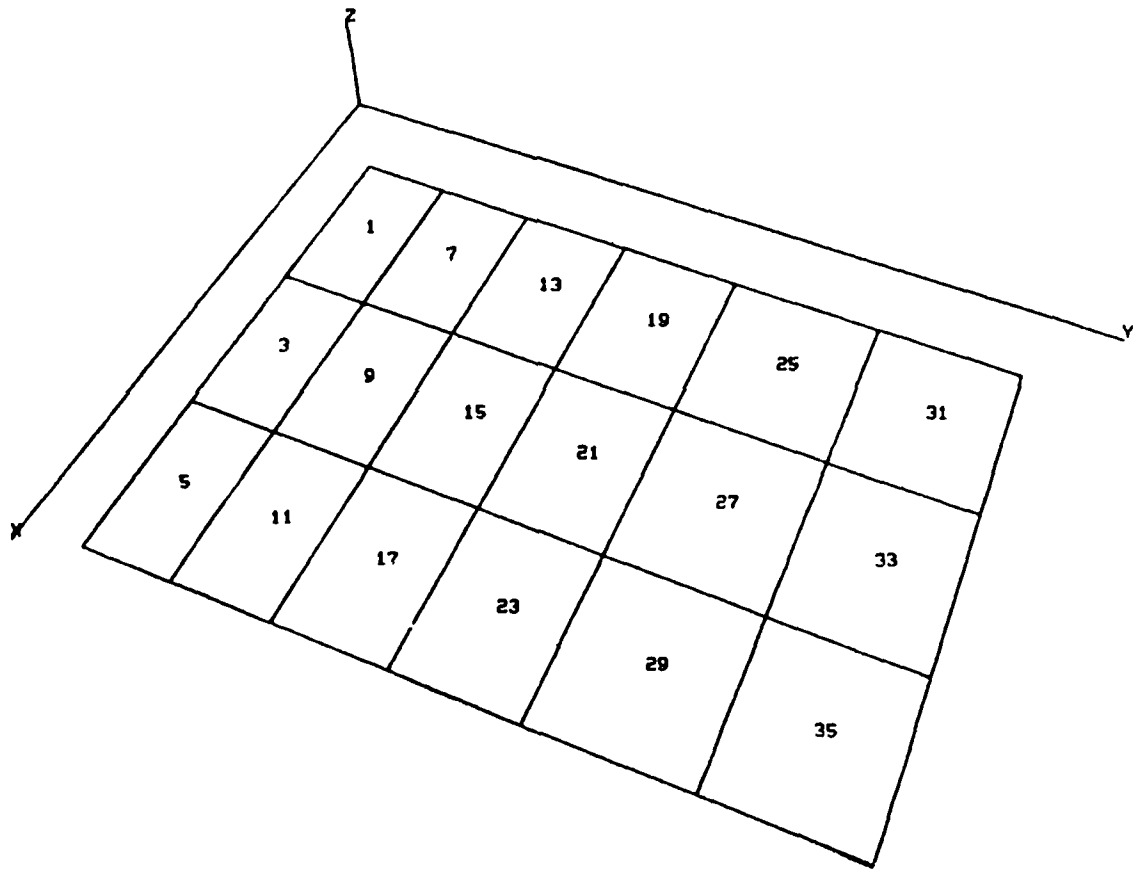

Figure 3.3b. Specimen 1 Finite Element Model - Lower Skin Membrane Elements.

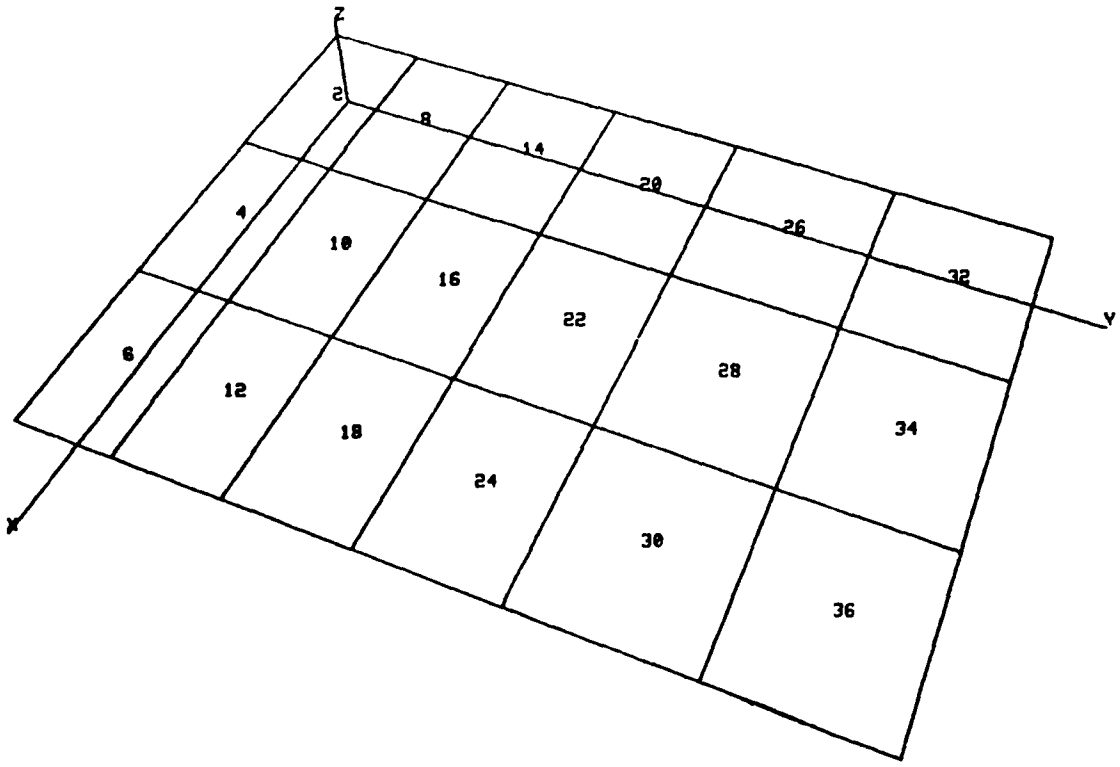

Figure 3.3c. Specimen 1 Finite Element Model - Upper Skin Membrane Elements.

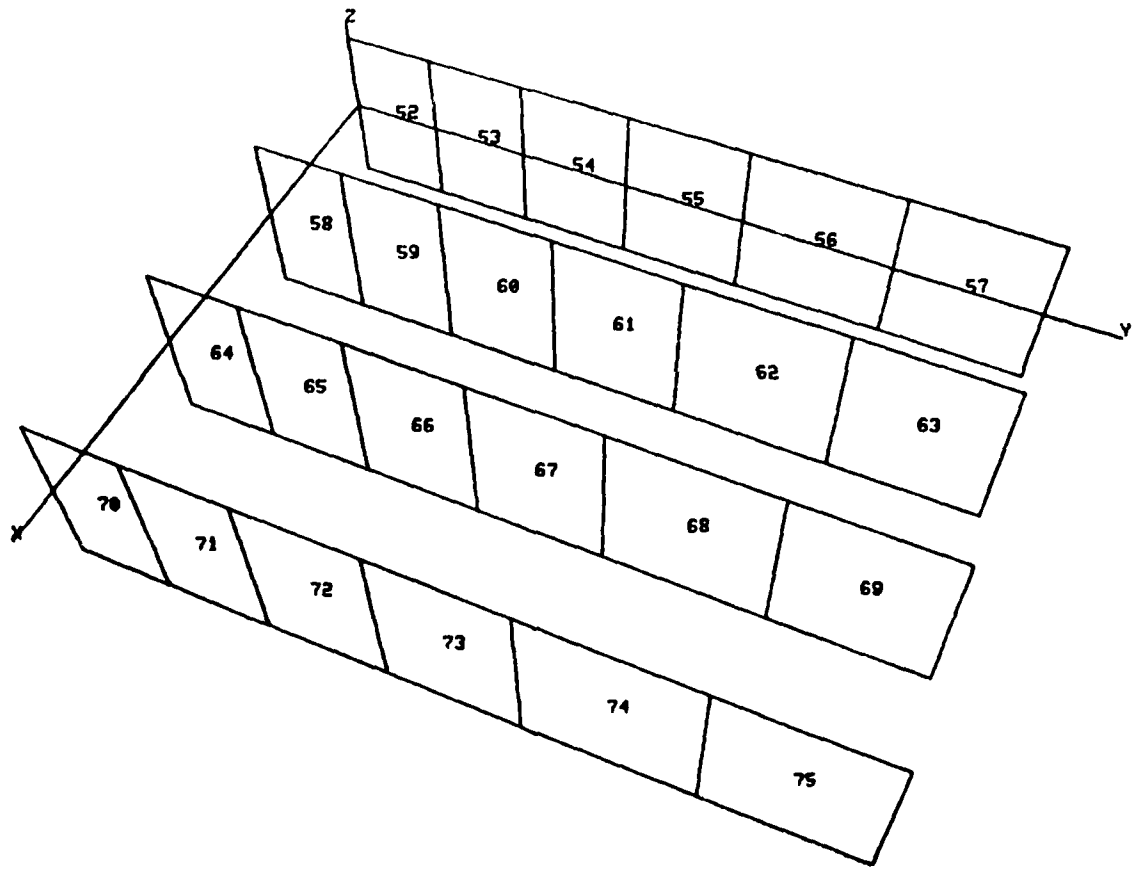

Figure 3.3d. Specimen 1 Finite Element Model - Spar Shear Panel Elements.

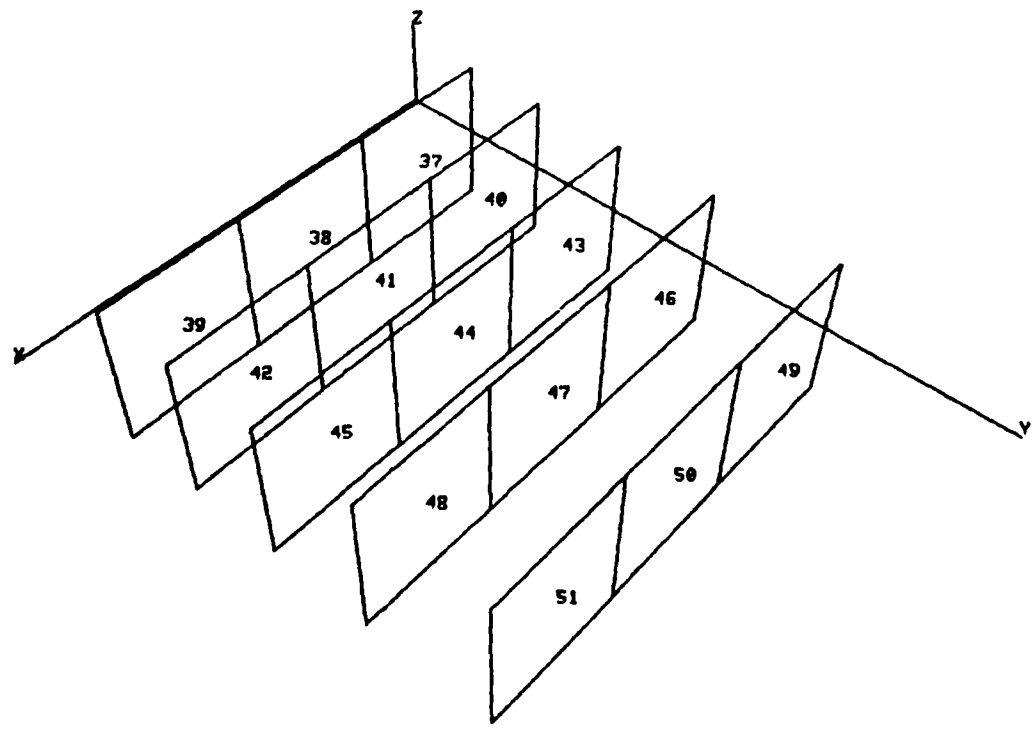

Figure 3.3e. Specimen 1 Finite Element Model - Rib Shear Panel Elements.

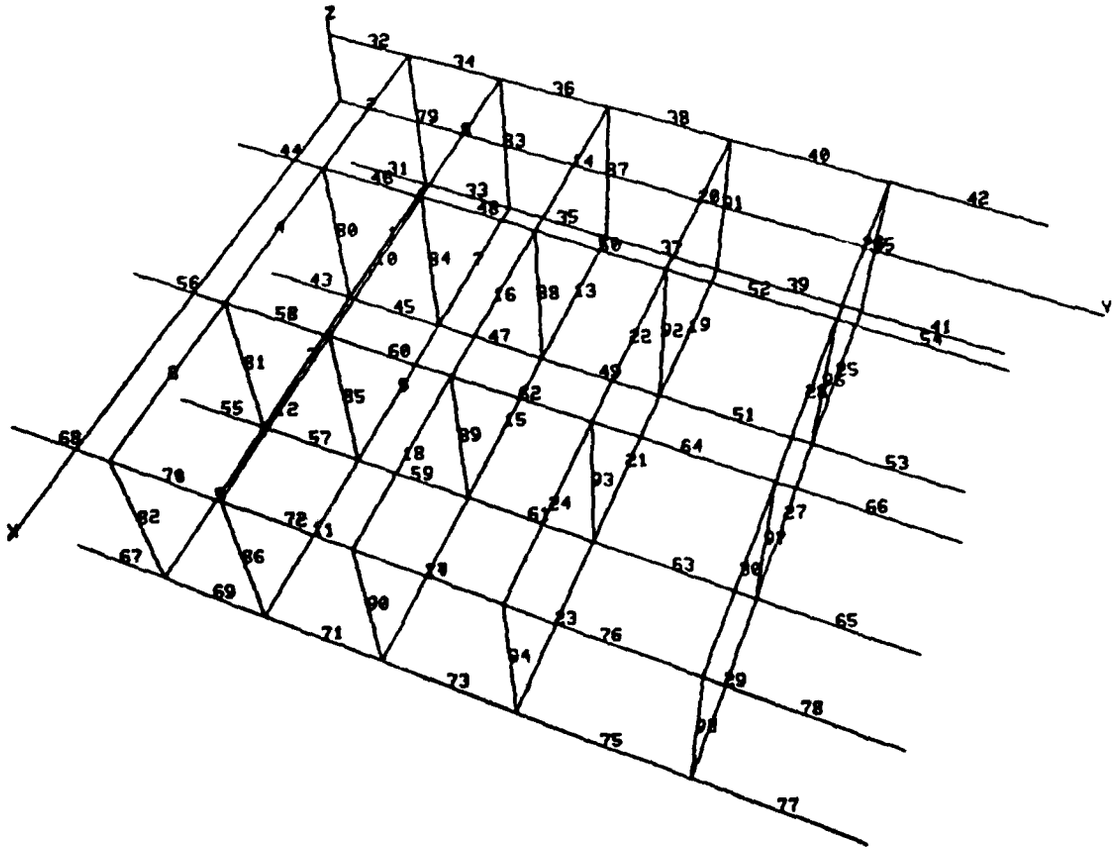

Figure 3.3f. Specimen 1 Finite Element Model - Cap Bar Elements.

parallel to the three coordinate axes. Eight of the nodes are clamped at the reaction end of the specimen. Therefore, the analysis model has 3 x 48 = 144 degrees of freedom.

3.2.5 Test/Analysis Results

The series of load cases defined in Paragraph 3.2.2 was used to determine if the experimental facility operated as it was designed. The maximum load levels were intentionally kept relatively low to ensure that no failure of the specimen would occur during the tests.

Each of the five loading cases was applied to the specimen by incrementing the individual actuator forces through the control console. The repeatability of the tests was checked by cycling through the tests twice. In each case the repeatability was excellent. The symmetric load cases produced symmetric strain gage readings. Also, the strains on the top and bottom surfaces of the specimen at the same planform locations were of the same magnitude but of opposite signs.

The comparison between the results obtained from the verification tests and those produced by the MAGNA finite element program was quite good. As mentioned above in Paragraph 2.2.2, the finite element model produced by the wing model preprocessor is a one-element-per-bay model. This type of model has been used by many aircraft stress analysts for analyzing undamaged wing structures with good success. Therefore, it was expected that the test/analysis comparison for the undamaged specimen tests would be good.

As an example, Figure 3.4 shows the comparison between a stress measured during the test of Case 1 (pure bending), and the stress predicted by the finite element program. The location of the compared stresses corresponded to rosette number 3 in Figure 3.2 and element 29 in Figure 3.3b. Figure 3.4 is a plot of the maximum principal stress at the indicated

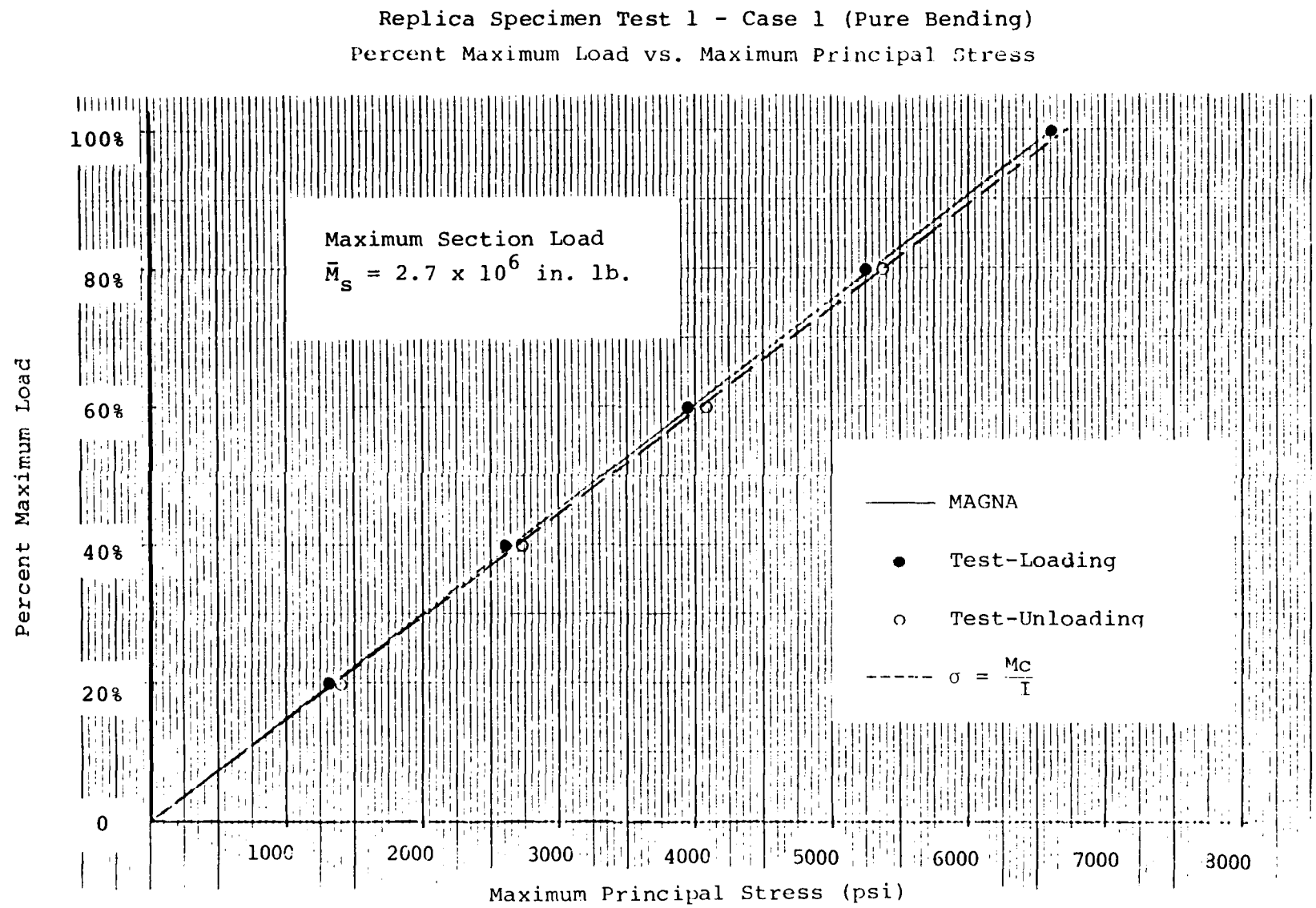

Figure 3.4. Comparison of Experimental/Analytical Results for Test 1, Case 1.

location versus the percentage of the maximum loading applied to the specimen. The figure shows that the test results and the finite element results are very close. Also plotted on the figure is the result obtained from the simple beam formula $\sigma = Mc/I$. The close agreement between the three results (test, finite elements, and beam theory) gives insight into why the bar/membrane/shear panel finite element modeling approach works so well for undamaged wings. That is, a wing box (undamaged) responds sufficiently like a classical beam so that a simplified finite element model provides accurate analytical results. However, this is not the case for some damaged wing structures (see Sections 3.3-3.6).

The results of the remaining verification tests were similar to those of Case 1 (pure bending) discussed above. Therefore, it was concluded that the experimental facility operated as designed. Some minor problems with the electrical and hydraulic systems were encountered, but these were considered to be more of a debugging nature rather than design deficiencies.

3.3 TEST 2 - DAMAGED SPECIMEN, NUMBER 2

The second test was performed on a specimen having a small amount of damage - one panel missing from the lower skin. A combination of spanwise bending and spanwise shear loads were applied. The intention was to increment the applied loads until failure of the specimen occurred. The following paragraphs describe Test 2 in detail.

3.3.1 Instrumentation

Figure 3.5 shows a schematic representation of the relative locations of strain gages monitored during Test 2. The numbers in circles identify strain gage rosettes, while the uncircled numbers indicate individual gages.

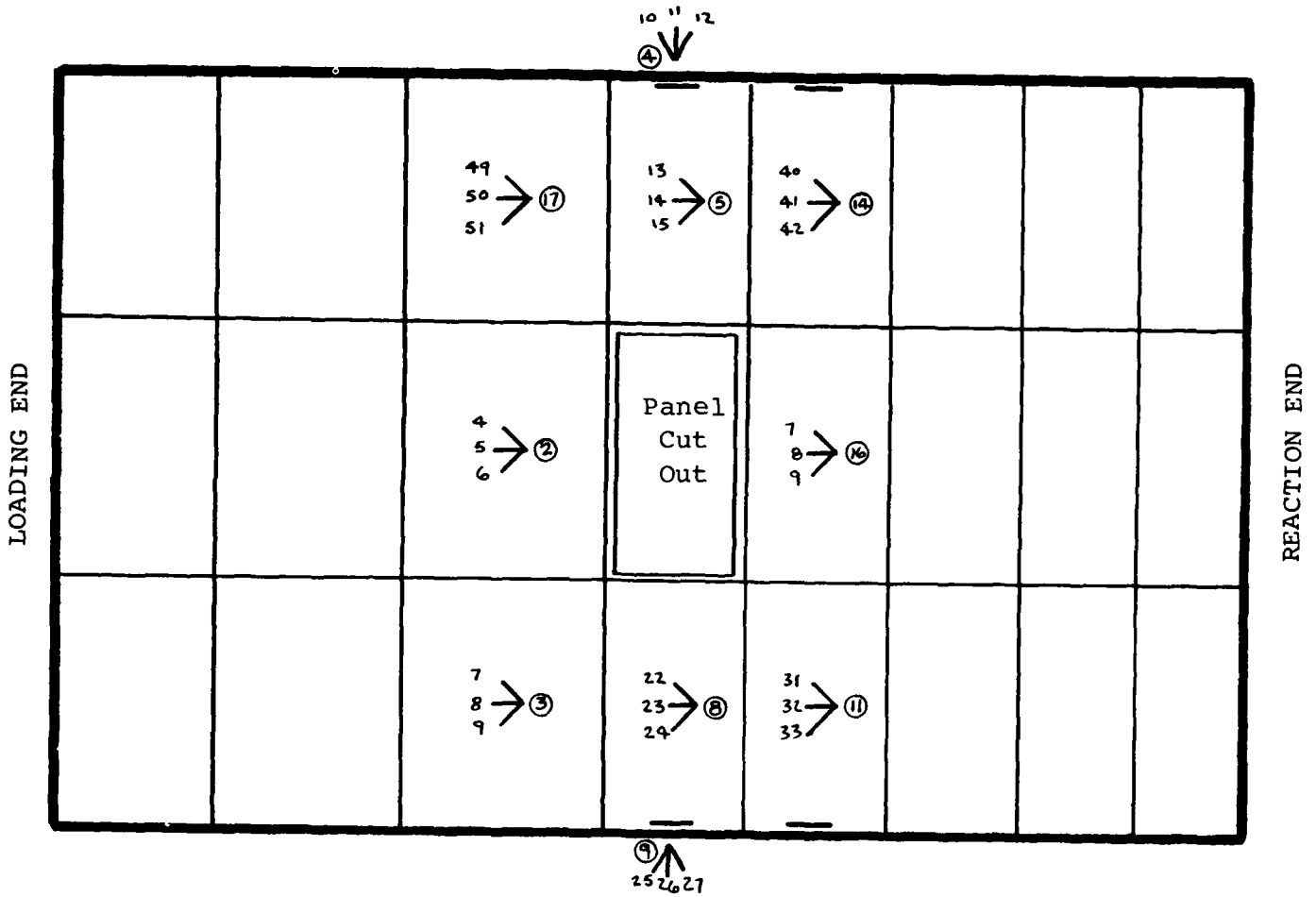

View of Bottom Skin

Figure 3.5. Strain Gage Locations - Specimen 2.

3.3.2 Loading

The maximum load applied to a specimen was a combination of spanwise bending moment and spanwise shear load ($\bar{M}_s = 5.4 \times 10^6$ in. lb. and $\bar{V}_s = 30{,}000$ lb). The individual actuator loads corresponding to these section loads were:

$T_1 = 45{,}573$ lb. Compression

$T_2 = 49{,}344$ lb. Compression

$T_3 = 25{,}497$ lb. Tension

$T_4 = 29{,}426$ lb. Tension

3.3.3 Load Incrementation and Data Collection

During the test the actuator loads were increased in 5 percent increments until failure of the specimen occurred. At each stage of the loading, strain gage readings were recorded by a minicomputer. A computer program converted the gage signals into units of strain, and computed the corresponding gage stresses. In the case of the rosettes, the maximum principal stress, the maximum shear stress, and the principal angle were calculated. An example of the output of the data reduction program for Test 2 is shown in Figure 3.6. The output shown corresponds to 35 percent of the maximum loads defined above.

3.3.4 Analysis Model

The finite element model of Specimen Number 2 is shown in Figure 3.7a-e. The modeled portion of the replica specimen is that part of Figure 2.12 which has the bays numbered. As mentioned before, in the experimental facility, the two end bays are clamped by mounting brackets, and are therefore not considered in the analysis. The model contains 56 nodes, 35 skin membrane elements, 24 spar web shear panel elements, 15 rib web shear panel elements, 48 spar cap bar elements, and 30 rib cap bar elements. Each of the 56 nodes has three degrees of freedom - the displacements parallel to

SPECIMEN 2: TEST 1 1/12/79 10:29:39 READING 1

E= 10.300 MU= .330

BASIC CHANNELS

CH	---MV---	-VALUE--	
1	-1597.265	-16.006	P1
2	-1723.242	-17.253	P2
3	847.851	8.485	P3
4	1371.679	13.665	P4
5	-2.734	-.006	P5
6	-3448.629	34.486	XL
7	-74.80540	598.000	MP
8	-3.125	-.031	D1
9	2.148	.021	D2
10	264.258	2.571	D3

STRAIN GAGE DATA				PRINCIPAL STRESS CALCULATIONS				
CH	MV(CORR)	USTRAIN	-STRESS- (PSI)	ROS-ETTE	MIN. PR. STRESS	MAX PR. STRESS	MAX SHEAR	ANGLE
1	.000	.00	.					
2	.000	.00	.					
3	.000	.00	.					
4	.216	83.50	1611.					
5	.711	271.02	3063.					
6	.445	169.31	2276.					
				1002	775.	3111.	1168	53.21
7	.679	258.16	4192.					
8	1.695	660.17	7305.					
9	.813	316.73	4646.					
				1003	1523.	7314	2895	47.25
10	.299	114.65	2215.					
11	.001	.58	1332.					
12	.612	233.30	3134.					
				1004	1255.	4094.	1419	123.51
13	.712	272.20	4285.					
14	-52.295	-20127.45	-153698.					
15	.780	298.41	4487.					
				1005	-153698.	162470	158084	134.99
16	.479	188.68	2086.					
17	.298	115.04	1515.					
18	-.065	-25.00	431.					
				1006	392.	2125.	866.	9.62

Figure 3.6. Sample Experimental Data - Test 2

19	.505	194.08	2015.						
20	.181	70.01	1054.						
21	-.155	-59.80	49						
				1007	49	2015	951	[illegible]	[illegible]
22	.657	252.21	3995.						
23	1.690	655.05	7105.						
24	.729	280.45	4204.						
				1008	1092	7107	3012	[illegible]	[illegible]
25	.016	33.68	-96223.						
26	.131	50.20	-96095.						
27	-.212	-25328.36	-292636.						
				1009	-333405.	-55454	[illegible]	[illegible]	[illegible]
28	2.013	769.37	7924						
29	1.738	667.87	6879						
30	.569	-58250.08	-599976						
31	.869	330.30	3402.						
32	1.827	705.60	7268						
33	.424	932.71	9607						
34	.000	.00							
35	1.541	592.87	6107.						
36	1.622	621.41	6400.						
37	.000	.00	.						
38	.158	635.33	6544						
39	.001	380.52	3919						
40	-7.069	36053.05	417913						
41	1.864	722.54	144300.						
42	.806	310.57	141110.						
				1014	66025	472998	[illegible]	[illegible]	[illegible]
43	2.040	790.21	8139						
44	1.699	656.97	6767						
45	.000	.00							
46	2.015	844.78	8701						
47	.732	282.38	2909						
48	.450	-1606718.	-1654920						
49	.811	312.48	3219.						
50	.000	.00							
51	1.659	643.27	6626						

Figure 3.6. (concluded).

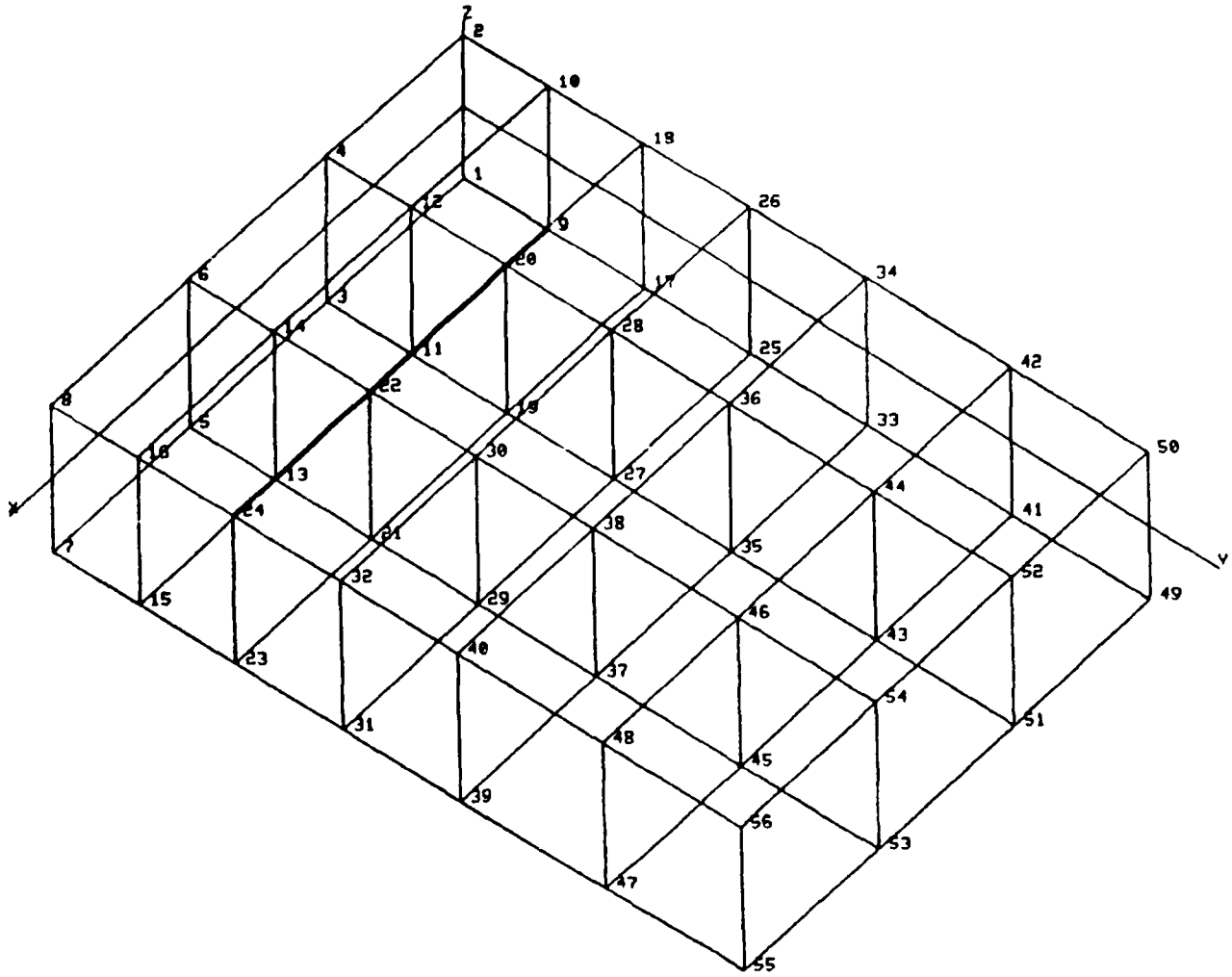

Figure 3.7a. Specimen 2 Finite Element Model - Node Numbers.

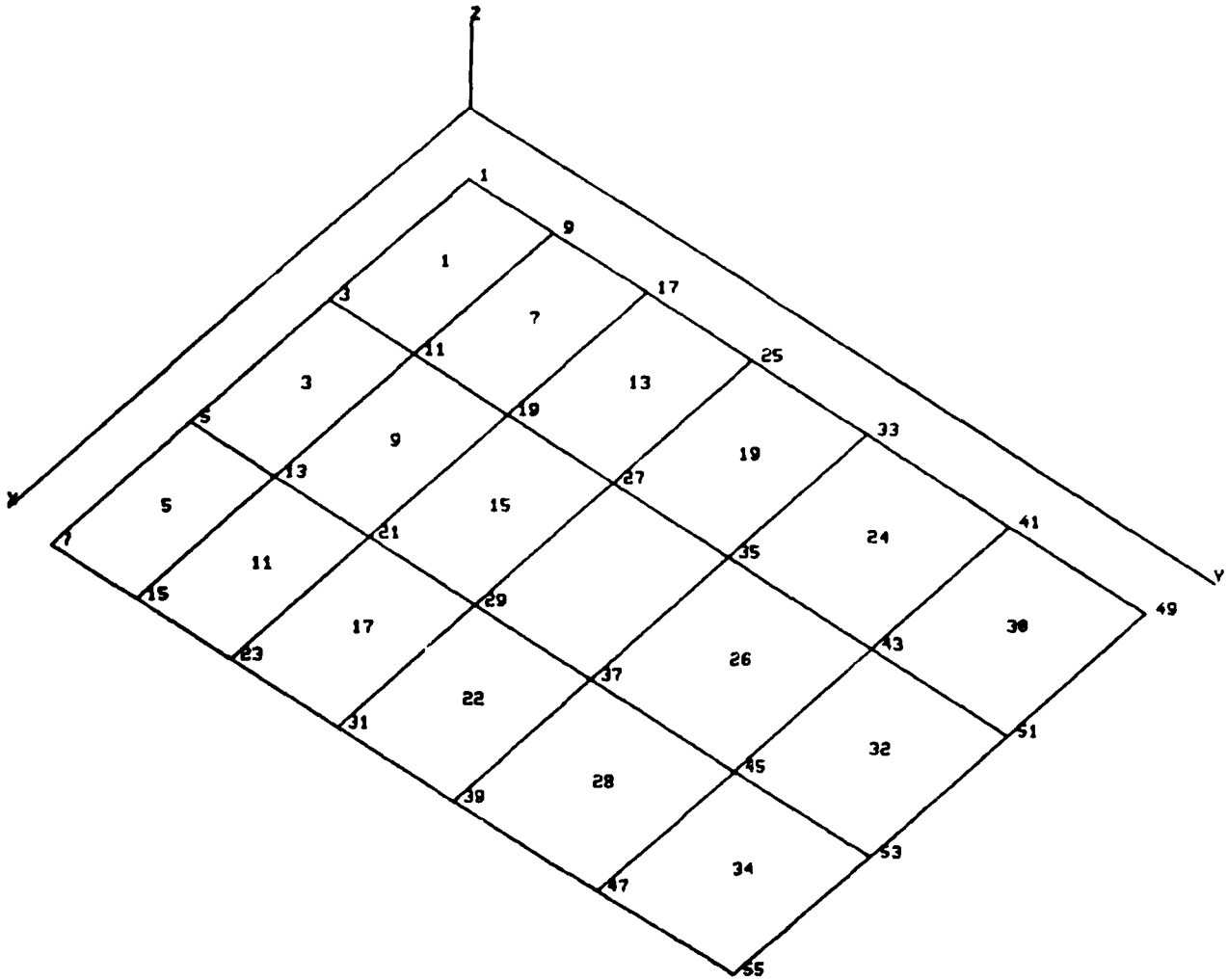

Figure 3.7b. Specimen 2 Finite Element Model - Lower Skin Membrane Elements.

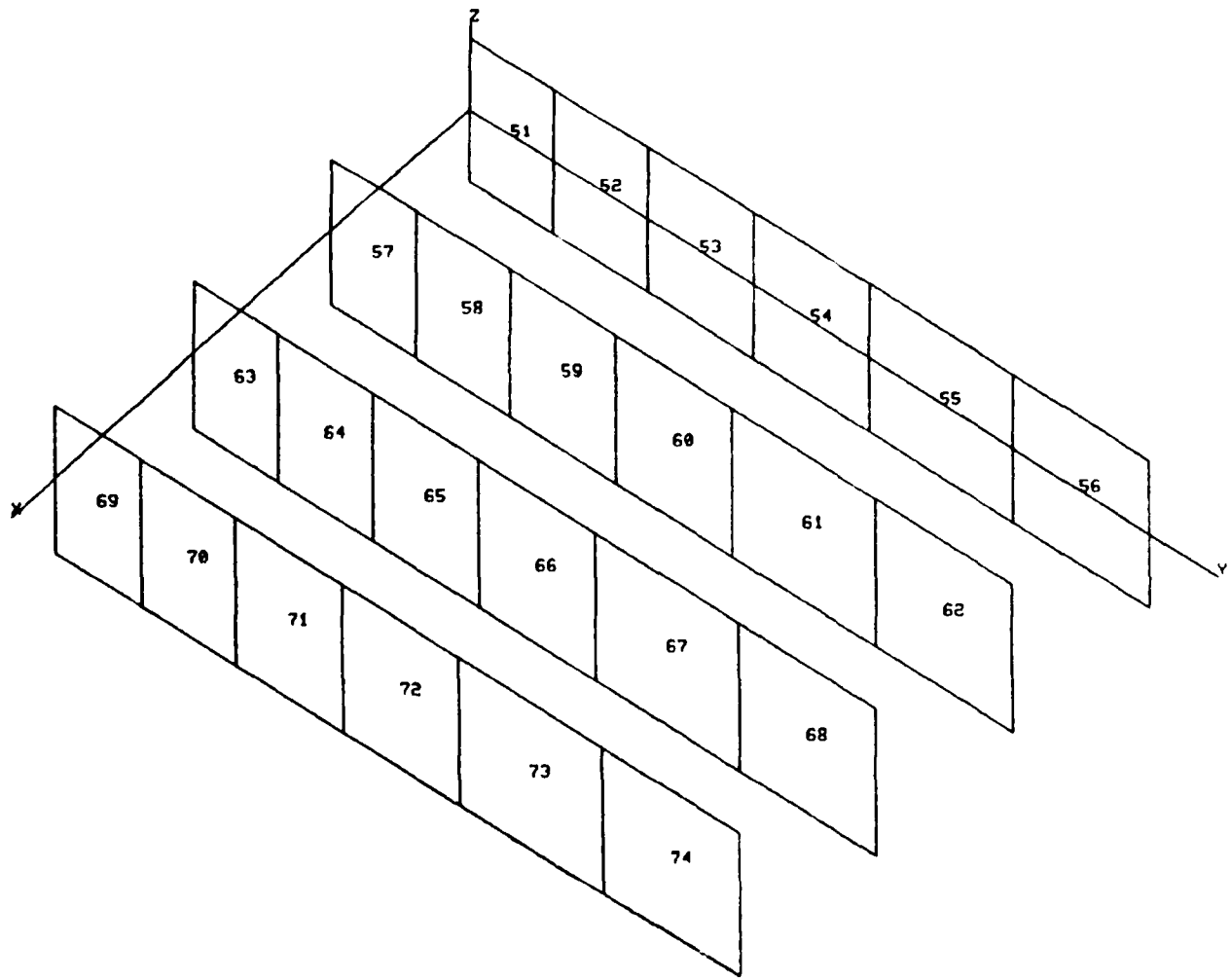

Figure 3.7c. Specimen 2 Finite Element Model - Spar Shear Panel Elements.

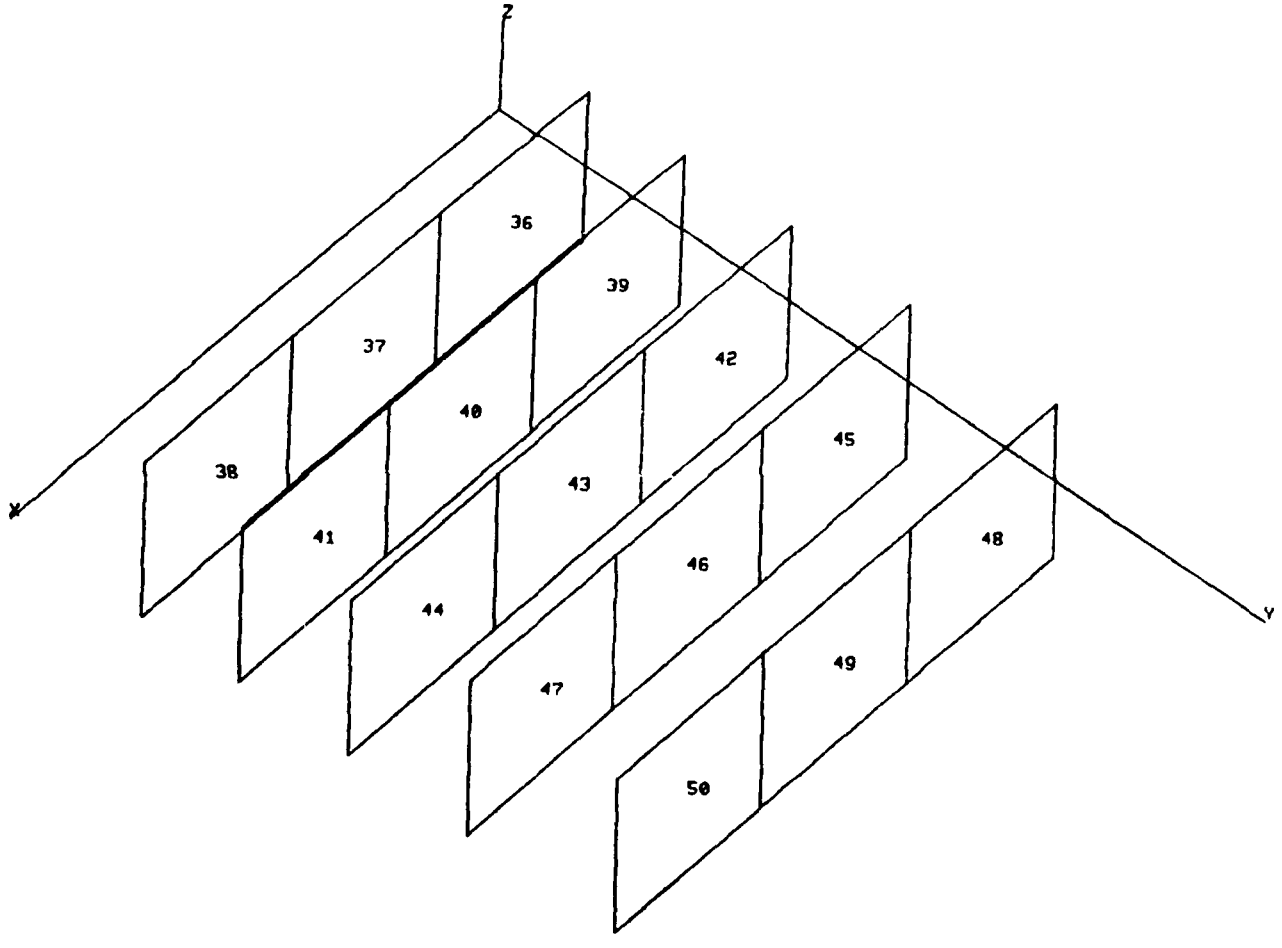

Figure 3.7d. Specimen 2 Finite Element Model - Rib Shear Panel Elements.

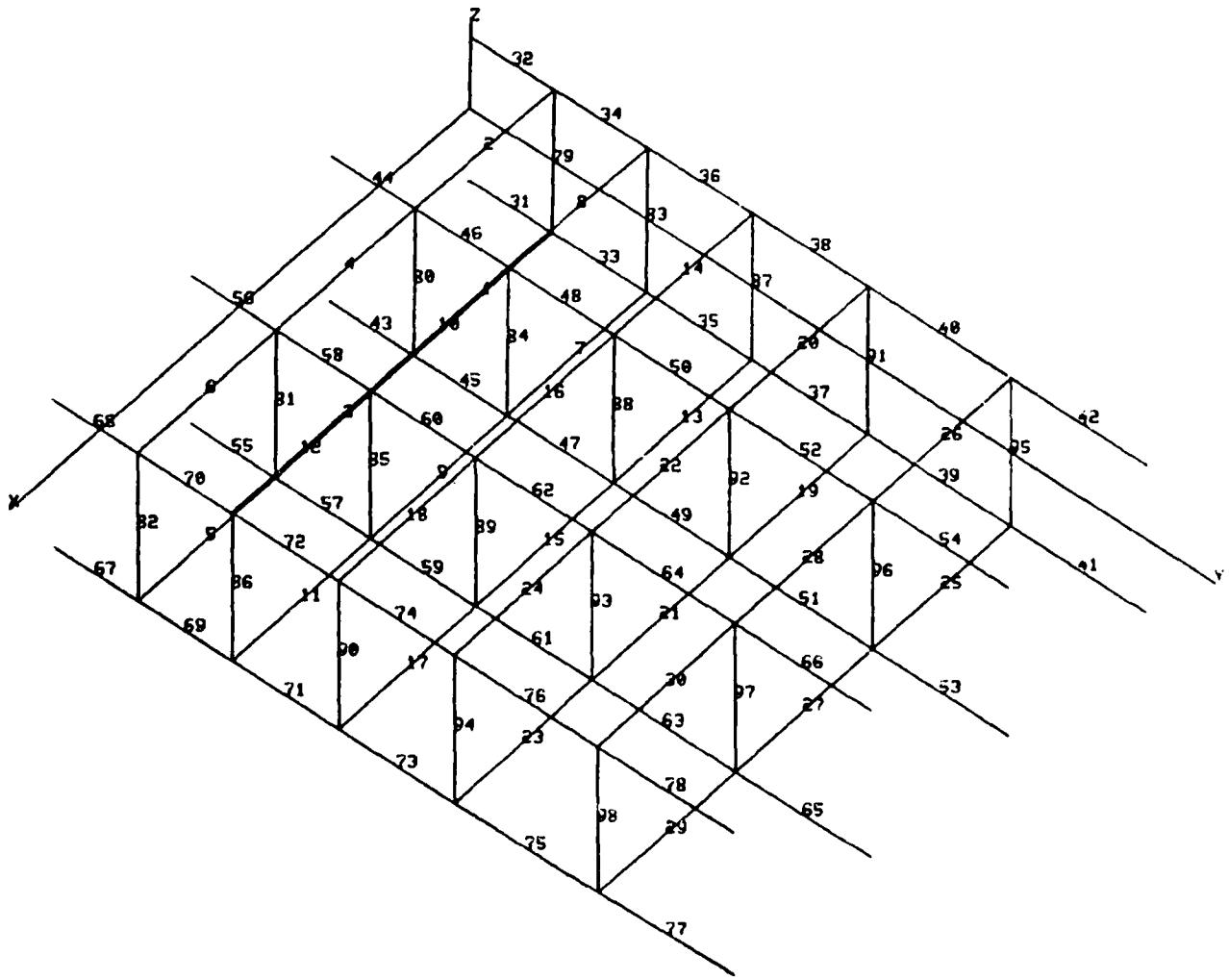

Figure 3.7e. Specimen 2 Finite Element Model - Cap Bar Elements.

the three coordinate axes. Eight of the nodes are clamped at the reaction end of the specimen. Therefore, the analysis model has 3 x 48 = 144 degrees of freedom.

3.3.5 Test/Analysis Results

The replica specimen number 2 had minimal damage, with a single skin panel missing on the lower skin and no other structural damage present. This small amount of damage was not expected to cause the response of the specimen to deviate much from that which would be predicted with a mathematical model based on the use of membranes, shear panels, and bars for the skins, webs, and caps, respectively. Comparison of the experimental and analytical results showed the expectation to be true. As an example, Figure 3.8 shows the experimentally and analytically obtained maximum principal stress for rosette number 8 (Figure 3.5) and finite element number 19 (Figure 3.7b). It can be seen that the analytical prediction is quite close to the experimental result.

The loads applied to the specimen were incremented to 85 percent of the maximum loads indicated in Paragraph 3.3.2. The test was terminated at this stage because of excessive local deformation of the specimen at the points of attachment to the reaction structure and to the loading frame. The response in the middle of the specimen remained quite linear, however, as seen in Figure 3.8.

3.4 TEST 3 - DAMAGED SPECIMEN, NUMBER 3

Specimen Number 3 (Paragraph 2.3) had more extensive damage than Specimen Number 2. Figure 3.9 shows a schematic representation of the damage which extends the entire depth of the specimen. Missing are skin panels on the upper and lower surfaces, the center two spar shear webs, and the upper and lower spar caps. A combination of spanwise bending moment and spanwise shear loads were applied to the specimen. The following paragraphs describe Test 3 in more detail.

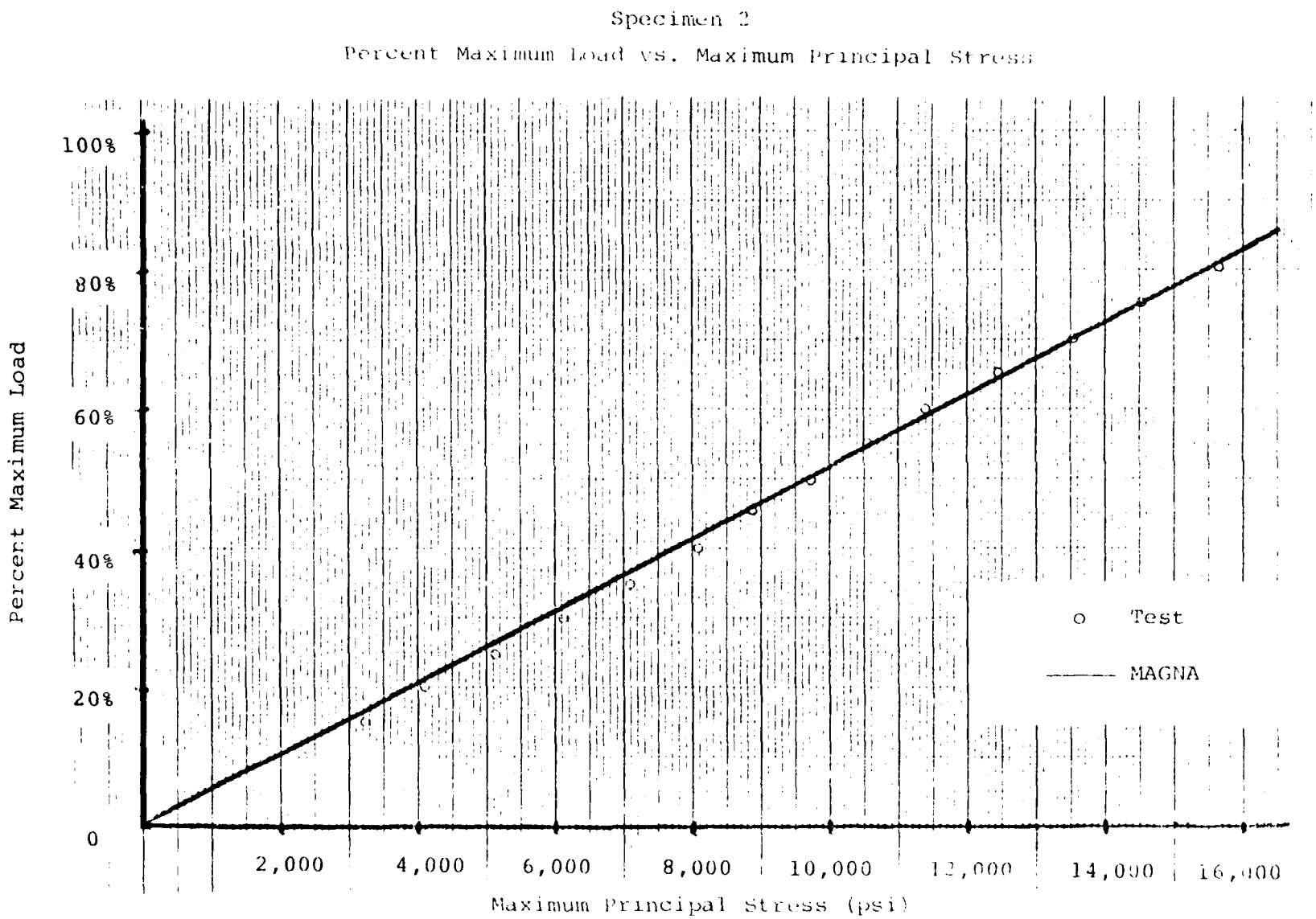

Figure 3.8. Comparison of Experimental/Analytical Results for Test 2.

3.4.1 Instrumentation

Figure 3.9 indicates the relative locations of strain gages monitored during Test 3. Both rosettes and individual gages are numbered.

3.4.2 Loading

The maximum load applied to the specimen was a combination of spanwise bending moment, $\bar{M}_s = 5.4 \times 10^6$ in. lb., and spanwise shear load, $\bar{V}_s = 30{,}000$ lb. The individual actuator forces corresponding to these section loads were (from Equations 3.2):

$T_1 = 45{,}573$ lb. Compression

$T_2 = 49{,}344$ lb. Compression

$T_3 = 25{,}497$ lb. Tension

$T_4 = 29{,}426$ lb. Tension

3.4.3 Load Incrementation and Data Collection

During the test the individual actuator forces were increased incrementally in steps equal to 5 percent of the maximum values given above. At each stage of the loading, strain gage readings were recorded by a minicomputer. A computer program coverted the gage signals into units of strain, and computed the associated material stresses. In the case of the rosettes, the minimum and maximum principal stresses, the maximum shear stress, and principal angle, and the Von Mises equivalent stress were computed. An example of the output of the data reduction program for Test 3 is shown in Figure 3.10. The output shown corresponds to 60 percent of the maximum loads defined above.

3.4.4 Analysis Model

The finite element model for specimen No. 3 is shown in Figure 3.11a-e. The modeled portion of the replica specimen is that part of Figure 2.12 which has the

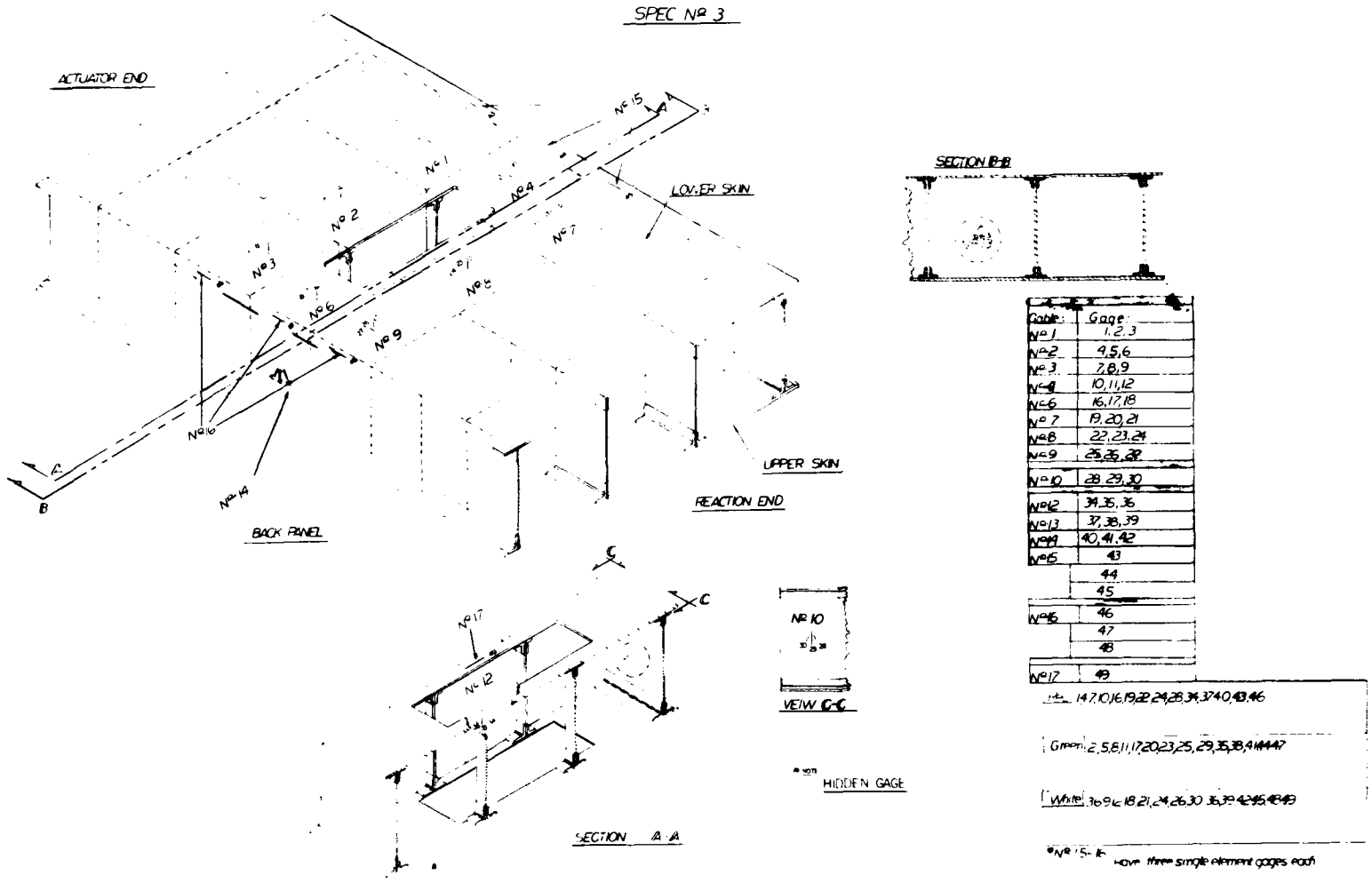

Figure 3.9. Strain Gage Locations - Specimen 3.

SPECIMEN #6, TEST #3 4/11/80 9 45 50 READING 9

E= 10 300 MU= 330

BASIC CHANNELS

CH	---MV---	-VALUE--	
1	-1568 000	-15 644	P1
2	-1463 000	-14 629	P2
3	393 500	3 939	P3
4	851 875	8 516	P4
5	23 875	241	P5
6	-5988 125	60 241	%1
7	-1489 375	-1262 170	MP
8	137 000	1 370	D1
9	134 687	1 347	D2
10	152 712	1 527	D3

DEFLECTION CHANNELS

	WEST SIDE	MIDDLE	EAST SIDE
DEFLECTION			
ANGLE (DEG)	6169	0000	.0000
TOP DEF	- 5409		.0000
BOT DEF.	.1536		.0000
BASE EFLECTION			
ANGLE (DEG)	.3811	3595	.3380
TOP DEF.	- 4219		-.3747
BOT DEF.	0071		-.0024
UNCORRECTED DEFLECTIONS			
D1 (2 12)	.1207		.0975
D2 (12 50)	.1787		2479
D3 (37 25)	.5156		.5513
D4 (54 37)	7569		7766
D5 (87 37)	1 3469		1 3700
D6 (93 25)		1 5271	
CORRECTED DEFLECTIONS			
D1 (2 12)	0767		0584
D2 (12 50)	.0189		.0892
D3 (37 25)	.1929		.2431
D4 (54 37)	.3194		.3717
D5 (87 37)	6899		7704
D6 (93 25)		.8604	

Figure 3.10. Sample Experimental Data - Specimen 3.

STRAIN GAGE DATA				PRINCIPAL STRESS CALCULATIONS					
CH	MV(CORR)	USTRAIN	-STRESS- (PSI)	POS-ETTE	MIN PR STRESS	MAX PR STRESS	MAX SHEAR	ANGLE	EQUIV STRESS
1	1.585	306.89	4316						
2	4.543	878.58	8744						
3	1.042	201.58	3501						
				1001	-944	8761	4852	42.59	9269
4	.162	31.24	735						
5	.760	147.00	1631						
6	.506	97.89	1251.						
				1002	304	1681	689	56.01	1552
7	1.051	203.45	3500						
8	4.436	857.89	8569						
9	1.559	301.05	4256						
				1003	-828	8583.	4705	47.30	9026
10	2.232	430.96	6902.						
11	5.601	1083.29	11853						
12	2.468	477.20	7160						
				1004	2104.	11857.	4876.	46.05	10957.
13	2.081	402.99	6337						
14	5.283	1021.93	11130						
15	2.280	440.11	6624						
				1005	1829	11132.	4652.	45.89	10340
16	1.205	233.12	4415						
17	5.679	1094.67	11087						
18	2.330	450.94	6101						
				1006	-631	11147.	5889	49.12	11476.
19	.220	42.55	731						
20	.815	157.83	1624						
21	.325	62.82	888						
				1007	-8	1628	818	47.75	1632
22	.000	.00							
23	-1.812	-344.41	-3547						
24	-3.668	-696.39	-7173						
25	-4.053	-770.42	-7935						
26	-4.494	-854.67	-8803						
27	-19.648	-926261	1-9540483						
28	2.386	460.43	6103						
29	5.170	999.41	10276						
30	1.059	204.55	4121						
				1010	-147	10371	5259	39.57	10445

Figure 3.10. (continued)

31	2.095	404.72	3204						
32	281	54.14	499						
33	-2.000	-386.37	-2922						
				1011	-2942.	3224	3083.	3.24	5342.
34	.046	9.90	217						
35	.132	25.53	345						
36	.155	29.85	379						
				1012	204	392	94.	74.78	339.
37	.164	31.62	353						
38	.236	45.54	461						
39	-.017	-3.20	84						
				1013	-59	496.	278.	30.47	528.
40	-1.610	-310.82	-2393						
41	.108	21.09	172						
42	1.620	313.16	2434						
				1014	-2403.	2439	2421.	88.17	4193.
43	3.359	646.16	9986						
44	3.815	736.51	10686						
45	3.415	659.95	10093.						
				1015	9391	10688.	648.	47.36	10102.
46	1.242	240.02	3869						
47	.731	141.17	3103						
48	1.486	286.92	4232.						
				1016	3086.	5015.	964.	129.57	4381.
49	.000	.00							
50	.000	.00							
51	.000	.00							
52	-4.322	-835.23	-11041						
53	-6.513	-1259.47	-14326						
54	-1.880	-363.50	-7388						
				1018	-14643.	-3786.	5429.	125.17	13165.
55	.115	22.25	158						
56	-.207	-40.09	-325						
57	-.135	-25.98	-215.						
				1019	-379.	321	350.	-28.88	607.
58	-1.529	-295.62	-5966						
59	-5.760	-1111.35	-12284						
60	-3.460	-668.33	-8853.						
				1020	-12493.	-2326.	5083.	-36.75	11507.

Figure 3.10. (continued).

61	-4.525	-860.02	-8858.						
62	.000	.00	.						
63	-4.079	-774.42	-7977.						
64	-3.584	-681.36	-7018.						
65	.000	.00	.						
66	3.440	657.78	6775.						
67	.357	69.04	1545.						
68	1.101	211.79	2651.						
69	1.027	195.88	2527.						
				1023	1250	2823	787.	64.32	2450
70	.000	.00							
71	3.872	735.67	7577.						
72	4.285	811.95	8363.						
73	4.104	783.69	8072.						
74	.000	.00	.						
75	.000	.00	.						
76	2.368	457.86	6843.						
77	-.579	-111.98	2430.						
78	4.907	950.89	10662.						
				2026	1889	11402	4756	46.19	10584
79	3.635	690.17	7109.						
80	4.070	771.52	7947.						
81	4.498	855.08	8807.						
82	3.198	610.23	6285.						
83	3.801	723.05	7447.						
84	4.400	834.60	8596.						

Figure 3.10. (concluded).

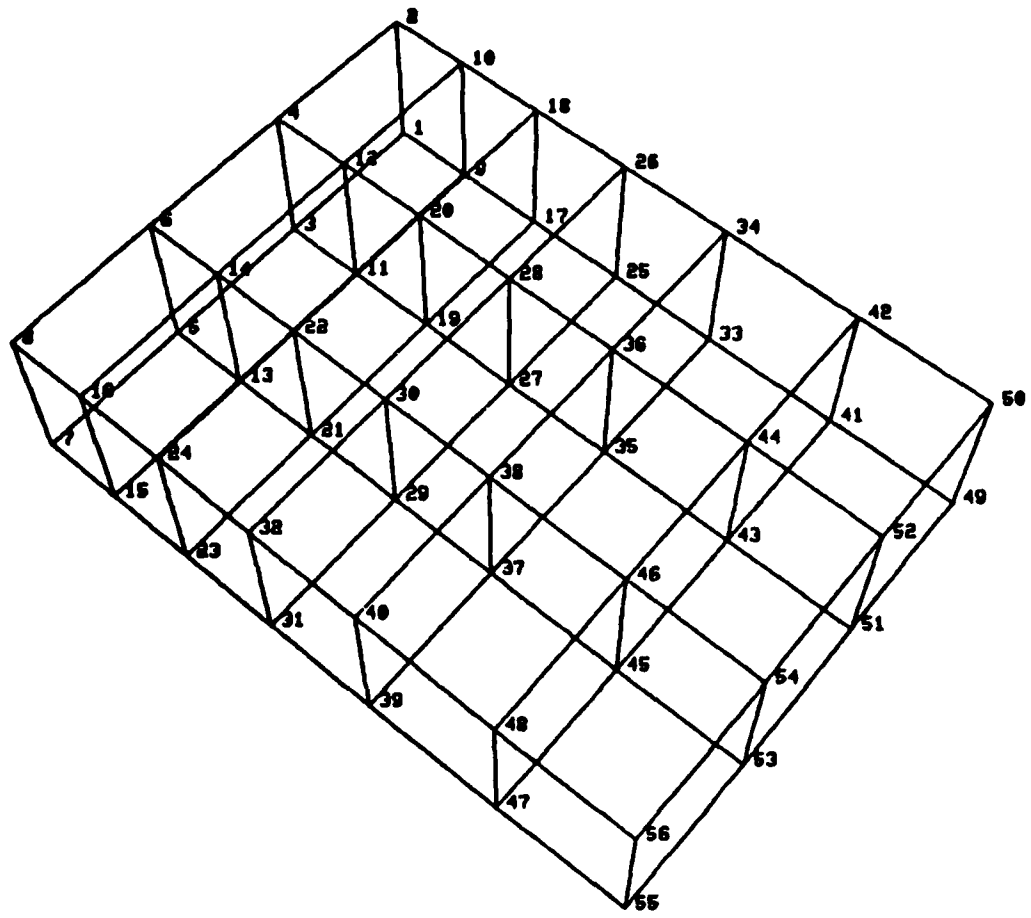

Figure 3.11a. Specimen 3 Finite Element Model - Node Numbers.

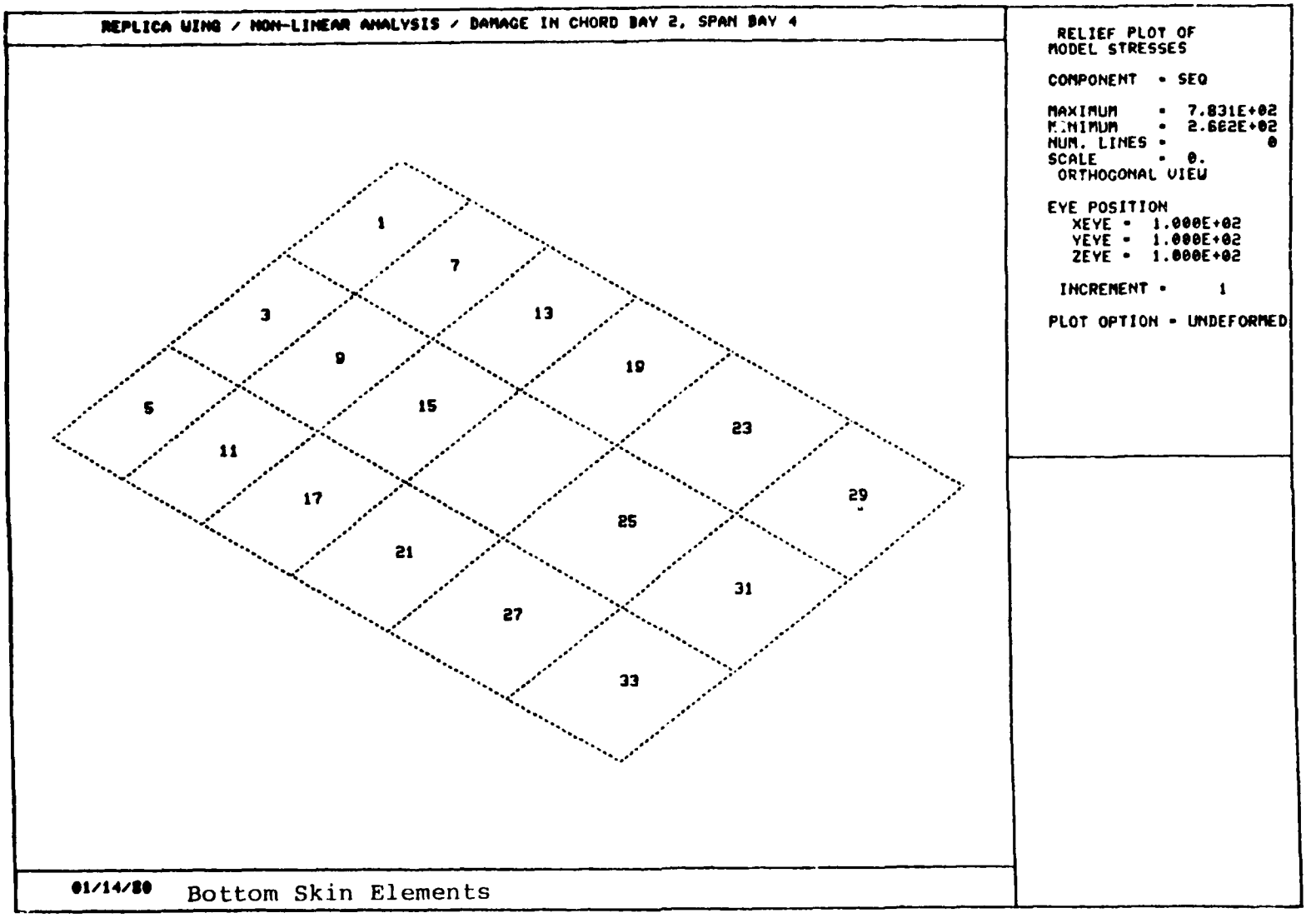

Figure 3.11b. Specimen 3 Finite Element Model - Bottom Skin Membrane Elements.

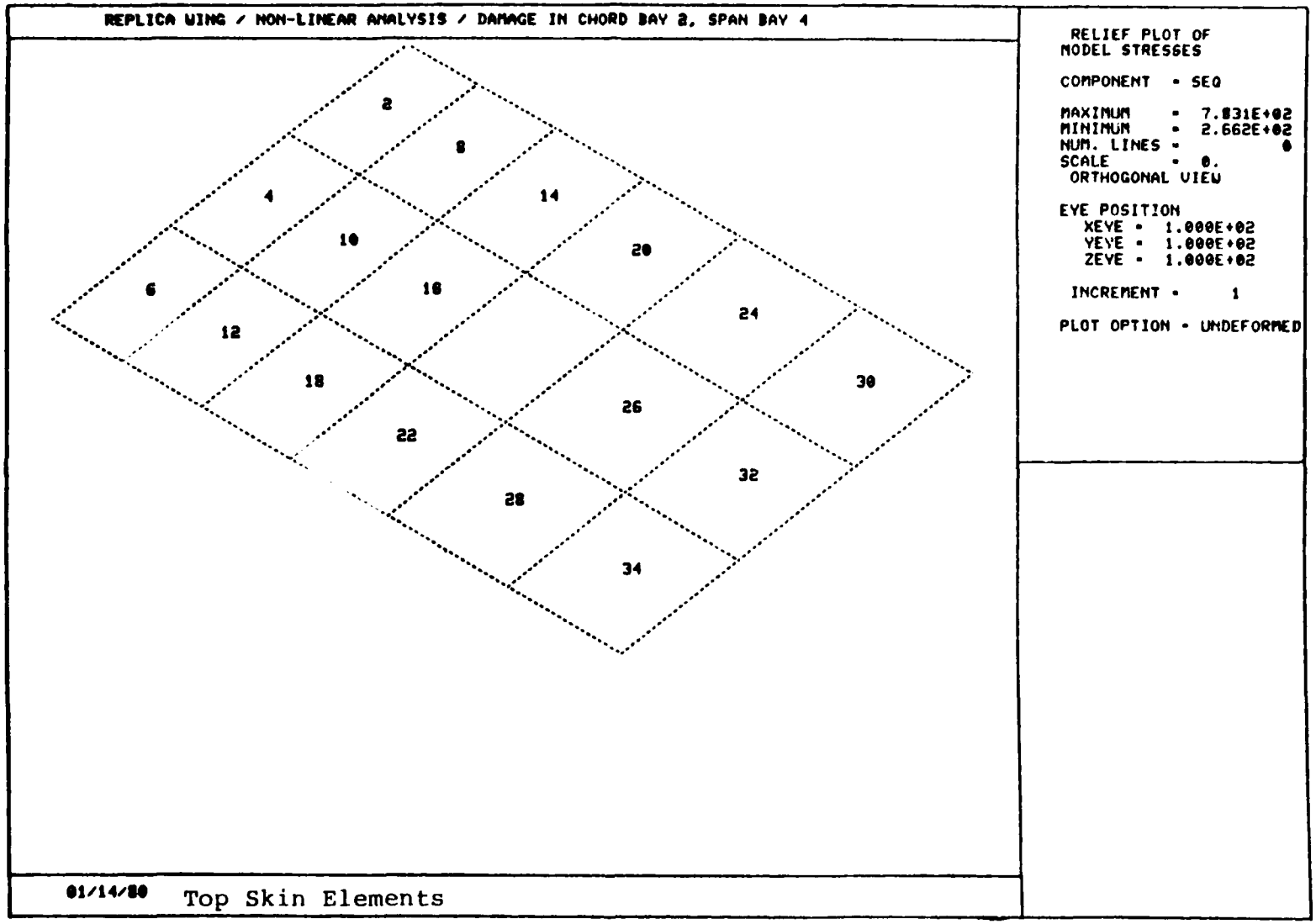

Figure 3.11c. Specimen 3 Finite Element Model - Top Skin Membrane Elements.

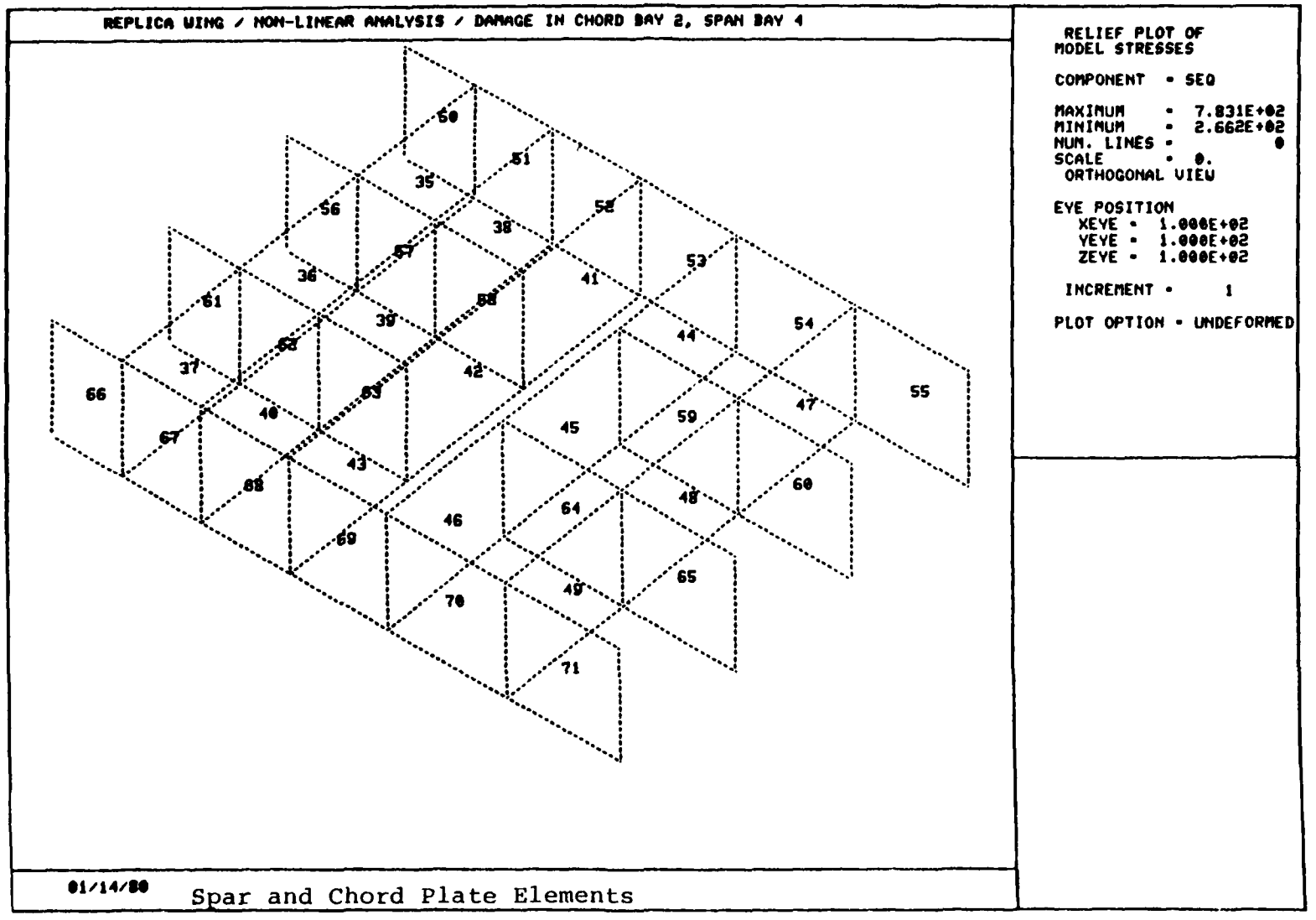

Figure 3.11d. Specimen 3 Finite Element Model - Spar and Rib Shear Panel Elements.

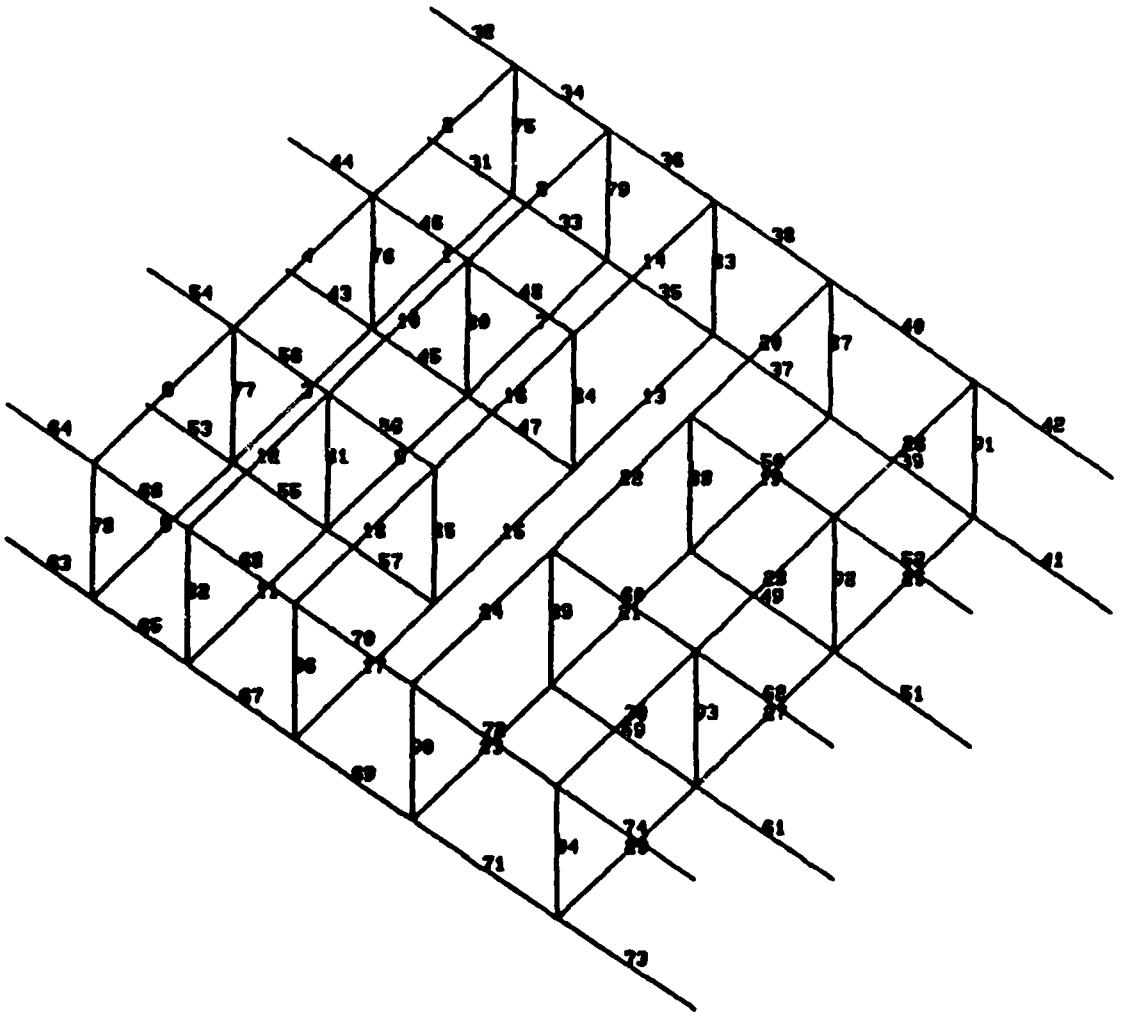

Figure 3.11e. Specimen 3 Finite Element Model - Cap Bar Elements.

bays numbered. As mentioned before, in the experimental facility, the two end bays are clamped by mounting brackets, and are therefore not considered in the analysis. The model contains 56 nodes, 34 skin membrane elements, 22 spar web shear panel elements, 15 rib web shear panel elements, 44 spar cap bar elemtns, and 30 rib cap bar elements. Each of the 56 nodes has three degrees of freedom, the displacements parallel to the three coordinate axes. Eight of the nodes are fixed at the reaction end of the specimen (Nodes 1 - 8). Therefore, the analysis model has 3 x 48 = 144 degrees of freedom.

3.4.5 Test/Analysis Results

When the console operator began the test on Specimen 3, a malfunction of one of the control systems caused one of the hydraulic actuators to overload. The result of the malfunction and overload was that Specimen 3 was damaged beyond use with no experimental data being collected. The spare specimen number 6 (Table 2.1) was then altered according to the damage of Specimen 3, and the control system was modified to prevent a reoccurrence of the malfunction. The modified specimen 6 is referred to hereafter as Specimen 3.

Figures 3.12a-p compare experimentally obtained stresses with corresponding stresses computed analytically with the finite element program. Of the eight skin stresses shown in Figures 3.12a-h, the stresses in elements 19 and 21 (those elements adjacent to the damaged area) compared most favorably; Figures 3.13a-e give some insight into why this is so. Figures 3.13a-e are postprocessor plots which present level contours of the equivalent stresses on the lower skin superposed on the finite element model of the lower skin. In the spanwise bays on either side of the damaged bay, the stress contours undergo considerable change as the stress "goes around" the damaged area. Apparently, the "one-element-per-bay" finite element model is not sufficient in this case to predict the stress redistribution in the transition areas.

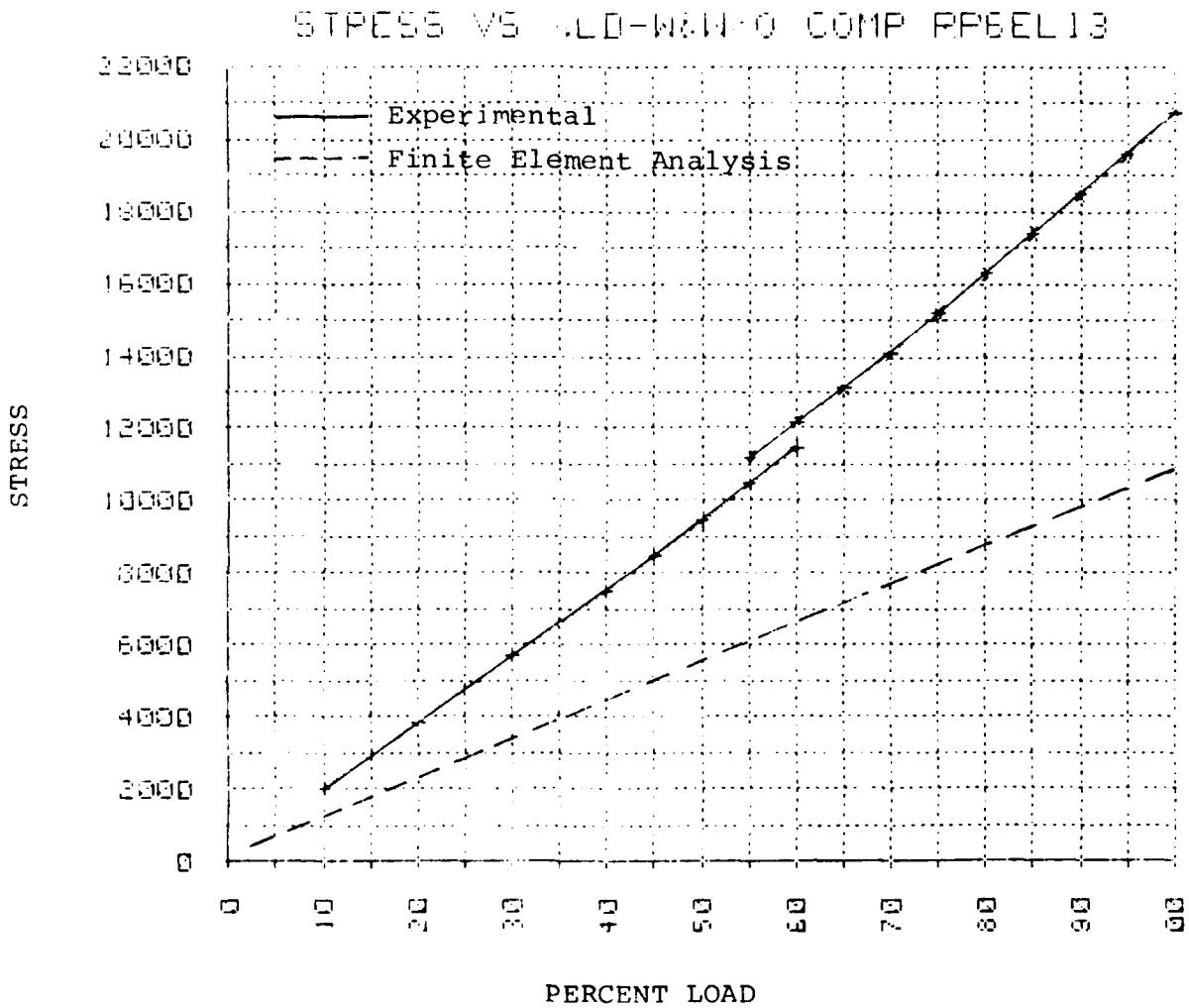

Figure 3.12a. Equivalent Stress-Skin Element 13.

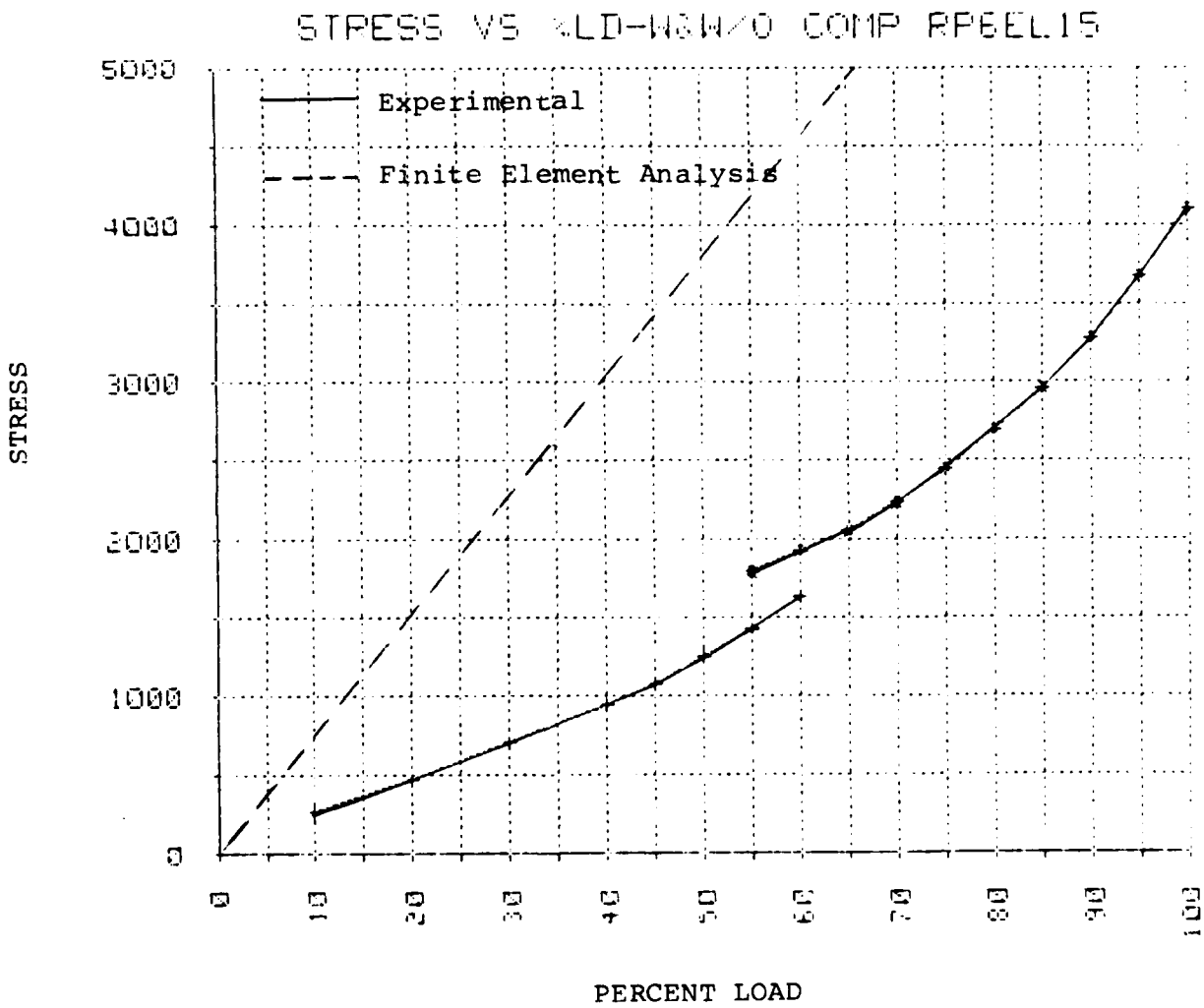

Figure 3.12b. Equivalent Stress-Skin Element 15.

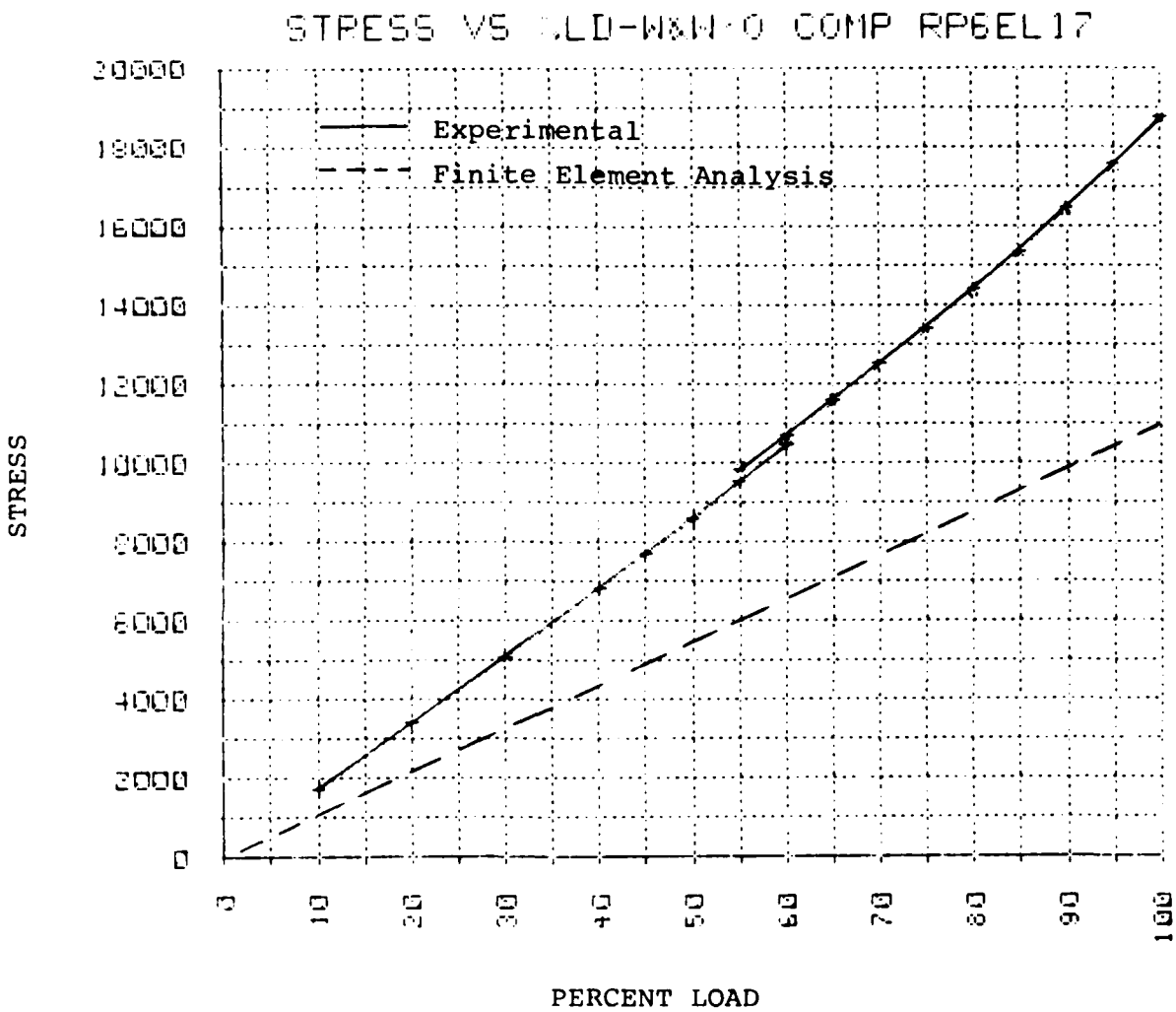

Figure 3.12c. Equivalent Stress-Skin Element 17.

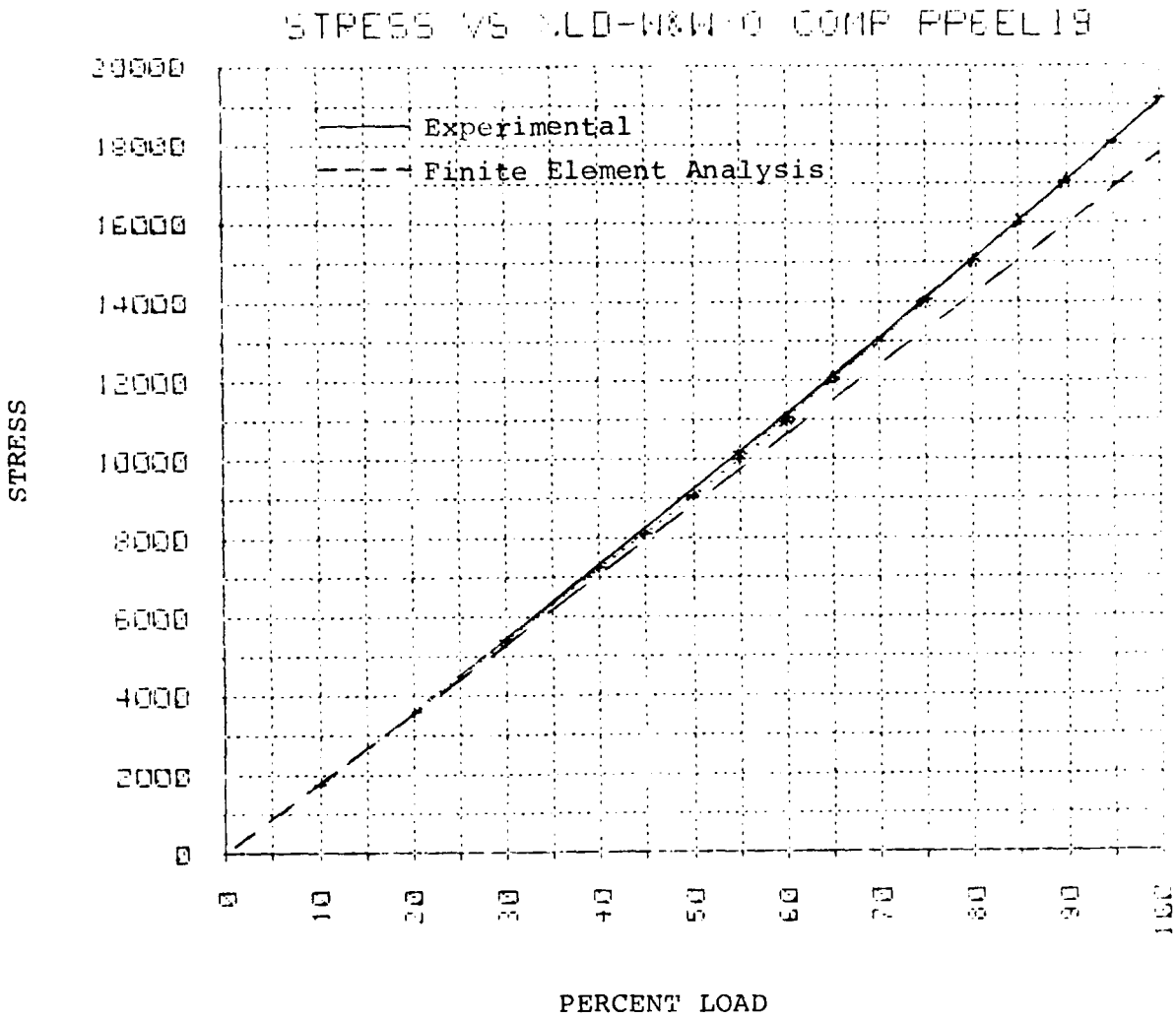

Figure 3.12d. Equivalent Stress-Skin Element 19.

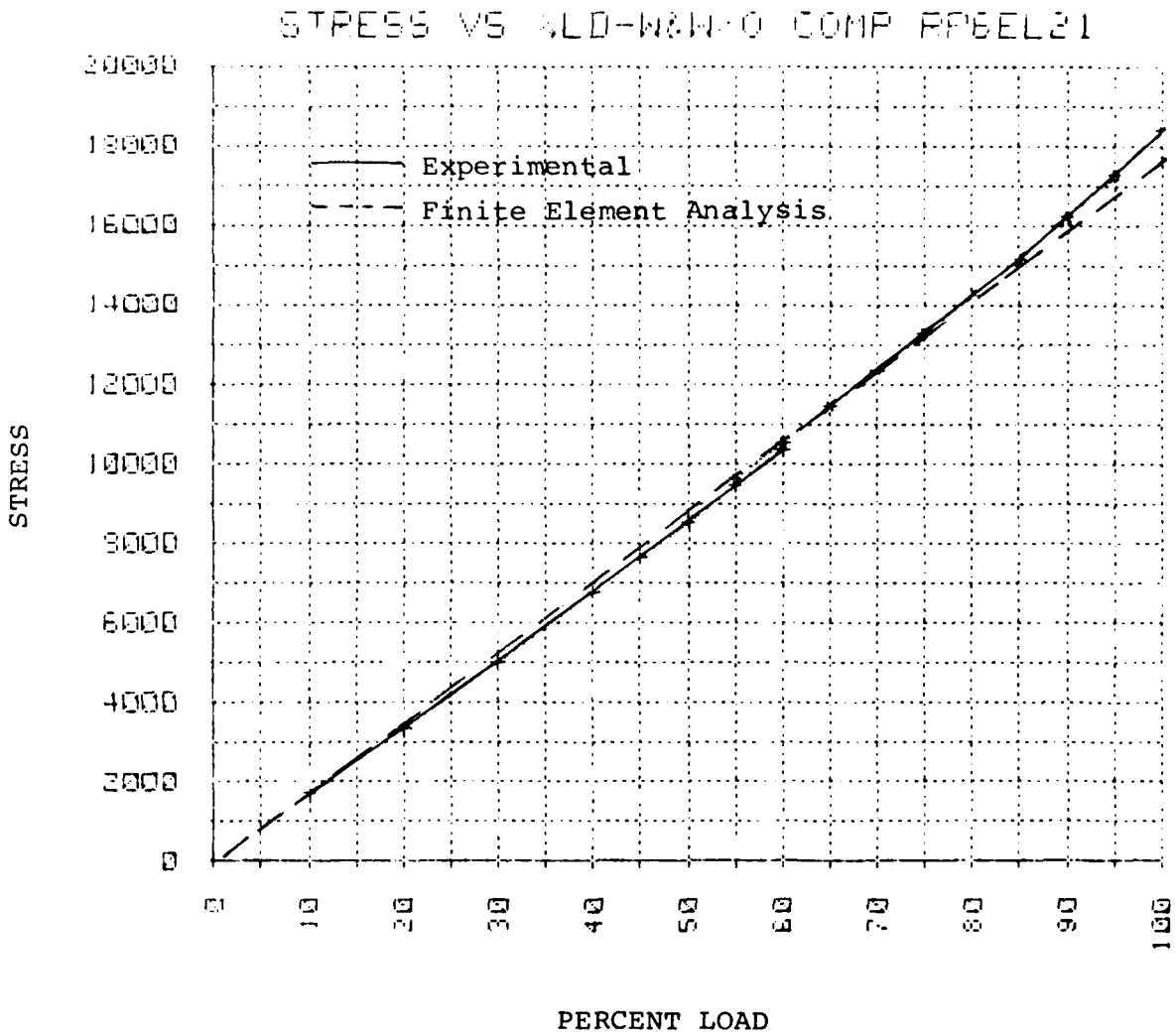

Figure 3.12e. Equivalent Stress-Skin Element 21.

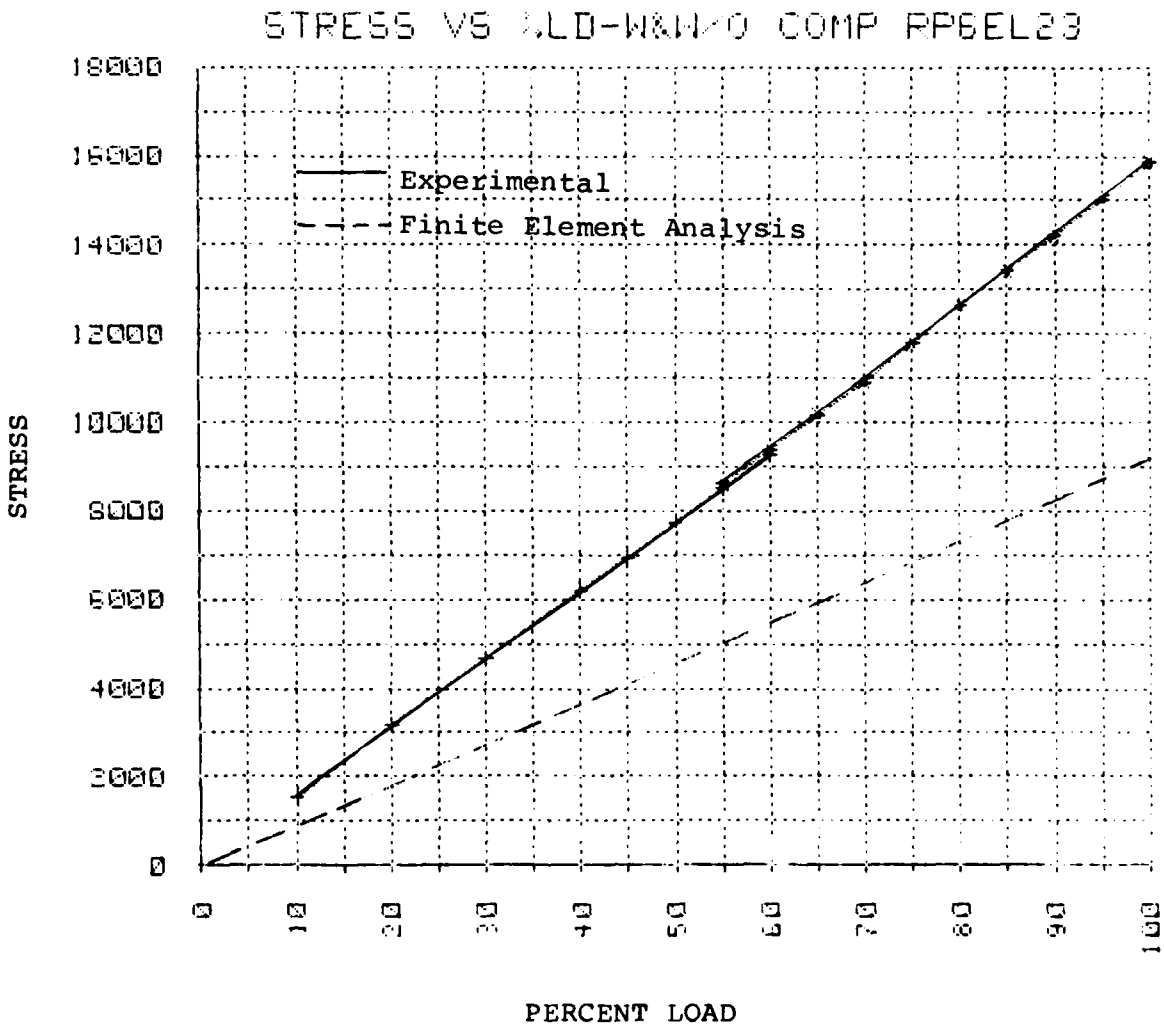

Figure 3.12f. Equivalent Stress-Skin Element 23.

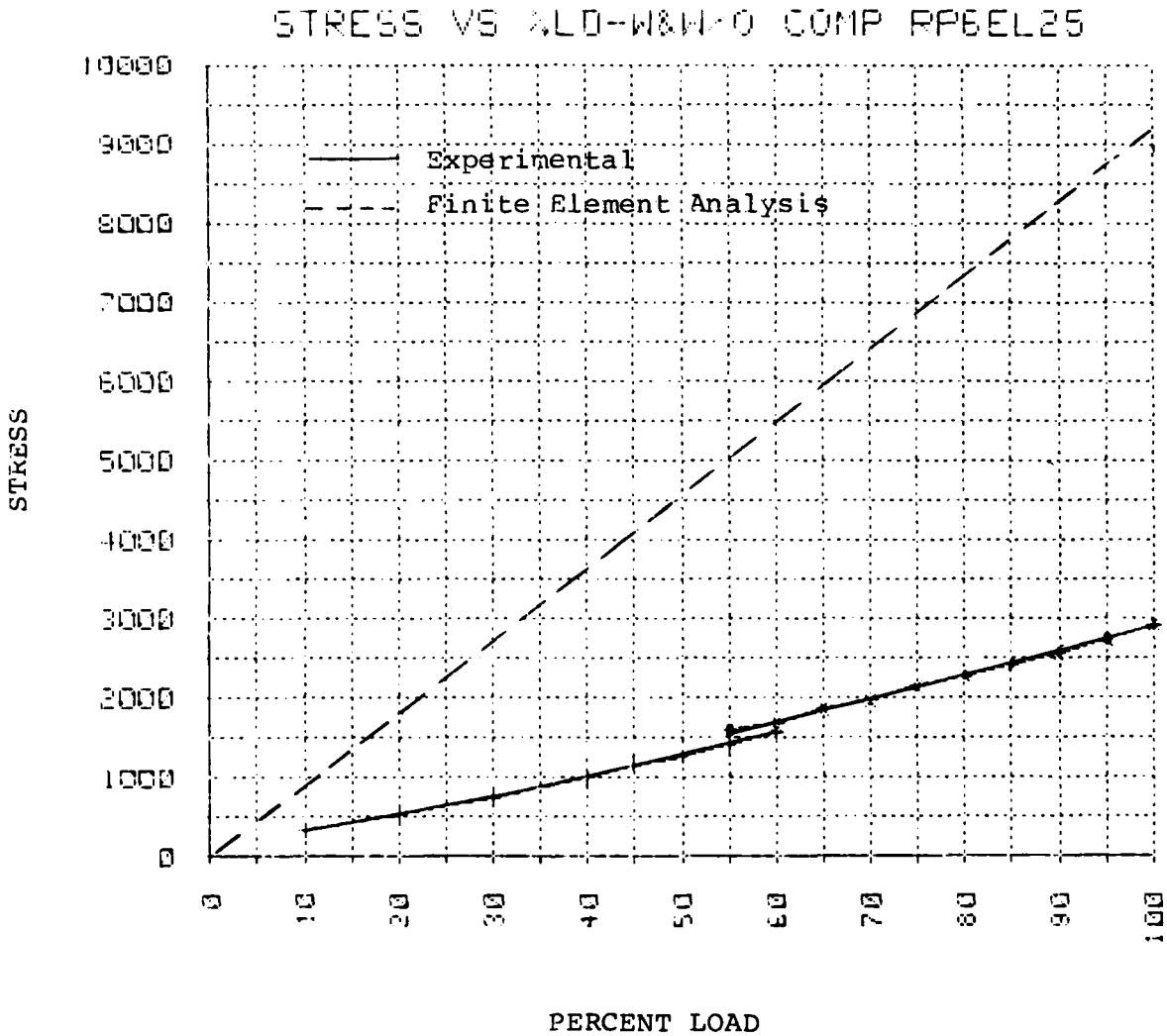

Figure 3.12g. Equivalent Stress-Skin Element 25.

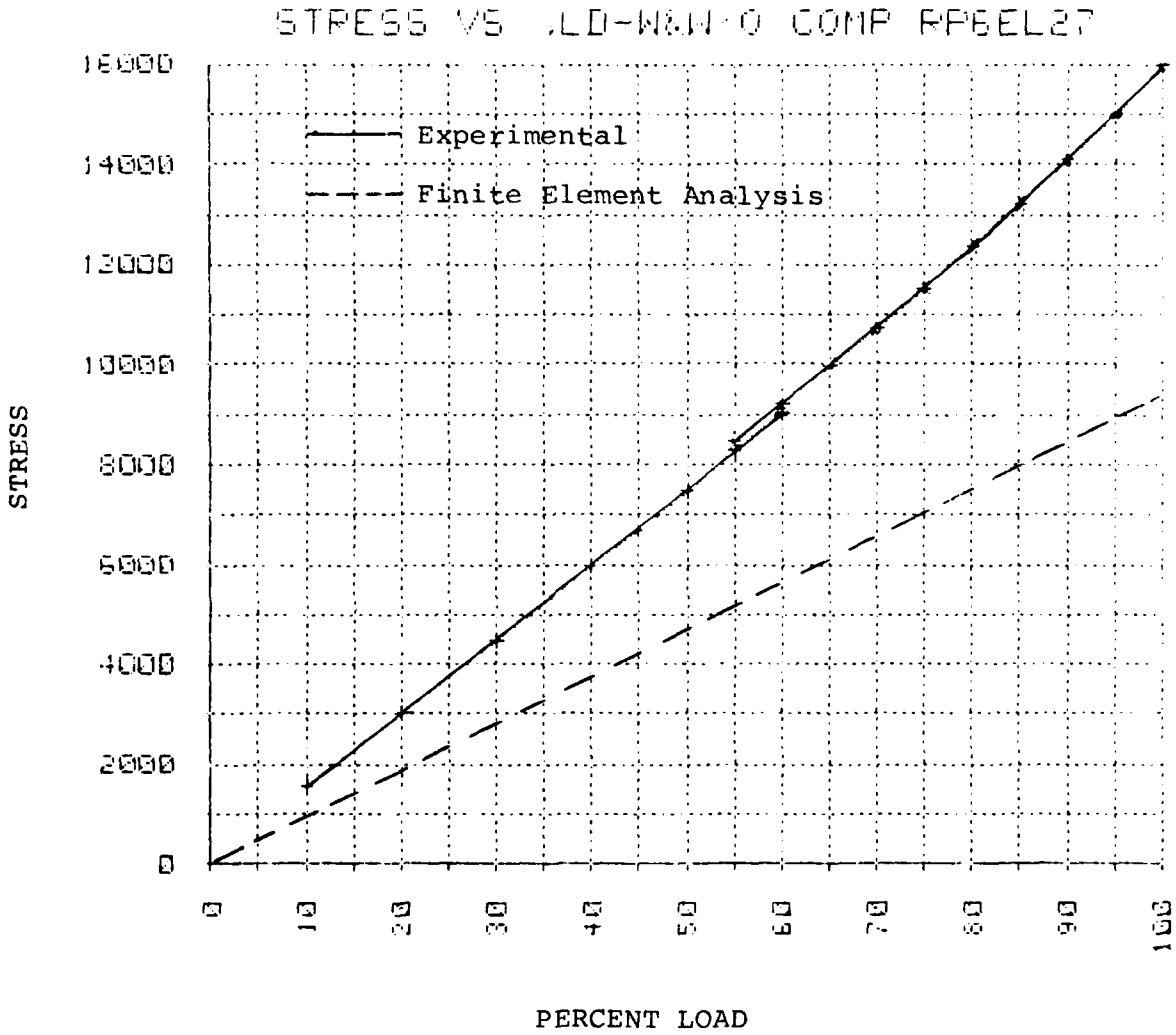

Figure 3.12h. Equivalent Stress-Skin Element 27.

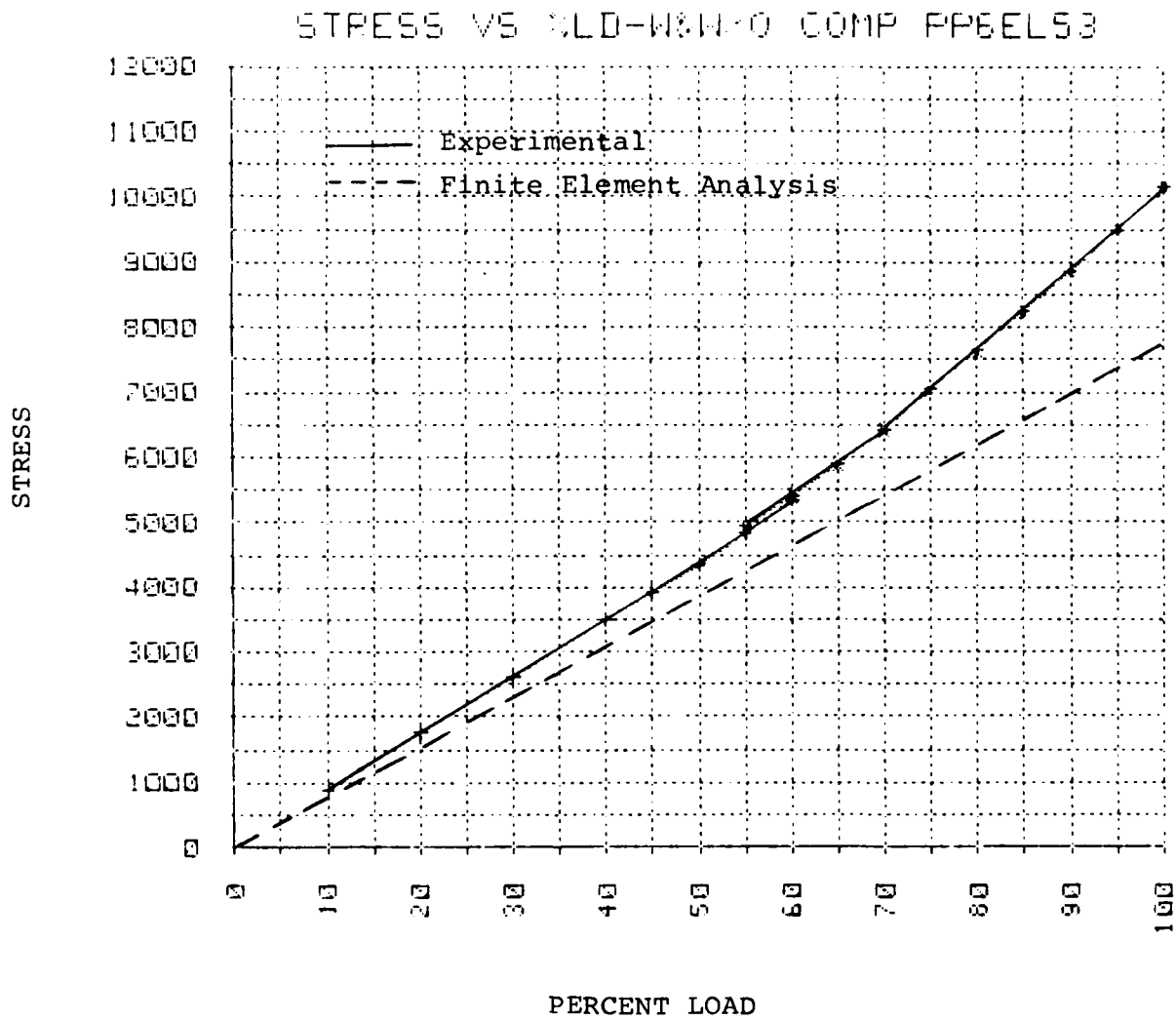

Figure 3.12i. Equivalent Stress-Spar Web Element 53.

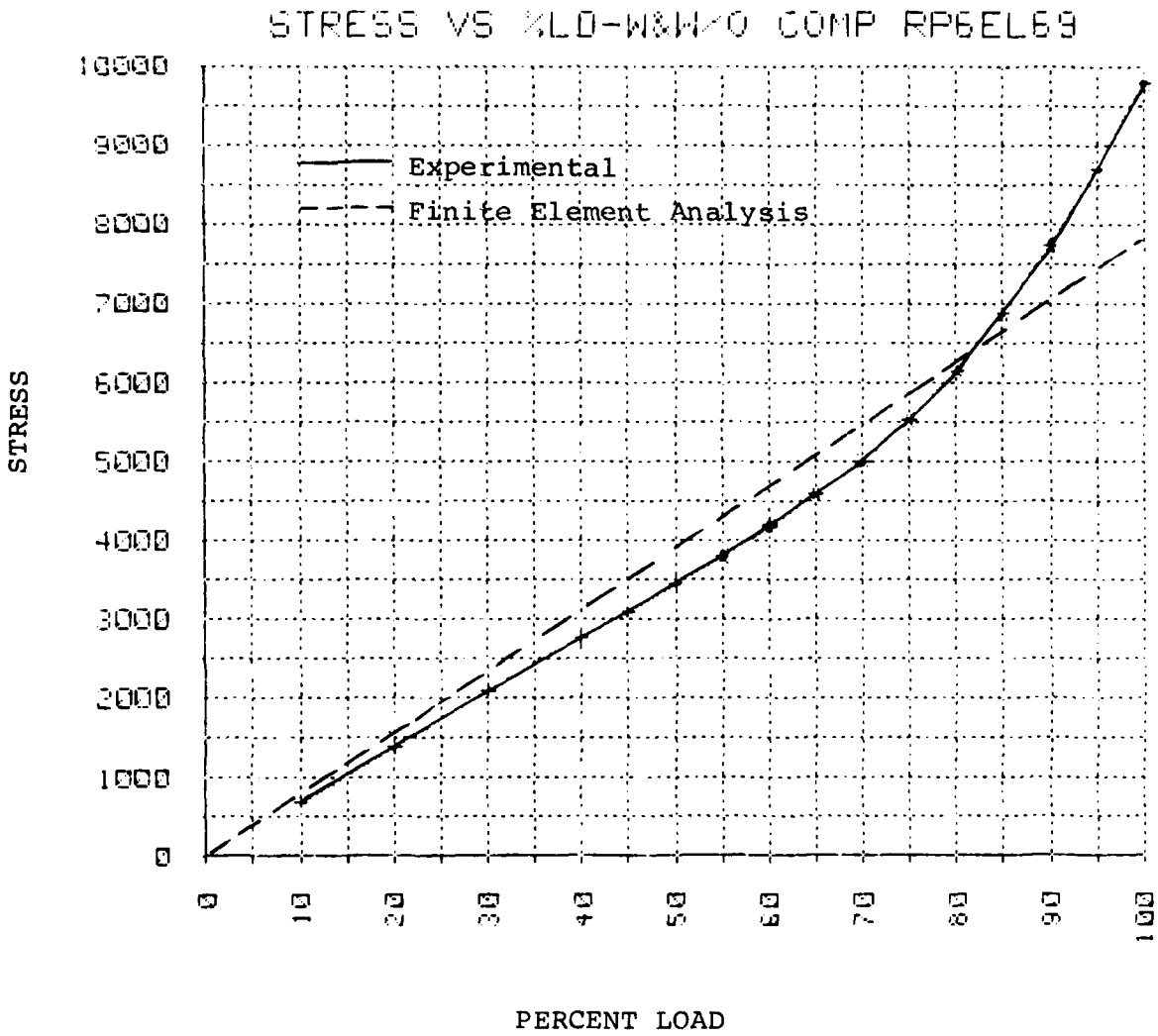

Figure 3.12j. Equivalent Stress-Spar Web Element 69.

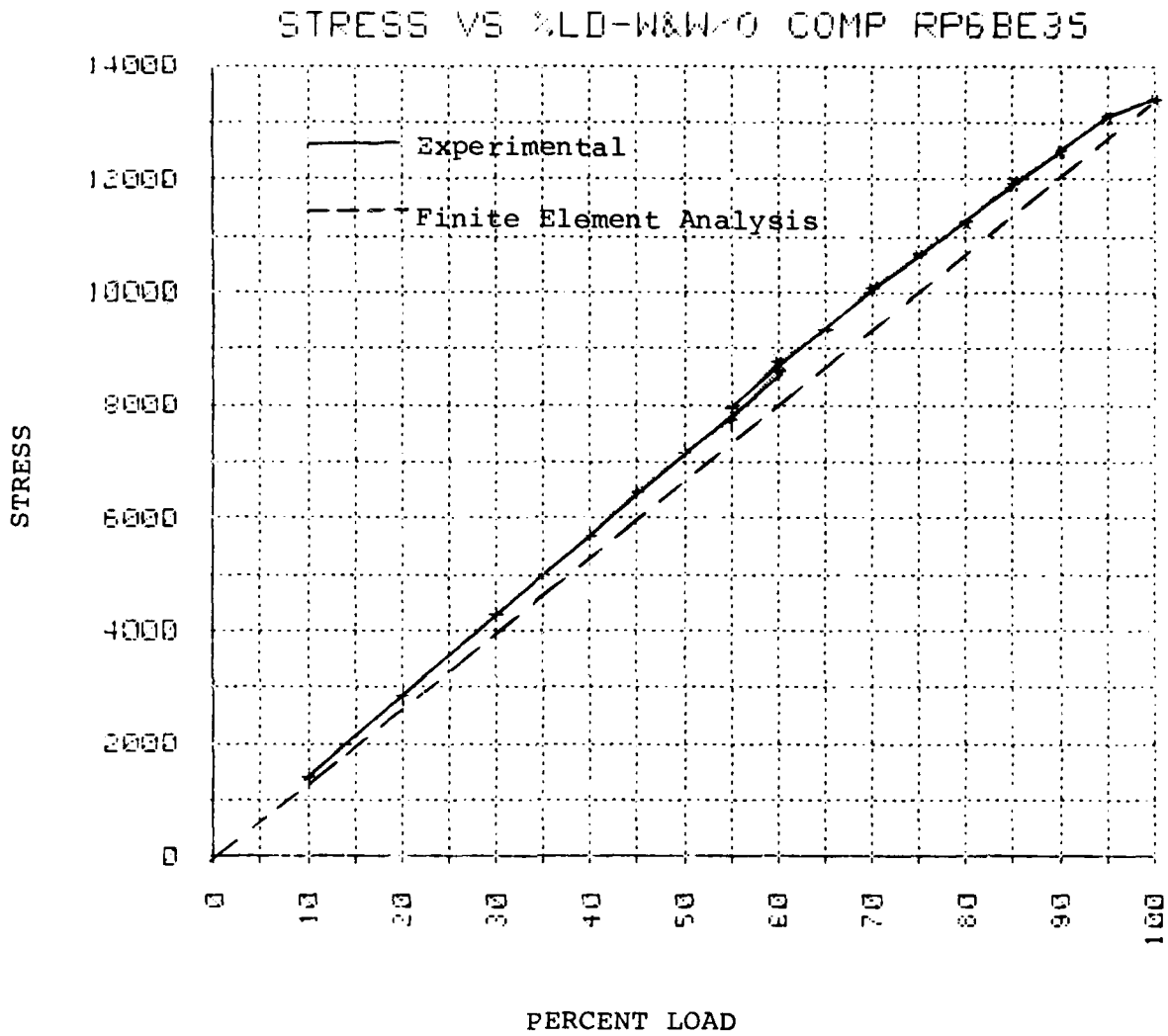

Figure 3.12k. Equivalent Stress-Spar Cap Element 35.

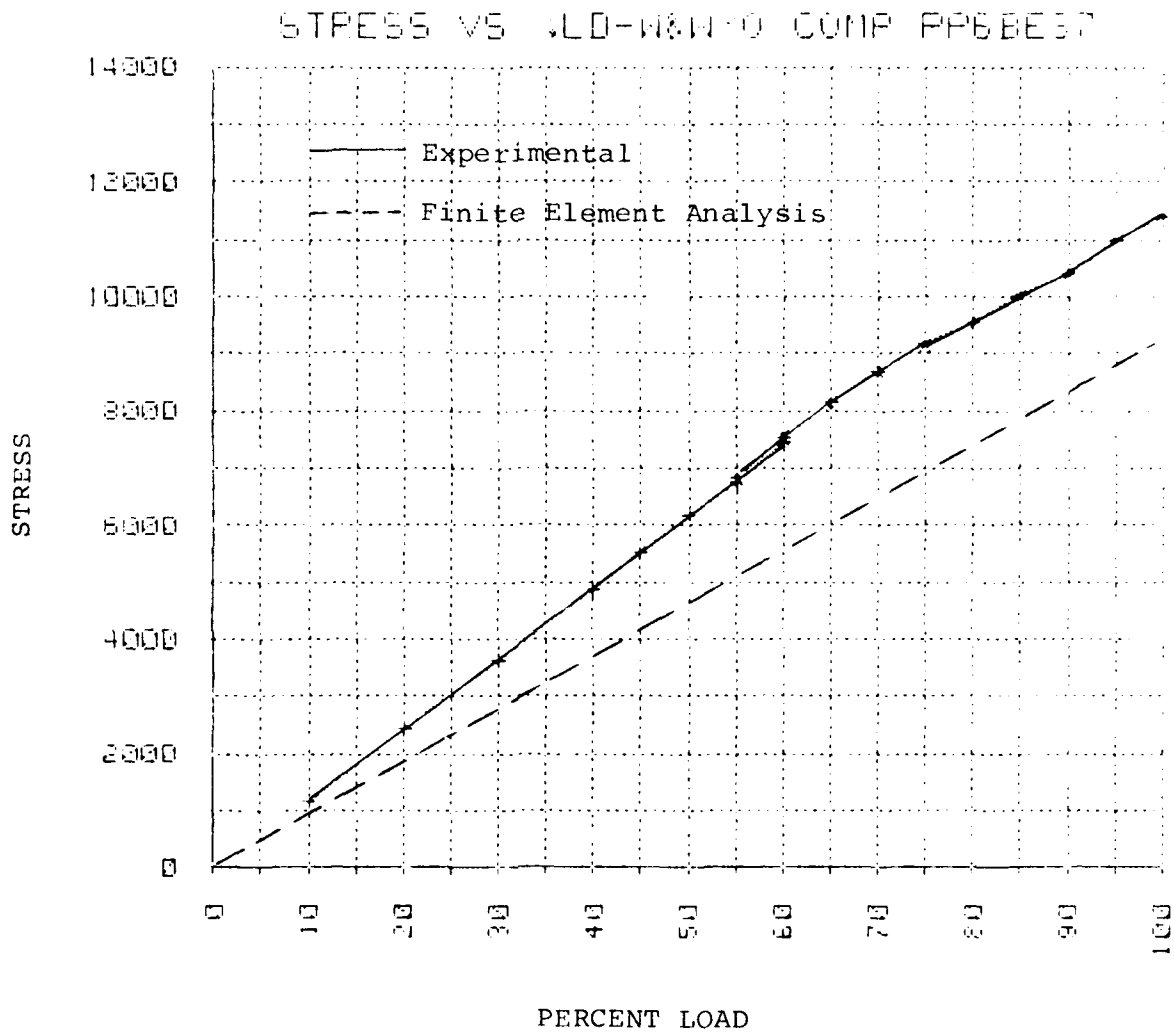

Figure 3.121. Equivalent Stress-Spar Cap Element 37.

AD-A096 572 DAYTON UNIV OH RESEARCH INST F/G 1/3
STRUCTURAL FLIGHT LOADS SIMULATION CAPABILITY. VOLUME I.(U)
NOV 80 F K BOGNER F33615-76-C-3135
UNCLASSIFIED UDR-TR-80-73-VOL-1 AFWAL-TR-80-3118-VOL-1 NL

2 OF 2
AD
A096572

END
DATE
FILMED
4-81
DTIC

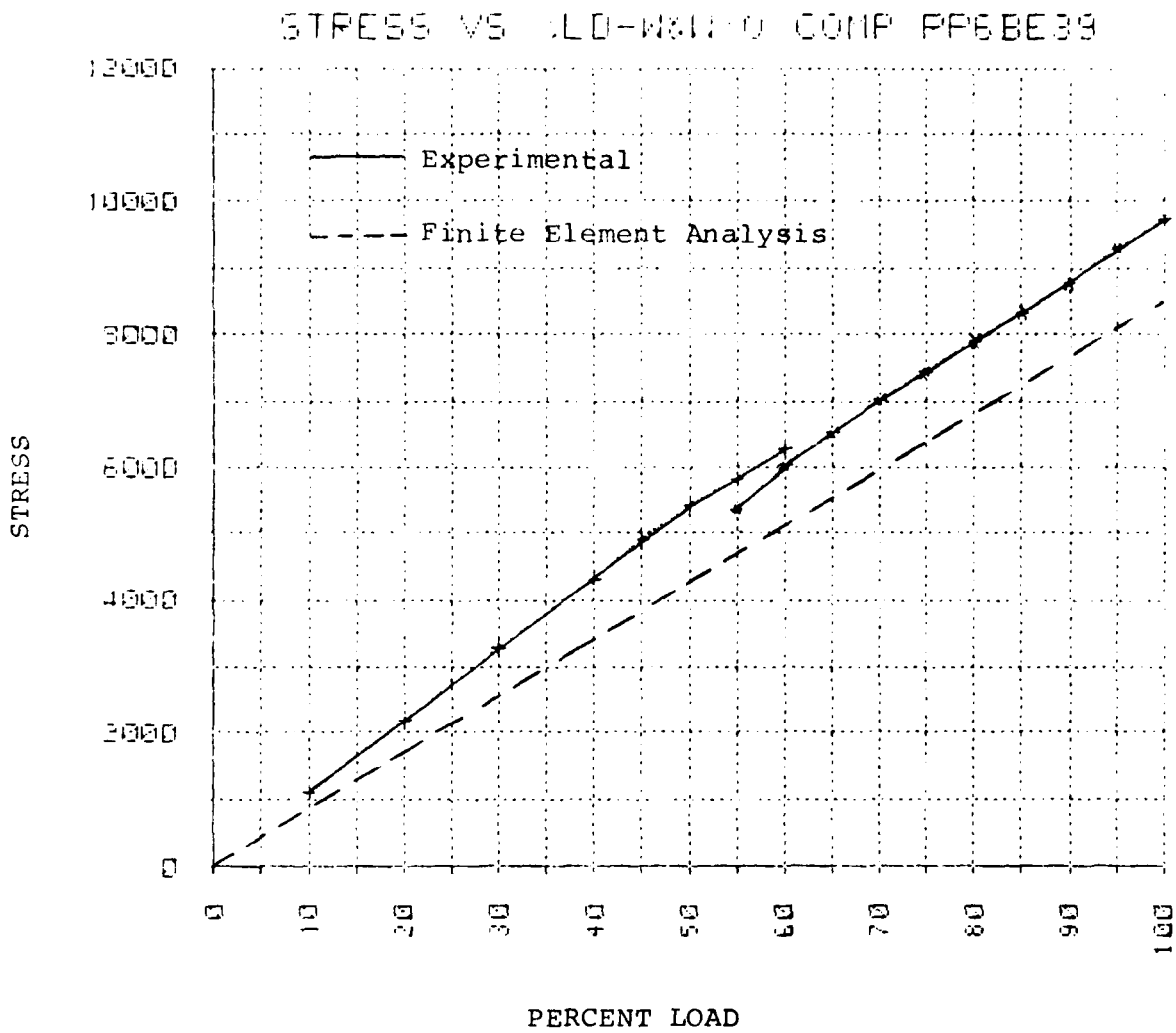

Figure 3.12m. Equivalent Stress-Spar Cap Element 39.

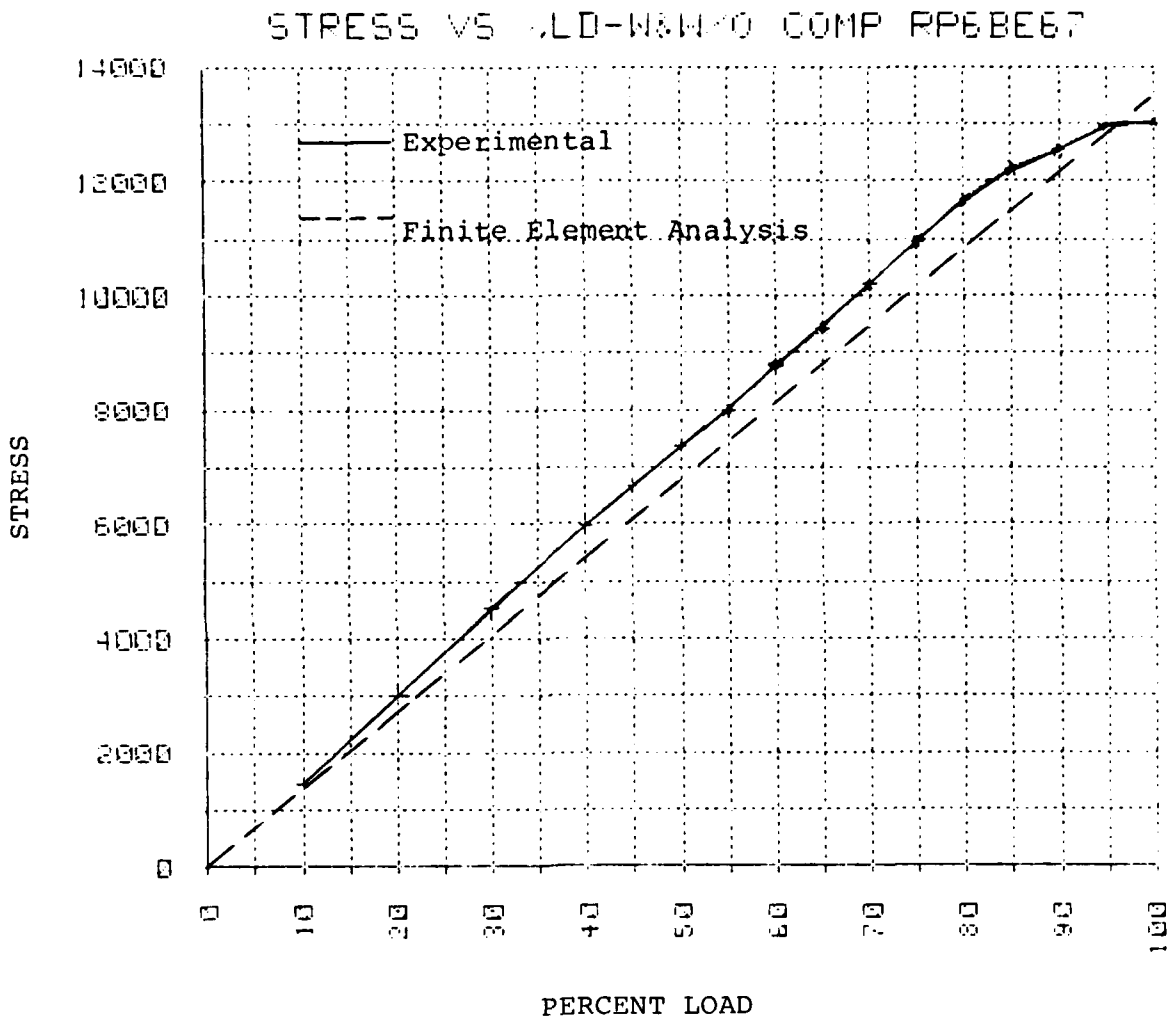

Figure 3.12n. Equivalent Stress-Spar Cap Element 67.

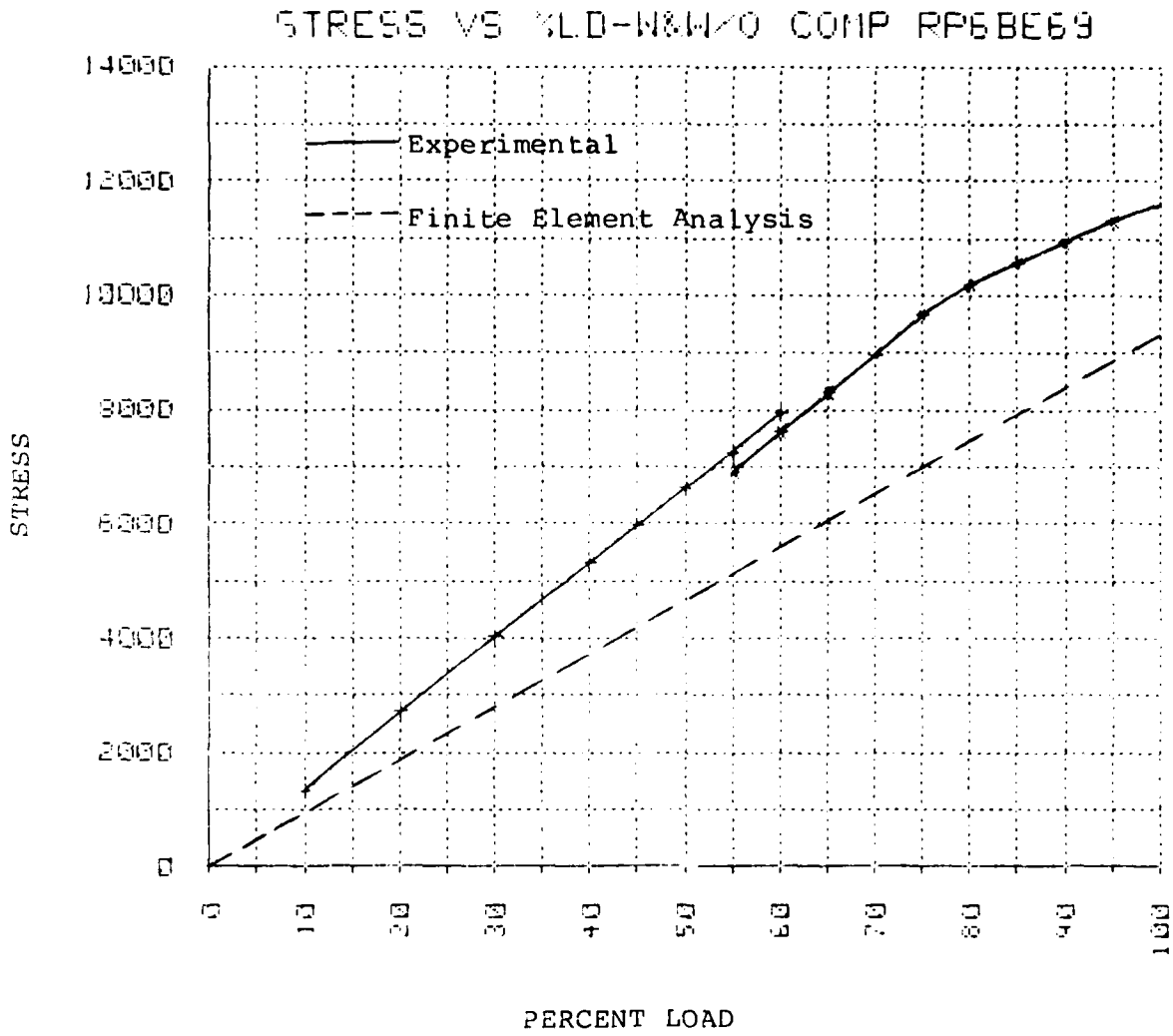

Figure 3.12o. Equivalent Stress-Spar Cap Element 69.

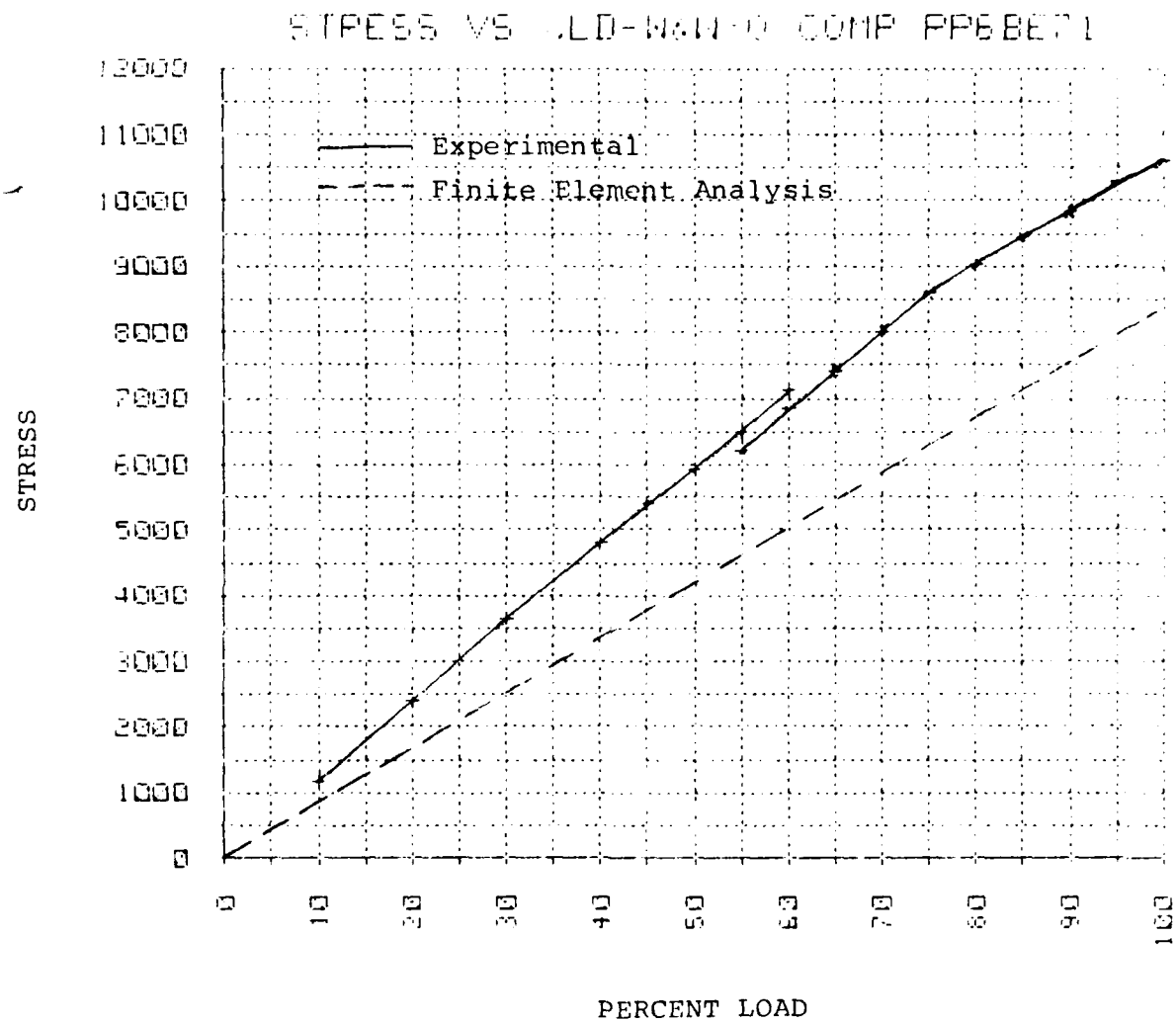

Figure 3.12p. Equivalent Stress-Spar Cap Element 71.

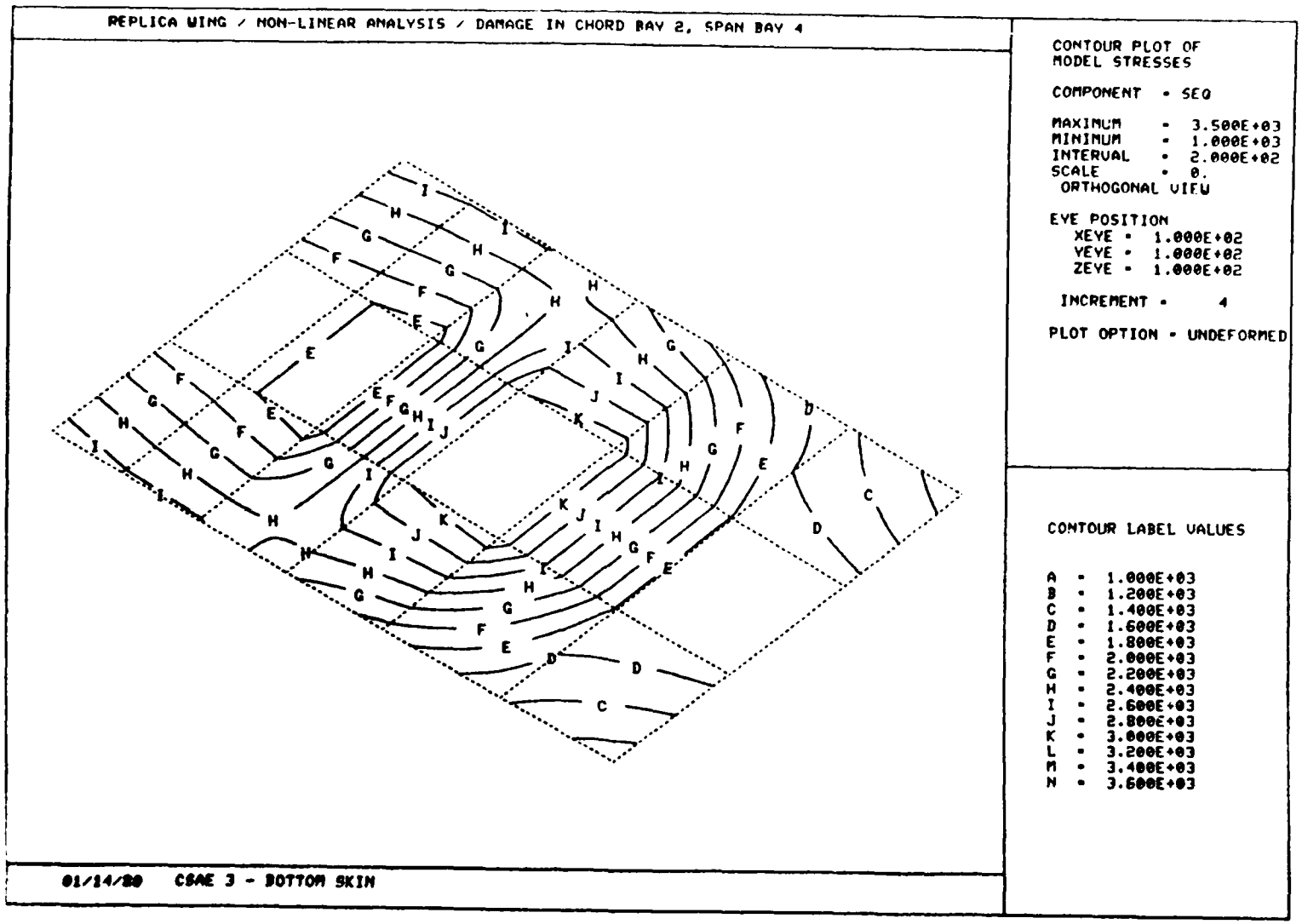

Figure 3.13a. Contours of Equivalent Stress - 20% Load.

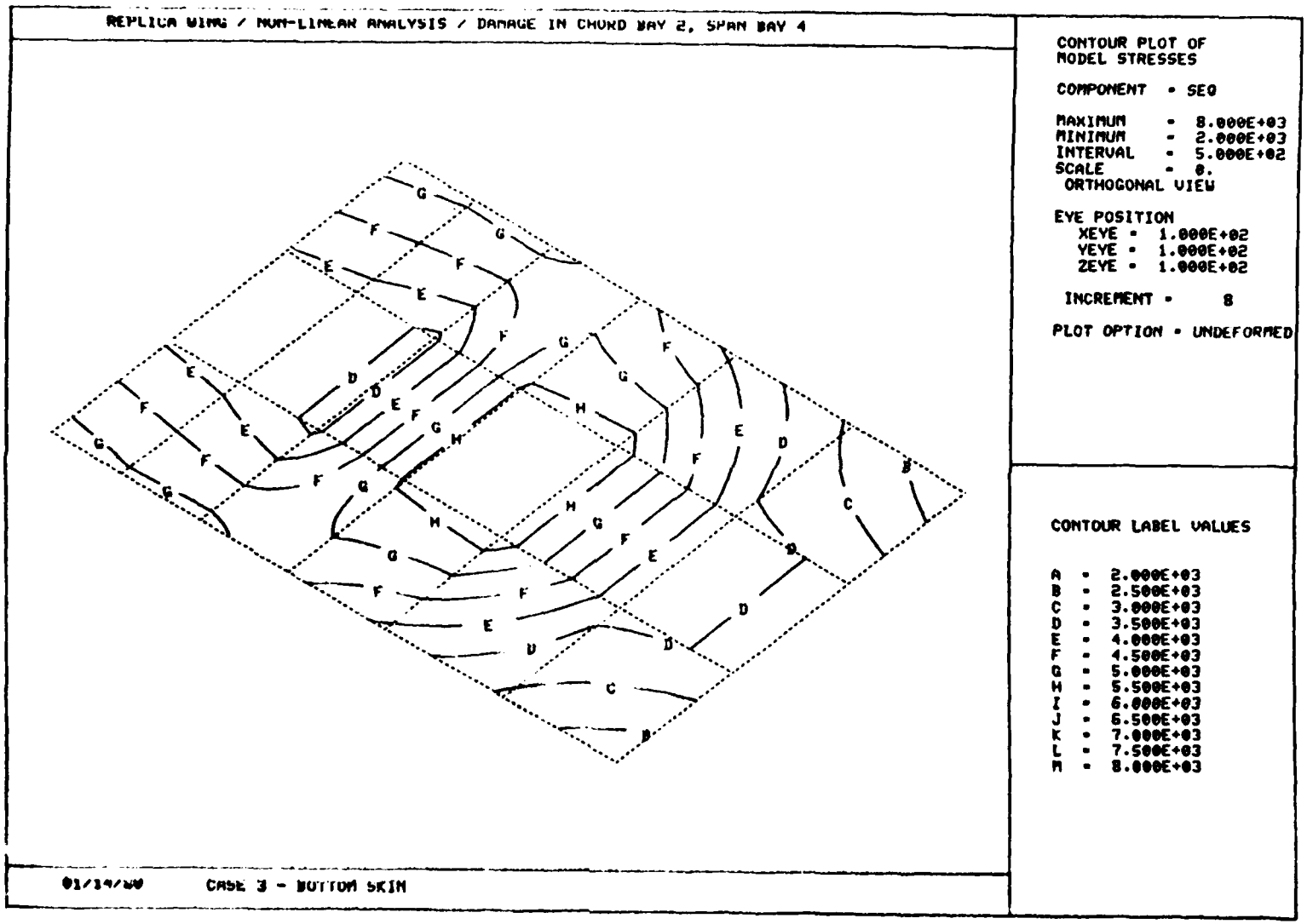

Figure 3.13b. Contours of Equivalent Stress - 40% Load.

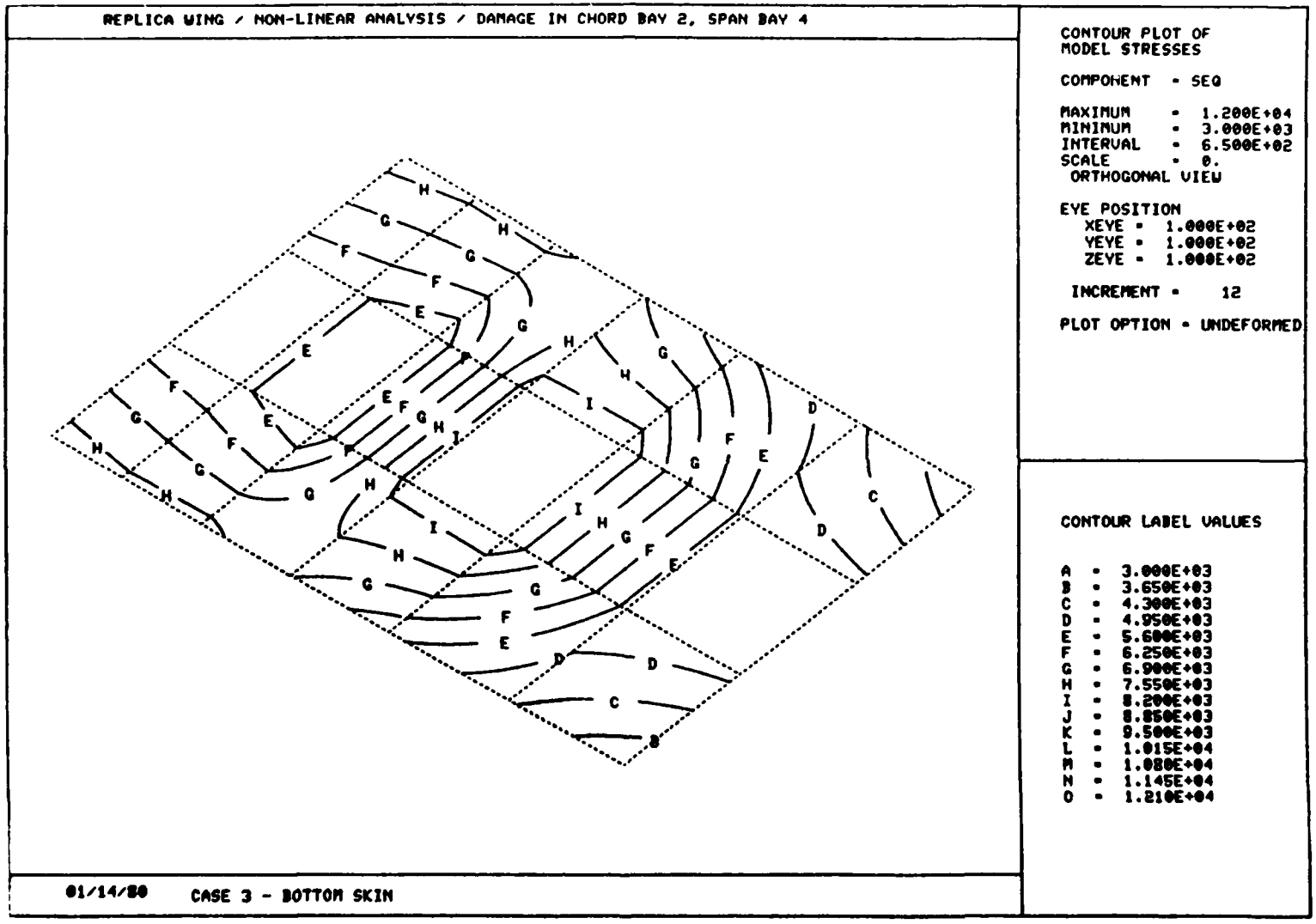

Figure 3.13c. Contours of Equivalent Stress - 60% Load.

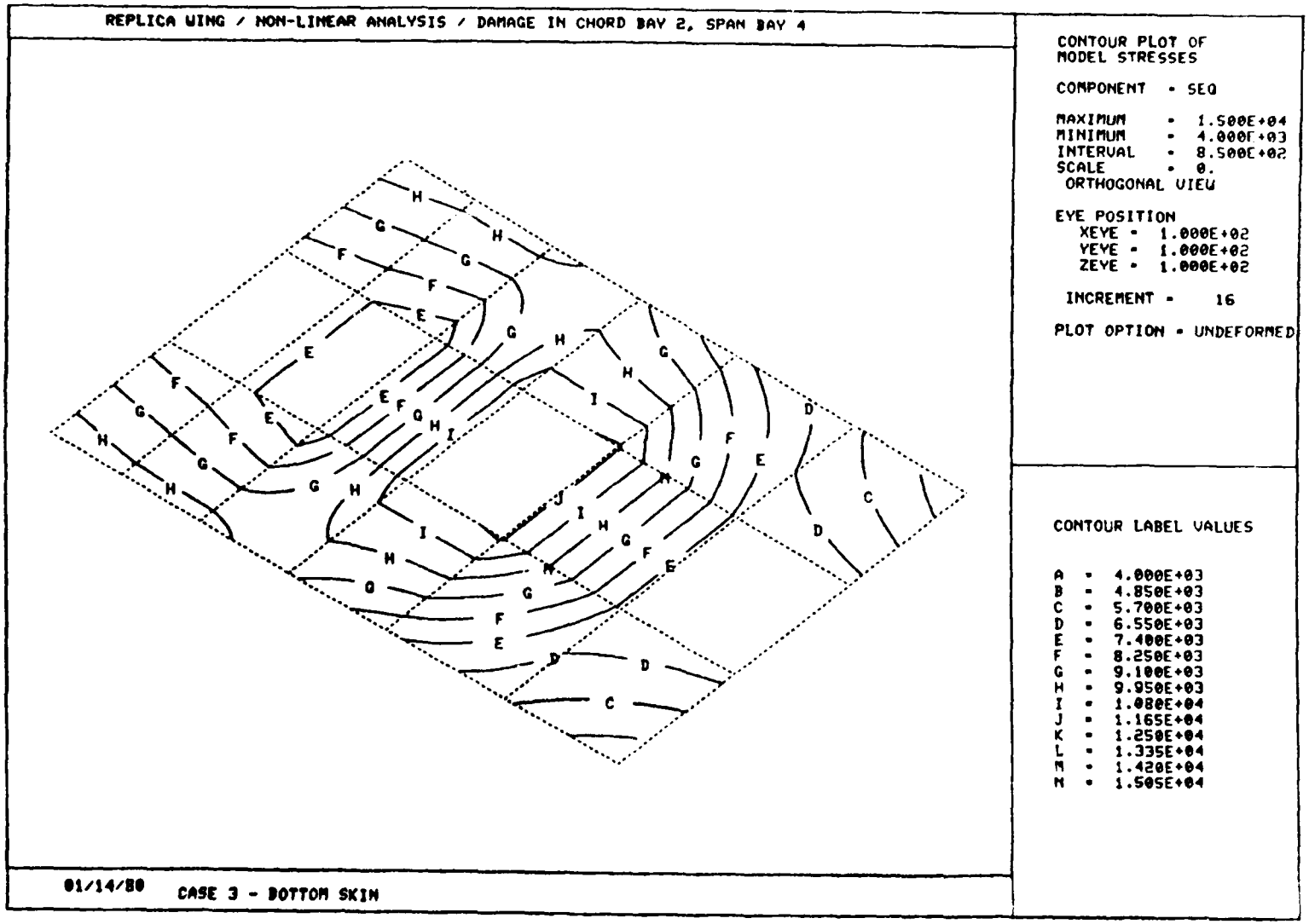

Figure 3.13d. Contours of Equivalent Stress - 80% Load.

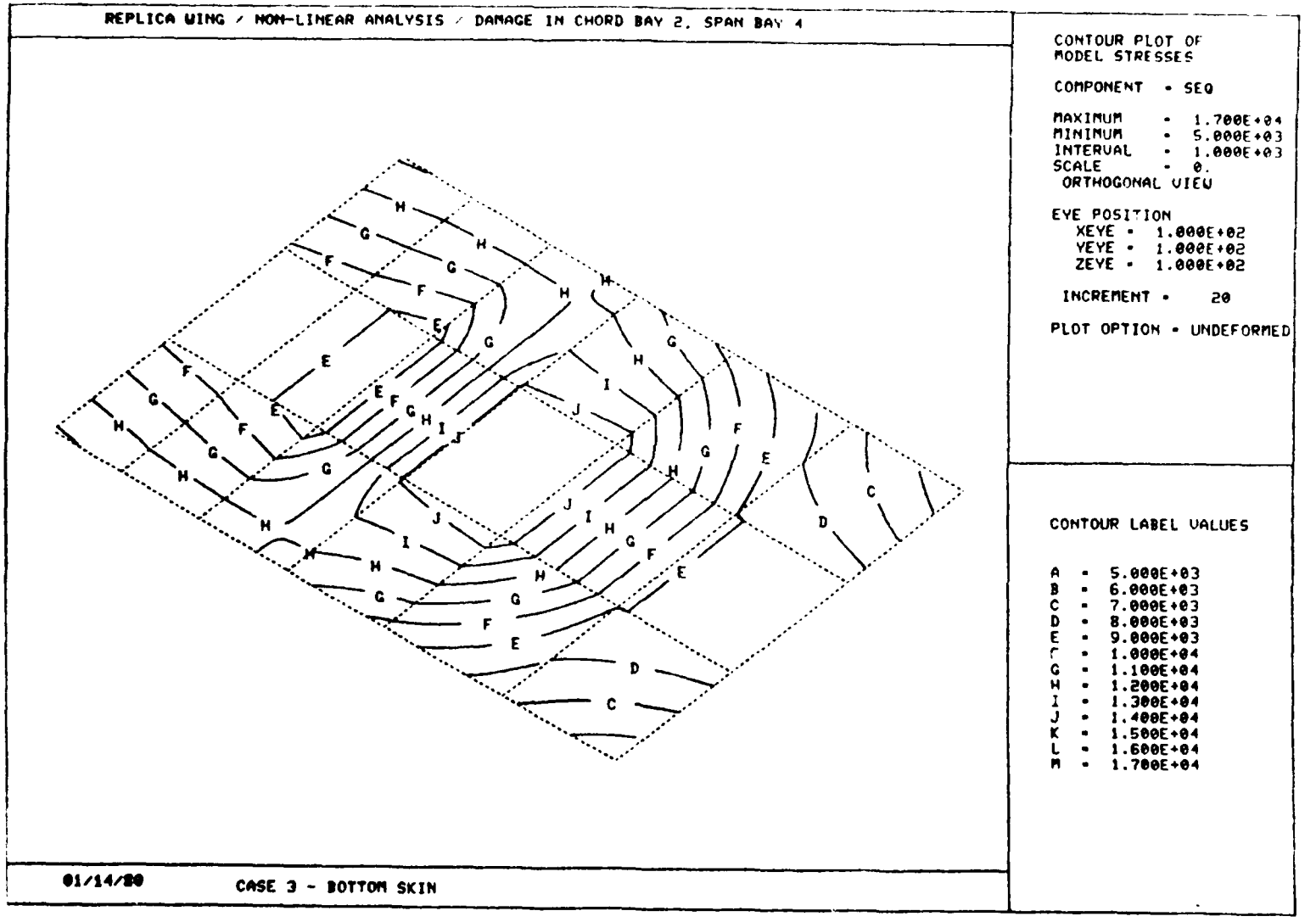

Figure 3.13e. Contours of Equivalent Stress - 100% Load.

The discontinuity which appears in the experimental data in Figures 3.12a-p occurred when two top skin panels (Elements 20 and 22 in Figure 3.11c) buckled. The buckling of the panels caused a readjustment in the stresses at other locations on the specimen. The simplified finite element model used is not capable of predicting local panel buckling. Also, the nonlinear and somewhat erratic behavior of the experimental results at the higher load levels is attributed not only to the compression skins buckling but also to the observed failure of rivets. The simplified finite element model also does not predict rivet failure.

3.5 TEST 4 - DAMAGED SPECIMEN, NUMBER 4

Specimen 4 is unsymmetrical having a "notch" in the leading edge and longitudinally split interior spar caps as indicated in Table 2.1. Again a combination of spanwise bending moment and spanwise shear load were applied to the specimen.

3.5.1 Instrumentation

Figure 3.14 shows the relative locations of strain gages monitored during Test 4. Both rosettes and individual gages are numbered in the figure.

3.5.2 Loading

The maximum load applied to the specimen was a combination of spanwise bending moment ($\bar{M}_s = 2.7 \times 10^6$ in. lb.) and spanwise shear load ($\bar{V}_s = 30{,}000$ lb.). The individual actuator forces corresponding to these section loads were (from Equations 3.2):

$T_1 = 45{,}573$ lb. Compression

$T_2 = 49{,}344$ lb. Compression

$T_3 = 25{,}497$ lb. Tension

$T_4 = 29{,}426$ lb. Tension

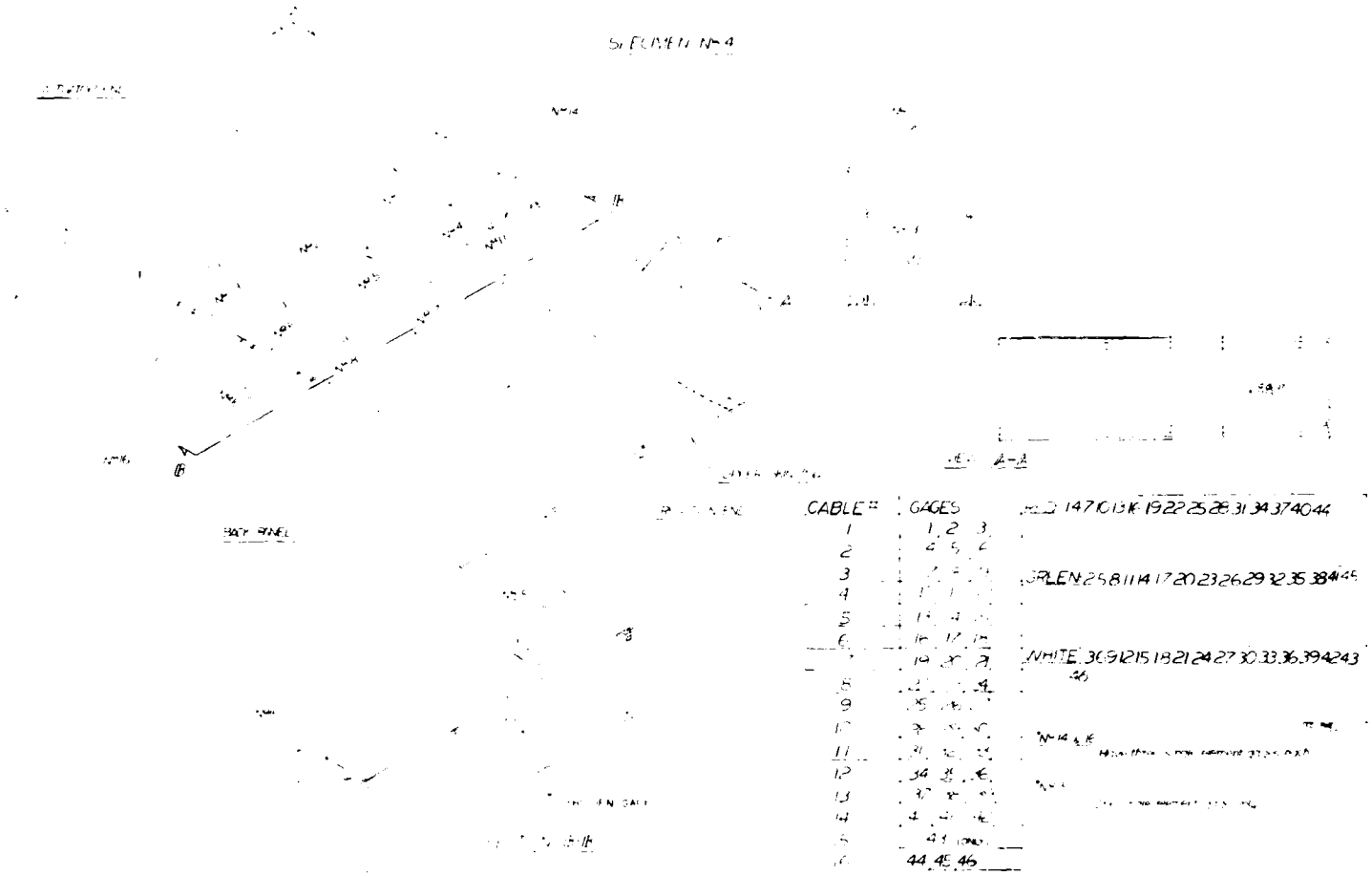

Figure 3.14. Strain Gage Locations - Specimen 4.

3.5.3 Load Incrementation and Data Collection

During the test of Specimen 4, the individual actuator forces were increased incrementally in steps equal to five percent of the maximum values given above. At each stage of the loading, strain gage readings were recorded by a mini-computer. A computer program converted the gage signals into units of strain and computed the associated material stresses. In the case of the rosettes, the minimum and maximum principal stresses, the maximum shear stress, the principal angles, and the Von Mises equivalent stress were computed. An example of the output of the data reduction program for Test 4 is shown in Figure 3.15. The output shown corresponds to 40 percent of the maximum loads defined above.

3.5.4 Analysis Model

The finite element model for specimen 4 is shown in Figure 3.16a-e. The modeled portion of the replica specimen is that part of Figure 2.12 which has the bays numbered. As mentioned before, in the experimental facility, the two end bays of the specimen are clamped by mounting brackets and are, therefore, not considered in the analysis. The model contains 56 nodes, 34 skin membrane elements, 23 spar web shear panel elements, 15 rib web shear panel elements, 46 spar cap bar elements and 30 rib cap bar elements. Each of the 56 nodes has three degrees of freedom, the displacements parallel to the three coordinate axes. Eight of the nodes are fixed at the reaction end of the specimen (nodes 1-8). Therefore, the analysis model has 3 x 48 = 144 degrees of freedom.

3.5.5 Test/Analysis Results

Figures 3.17a-m compare experimentally obtained stresses with corresponding stresses computed analytically with the finite element program. Each plot has two experimental results displayed. The strain gages on the specimen were zeroed with the loading apparatus hanging from the specimen. The lower curve was obtained assuming that the gages had zero readings when

```
SPECIMEN #4. TEST [illegible] 11-[illegible]                    3 3 24 READING 442

                                  E=   10 [illegible]   NO=   330

BASIC CHANNELS
CH ---MV--- -VALUE-
 1-1074 250  -10 [illegible]     F1
 2-1005 000  -10 0[illegible]4     F2
 3   34 250      [illegible]42     F3
 4  [illegible] 125    4 [illegible]     F4
 5  -65 250    [illegible]3     F5
 6-[illegible] 500   4[illegible]     [illegible]
 7-11[illegible] 625-1252 [illegible]4     [illegible]
 8  137 150    1 [illegible]72     D1
 9  124 375    1 [illegible]44     D2
10  141 925    1 41[illegible]     D3

 ----------------------------------------------------------------------

DEFLECTION CHANNELS
                  WEST      MIDDLE     EAST
                  SIDE                 SIDE

DEFLECTION
 ANGLE (DEG)      [illegible]      0000      .0000
  TOP DEF        - [illegible]                 0000
  BOT DEF          [illegible]                 0000

 BASE
DEFLECTION
 ANGLE (DEG)      [illegible]      2674      2633
  TOP DEF        - [illegible]              - 26[illegible]
  BOT DEF        - [illegible]                 0305

UNCORRECTED
DEFLECTIONS
D1 ([illegible]2 00)        1[illegible]25                 0588
D2 (1[illegible] 62)        14[illegible]                 1632
D3 (2[illegible] 00)        [illegible]157                .3443
D4 (41 00)          [illegible]                 5057
D5 ([illegible] 00)      1 [illegible]715              1.2438
D6 ([illegible] 25)                1 41[illegible]2
 CORRECTED
DEFLECTIONS
D1 ([illegible]2 00)        [illegible]24                 0233
D2 (12 62)          0124                 0557
D3 (28 00)          0133                 1635
D4 (41 00)          [illegible]469                 263[illegible]
D5 (83 00)          [illegible]906                 7814
D6 ([illegible] 25)                [illegible]232

 ----------------------------------------------------------------------
```

Figure 3.14. Sample Experimental Data - Specimen 4.

STRAIN GAGE DATA				PRINCIPAL STRESS CALCULATIONS					
CH	MV(CORR)	USTRAIN	-STRESS- (PSI)	ROS-ETTE	MIN PR STRESS	MAX PR STRESS	MAX. SHEAR	ANGLE	EQUIV. STRESS
1	1.469	284.17	2907						
2	1.632	315.47	3149						
3	- .512	-99.11	-92						
				1001	-654	3699.	2277.	24.66	4192.
4	1.031	199.12	2787.						
5	2.959	571.52	5671						
6	.658	127.20	2230						
				1002	-666	5683.	3175.	42.48	6044.
7	.246	47.43	1393						
8	2.312	446.91	4487						
9	1.146	221.53	2742						
				1003	-444	4579.	2512.	52.78	4817.
10	1.663	321.73	3188						
11	.700	135.39	1745						
12	- .720	-139.21	-982.						
				1004	-414.	3220.	1817.	5.42	3446.
13	1.264	244.45	5415						
14	1.519	293.76	5797						
15	3.513	678.79	8778						
				1005	4971.	9222.	2126.	108.85	7995.
					951	7315	3178		6836
16	.509	98.21	1978						
17	2.559	494.92	5050.						
18	1.141	220.82	2927.						
				1006	-188.	5093.	2641.	50.18	5190.
19	2.246	434.26	6078						
20	3.658	707.10	8191						
21	1.436	277.45	4863.						
				1007	2684.	8258	2787.	38.71	7296.
22	.000	.00							
23	2.367	449.60	4631						
24	1.833	348.87	3593.						
25	2.520	479.27	4937						
26	3.567	677.53	6979.						
27	8.166	-144460.8	-1487946.						
28	1.246	240.87	1742.						
29	- .299	-57.84	-571.						
30	-1.411	-273.23	-2239.						
				1010	-2265.	1768.	2017.	-4.60	3502.

Figure 3.14. (continued).

31	- 140	-27 17	-253						
32	- 016	-3 19	-60						
33	082	15 92	80						
				1011	-254	81.	168	86. 77	303.
34	-2 073	-400 65	-1952						
35	393	76 02	1840						
36	3 757	728 68	6894						
				1012	-1904.	6947.	4426.	94. 43	8070.
37	-1 442	-278 33	-2969						
38	- 360	-69 62	-1352						
39	337	65 17	-308						
				1013	-2999	-278.	1361.	83. 93	2870.
40	1 047	202 47	3110						
41	2 774	536 14	5994						
42	1 044	201 92	3105						
				1014	521.	5694.	2587.	44. 97	5452.
43	- 768	16888 26	194549						
44	399	75 90	782						
45	- 080	-15 20	-157.						
46	- 051	-9 88	-114						
47	- 079	-15 27	-156						
48	.000	.00	-35.						
				1016	-165.	13.	89.	122. 21	171.
49	579	110. 44	1138.						

Figure 3.14 (concluded).

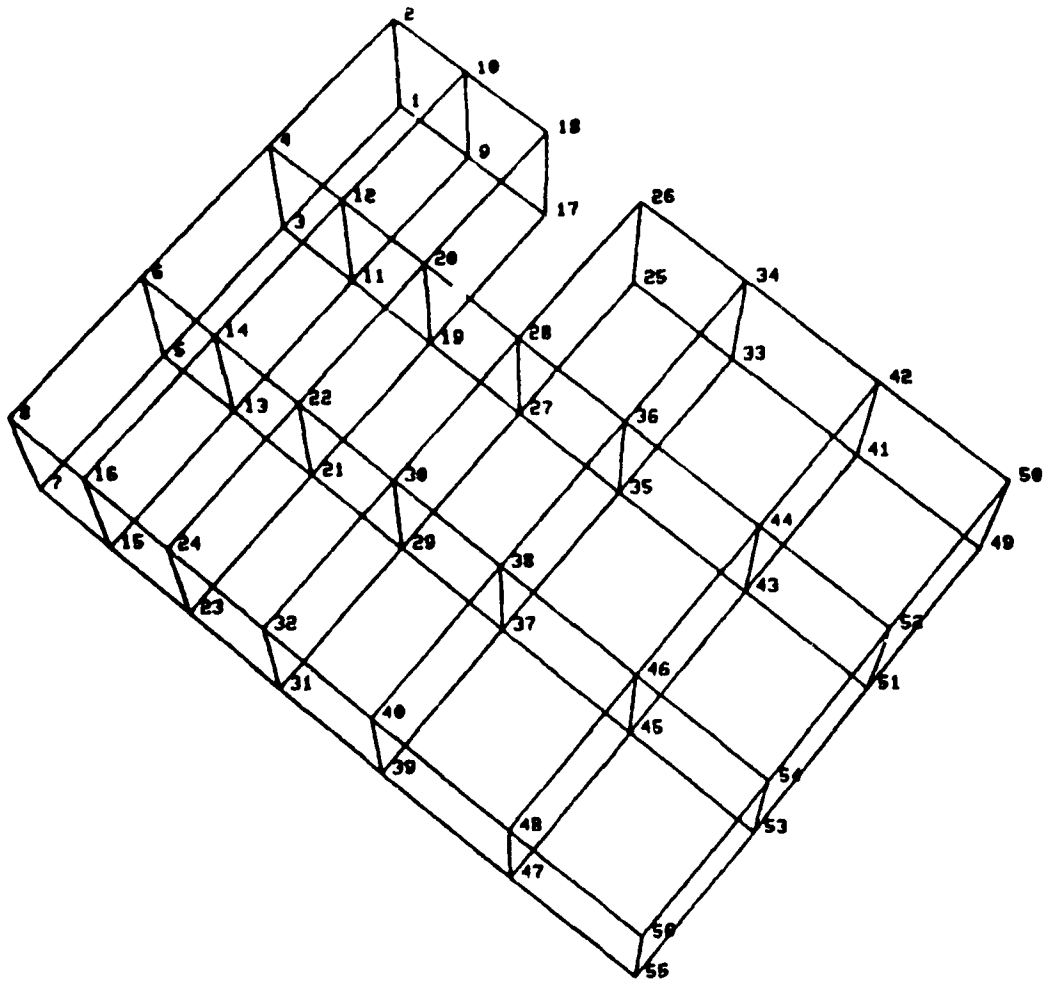

Figure 3.16a. Specimen 4 Finite Element Model - Node Numbers.

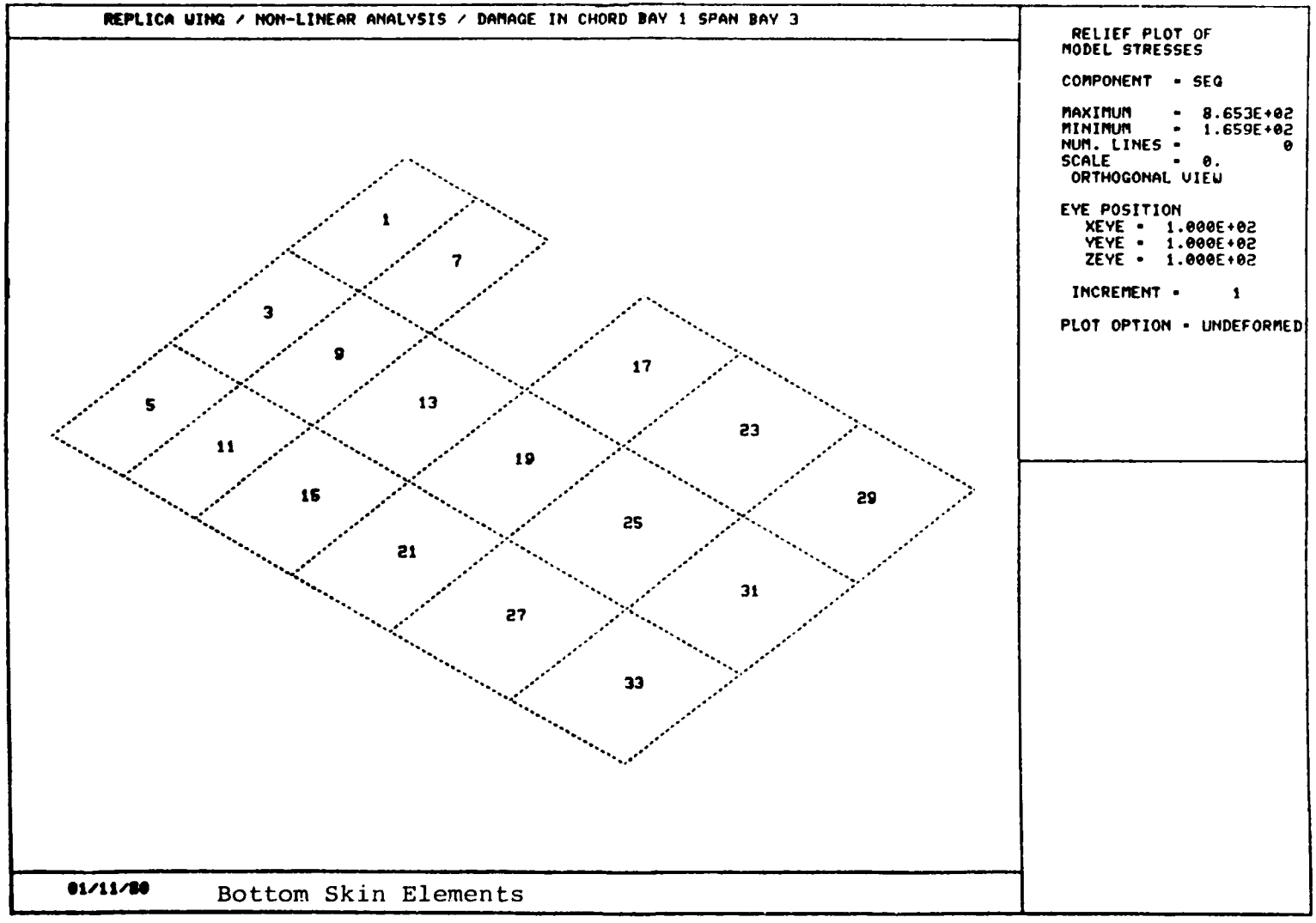

Figure 3.16b. Specimen 4 Finite Element Model - Bottom Skin Membrane Elements.

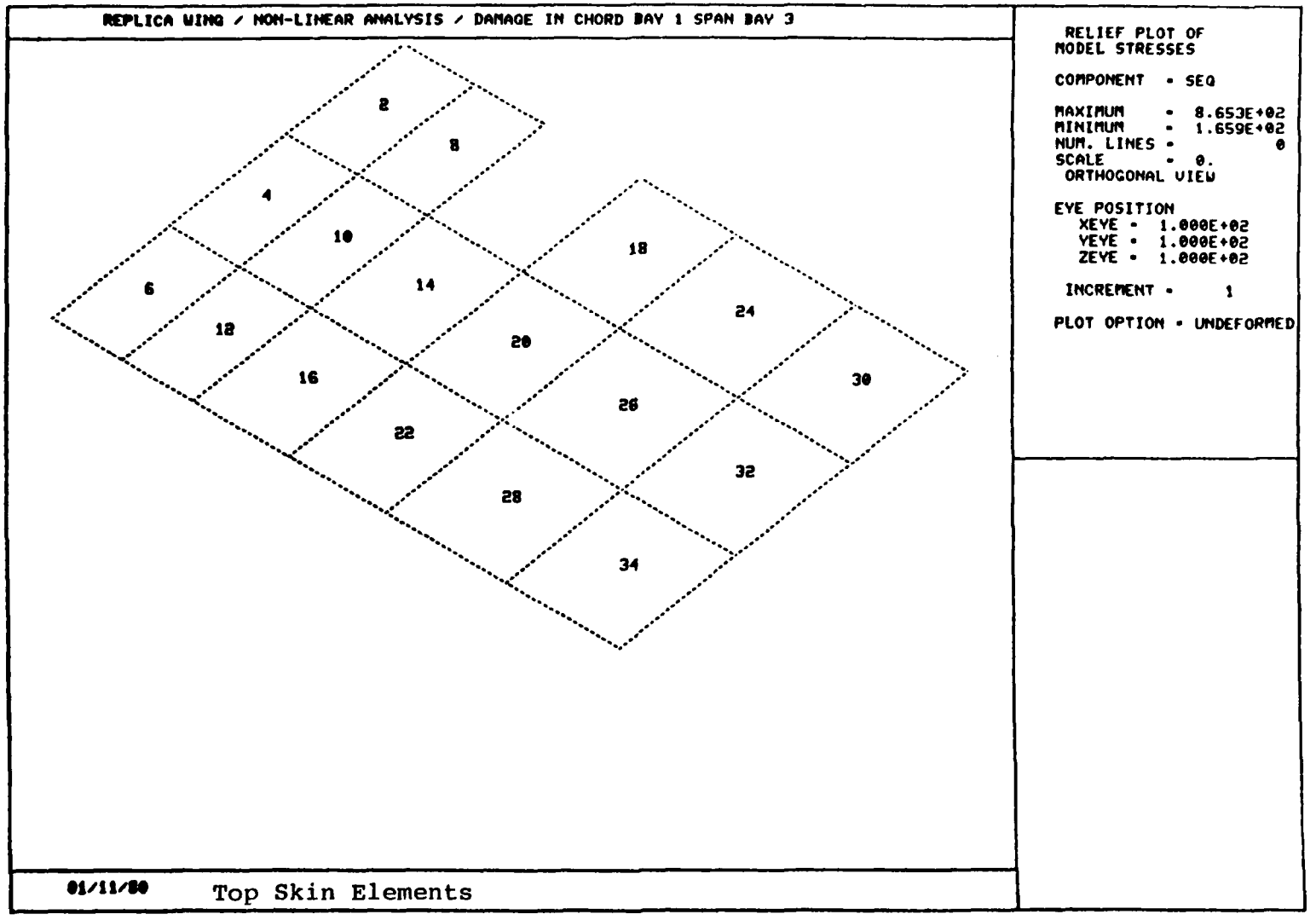

Figure 3.16c. Specimen 4 Finite Element Model - Top Skin Membrane Elements.

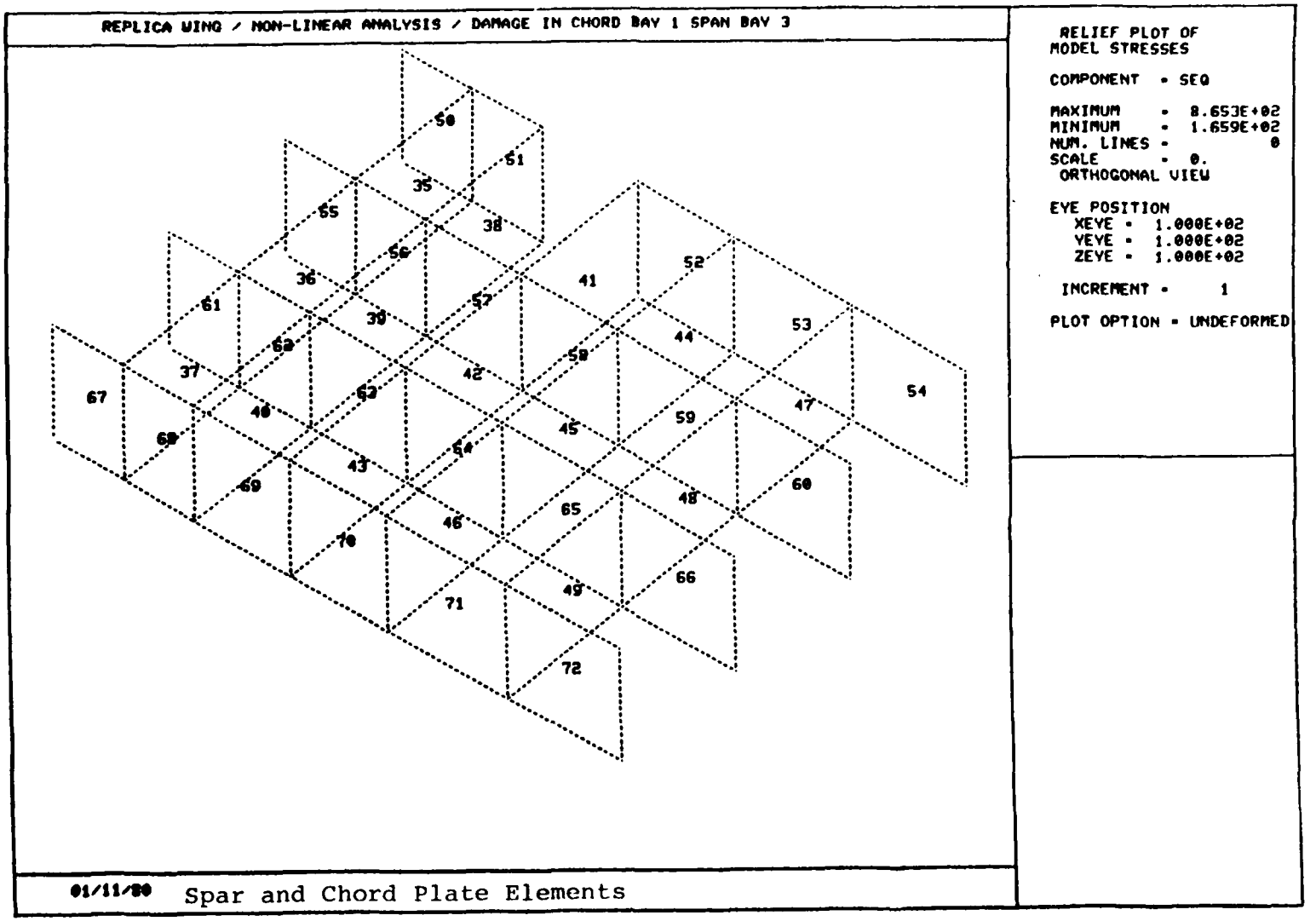

Figure 3.16d. Specimen 4 Finite Element Model - Spar and Rib Shear Panel Elements.

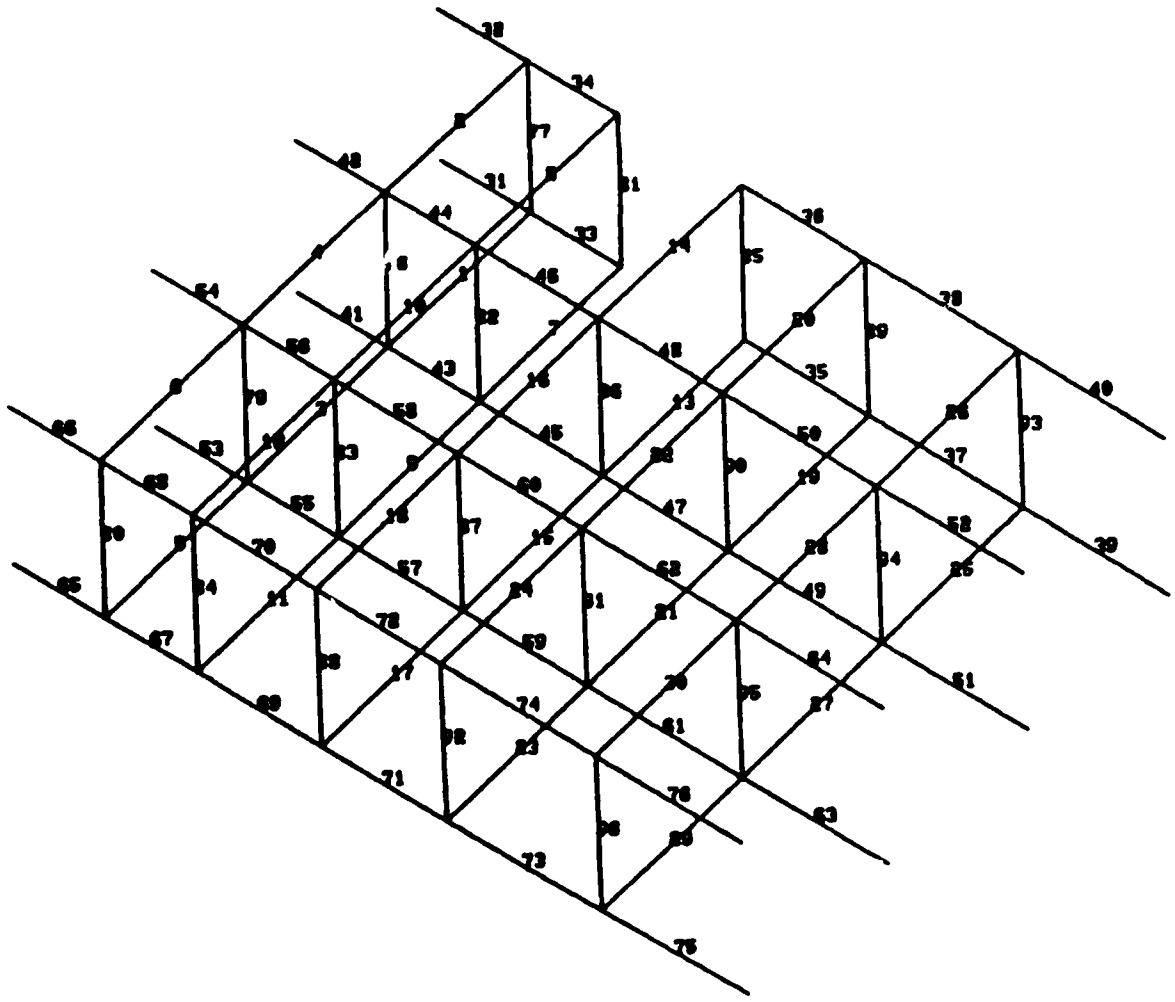

Figure 3.16e. Specimen 4 Finite Element Model - Cap Bar Elements.

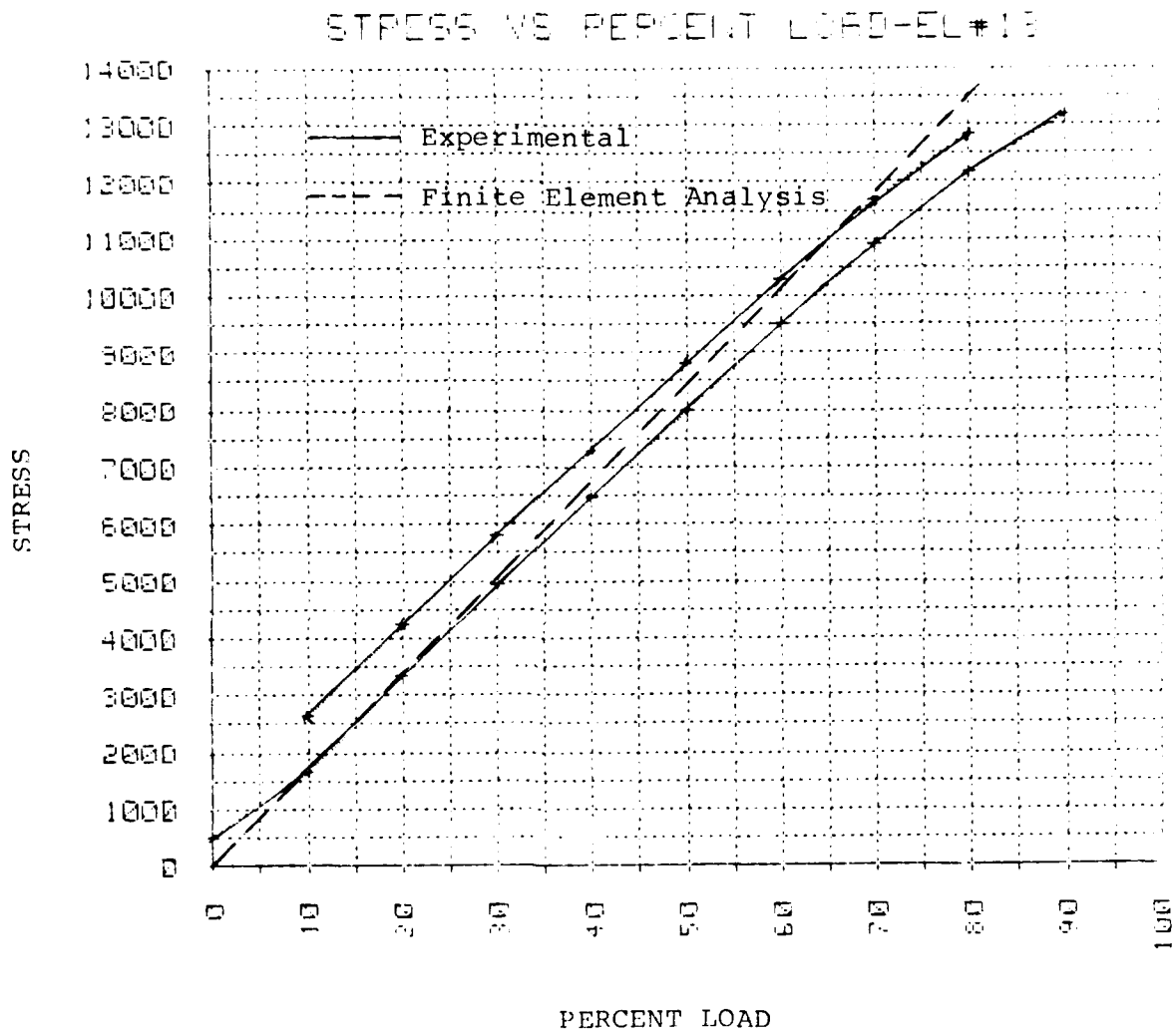

Figure 3.17a. Equivalent Stress-Skin Element 13.

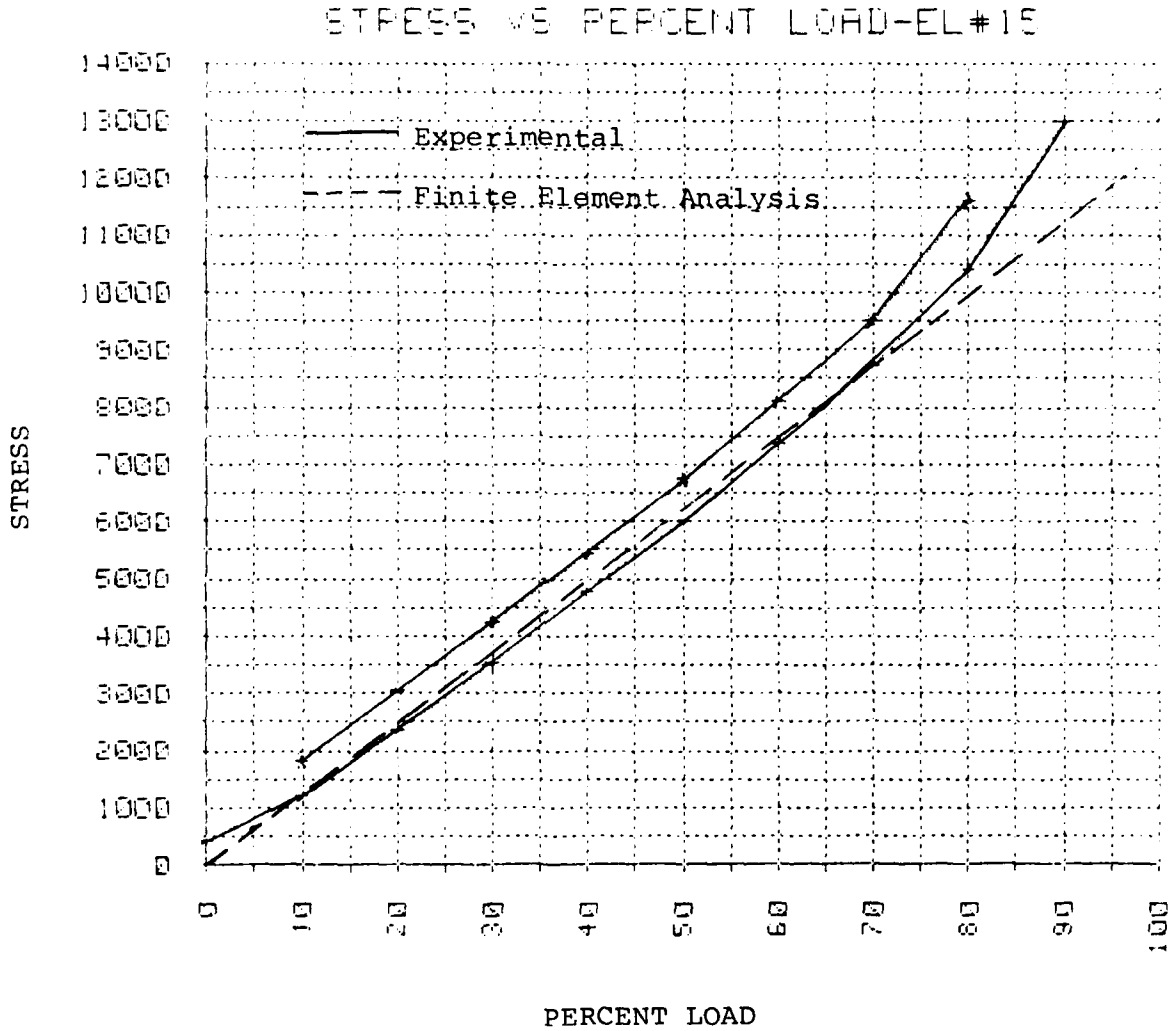

Figure 3.17b. Equivalent Stress-Skin Element 15.

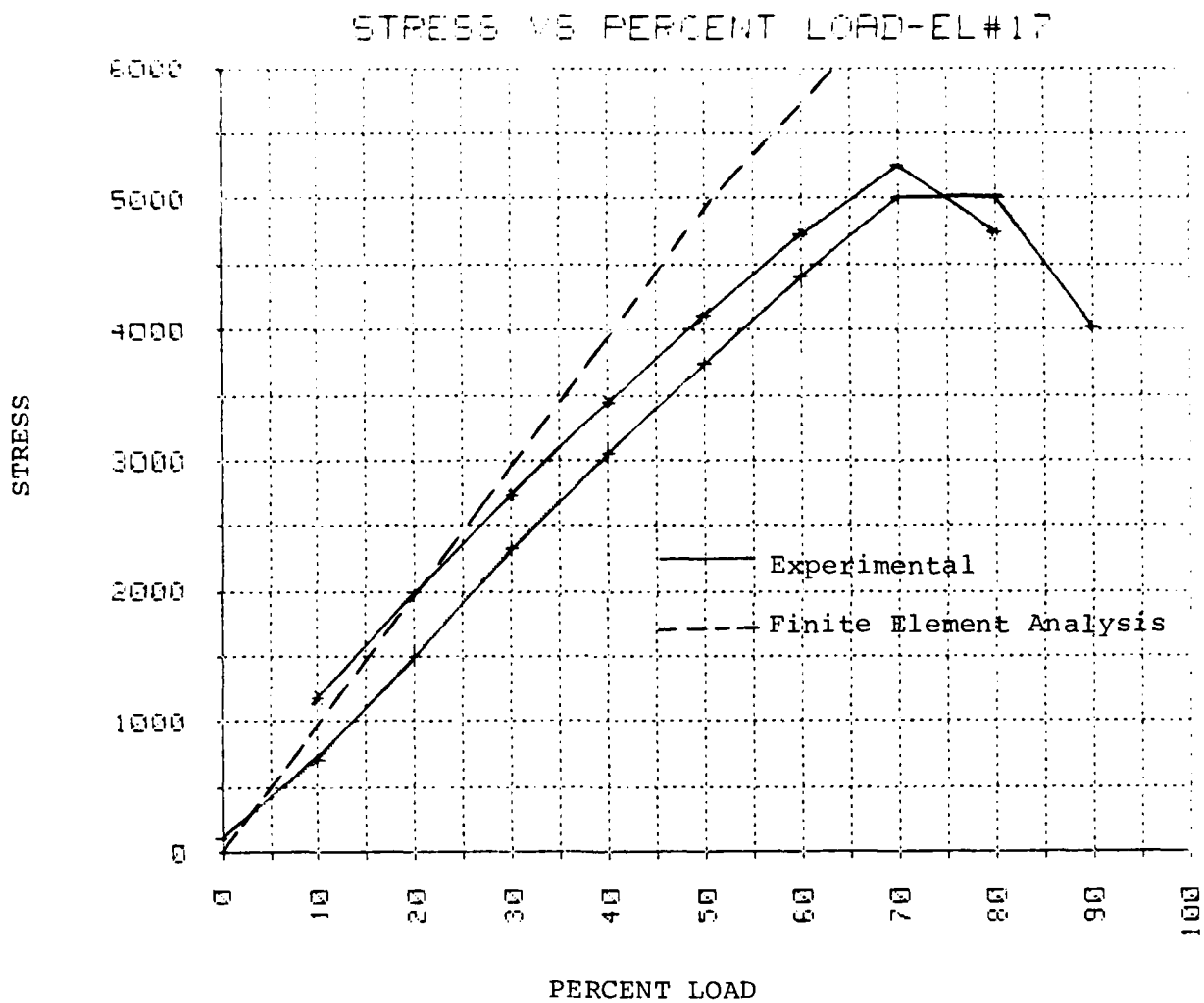

Figure 3.17c. Equivalent Stress-Skin Element 17.

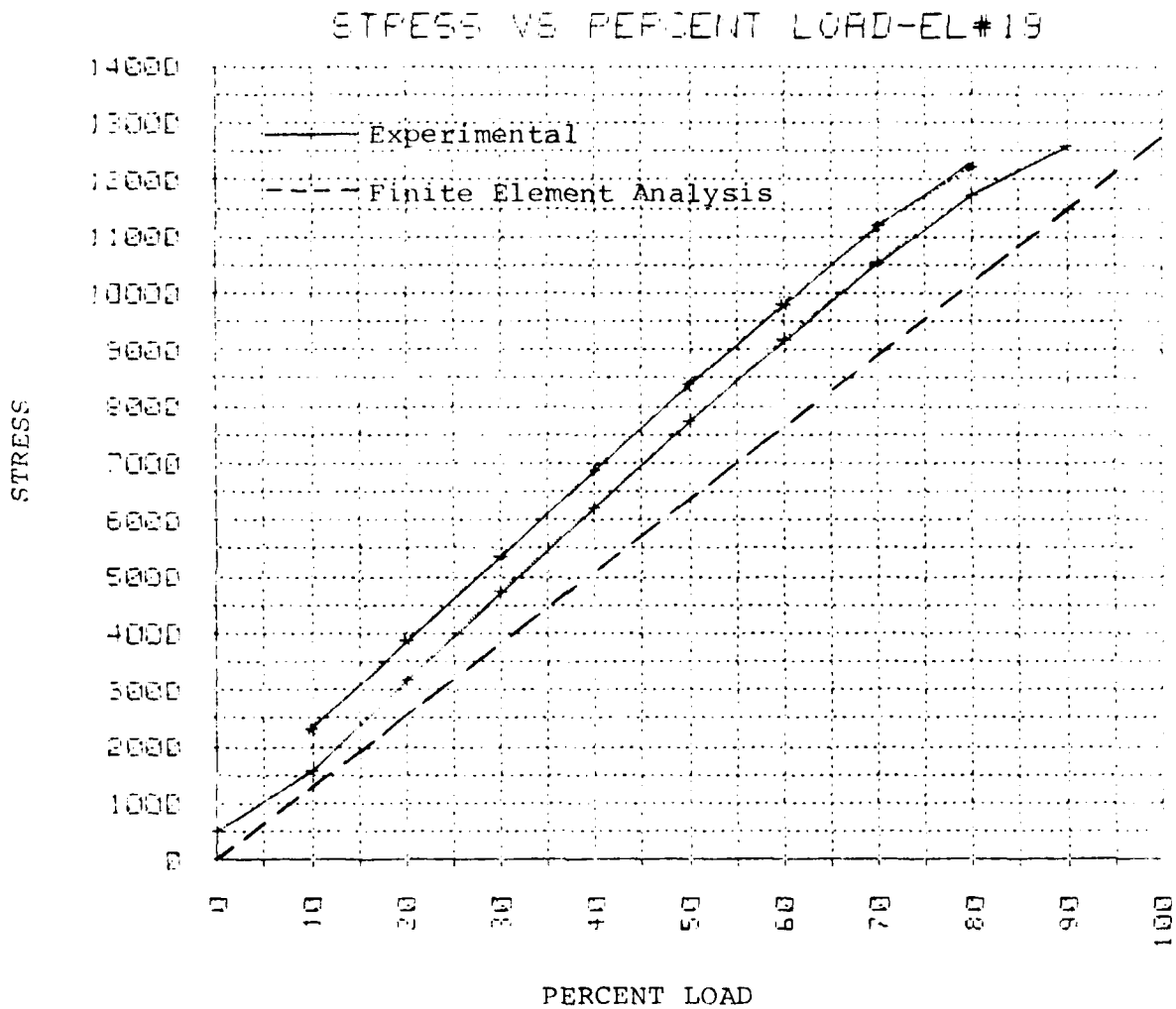

Figure 3.17d. Equivalent Stress-Skin Element 19.

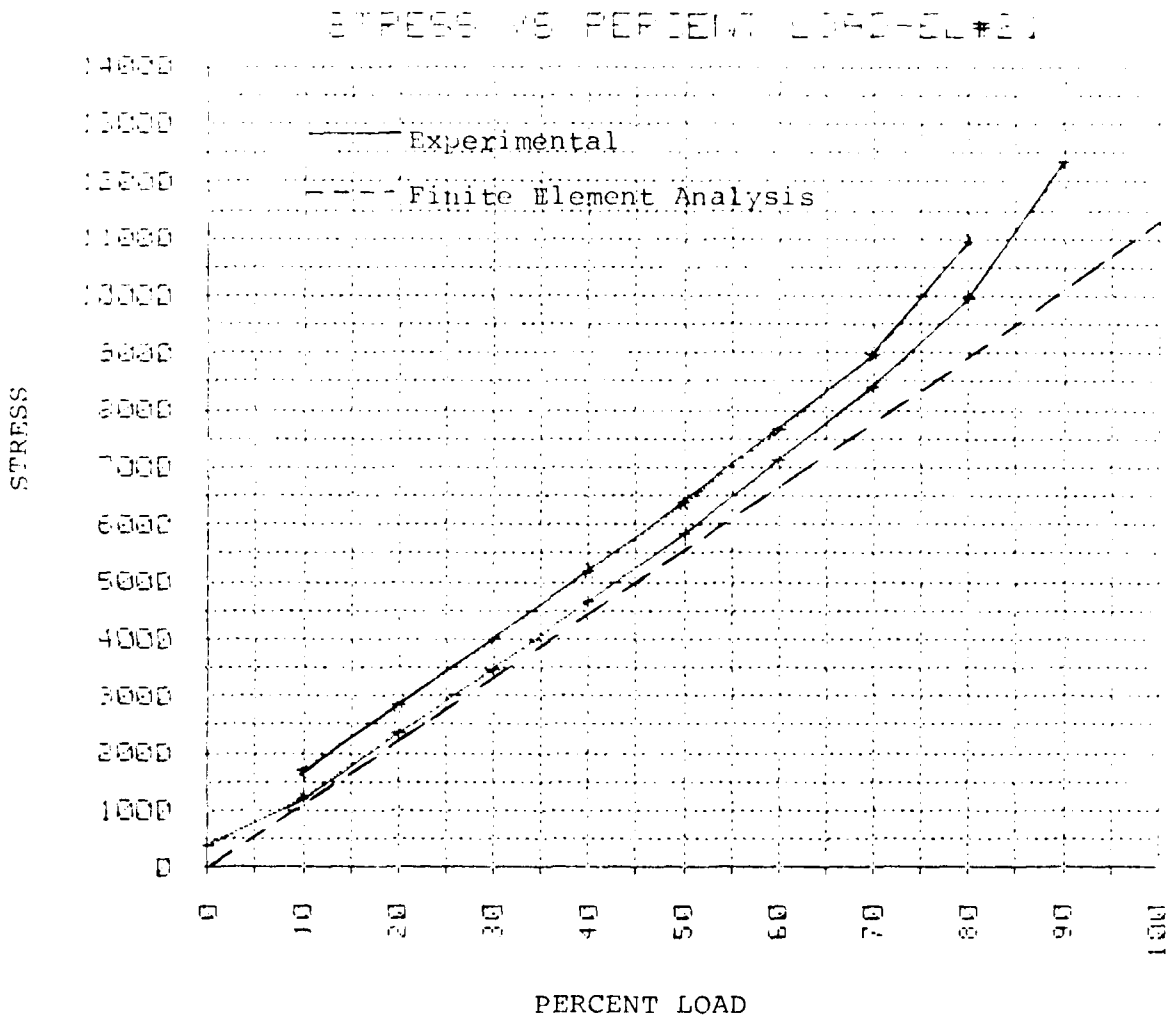

Figure 3.17e. Equivalent Stress-Skin Element 21.

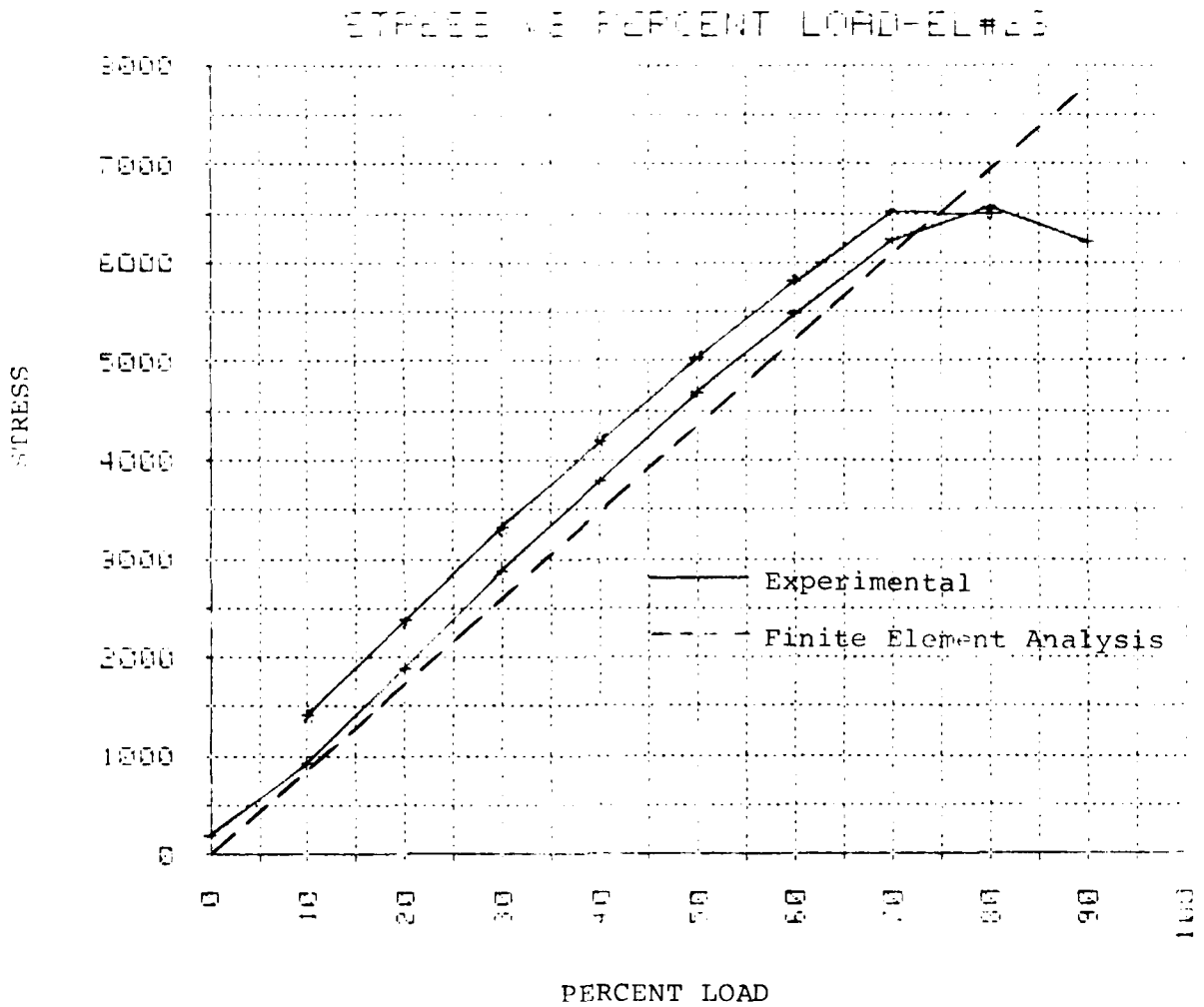

Figure 3.17f. Equivalent Stress-Skin Element 23.

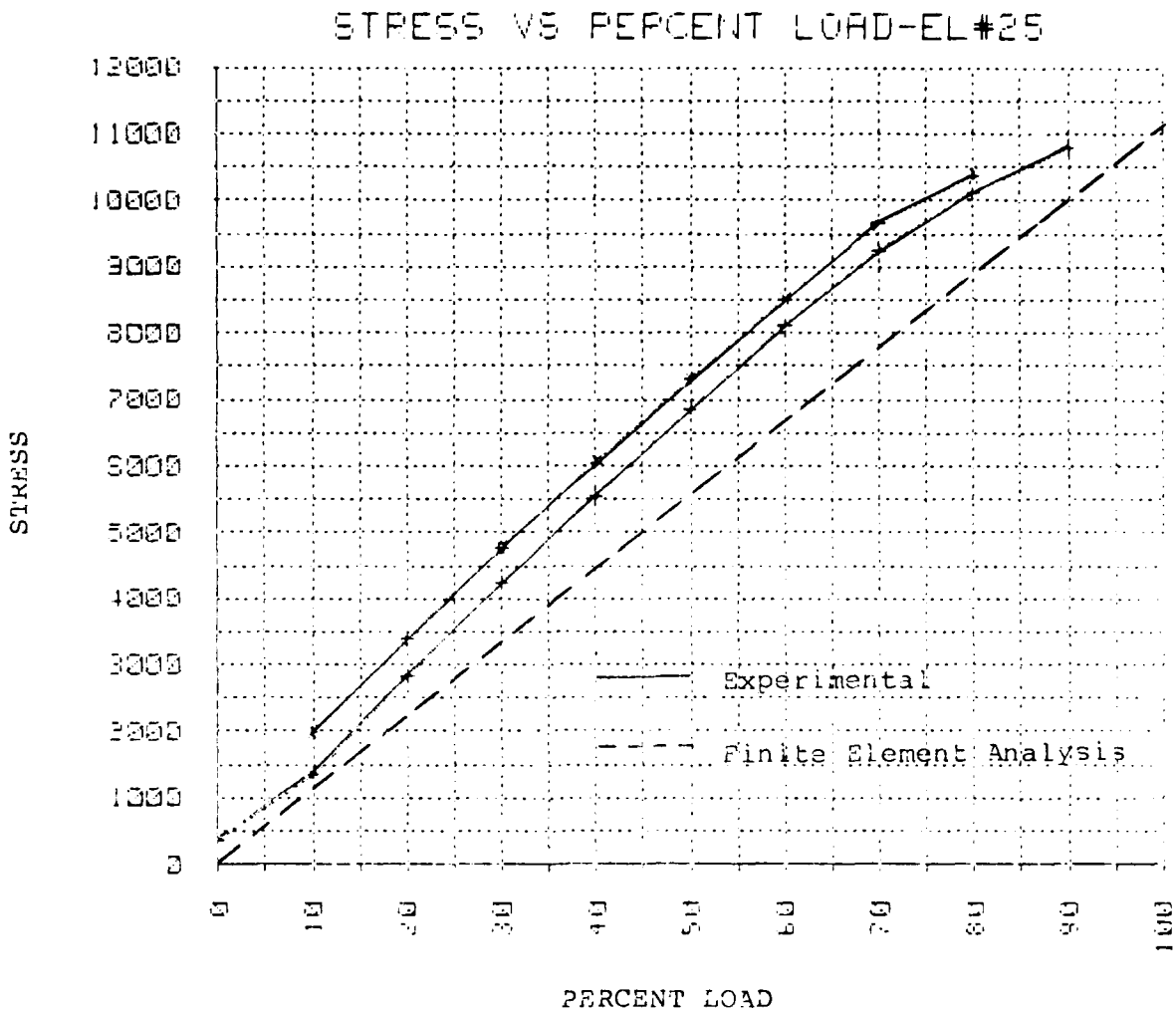

Figure 3.17g. Equivalent Stress-Skin Element 25.

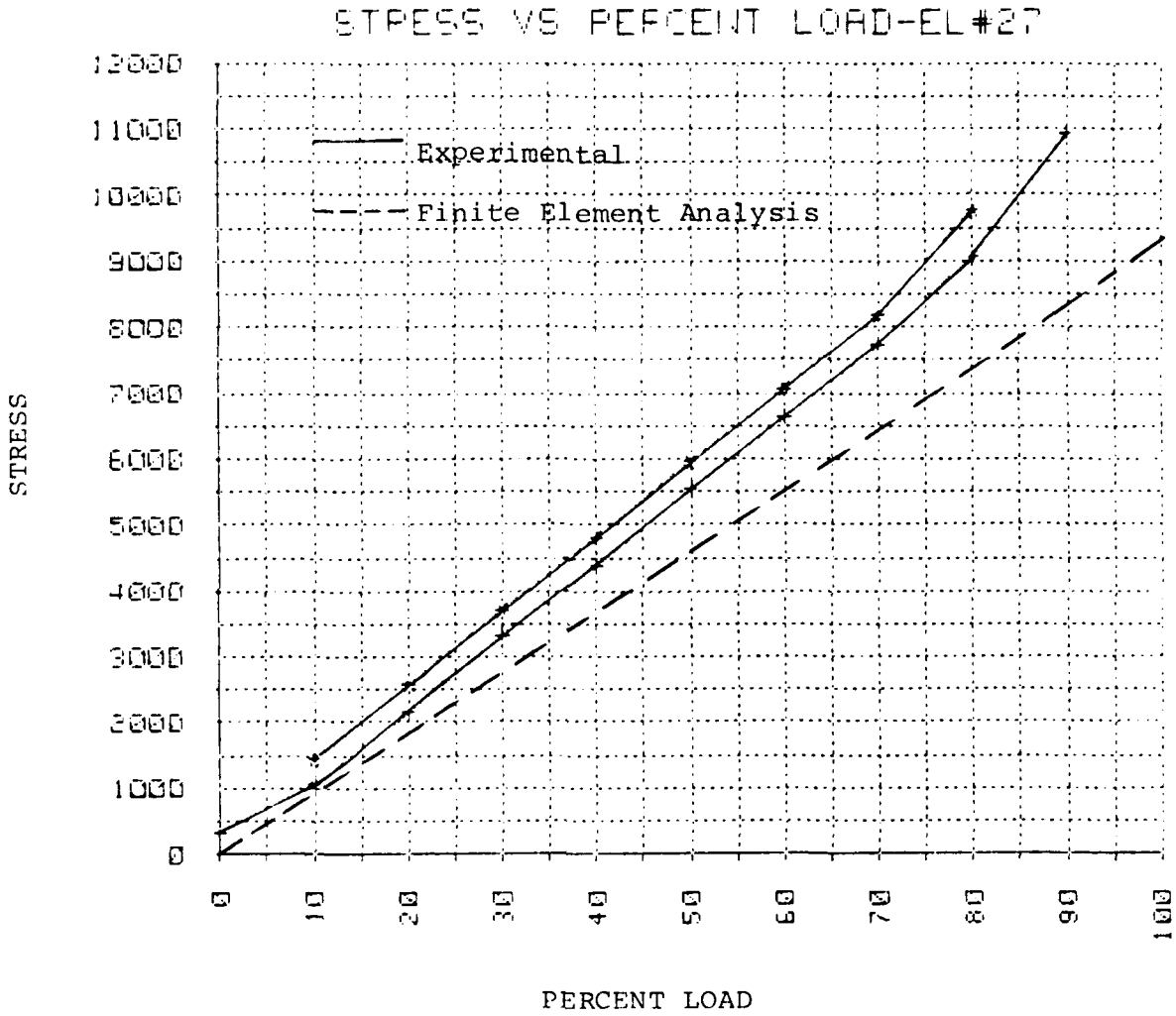

Figure 3.17h. Equivalent Stress-Skin Element 27.

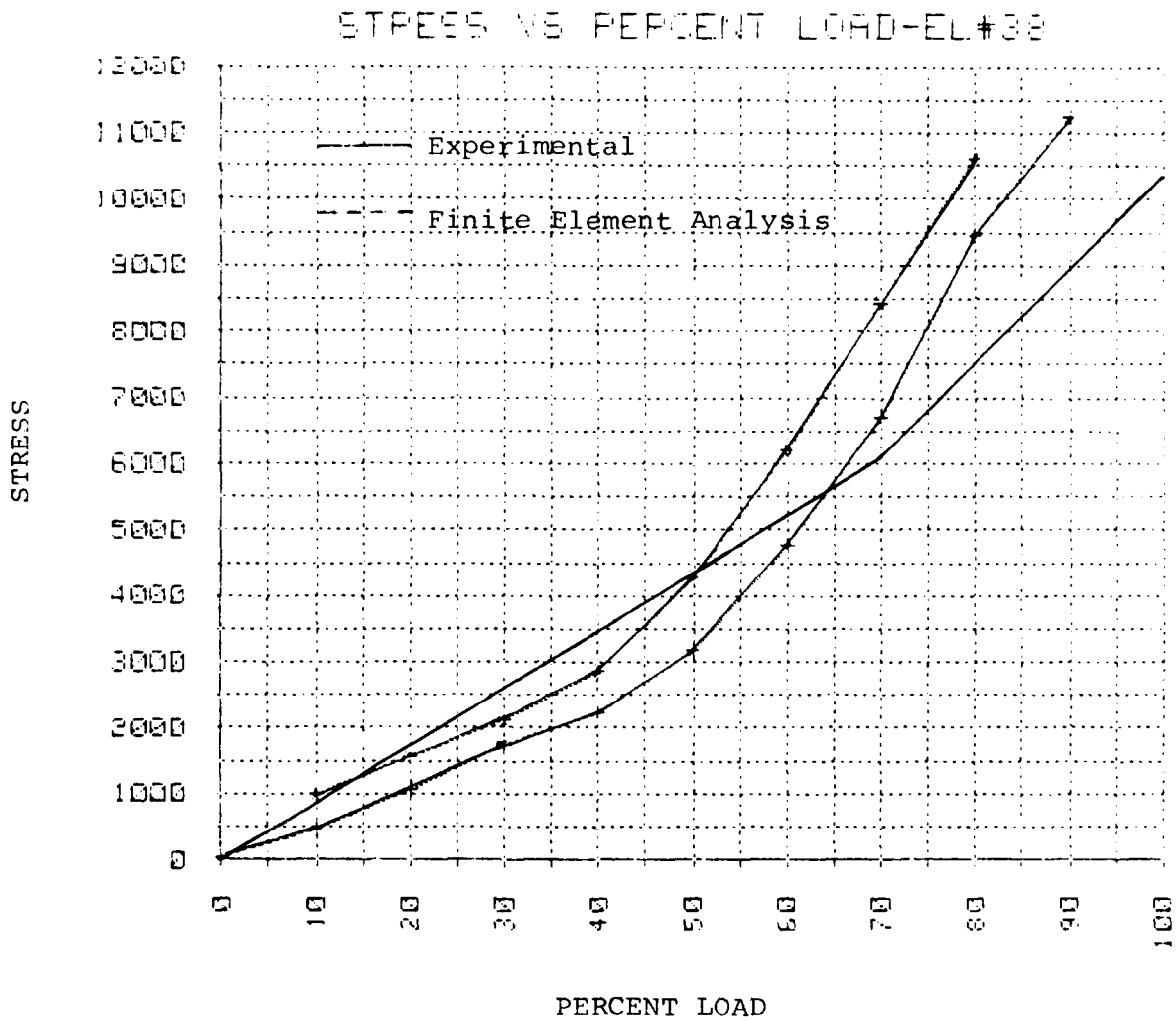

Figure 3.17i. Equivalent Stress-Rib Web Element 38.

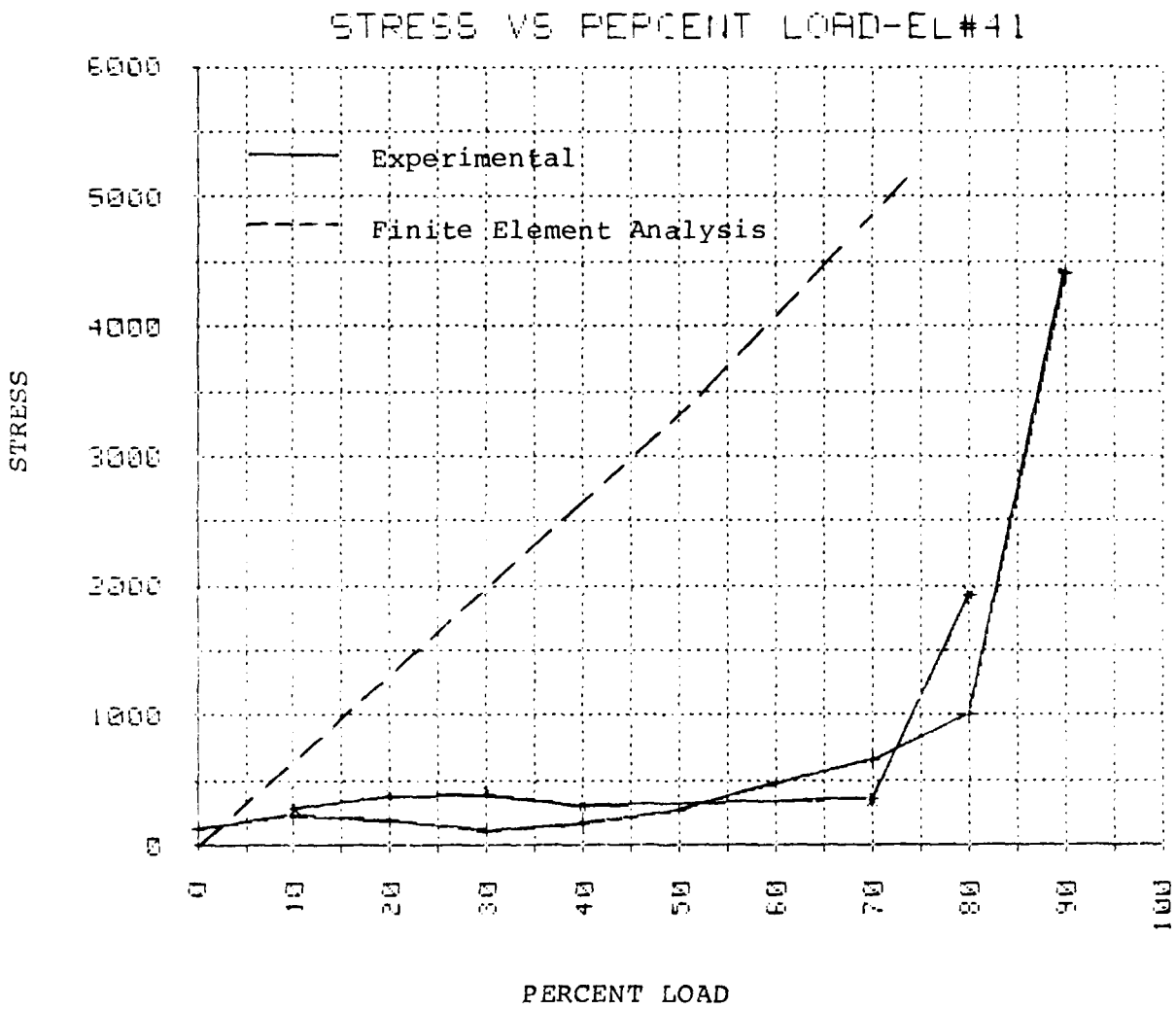

Figure 3.17j. Equivalent Stress-Spar Web Element 41.

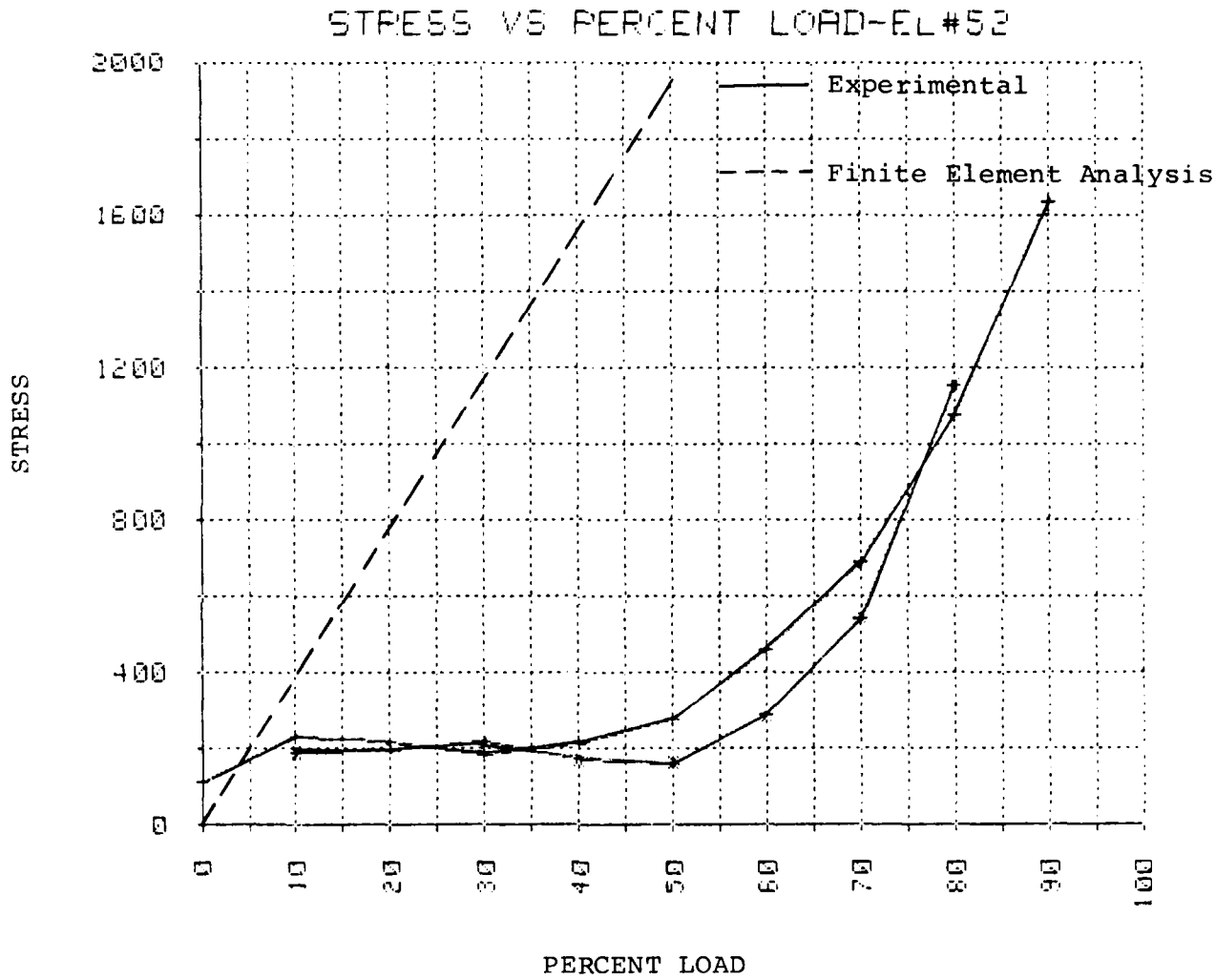

Figure 3.17k. Equivalent Stress-Spar Web Element 52.

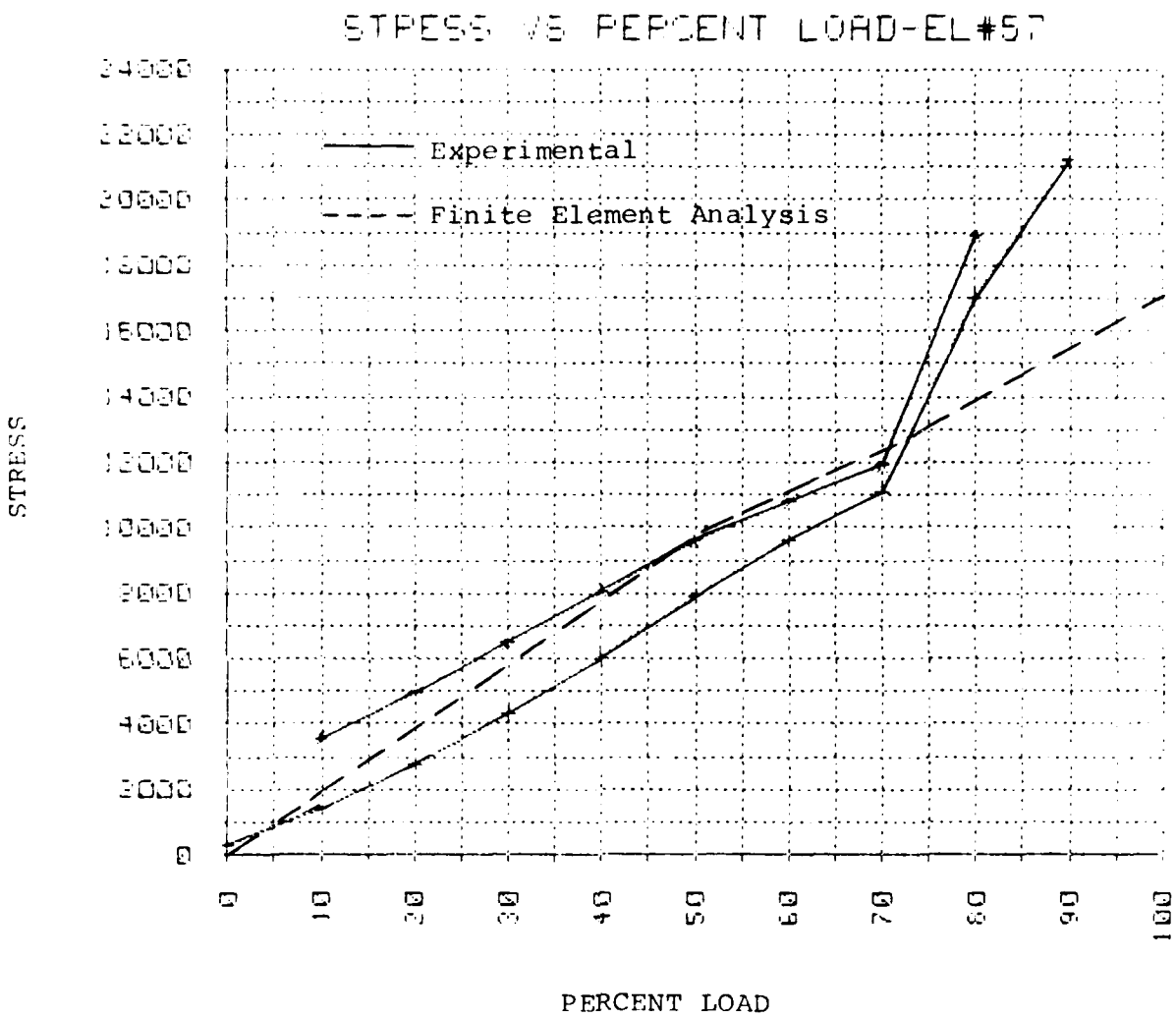

Figure 3.171. Equivalent Stress-Spar Web Element 57.

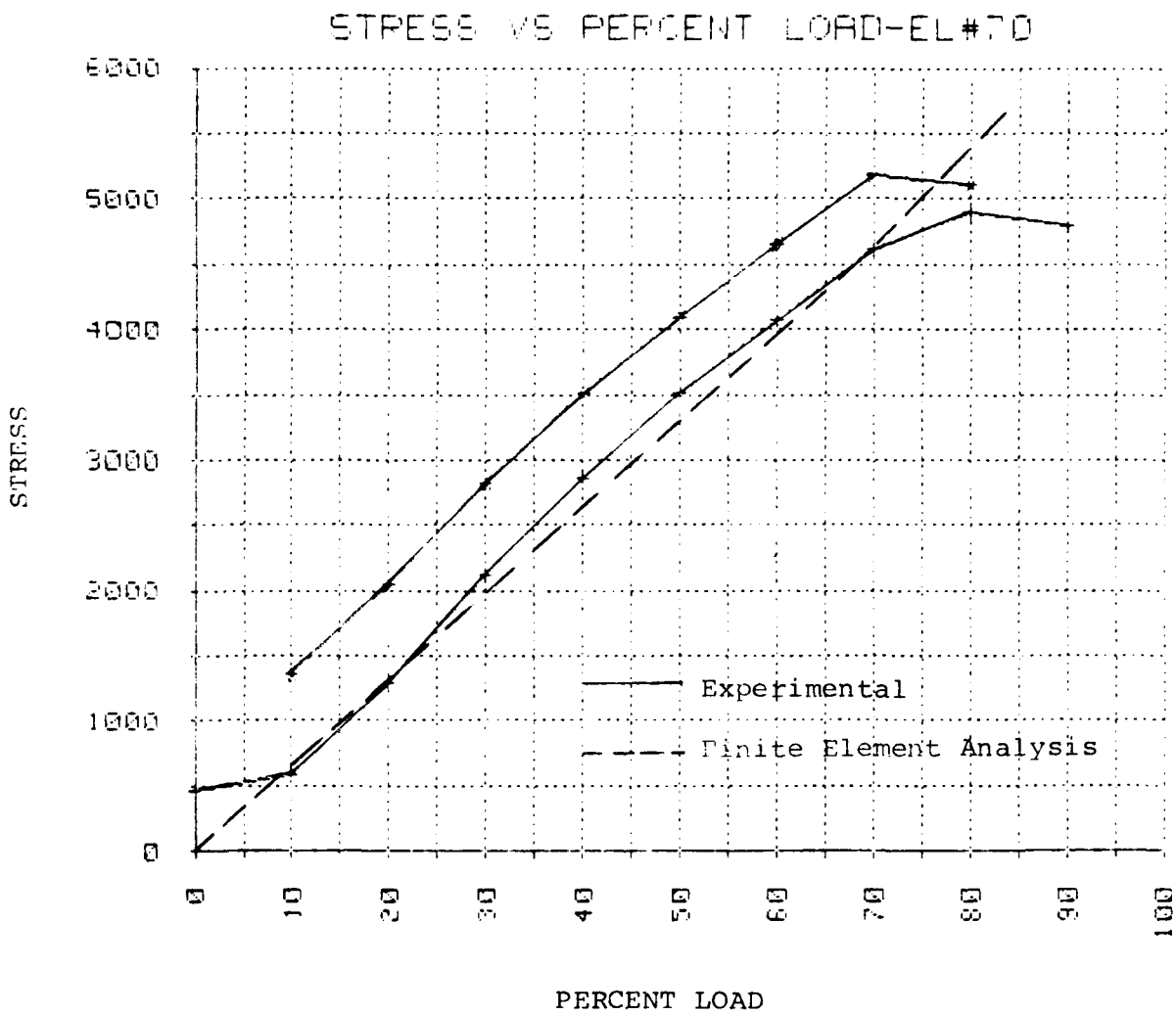

Figure 3.17m. Equivalent Stress-Spar Web Element 70.

the actuator forces were zero. The upper curve was obtained by taking into account the initial shear and moment applied to the specimen due to the weight of the loading plate.

There was rather good comparison between the experimentally obtained and analytically computed stresses of skin elements 13 and 15 (Figure 3.17a and b), the elements adjacent to the damaged section (Figure 3.16b). There was only fair agreement, however, for the other skin elements. This again indicates that the bar/membrane/shear panel finite element model is not sufficient to predict accurately the redistribution of stresses around a damaged area. Figures 3.17i-m refer to shear webs. The analytical/experimental comparisons for the shear web, run from fair (Figures 3.17i, l, m, n) to poor (Figures 3.17j, k). The erratic behavior of the gages attached to elements 41 and 52 indicate that there might have been some malfunction of these channels, however. The experimentally measured data showed a sudden change in the rate of stress growth at about the 70 percent load level. This was due to buckling of the compression skin around the area of the split spar caps. The bar/membrane/shear panel model does not capture this buckling effect.

Figures 3.18a-e present plots of level contours of the Von Mises equivalent stress at various stages of the load incrementation.

3.6 TEST 5 - DAMAGED SPECIMEN, NUMBER 5

Specimen 5 had the largest amount of damage with all of the bottom skin and all of the interior spar webs and spar caps in one bay of the specimen missing. The same combination of spanwise bending and spanwise shear was applied to this specimen as was applied to the other damaged specimens. The loading was increased proportionally until failure of the specimen occurred.

3.6.1 Instrumentation

Figure 3.19 shows the relative locations of strain gages monitored during Test 5. Both the rosettes and individual gages are numbered in the figure.

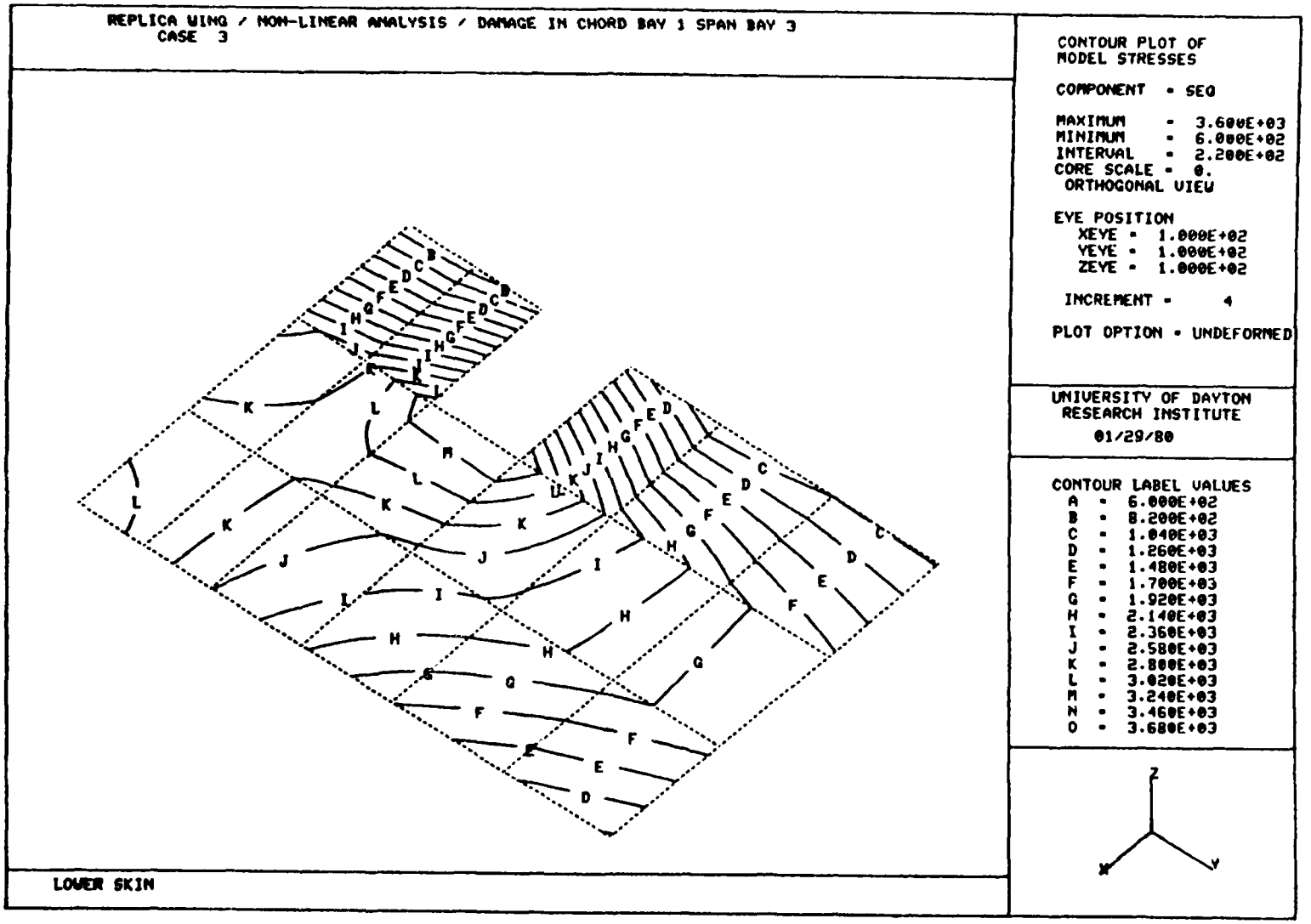

Figure 3.18a. Contours of Equivalent Stress - 20% Load.

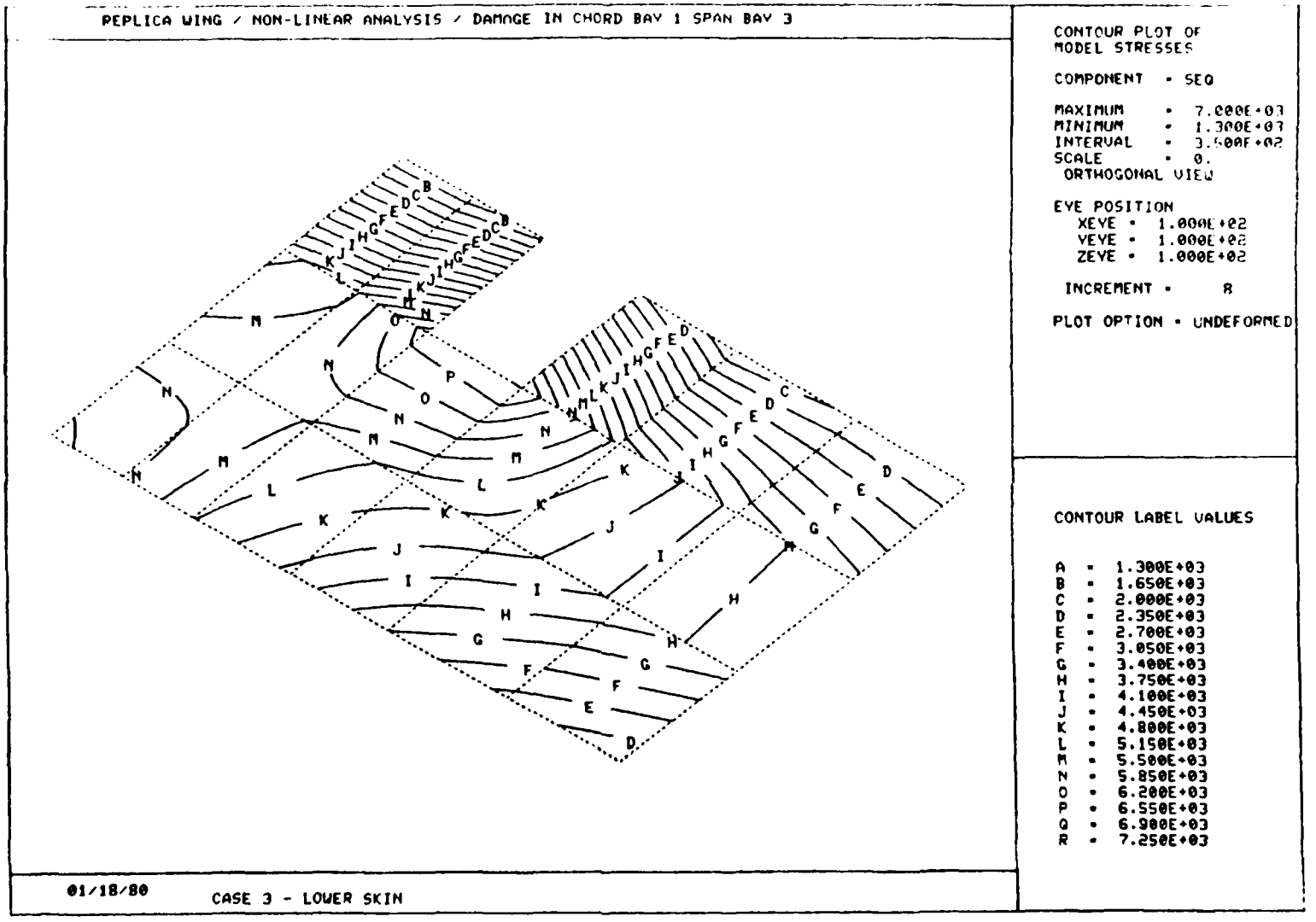

Figure 3.18b. Contours of Equivalent Stress - 40% Load.

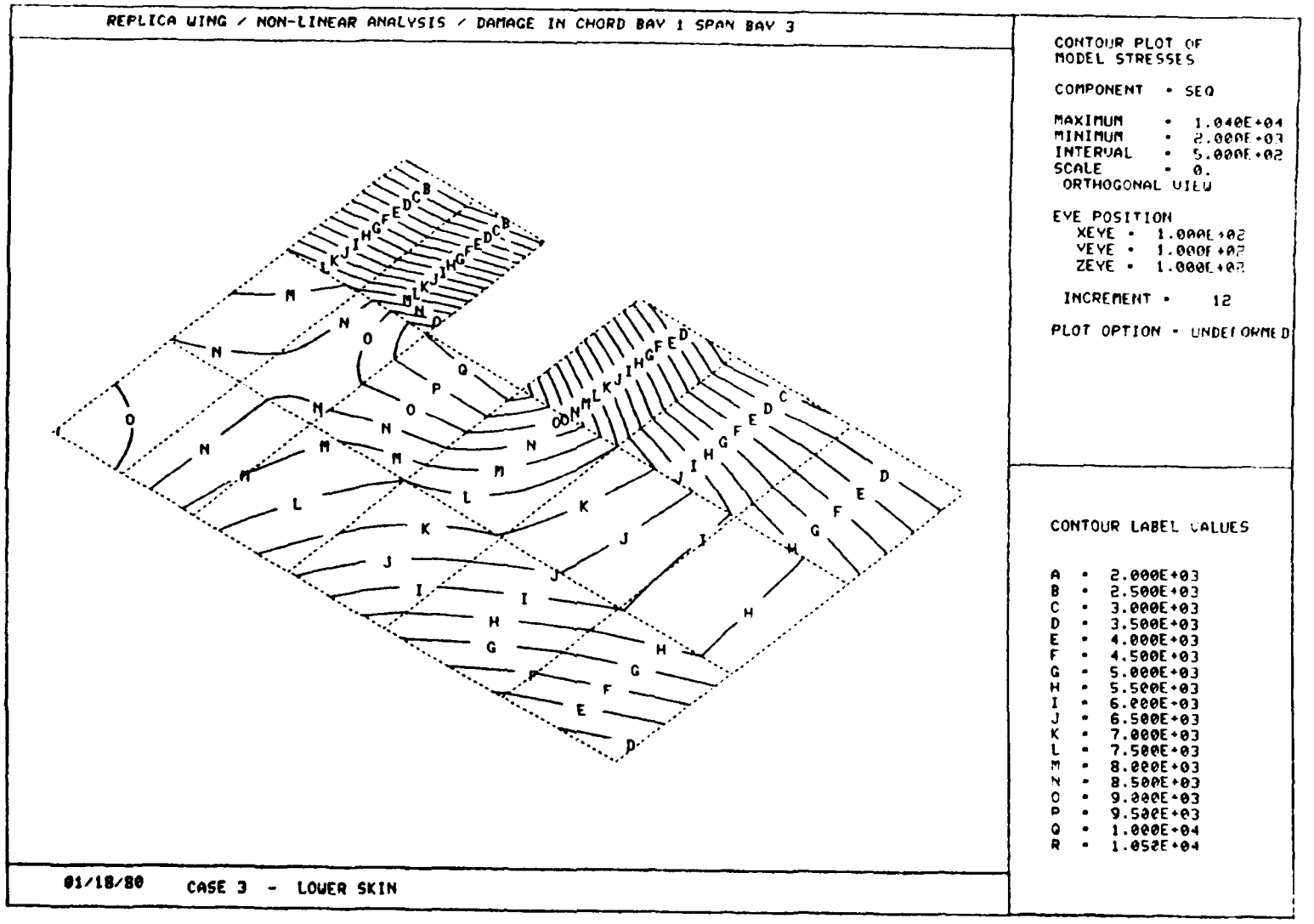

Figure 3.18c. Contours of Equivalent Stress - 60% Load.

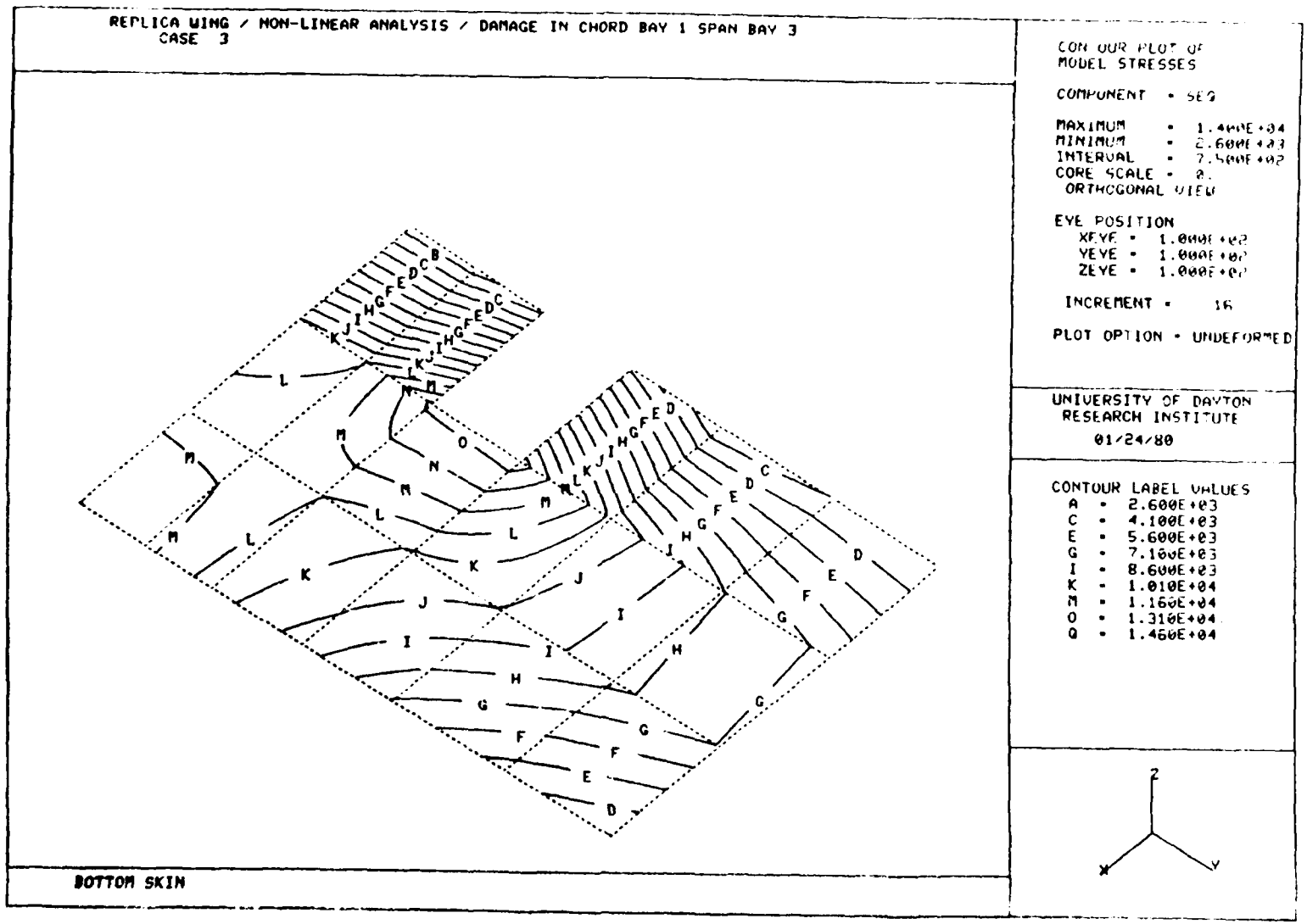

Figure 3.18d. Contours of Equivalent Stress - 80% Load.

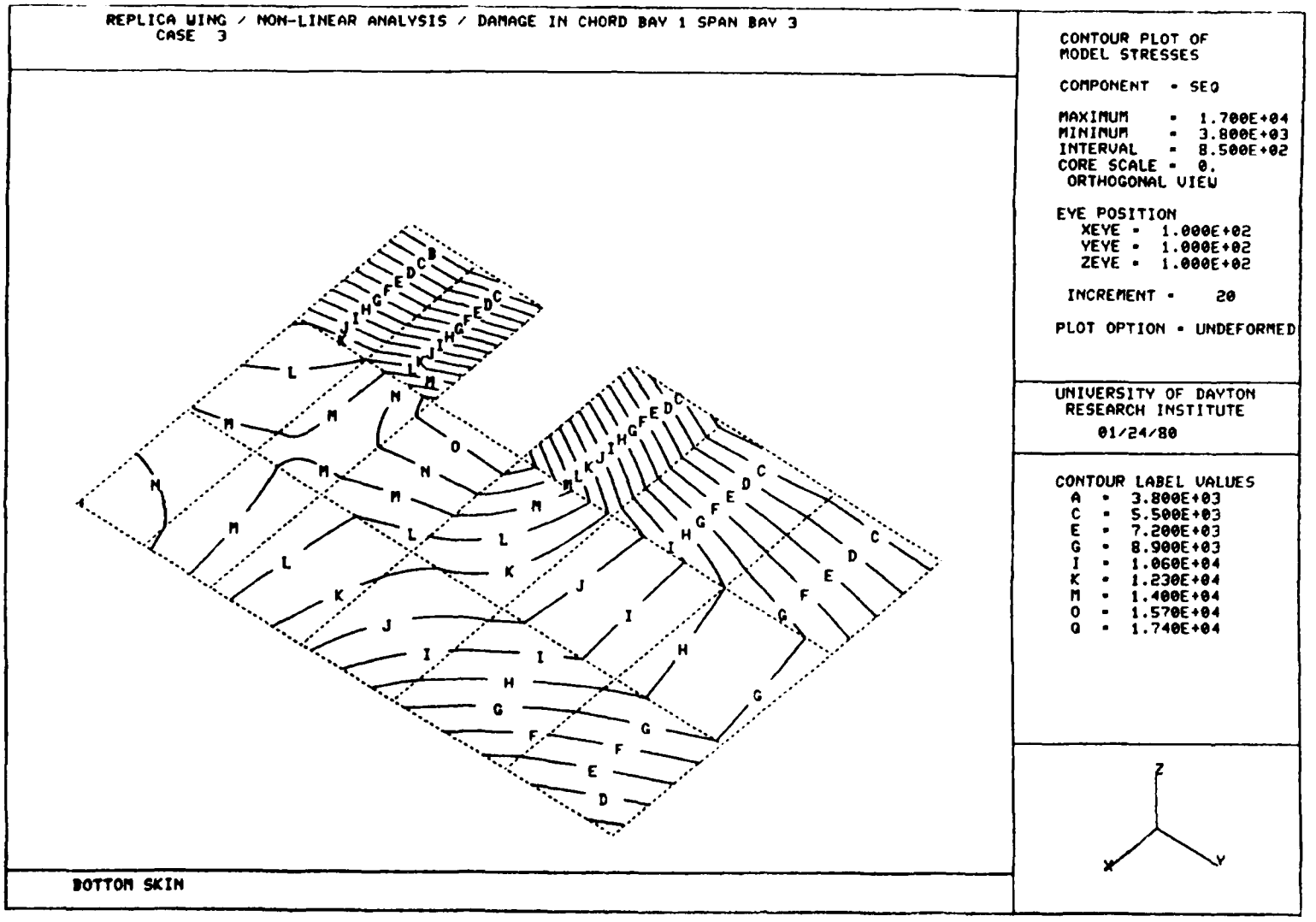

Figure 3.18e. Contours of Equivalent Stress - 100% Load.

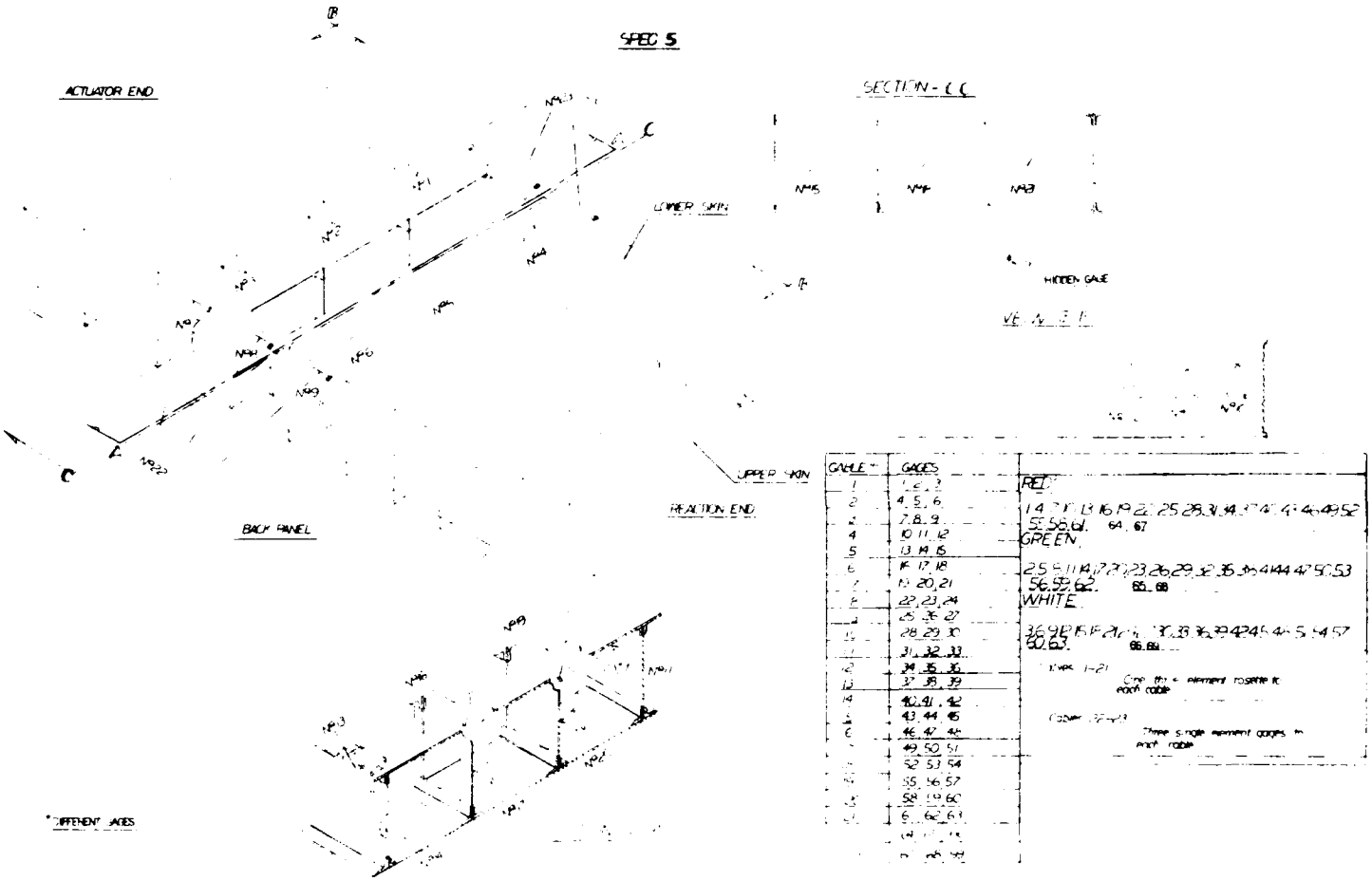

Figure 3.19. Strain Gage Locations - Specimen 5.

3.6.2 Loading

The maximum load set up at the control console corresponded to a combination of spanwise bending moment ($\bar{M}_s = 5.4 \times 10^6$ in. lb.) and spanwise shear load ($\bar{V}_s = 30{,}000$ lb.). The individual actuator loads corresponding to these section loads were (from Equations 3.2):

$T_1 = 45{,}573$ lb. Compression

$T_2 = 49{,}344$ lb. Compression

$T_3 = 25{,}497$ lb. Tension

$T_4 = 29{,}426$ lb. Tension

3.6.3 Load Incrementation and Data Collection

During the test of Specimen 5, the individual actuator forces were increased incrementally in steps equal to 5 percent of the maximum values given above. At each stage of the loading, strain gage readings were recorded by a minicomputer. A computer program converted the gage signals into units of strain, and computed the associated material stresses. In the case of the rosettes, the minimum and maximum principal stresses, the maximum shear stress, the principal angle, and the Von Mises equivalent stress were computed. An example of the output of the data reduction program for Test 5 is shown in Figure 3.20. The output corresponds to 20 percent of the maximum loads defined above.

3.6.4 Analysis Model

The finite element model for specimen 5 is shown in Figure 3.21a-e. The modeled portion of the replica specimen is that part of Figure 2.12 which has the bays numbered. As mentioned before, in the experimental facility the two end bays of the specimen are clamped by mounting brackets, and are therefore not considered in the analysis. The model contains 56 nodes, 33 skin membrane elements, 22 spar web panel elements, 15 rib web shear panel elements, 44 spar cap bar elements, and

SPECIMEN #5, TEST #7 4/ 1/80 12 :1.20 READING 149

E= 10 300 MU= .330

BASIC CHANNELS

CH	---MV---	-VALUE--	
1	-497.000	-4.959	P1
2	-466.750	-4.664	P2
3	153.750	1.540	P3
4	301.000	3.011	P4
5	-3.250	- .007	P5
6	-1960.500	19.997	%L
7	27.500	450.628	MP
8	57.150	.571	D1
9	56.012	.560	D2
10	63.137	.631	D3

DEFLECTION CHANNELS

	WEST SIDE	MIDDLE	EAST SIDE
DEFLECTION			
ANGLE (DEG)	.2671	.0000	.0000
TOP DEF	- .2273		.0000
BOT DEF.	.0734		.0000
BASE EFLECTION			
ANGLE (DEG)	.1363	.1221	.1080
TOP DEF.	-.1570		-.1188
BOT DEF.	-.0036		-.0020
UNCORRECTED DEFLECTIONS			
D1 (2.12)	.0368		.0128
D2 (12.62)	.0673		.0705
D3 (39.25)	.1917		.2127
D4 (55.75)	.2987		.3005
D5 (87.25)	.5601		.5715
D6 (93.50)		.6314	
CORRECTED DEFLECTIONS			
D1 (2.12)	.0216		.0008
D2 (12.62)	.0162		.0384
D3 (39.25)	.0773		.1304
D4 (55.75)	.1442		.1864
D5 (87.25)	.3310		.3983
D6 (93.50)		.4163	

Figure 3.20. Sample Experimental Data - Specimen 5.

STRAIN GAGE DATA				PRINCIPAL STRESS CALCULATIONS					
CH	MV(CORR)	USTRAIN	-STRESS- (PSI)	ROS-ETTE	MIN PR STRESS	MAX PR STRESS	MAX SHEAR	ANGLE	EQUIV STRESS
1	- 521	-100 78	-495						
2	534	103 38	1087						
3	.567	109 82	1136						
				2001	-495	1647	1071	90 77	1943
4	- 217	-42 03	-414						
5	.217	41 88	236						
6	-.180	-34 71	-357.						
				2002	-594	237	416	62 26	742
7	.522	100 89	992						
8	.467	90 40	911						
9	- 561	-108 49	-630						
				2003	-631	1479	1055	28 73	1876
10	.615	118 91	1230						
11	640	123 65	1267						
12	- 625	-120 86	-627						
				2004	-627	1874	1250	30 49	2254
13	- 318	-61 51	-675						
14	319	61 70	279						
15	-.405	-78 22	-804						
				2005	-1083.	284	683	56 86	1249.
16	-.799	-154 67	-999						
17	.604	116 81	1104						
18	.600	116 20	1099.						
				2006	-999.	1802.	1400.	89 94	2458.
19	-.372	-71 85	-294						
20	-.132	-25 54	65						
21	1 039	200 73	1817						
				2007	-775.	1834	1304	115 43	2320
22	.000	.00							
23	-1.116	-212 56	-2189.						
24	-1.329	-252 86	-2604						
25	-1 268	-242 22	-2495						
26	-.993	-188 87	-1945.						
27	-2.650	-119046.	4-1226178.						
28	-.238	-46 02	-100.						
29	-.154	-29 78	26.						
30	914	176 70	1625.						
				2010	-593	1627.	1110.	118 13	1991.

Figure 3.20. (continued).

31	071	13.73	522.						
32	-.061	-11.80	324						
33	.837	161.51	1666.						
				2011	1	1674	837.	123.92	1674.
34	.381	73.67	900						
35	.000	.00	329						
36	.288	55.76	761.						
				2012	320.	1007	344.	-23.26	891
37	.159	30.83	189						
38	-.035	-6.86	-103						
39	-.224	-43.46	-386						
				2013	-432.	232.	332.	14.75	584.
40	-.134	-25.79	-761						
41	-1.000	-193.41	-2059						
42	-.009	-1.65	-574						
				2014	-2066.	-198	934.	-33.32	1974
43	-.201	-38.68	45.						
44	.214	41.58	667.						
45	.686	132.57	1371						
				2015	-72.	1460.	766.	106.03	1498
46	.000	.00	-25						
47	-.025	-4.93	-63						
48	-.026	-5.02	-64						
				2016	-77.	-25	26	.48	68
49	-1.221	-232.88	-2399						
50	-1.275	-243.04	-2503.						
51	.000	.00							
52	.076	14.69	213.						
53	.059	11.39	188						
54	.067	13.05	201.						
				2018	186	215	15	-15.10	202
55	-.244	-47.15	-339						
56	.021	4.06	58						
57	.277	53.53	441						
				2019	-397	504	450	104.71	782
58	-.076	-14.68	-686						
59	-1.023	-197.38	-2101						
60	-.067	-12.93	-672						
				2020	-2101	-205	948	-30.24	2006
61	2.379	449.94	4634						
62	.000	.00							
63	2.404	456.99	4707						

Figure 3.20. (continued).

64	.000	.00	.						
65	.000	.00	.						
66	.000	.00	.						
67	-.172	-33.32	49.						
68	-.097	-18.86	161.						
69	.893	172.73	1644.						
				2023	-411.	1646.	1029.	118.20	1886.
70	.000	.00							
71	2.642	501.06	5161.						
72	2.338	443.59	4569.						
73	2.321	440.48	4537.						
74	2.773	525.91	5417.						
75	.000	.00	.						
76	.196	38.00	536.						
77	-.108	-20.89	80.						
78	.400	77.77	844.						
				2026	42.	930.	444.	-41.81	910.
79	-.106	-20.43	-689.						
80	-.812	-157.14	-1748.						
81	-.162	-31.31	-774.						
				2027	-1750.	-391.	679.	-27.95	1591.
82	.561	108.58	965.						
83	.060	11.70	215.						
84	-.370	-71.39	-429.						
				2028	-555.	1056.	805.	13.73	1417.

Figure 3.20. (concluded).

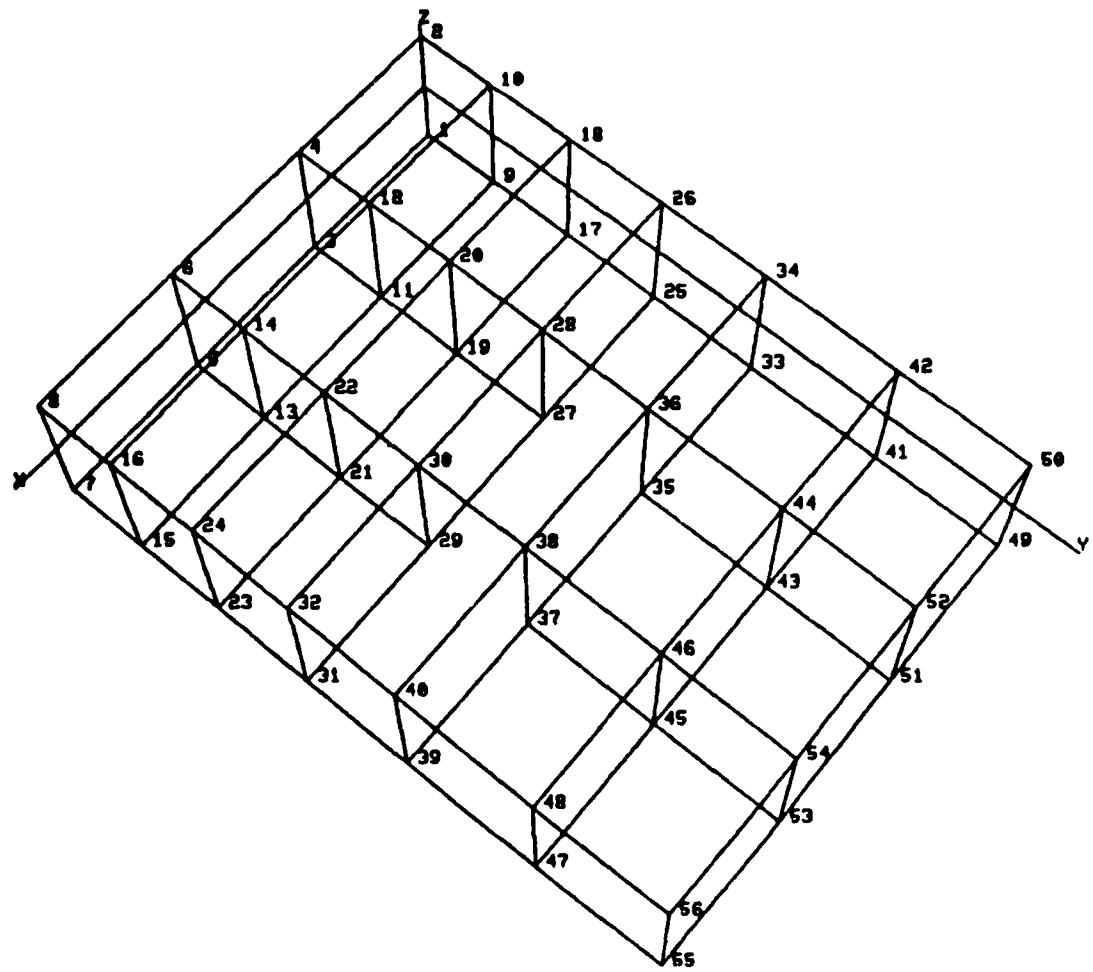

Figure 3.21a. Specimen 5 Finite Element Model - Node Numbers.

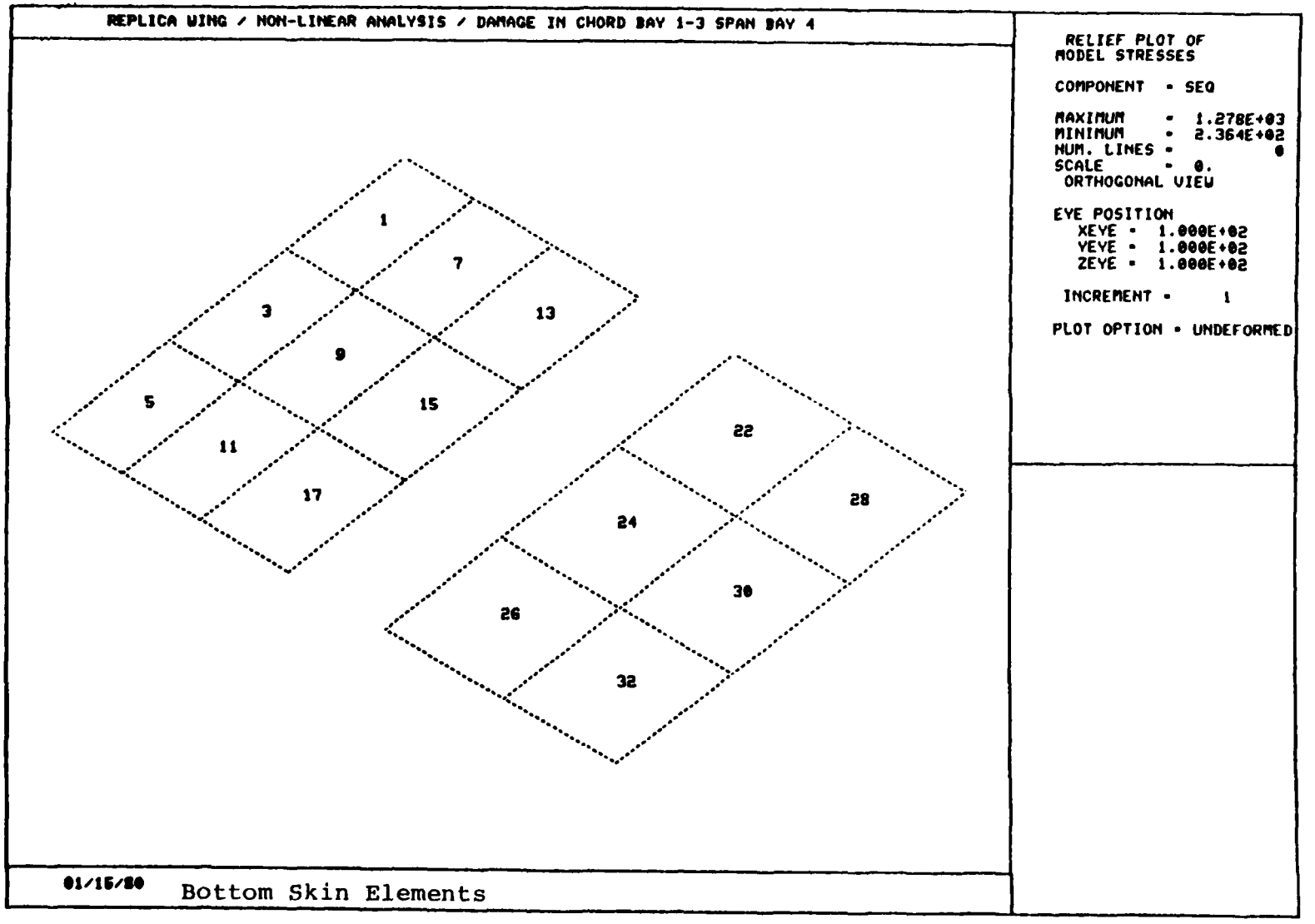

Figure 3.21b. Specimen 5 Finite Element Model - Bottom Skin Membrane Elements.

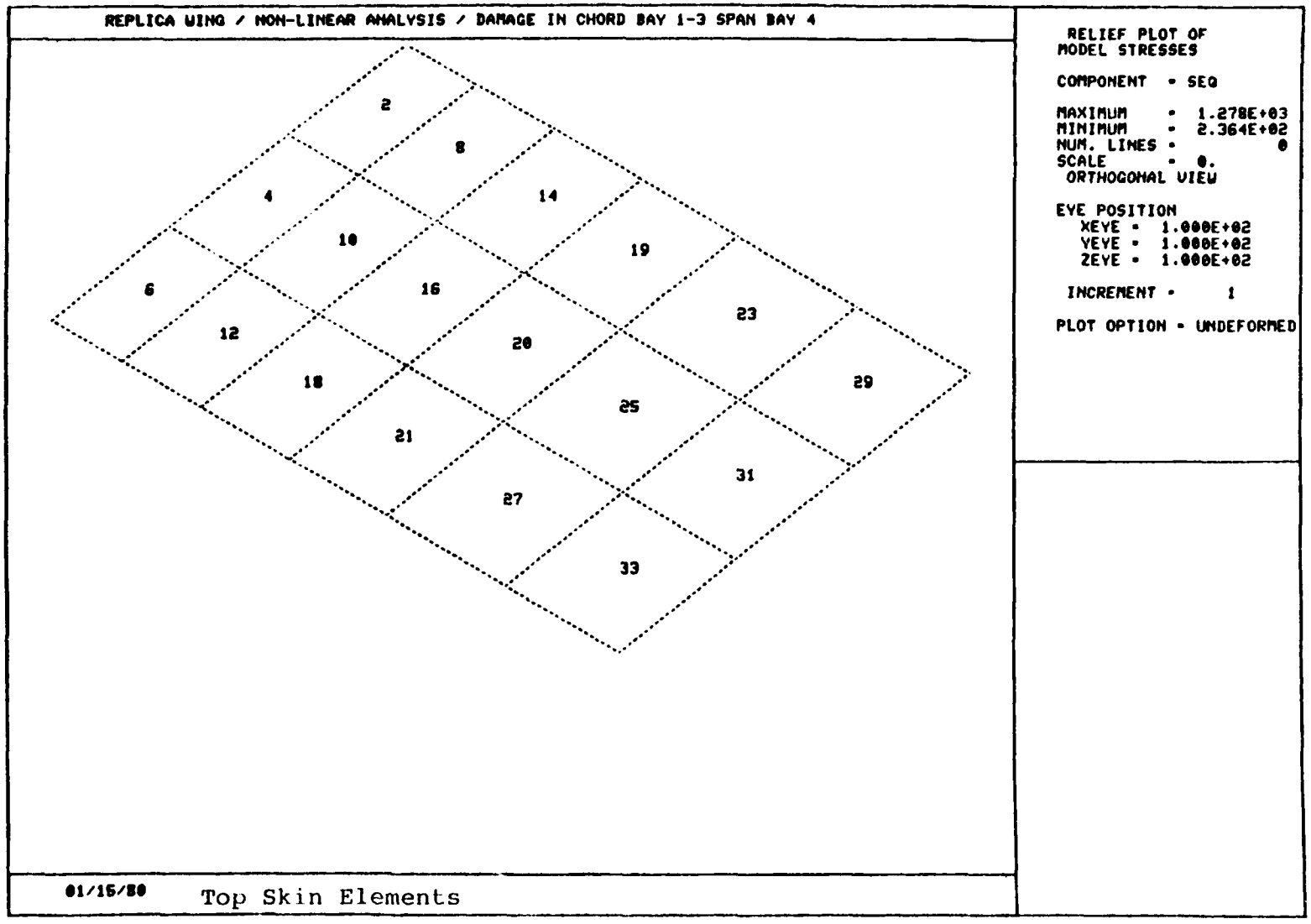

Figure 3.21c. Specimen 5 Finite Element Model - Top Skin Membrane Elements.

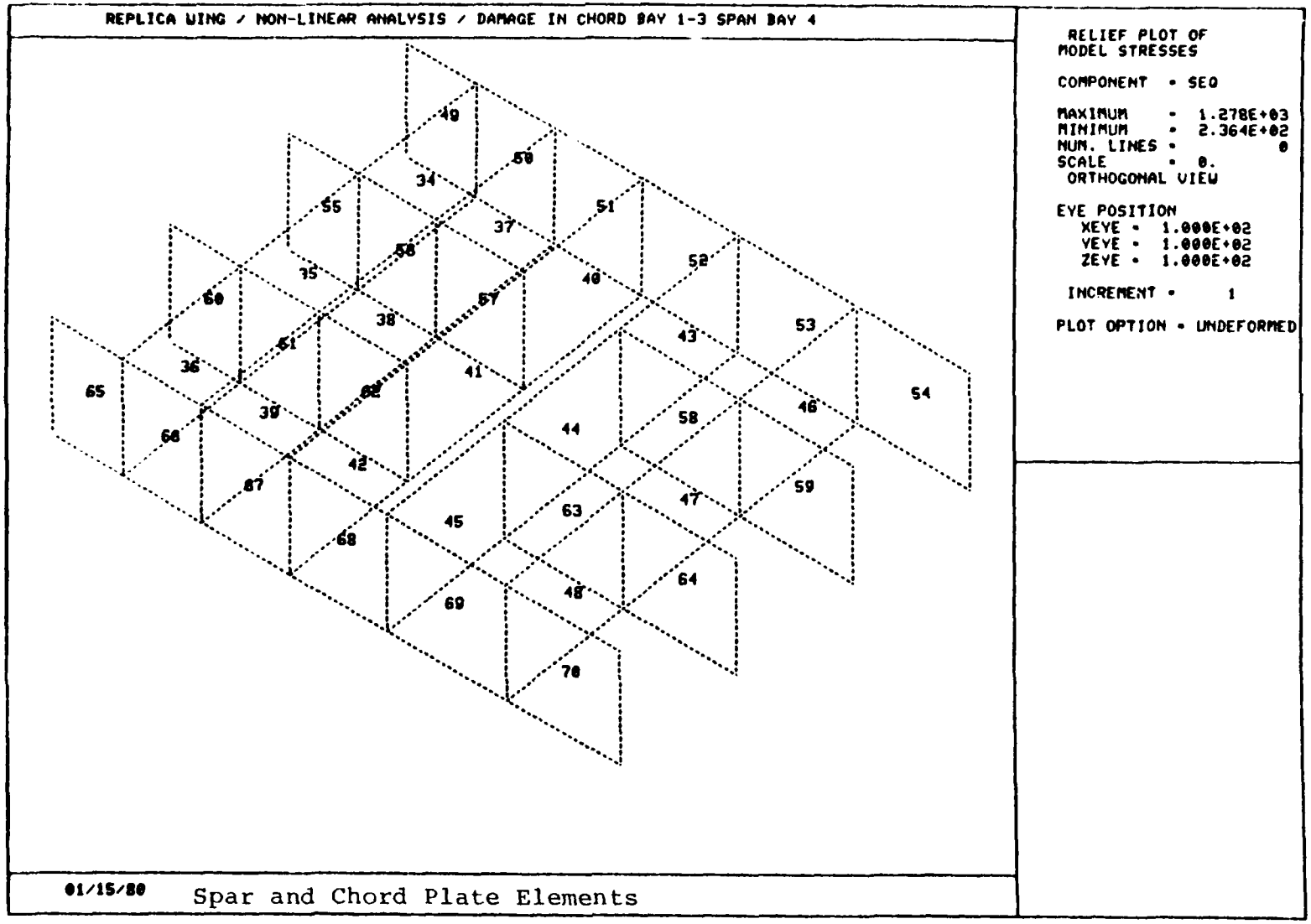

Figure 3.21d. Specimen 5 Finite Element Model - Spar and Rib Shear Panel Elements.

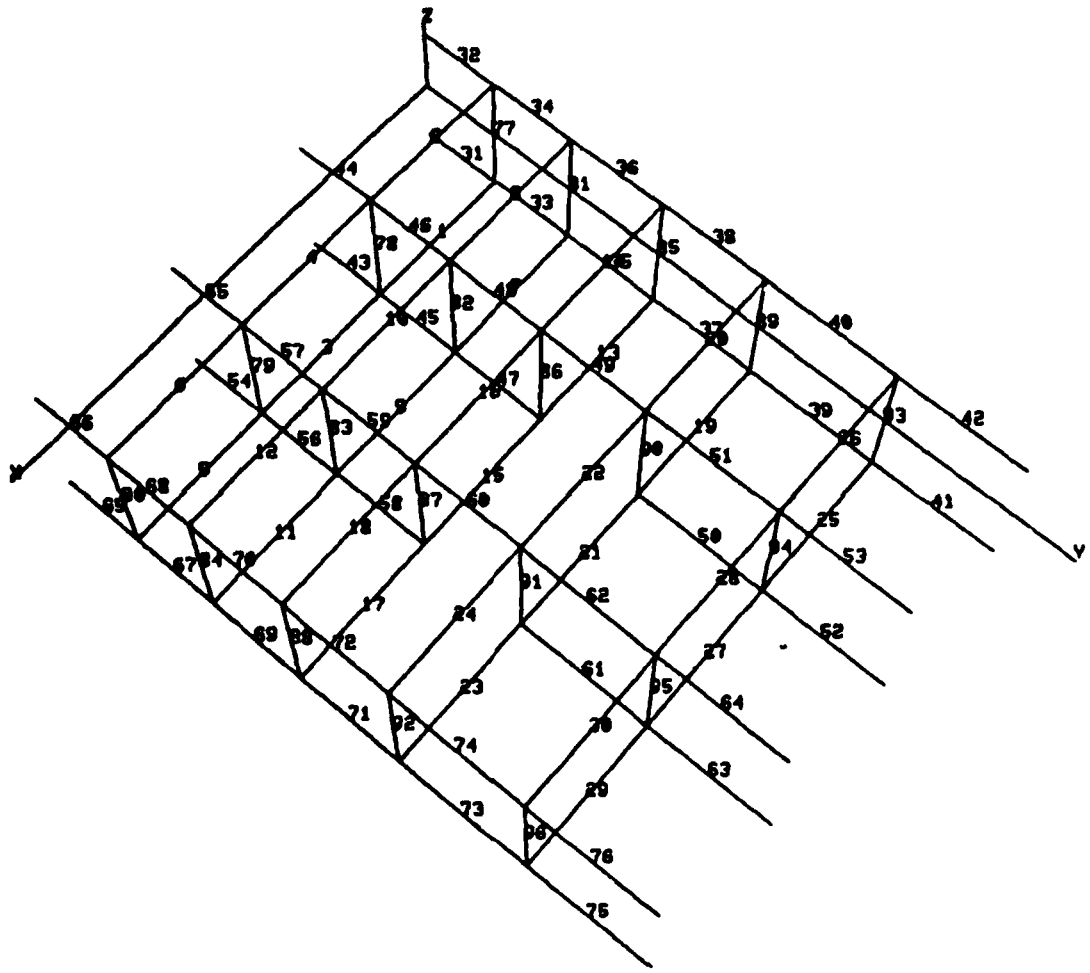

Figure 3.21e. Specimen 5 Finite Element Model - Spar and Rib Cap Bar Elements.

30 rib cap bar elements. Each of the 56 nodes has three degrees of freedom, the displacements parallel to the three coordinate axes. Eight of the nodes are fixed at the reaction end of the specimen (nodes 1-8). Therefore, the analysis model has 3 x 48 = 144 degrees of freedom.

3.6.5 Test/Analysis Results

Figures 3.22a-gg compare experimentally determined stresses with corresponding stresses computed with the finite element program. The skin element stresses are considered in Figure 3.22a-i. The best comparison between experimental and analytical determinations of skin stresses are for elements 19, 20, 21 (Figure 3.21c), the elements on the undamaged top surface. For skin elements 13, 15, 17, 22, 24, 26, the comparisons are not so close. This lack of comparison is again attributed to the inability of the simplified bar/membrane/shear panel finite element model to capture the redistribution of stresses about a damaged area. Figures 3.23a-d show plots of level contours of equivalent stress in the bottom skin for various load levels. All of the stress in the damaged skin must be directed around the damaged area through the spar webs and spar caps which bound the damaged area. Apparently the simplified finite element model is too coarse to predict the stress redistribution accurately.

The stresses in rib web panels 40-45 are considered in Figures 3.22j-o. Except for panel 43 the analytical and experimental results do not agree well. The stresses compare quite well in the case of the spar web panels 51, 52, 53, 67, 68, 69. The agreement is especially good for loading to about the 70 percent levels; above 70 percent the two results deviated substantially in many cases. This deviation at the higher load levels is attributed to the occurrence of local phenomena such as the failure of rivets and the buckling of compression panels which were observed during the test.

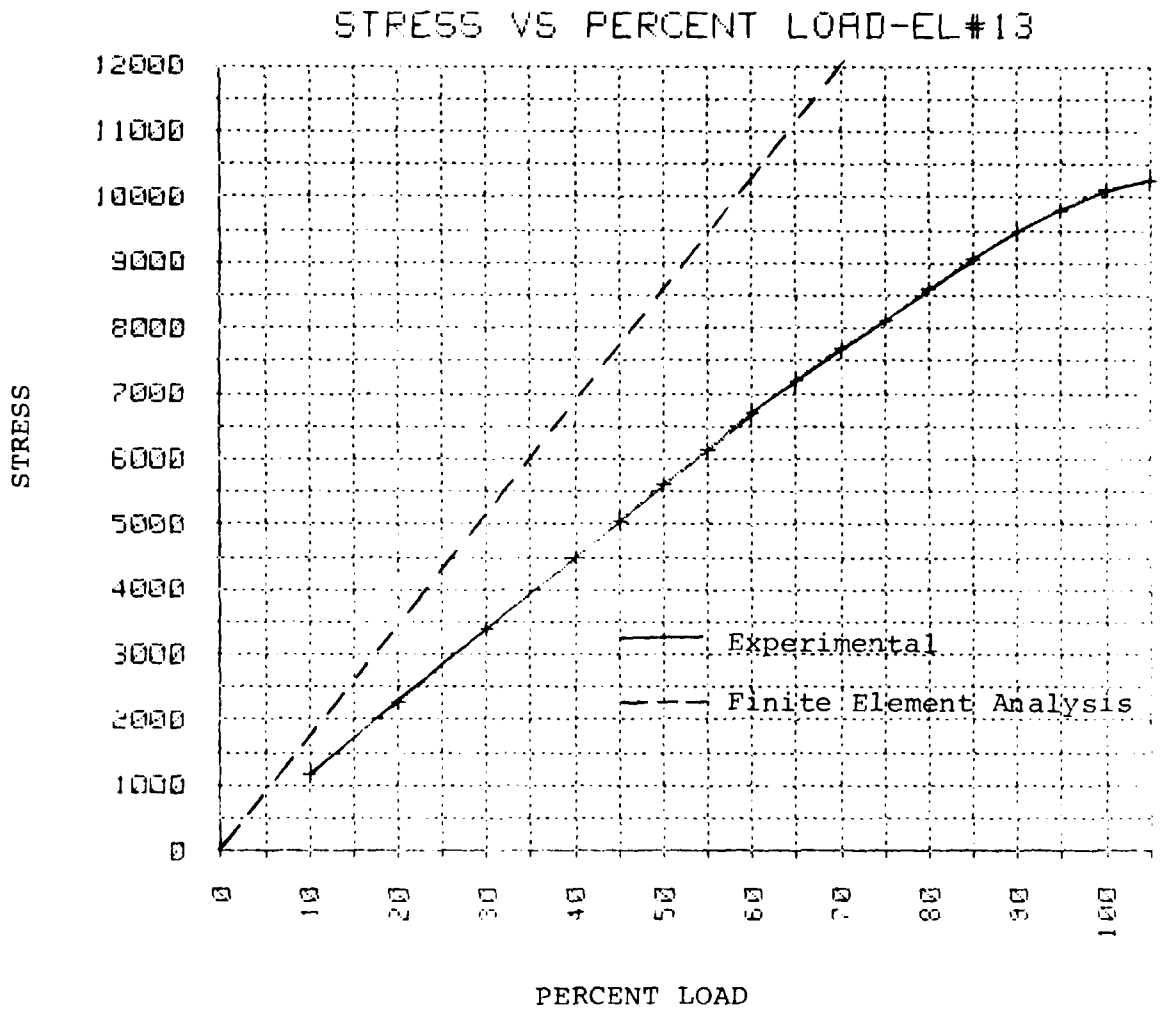

Figure 3.22a. Equivalent Stress-Skin Element 13.

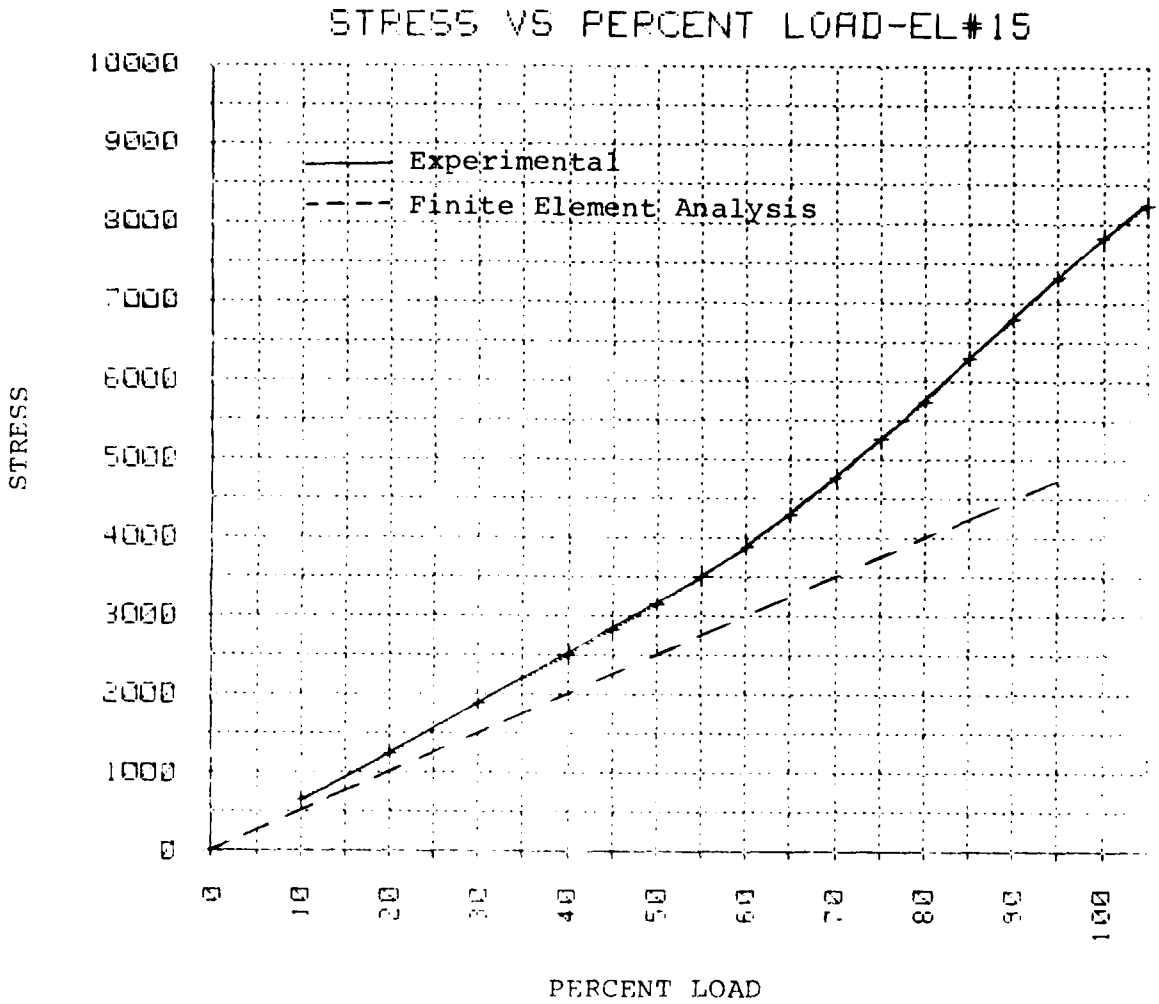

Figure 3.22b. Equivalent Stress-Skin Element 15.

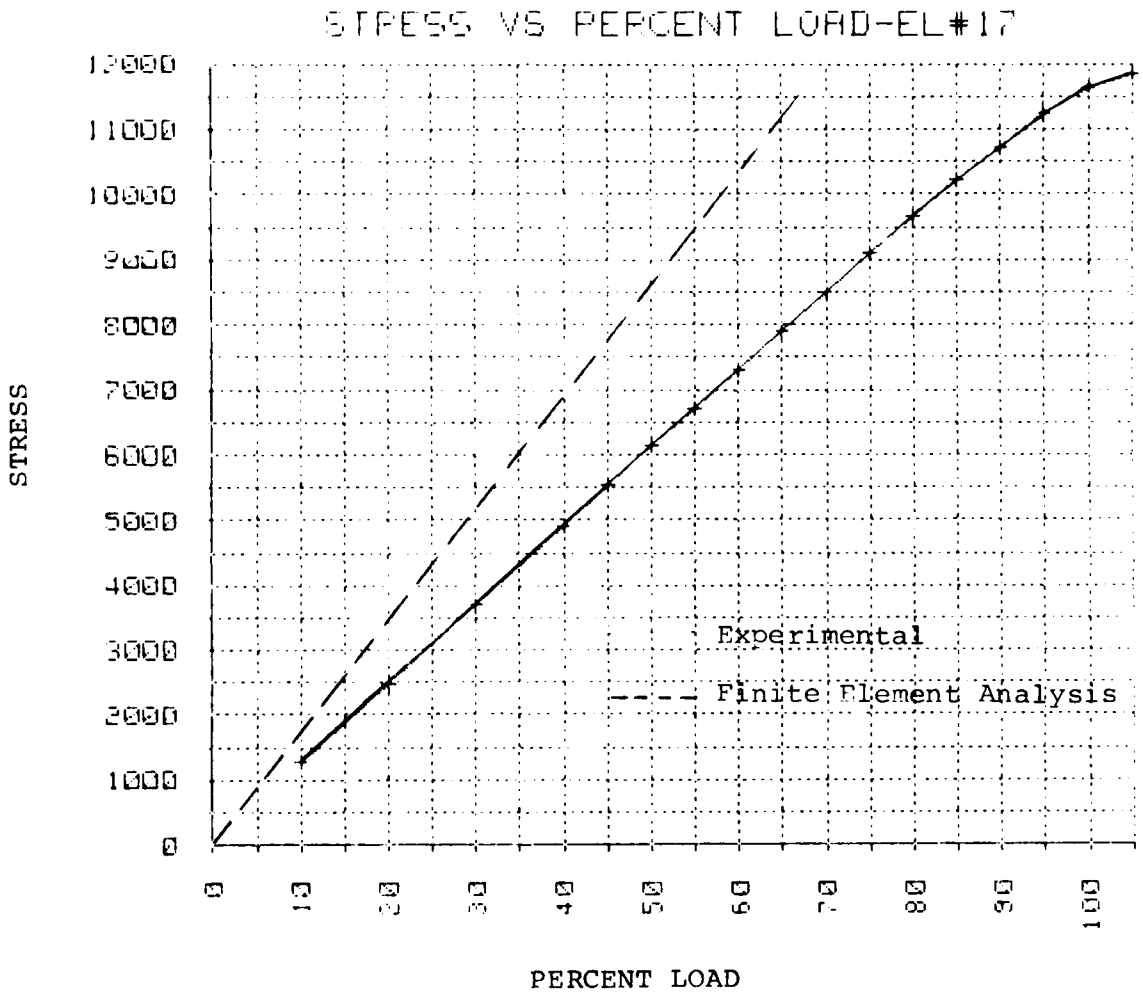

Figure 3.22c. Equivalent Stress-Skin Element 17.

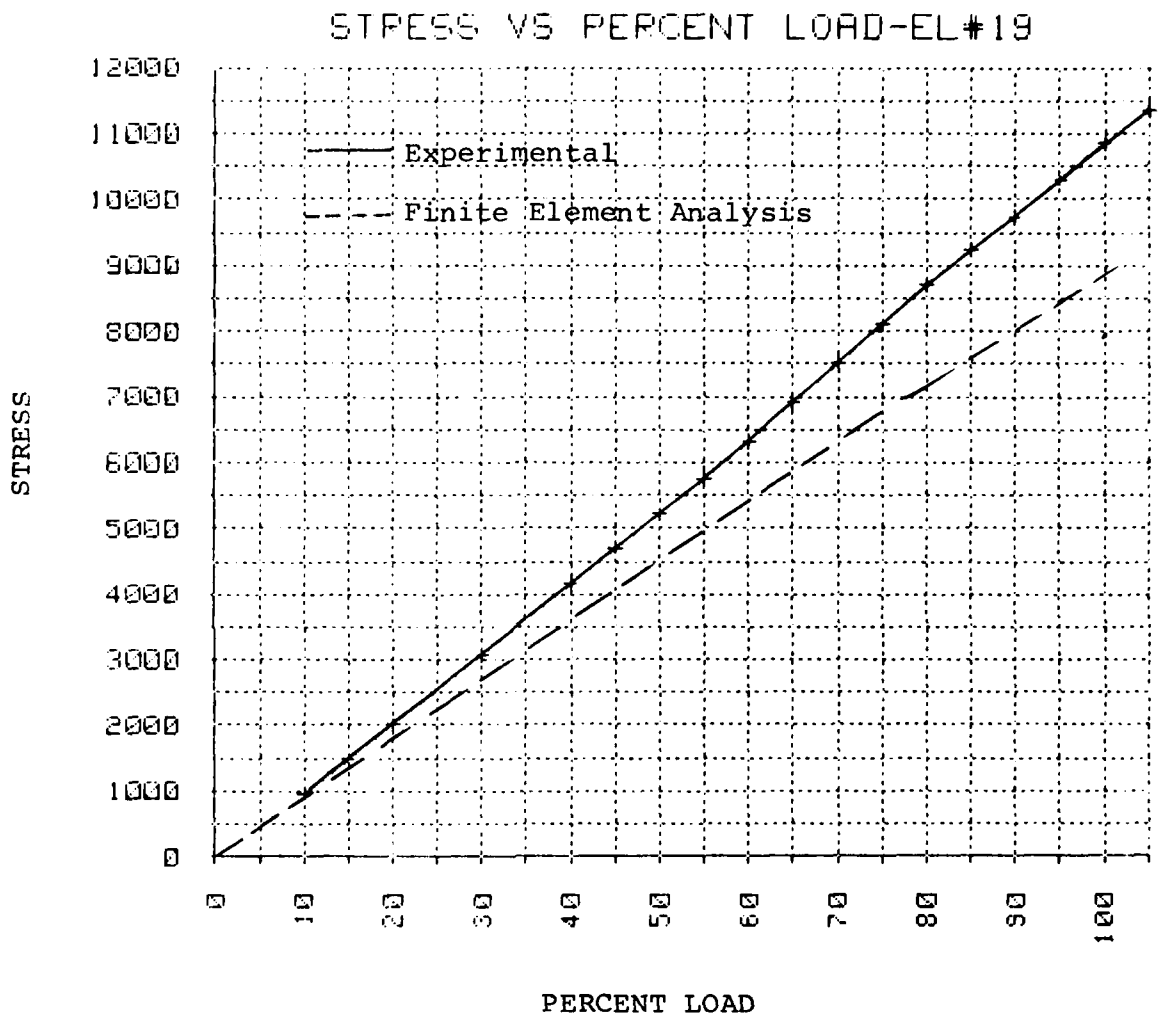

Figure 3.22d. Equivalent Stress-Skin Element 19.

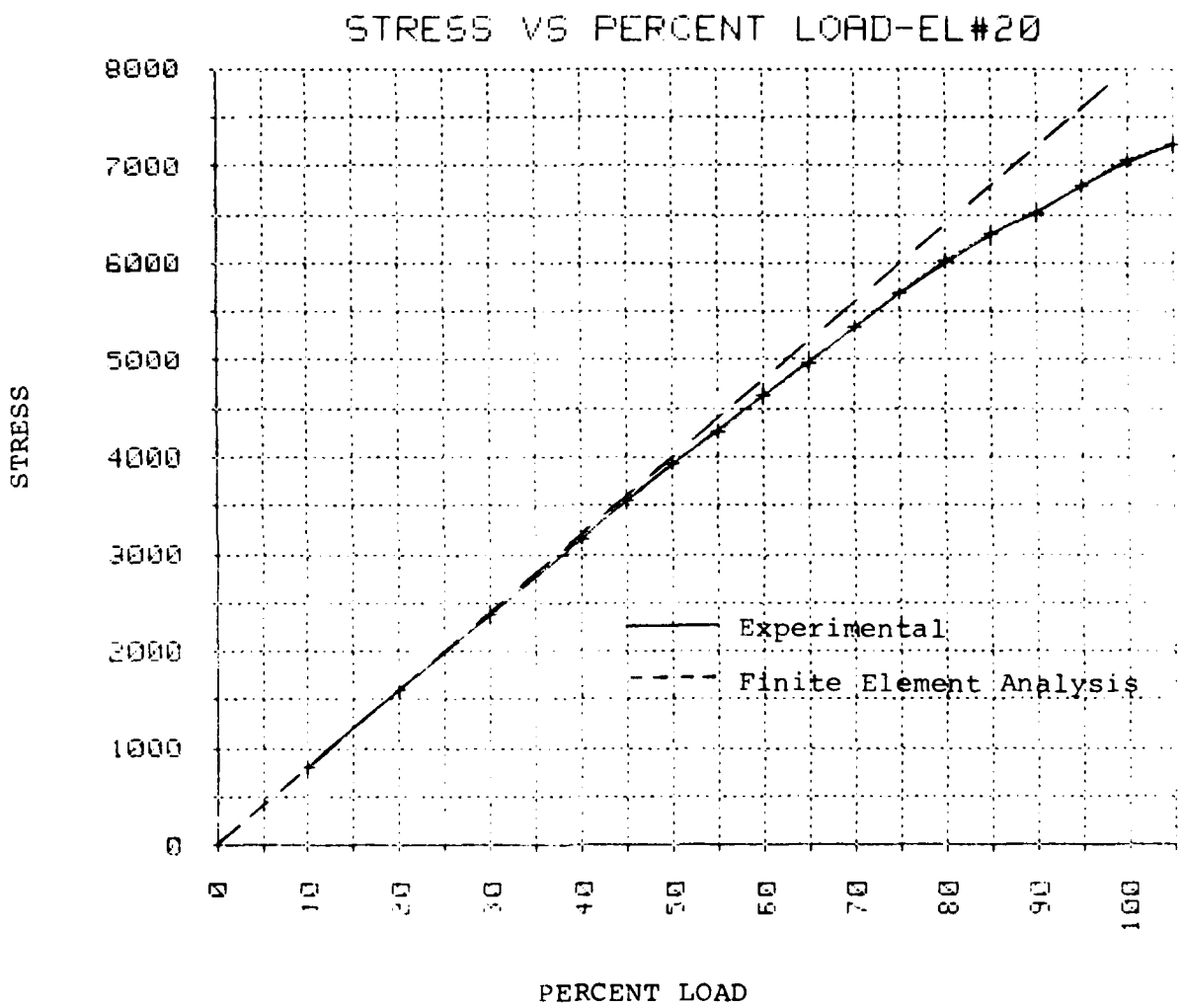

Figure 3.22e. Equivalent Stress-Skin Element 20.

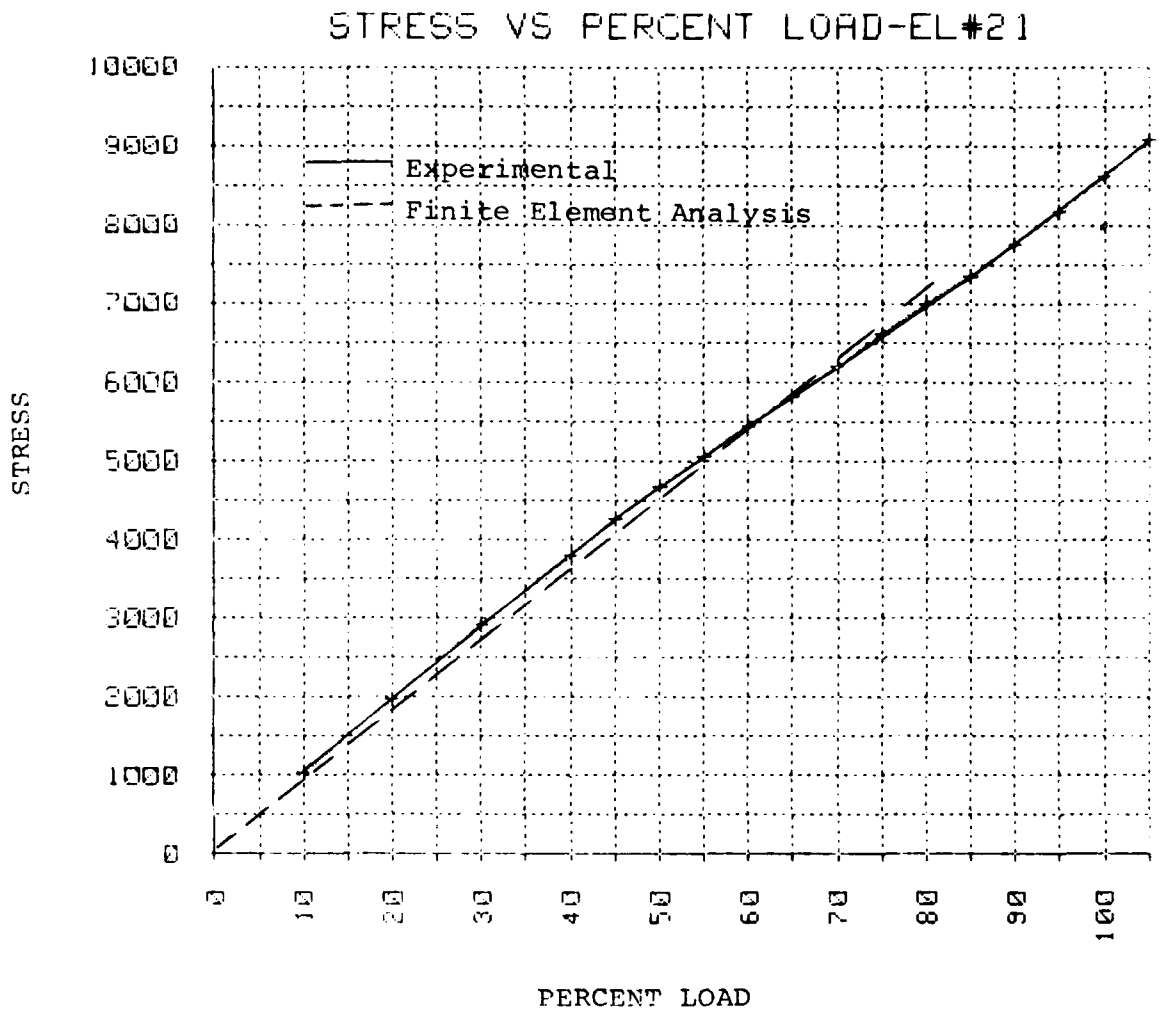

Figure 3.22f. Equivalent Stress-Skin Element 21.

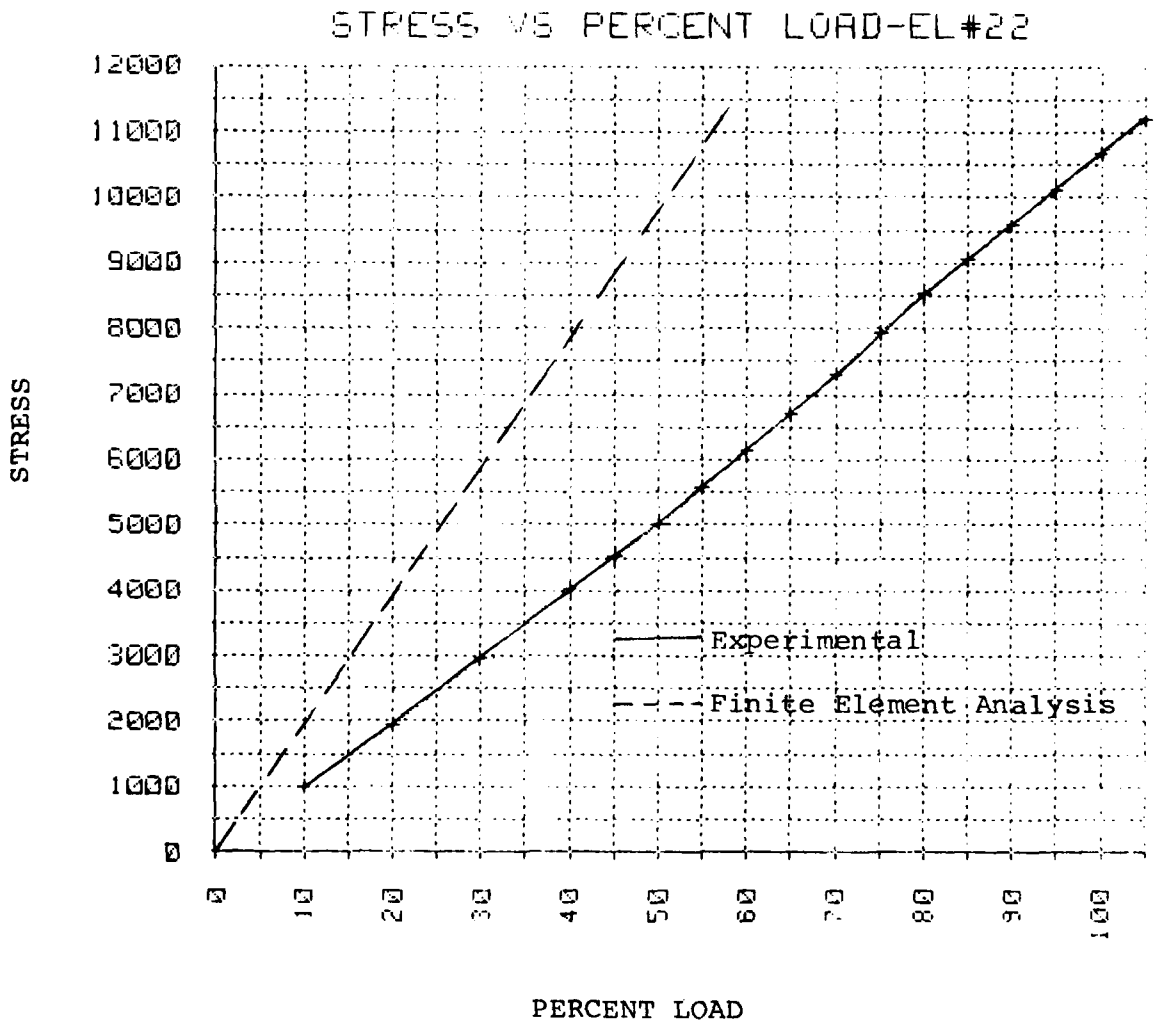

Figure 3.22g. Equivalent Stress-Skin Element 22.

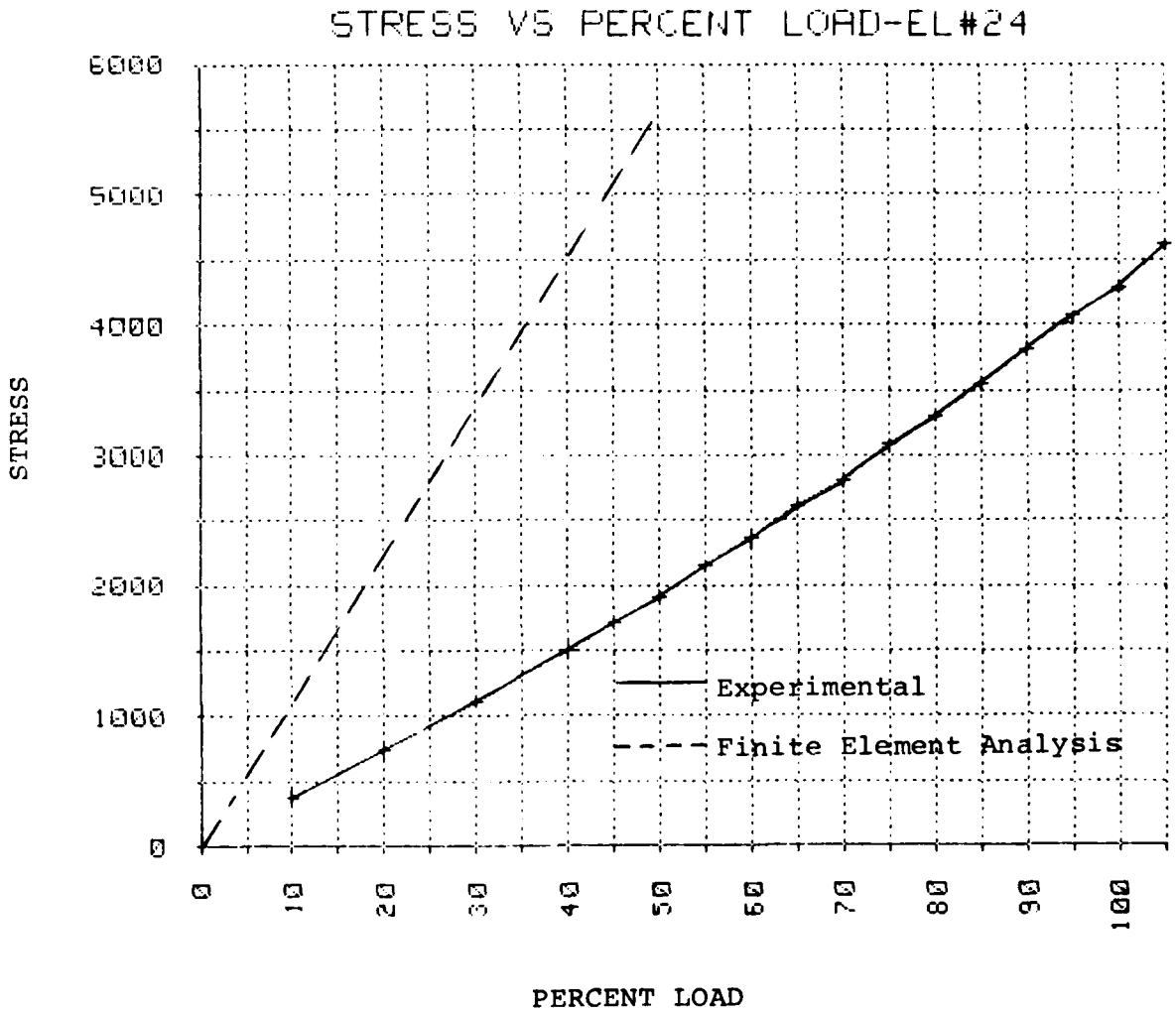

Figure 3.22h. Equivalent Stress-Skin Element 24.

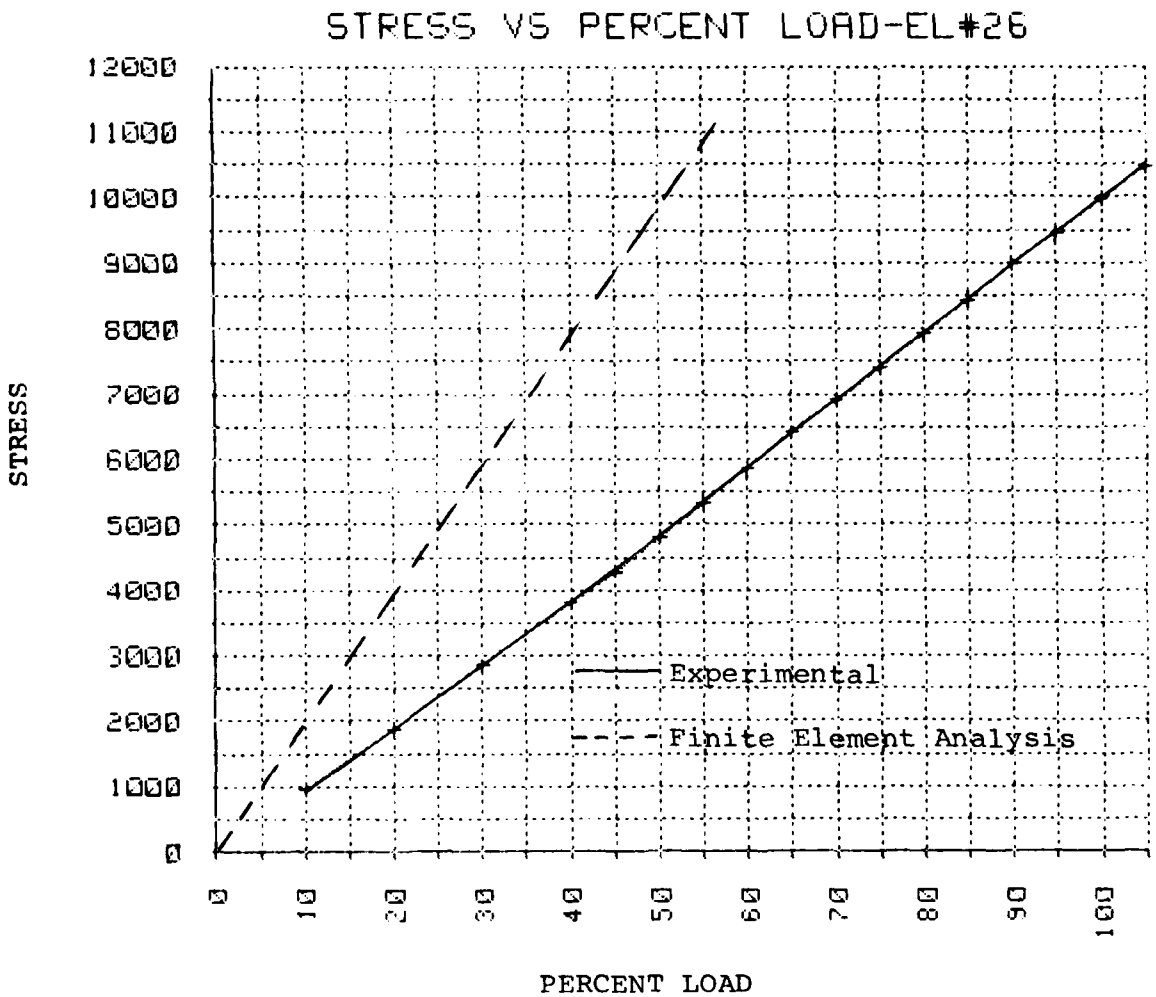

Figure 3.22i. Equivalent Stress-Skin Element 26.

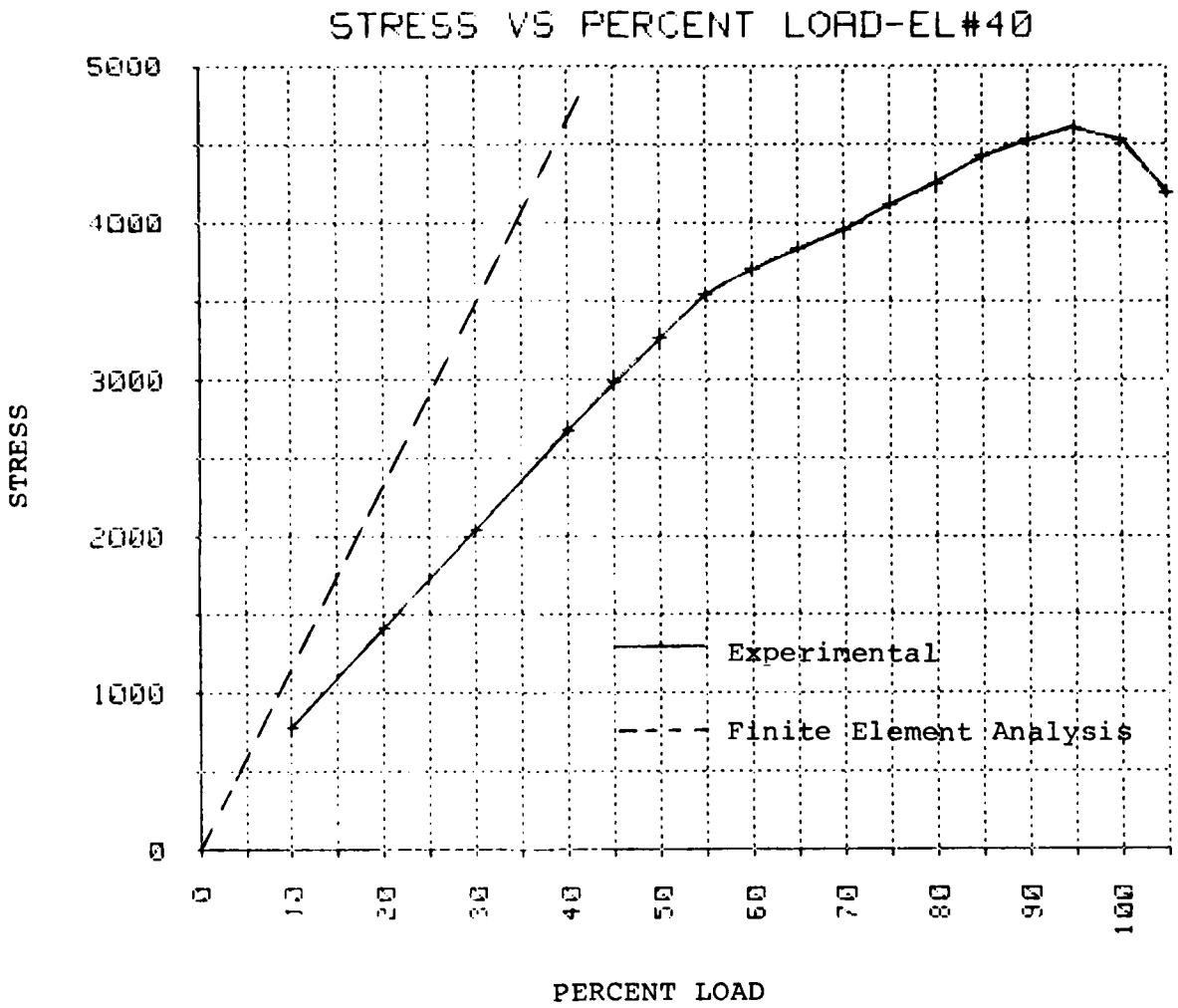

Figure 3.22j. Equivalent Stress-Skin Element 40.

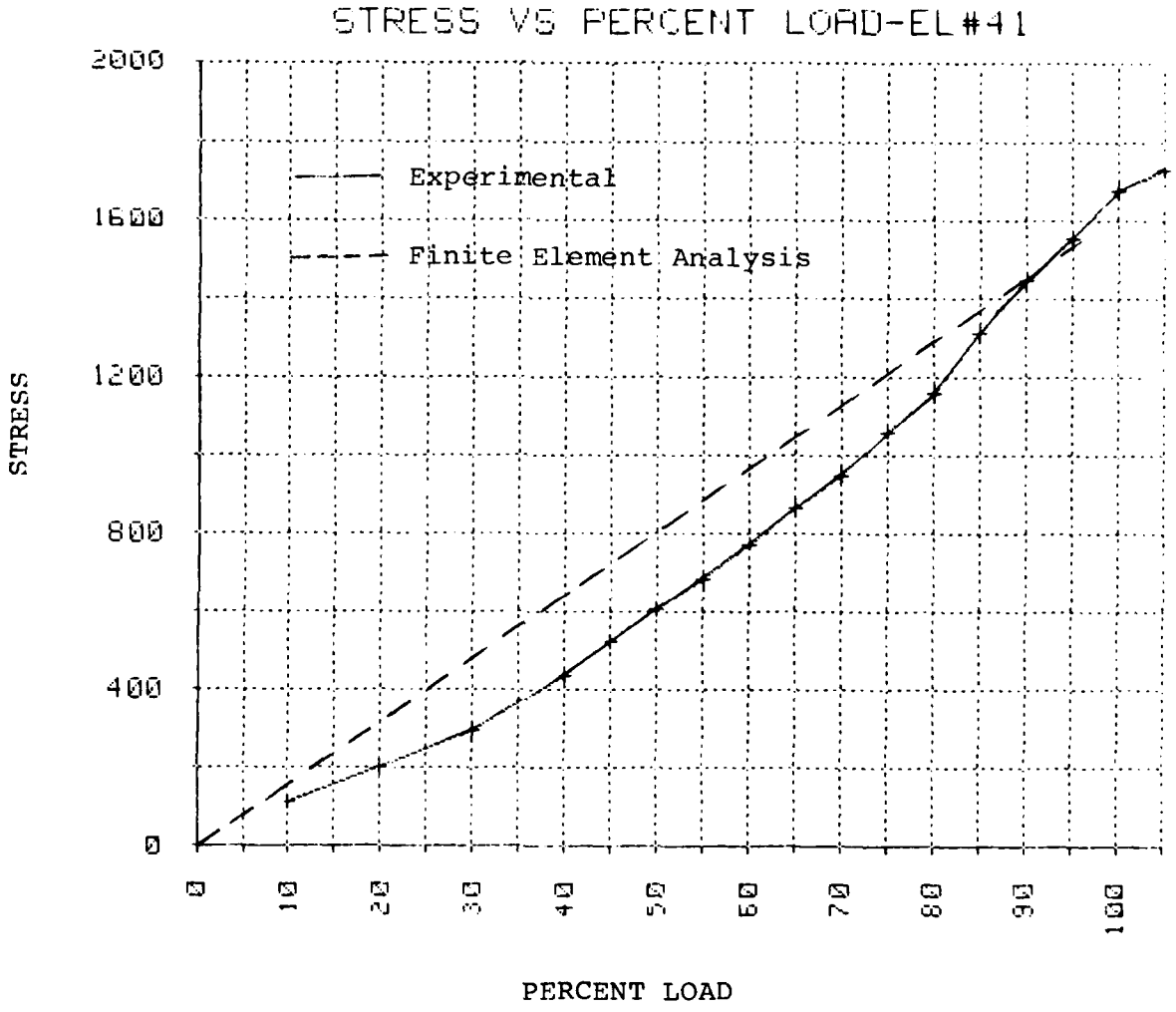

Figure 3.22k. Equivalent Stress-Rib Web Element 41.

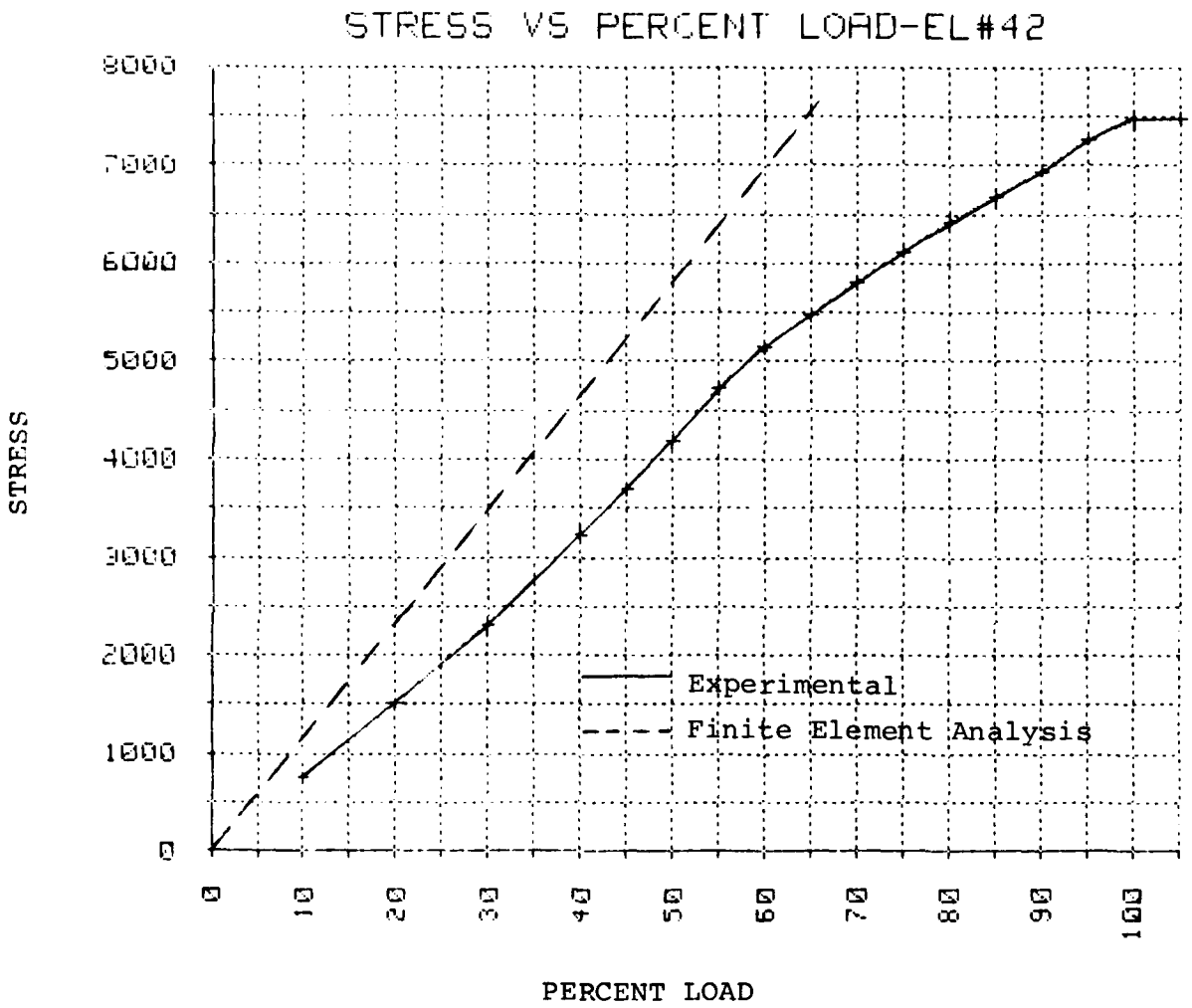

Figure 3.221. Equivalent Stress-Rib Web Element 42.

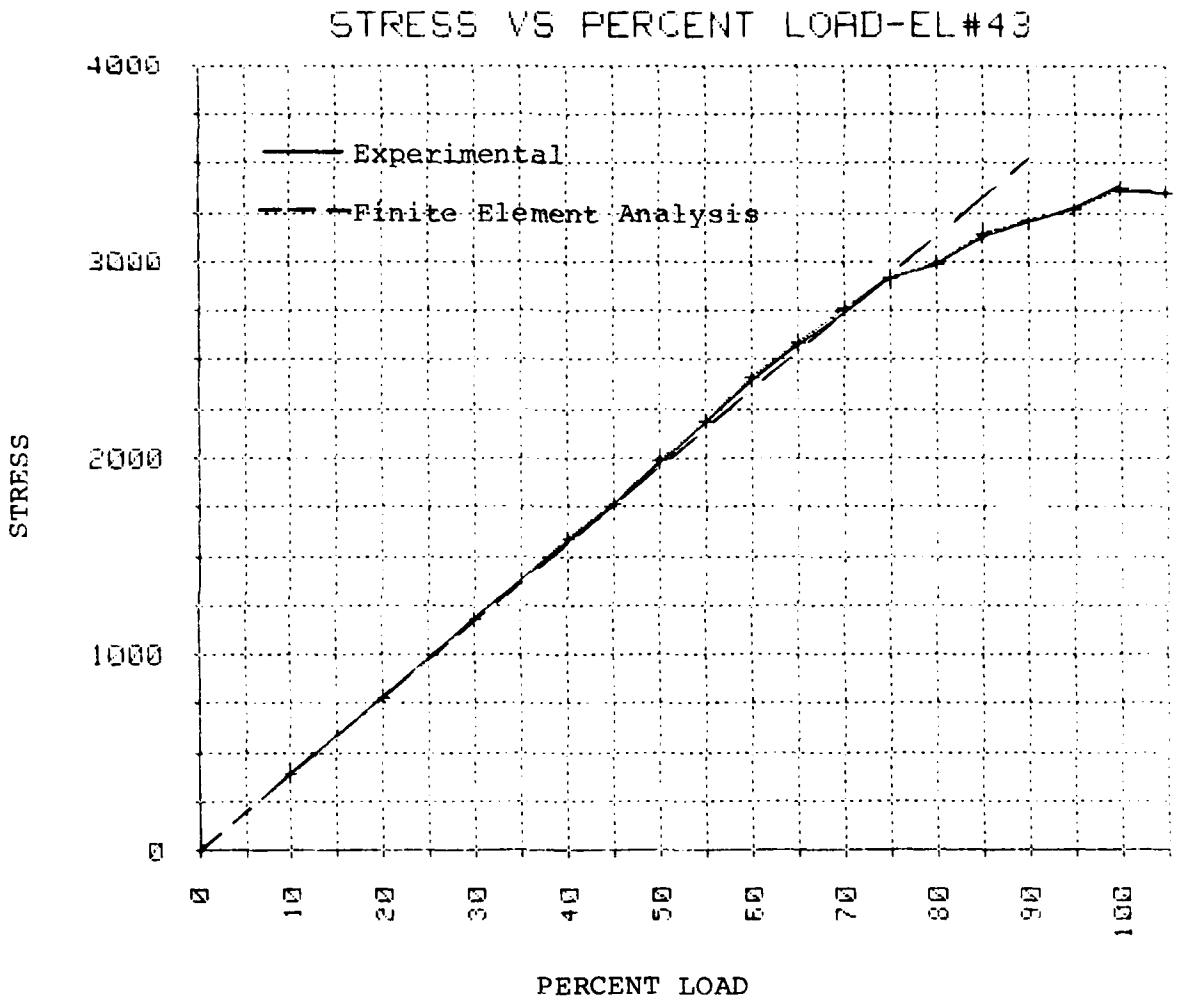

Figure 3.22m. Equivalent Stress-Rib Web Element 43.

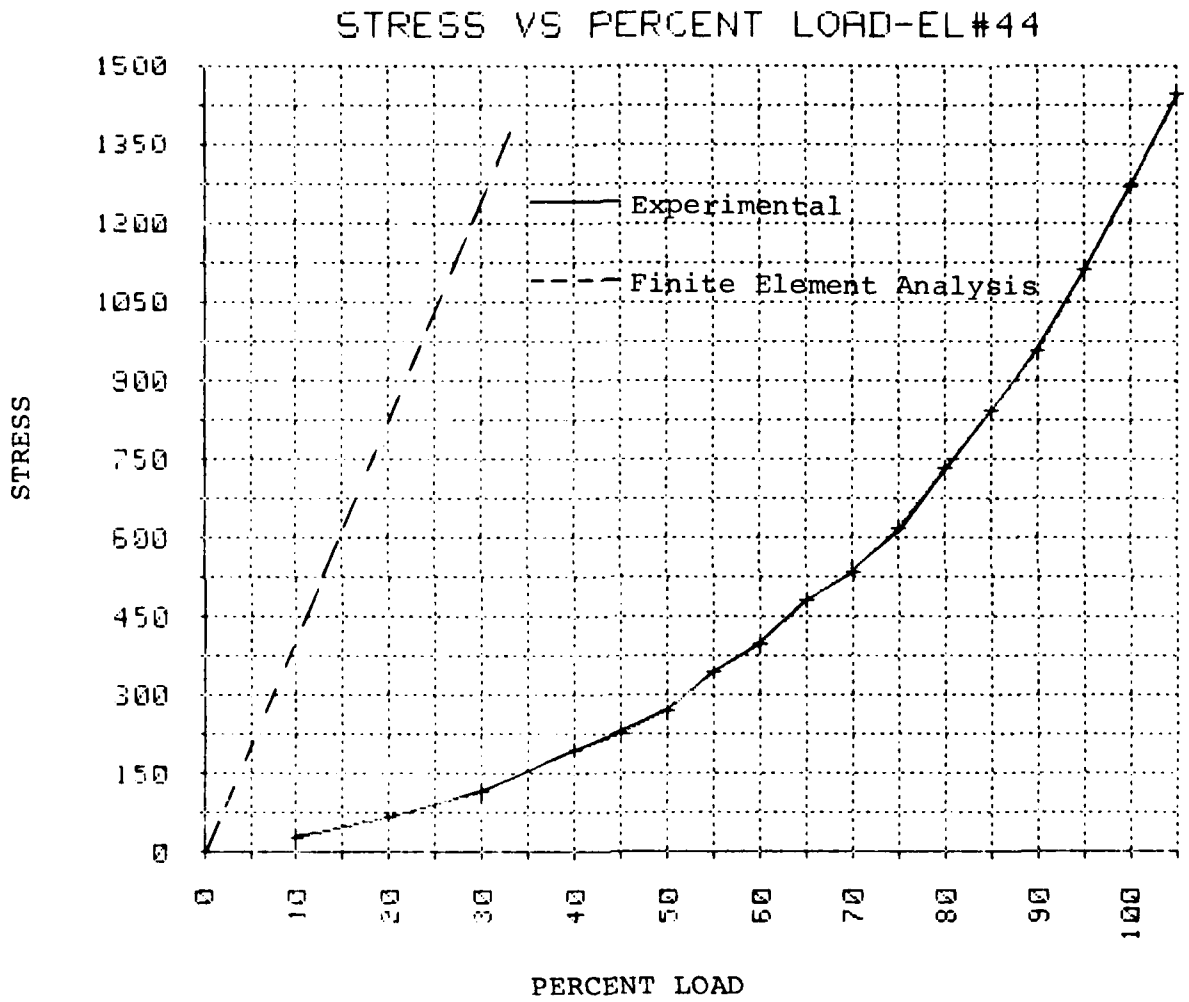

Figure 3.22n. Equivalent Stress-Rib Web Element 44.

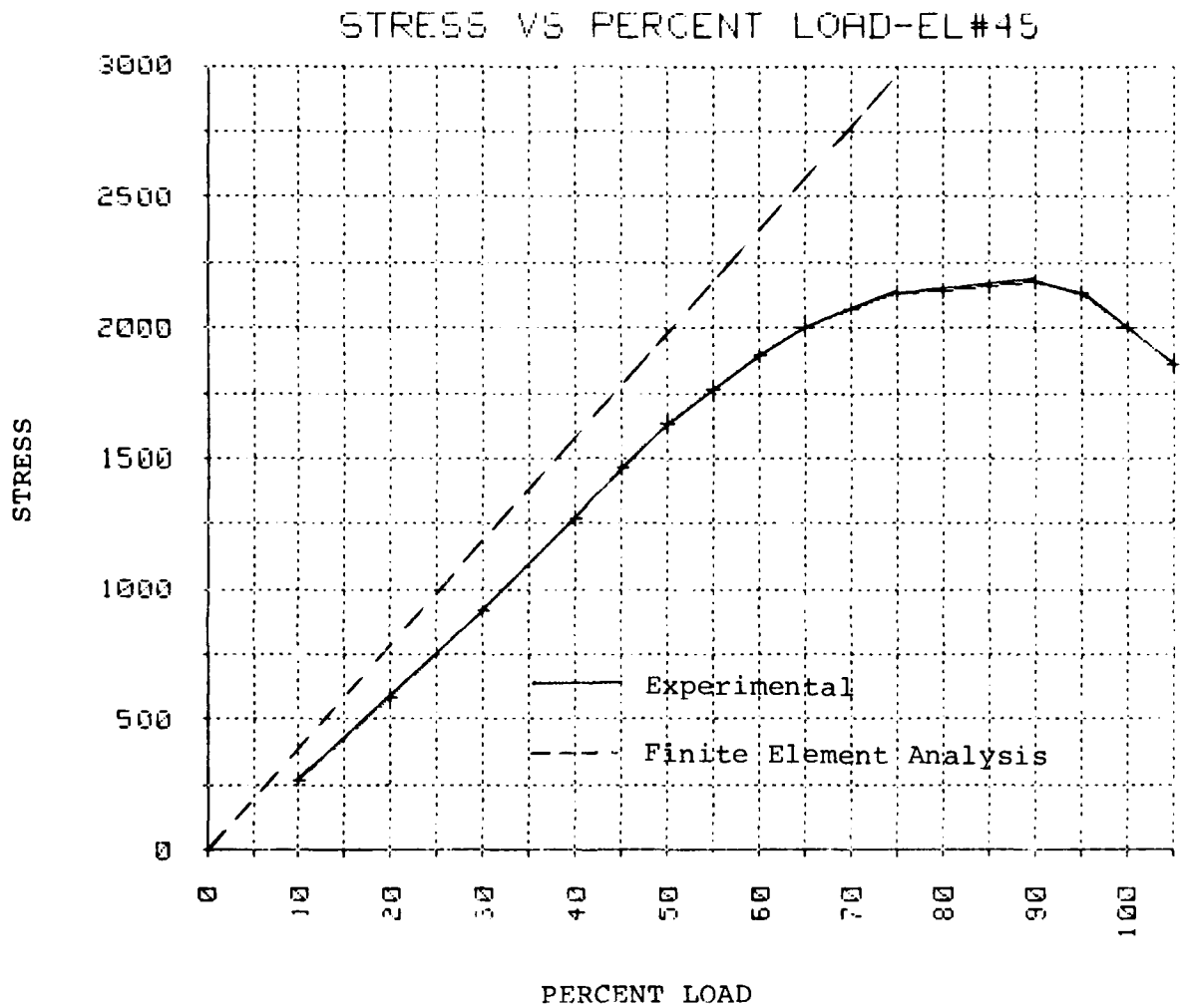

Figure 3.22o. Equivalent Stress-Rib Web Element 45.

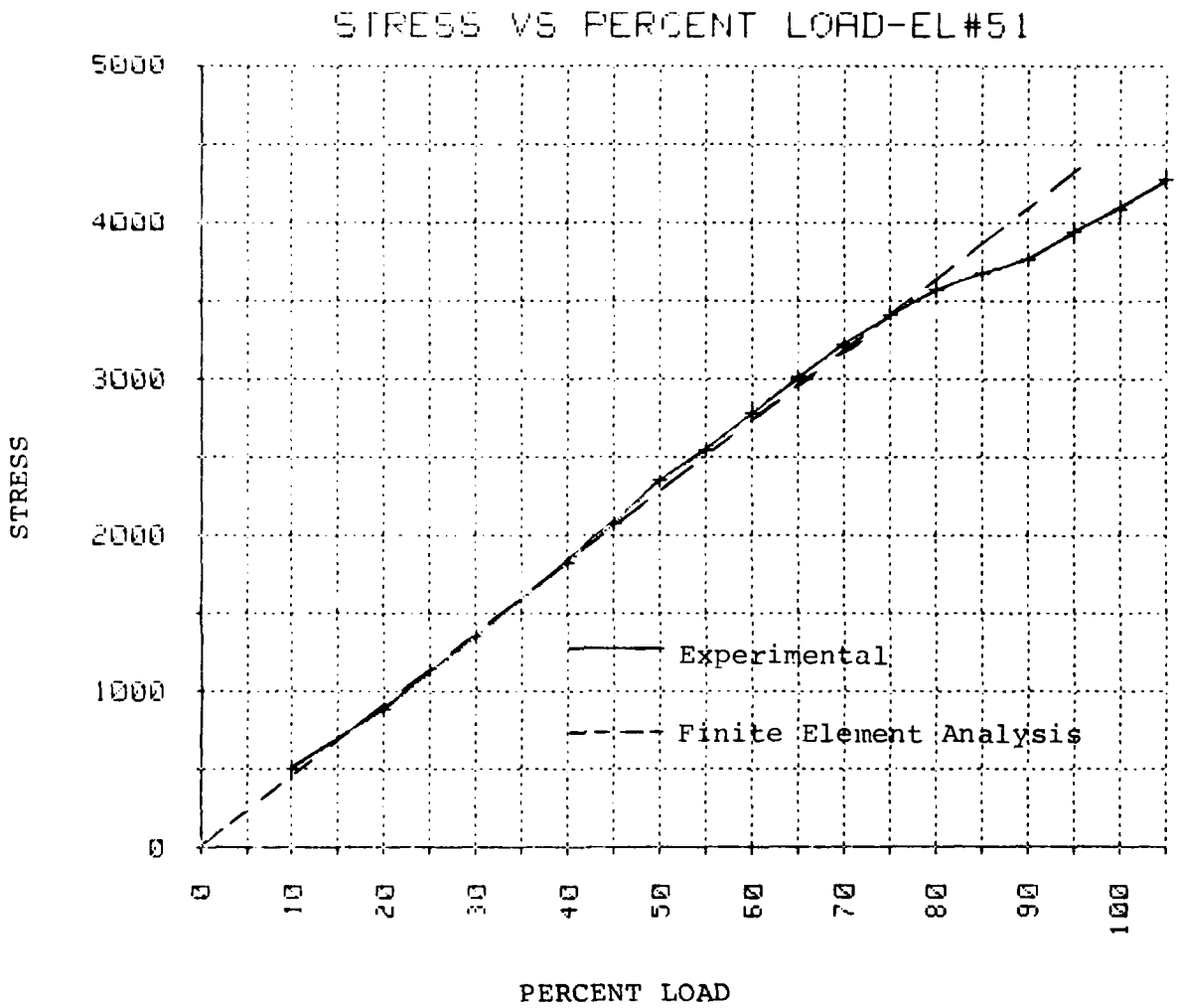

Figure 3.22p. Equivalent Stress-Spar Web Element 51.

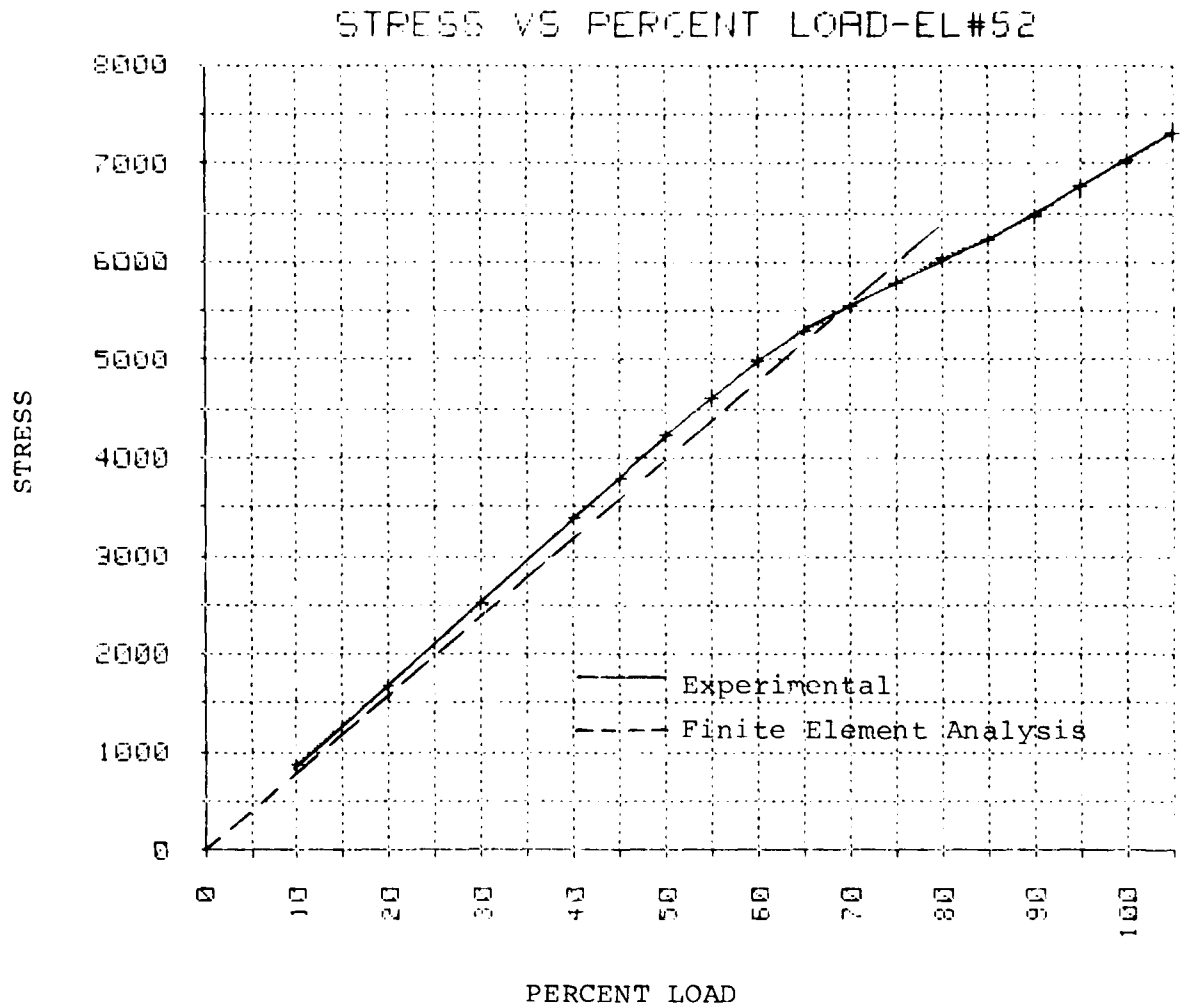

Figure 3.22q. Equivalent Stress-Spar Web Element 52.

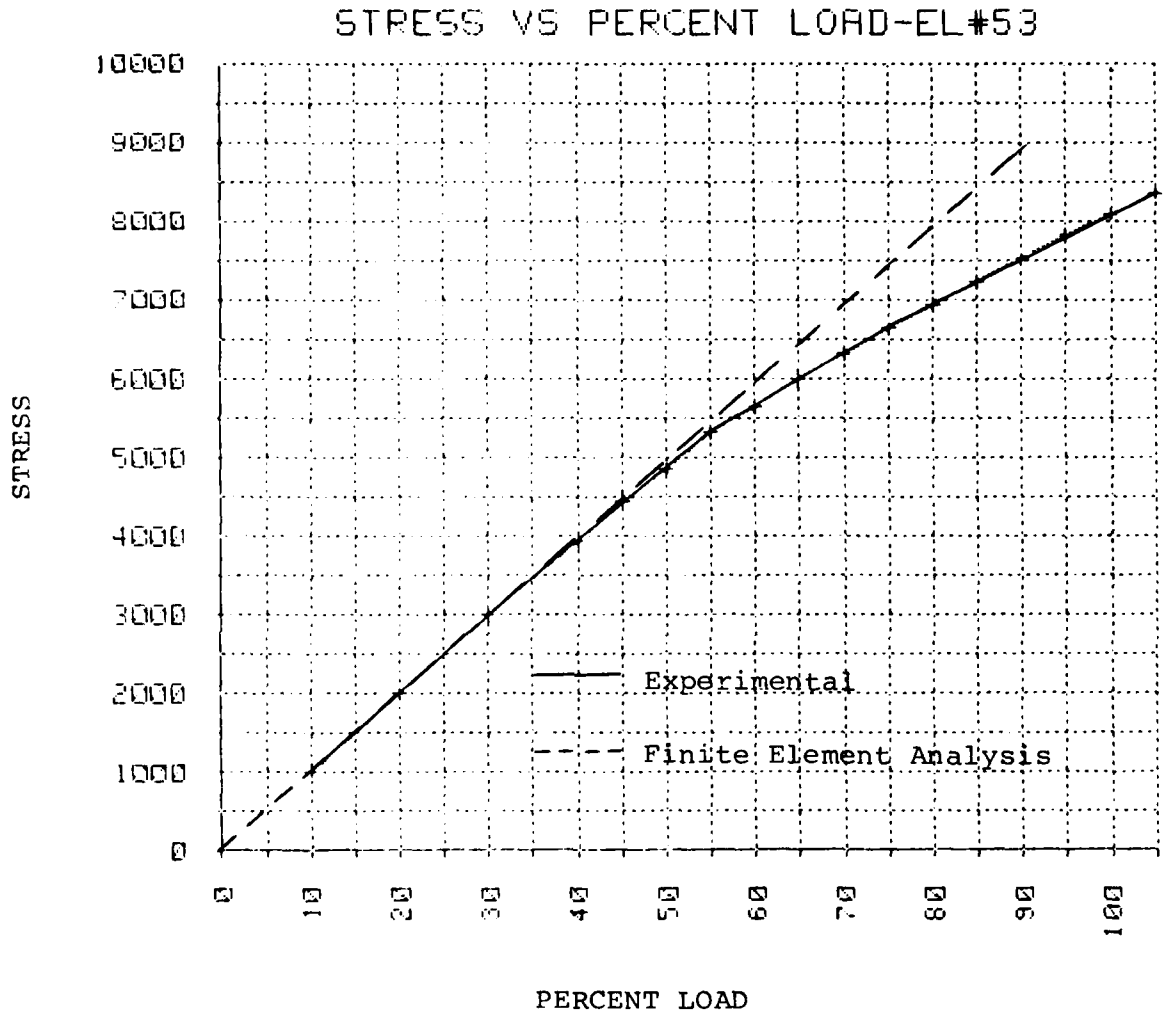

Figure 3.22r. Equivalent Stress-Spar Web Element 53.

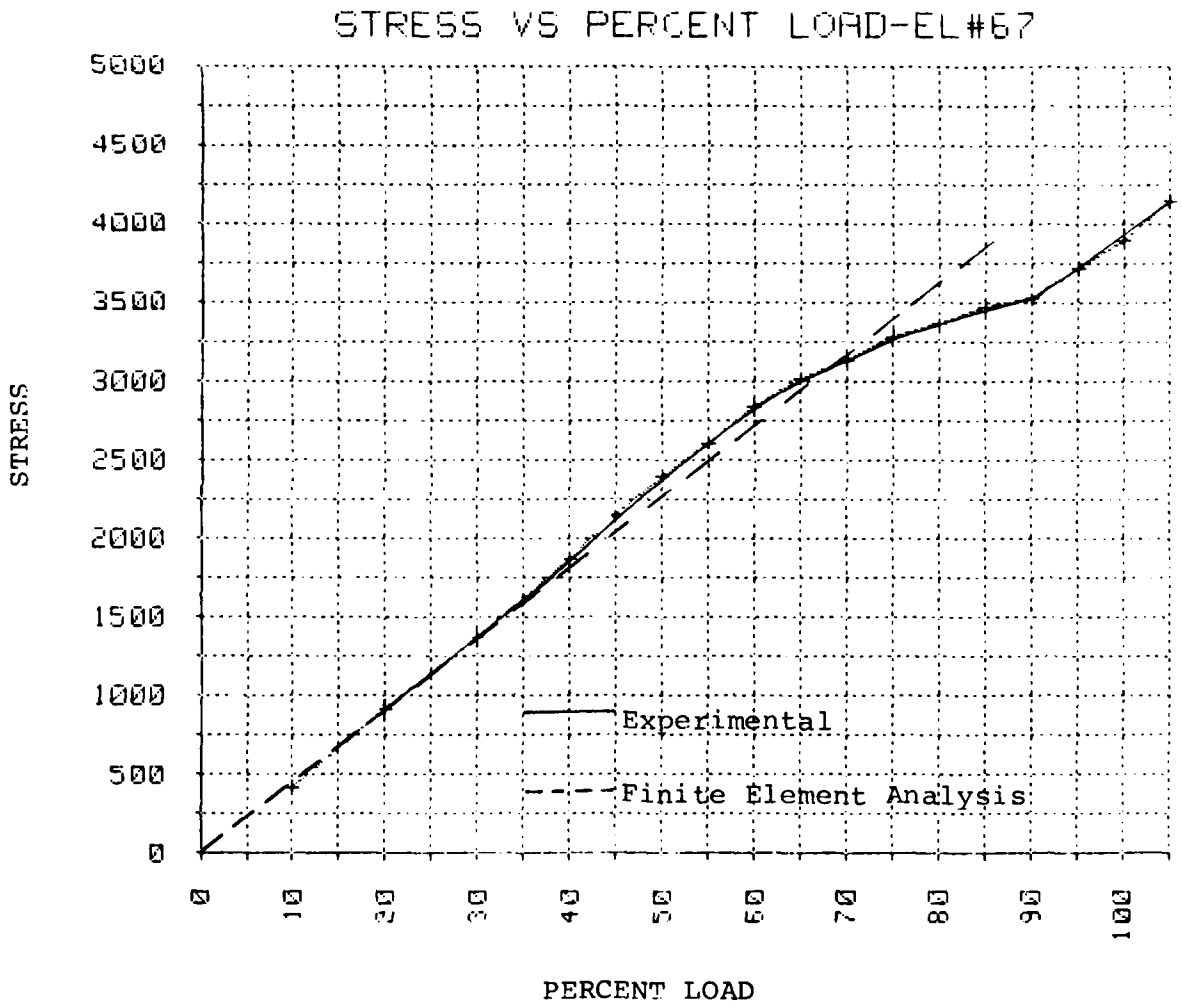

Figure 3.22s. Equivalent Stress-Spar Web Element 67.

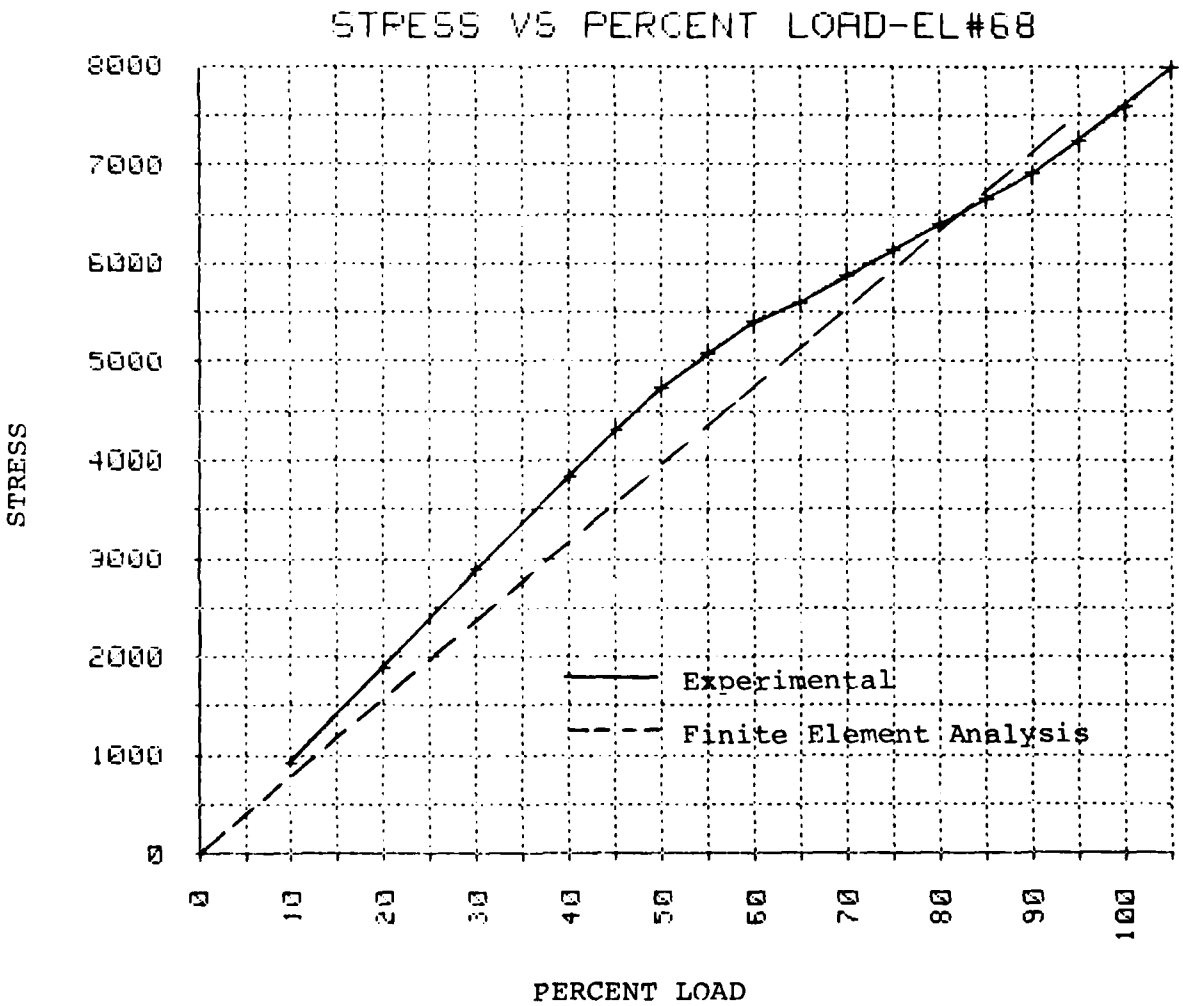

Figure 3.22t. Equivalent Stress-Spar Web Element 68.

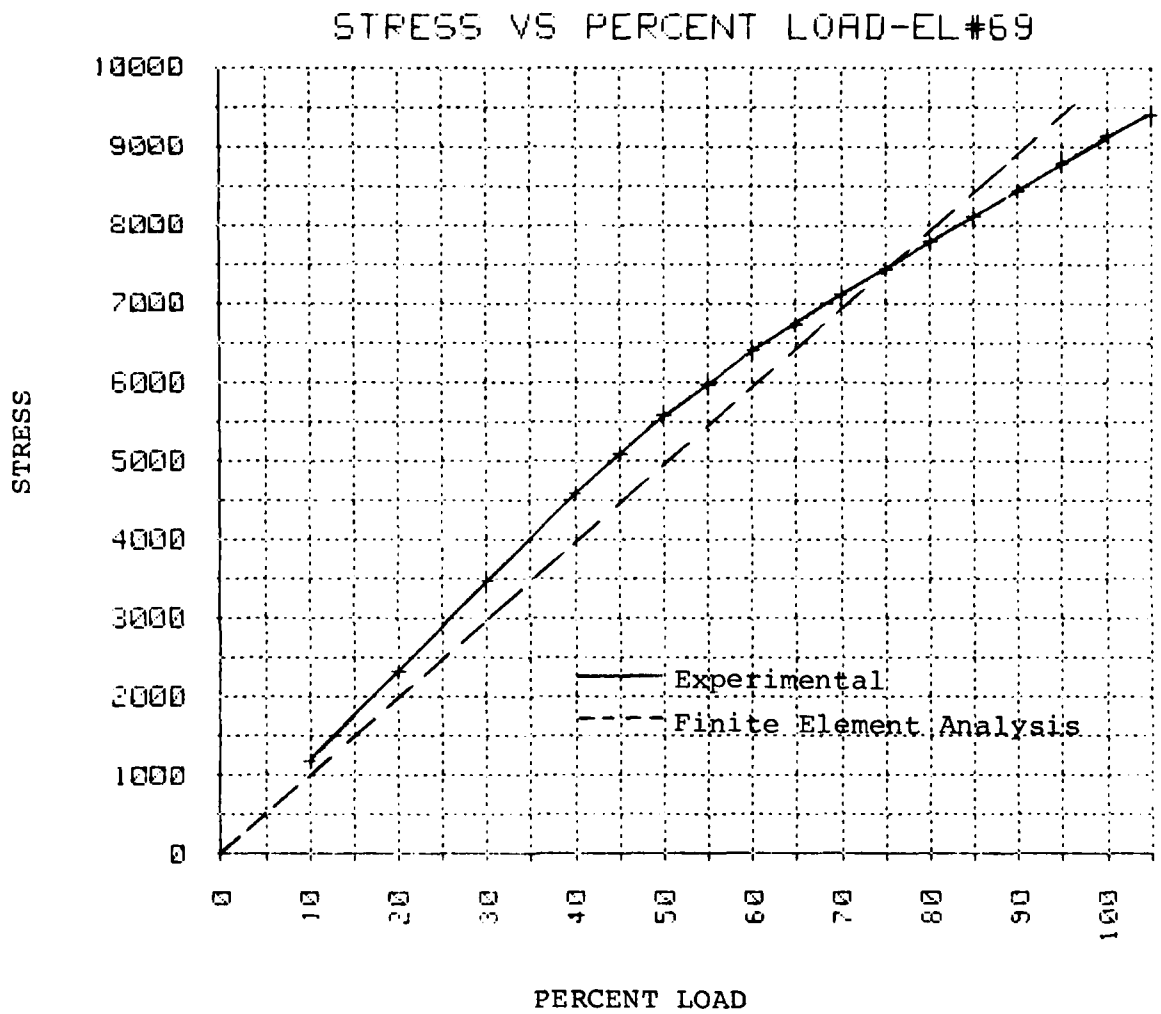

Figure 3.22u. Equivalent Stress-Spar Web Element 69.

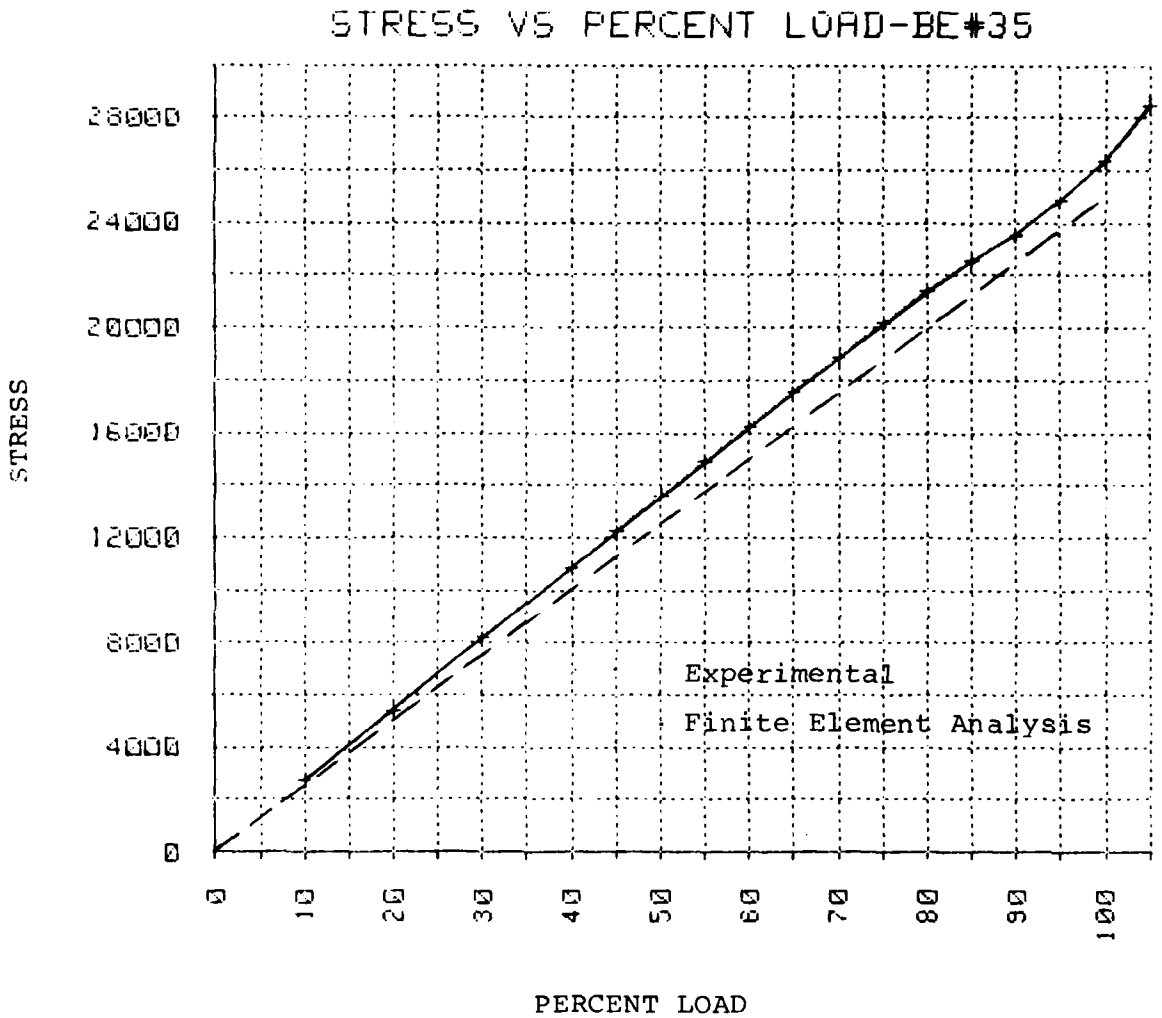

Figure 3.22v. Axial Stress-Spar Cap Element 35.

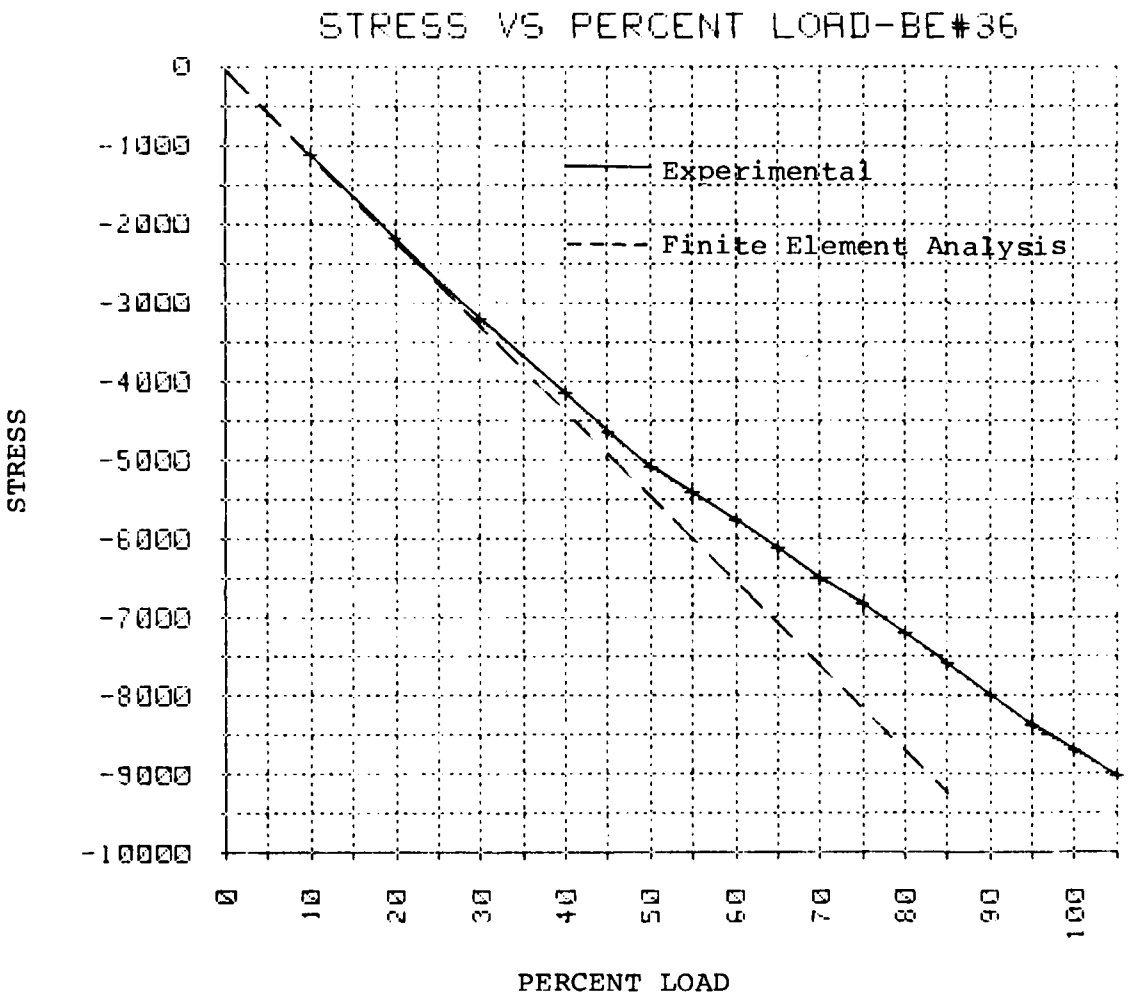

Figure 3.22w. Axial Stress-Spar Cap Element 36.

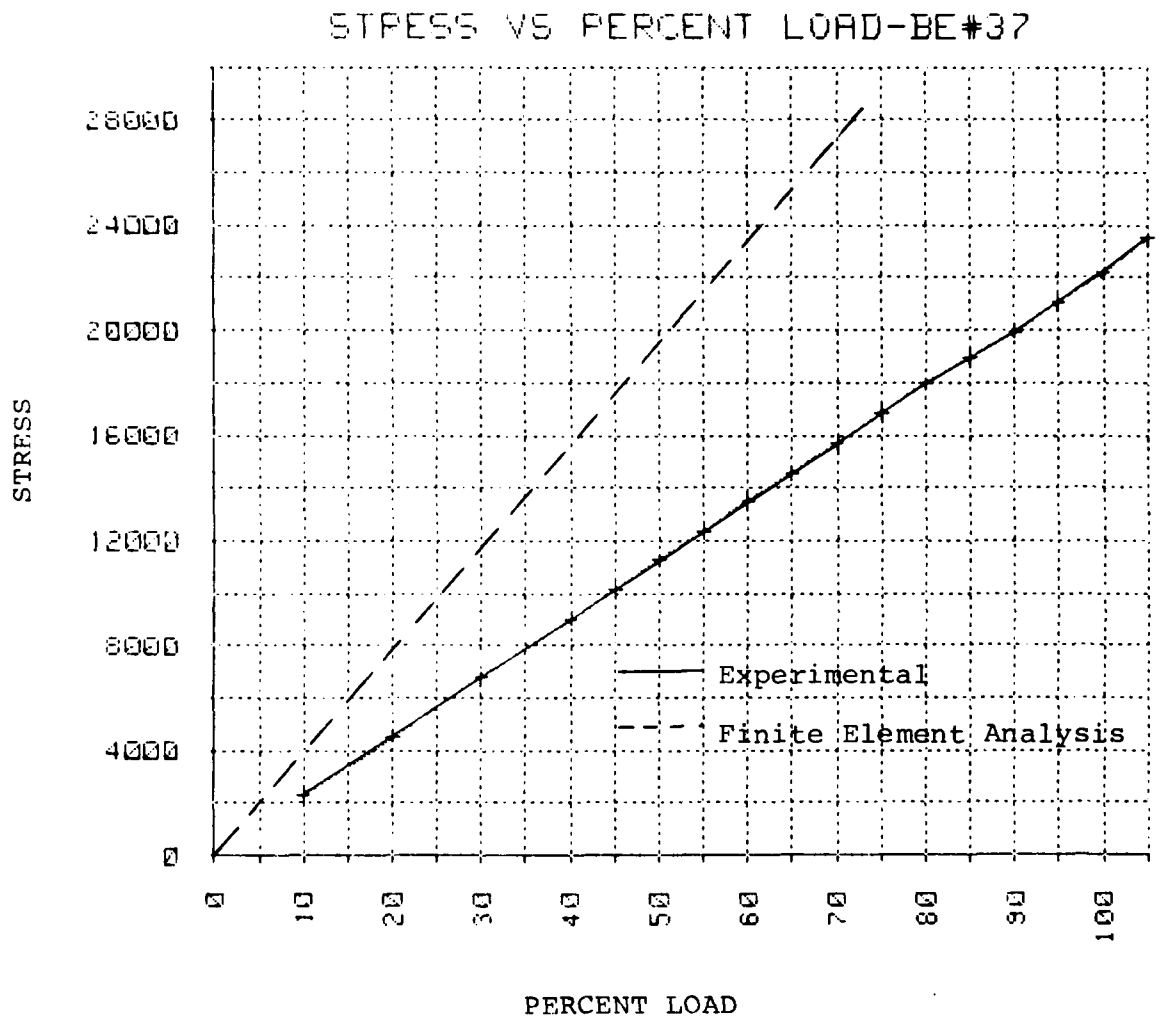

Figure 3.22x. Axial Stress-Spar Cap Element 37.

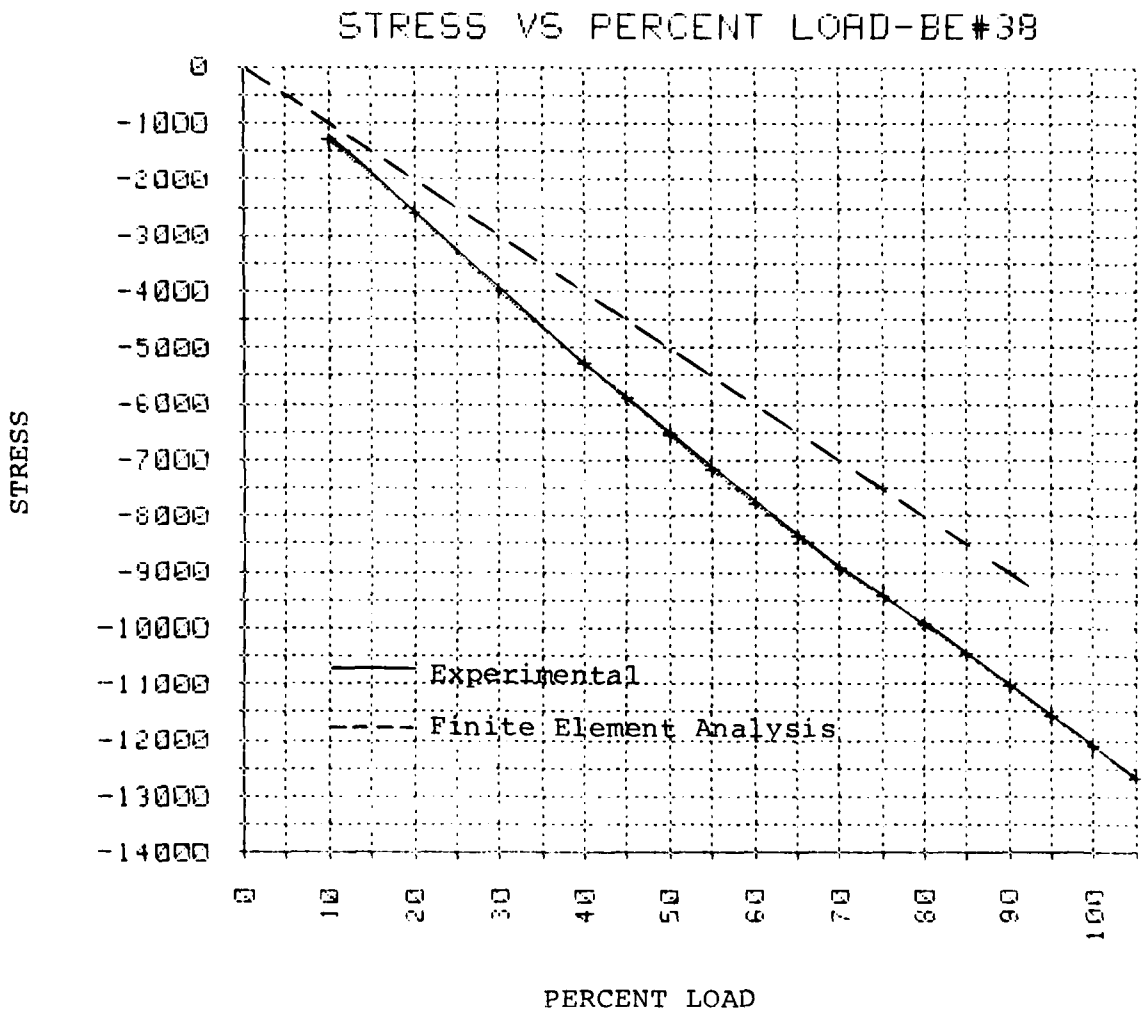

Figure 3.22y. Axial Stress-Spar Cap Element 38.

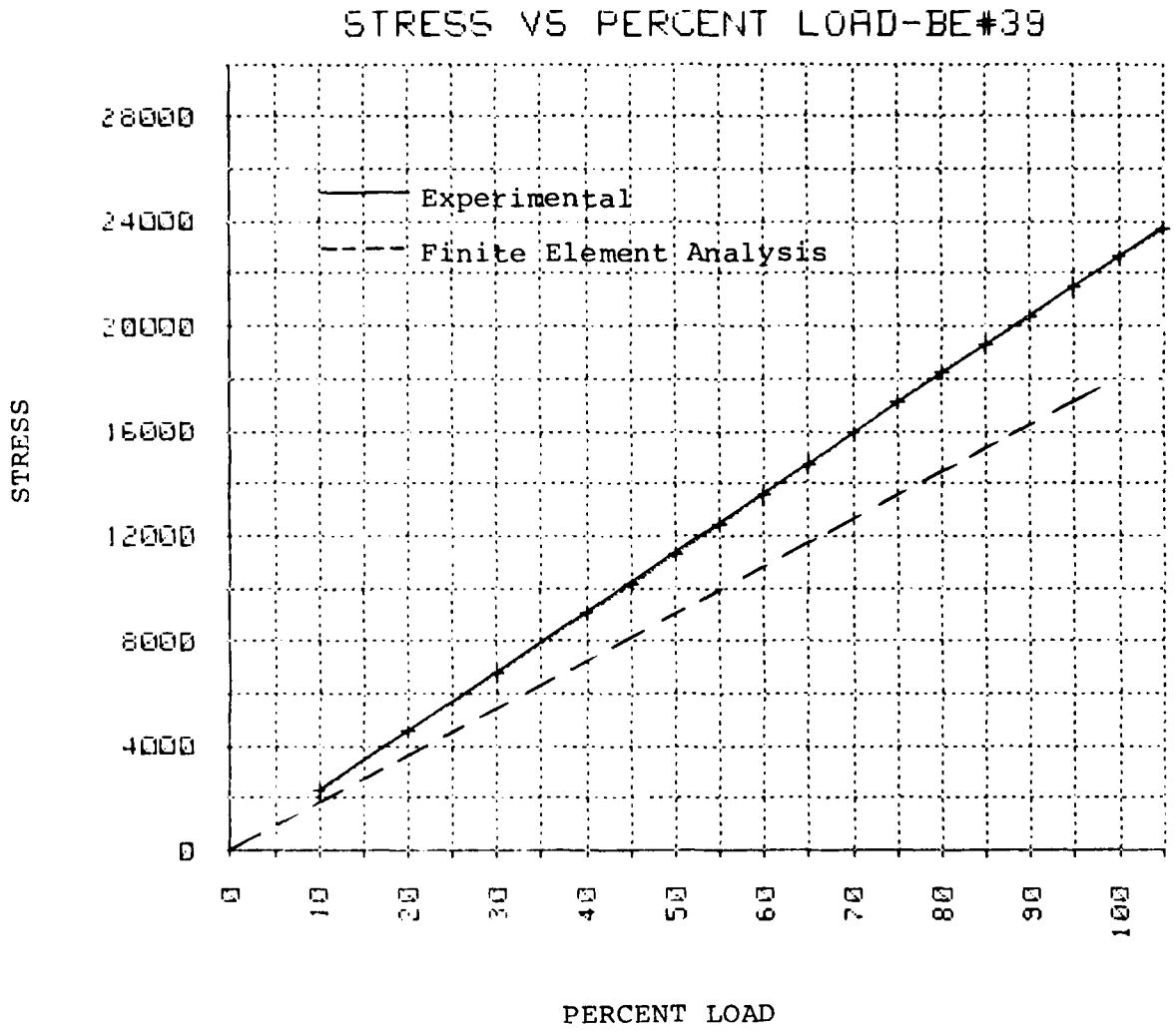

Figure 3.22z. Axial Stress-Spar Cap Element 39.

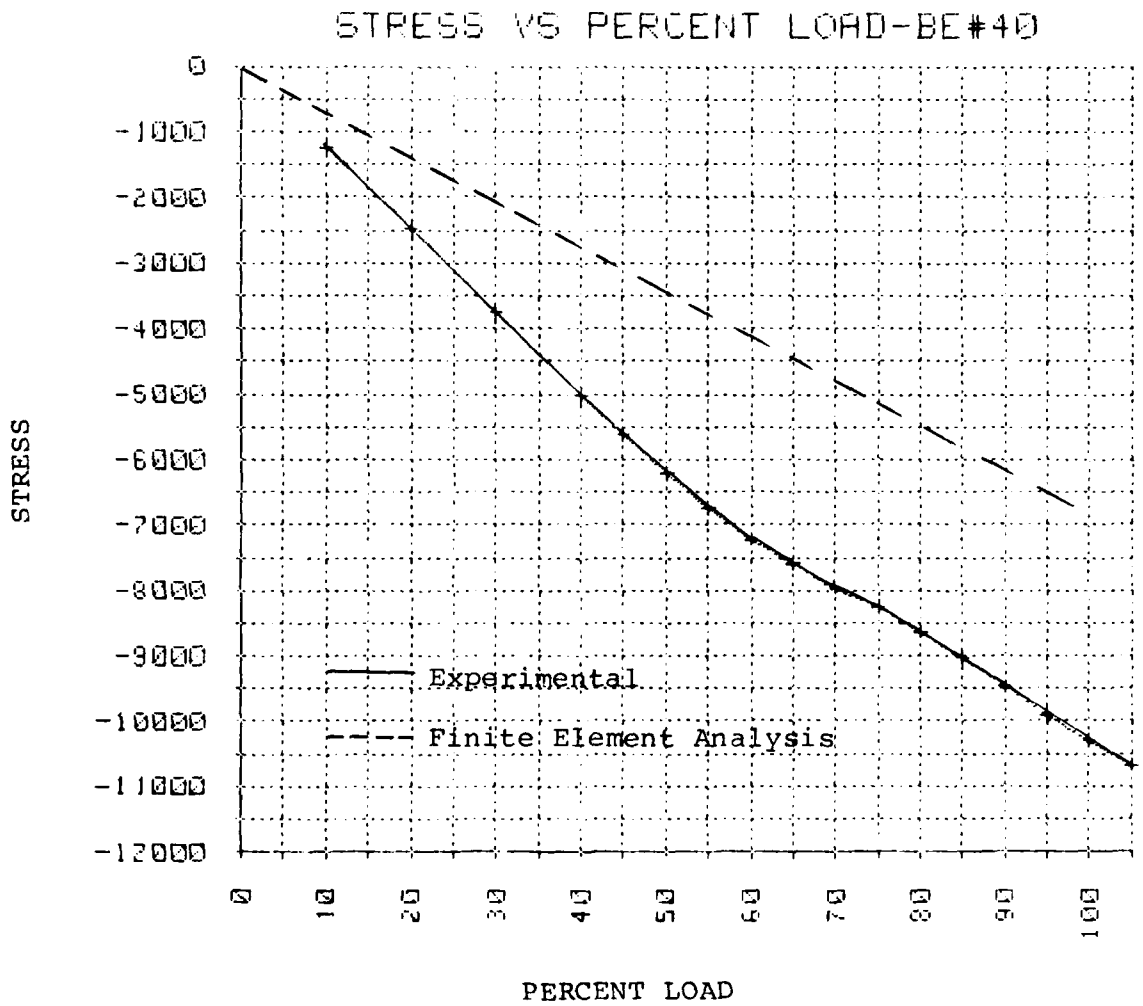

Figure 3.22aa. Axial Stress-Spar Cap Element 40.

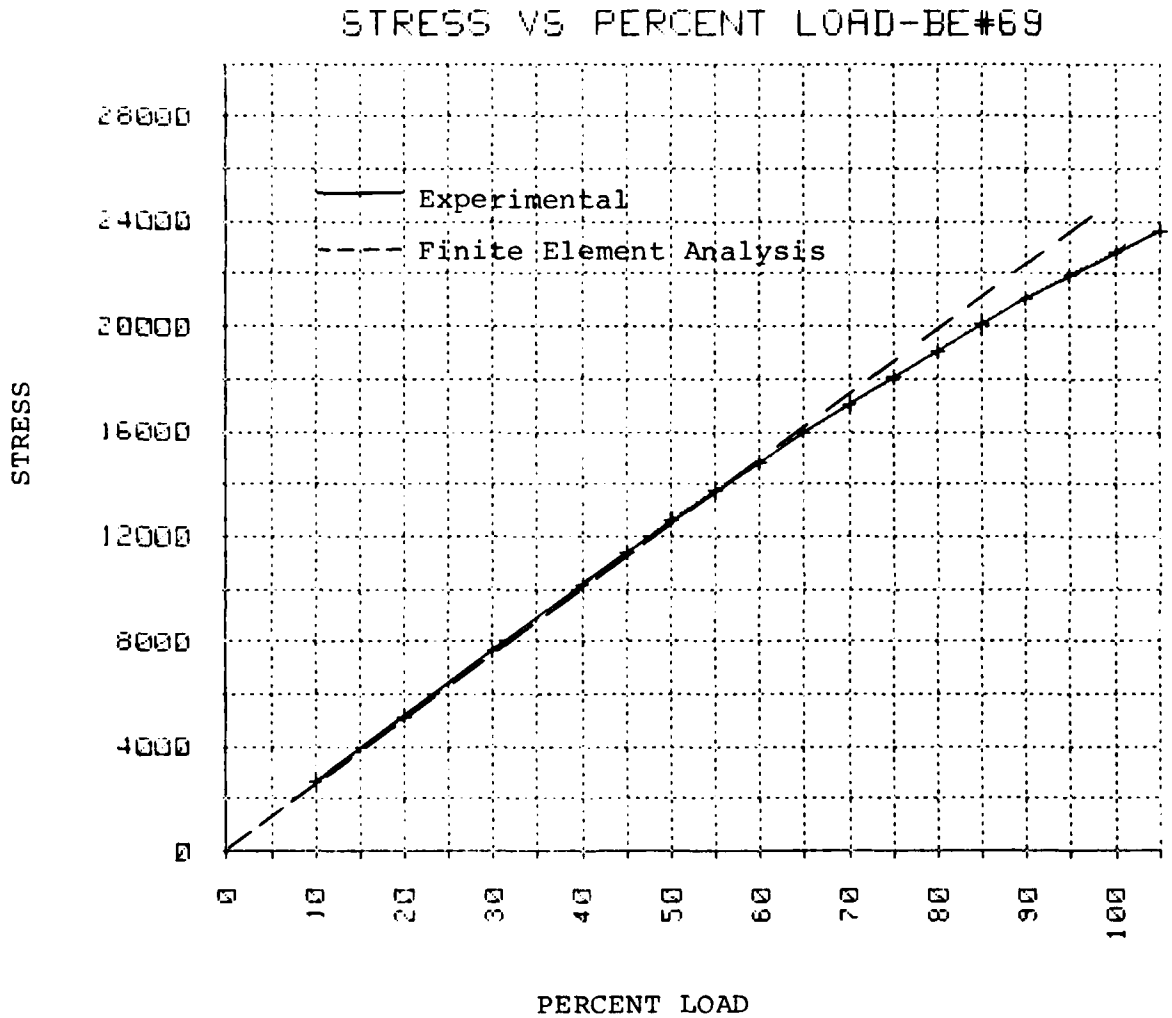

Figure 3.22bb. Axial Stress-Spar Cap Element 69.

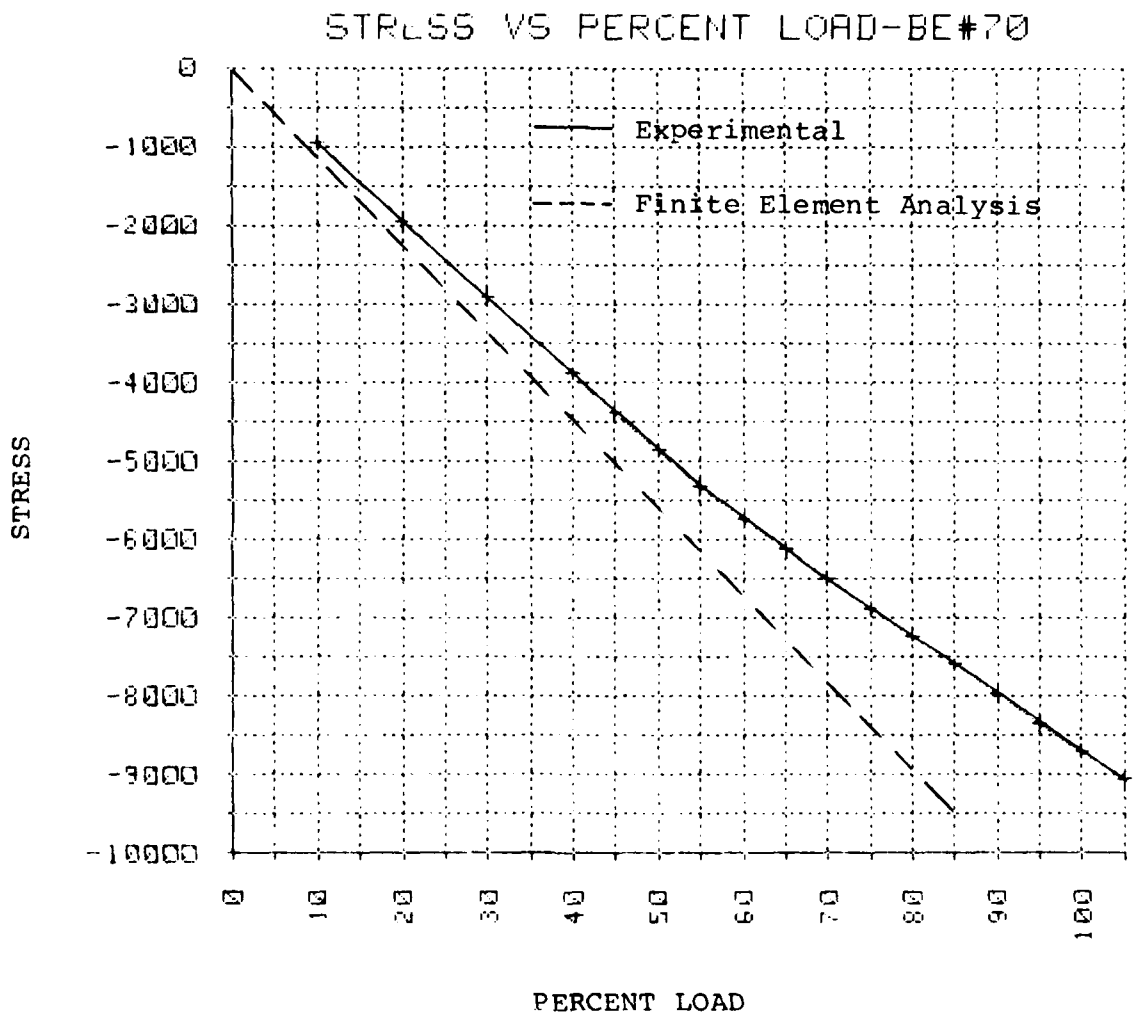

Figure 3.22cc. Axial Stress-Spar Cap Element 70.

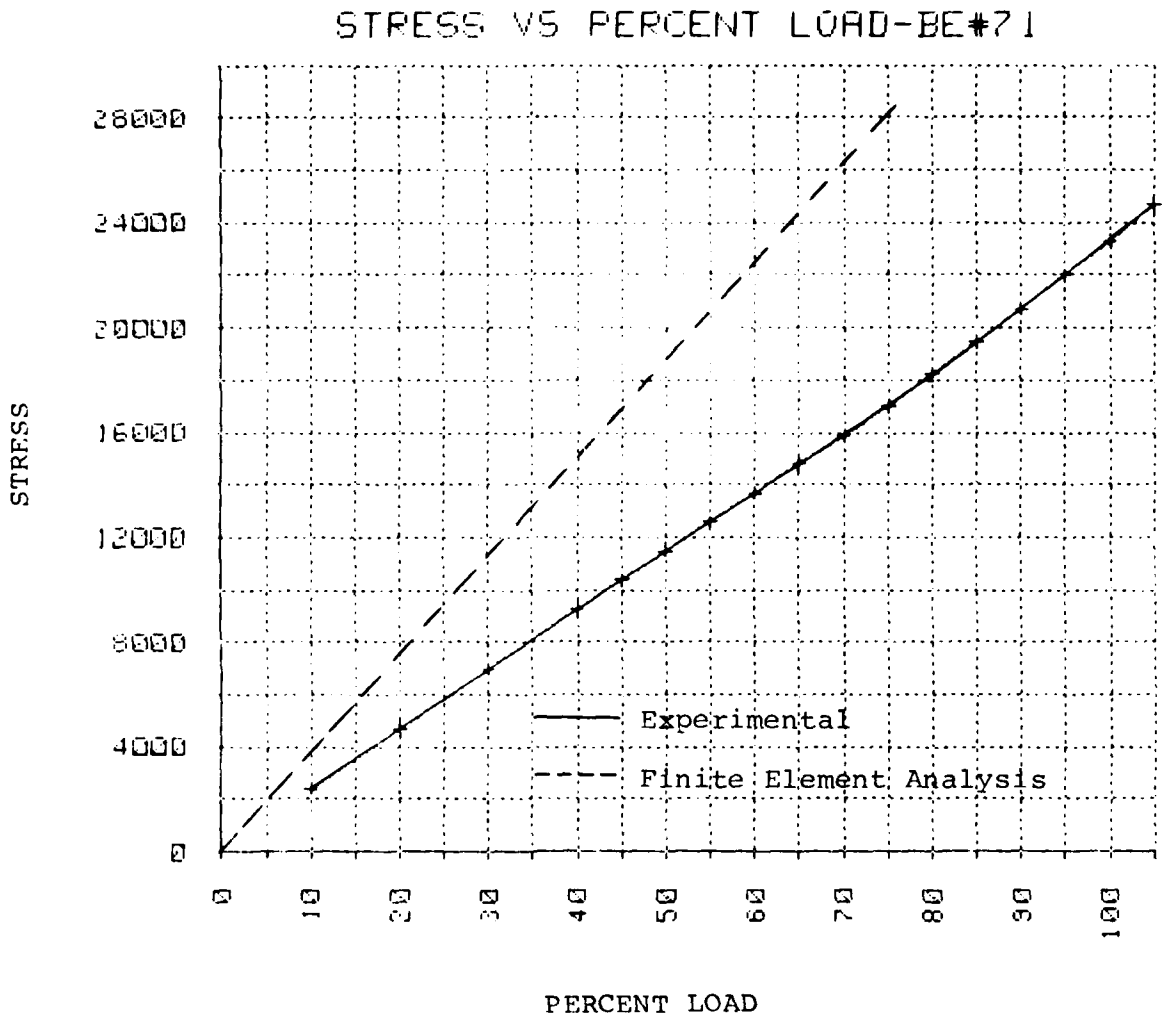

Figure 3.22dd. Axial Stress-Spar Cap Element 71.

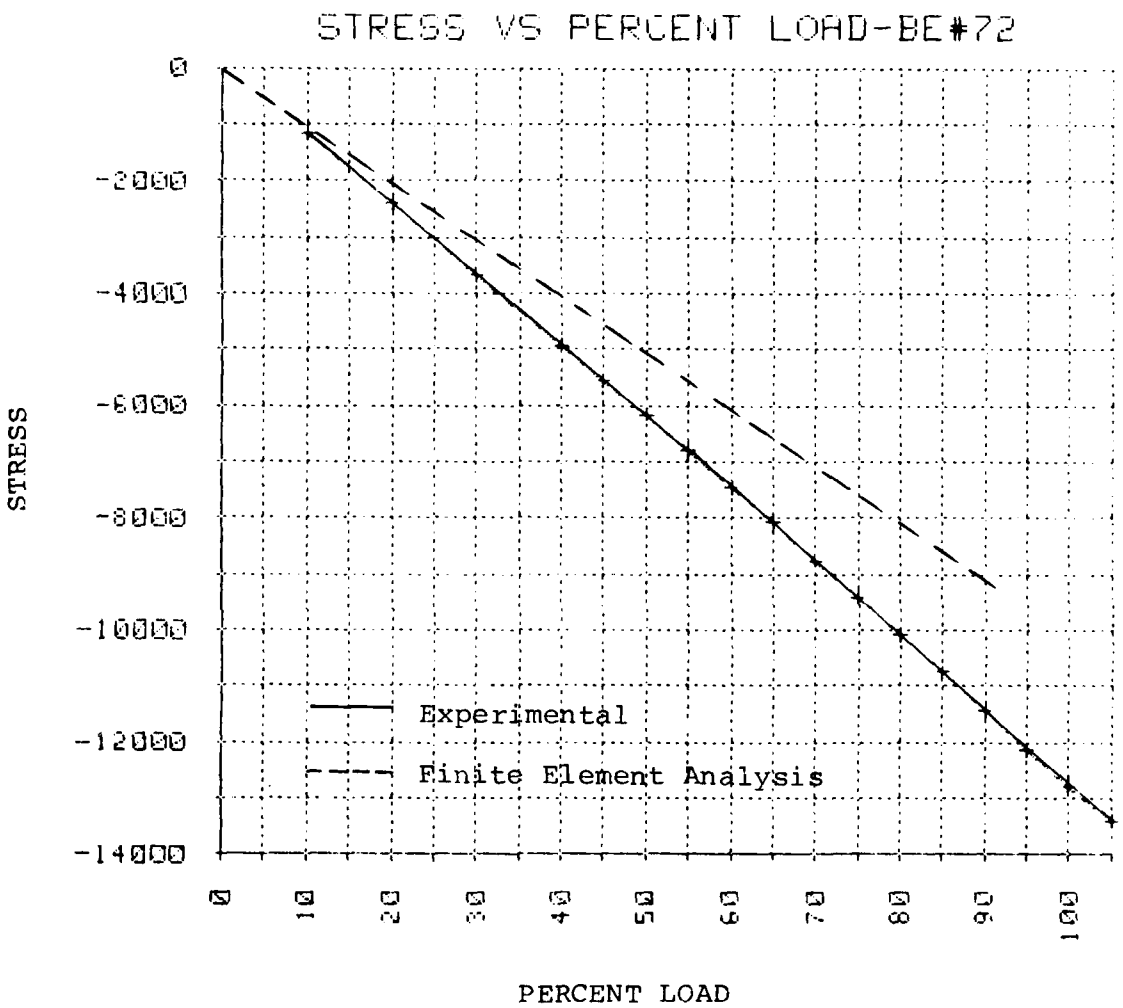

Figure 3.22ee. Axial Stress-Spar Cap Element 72.

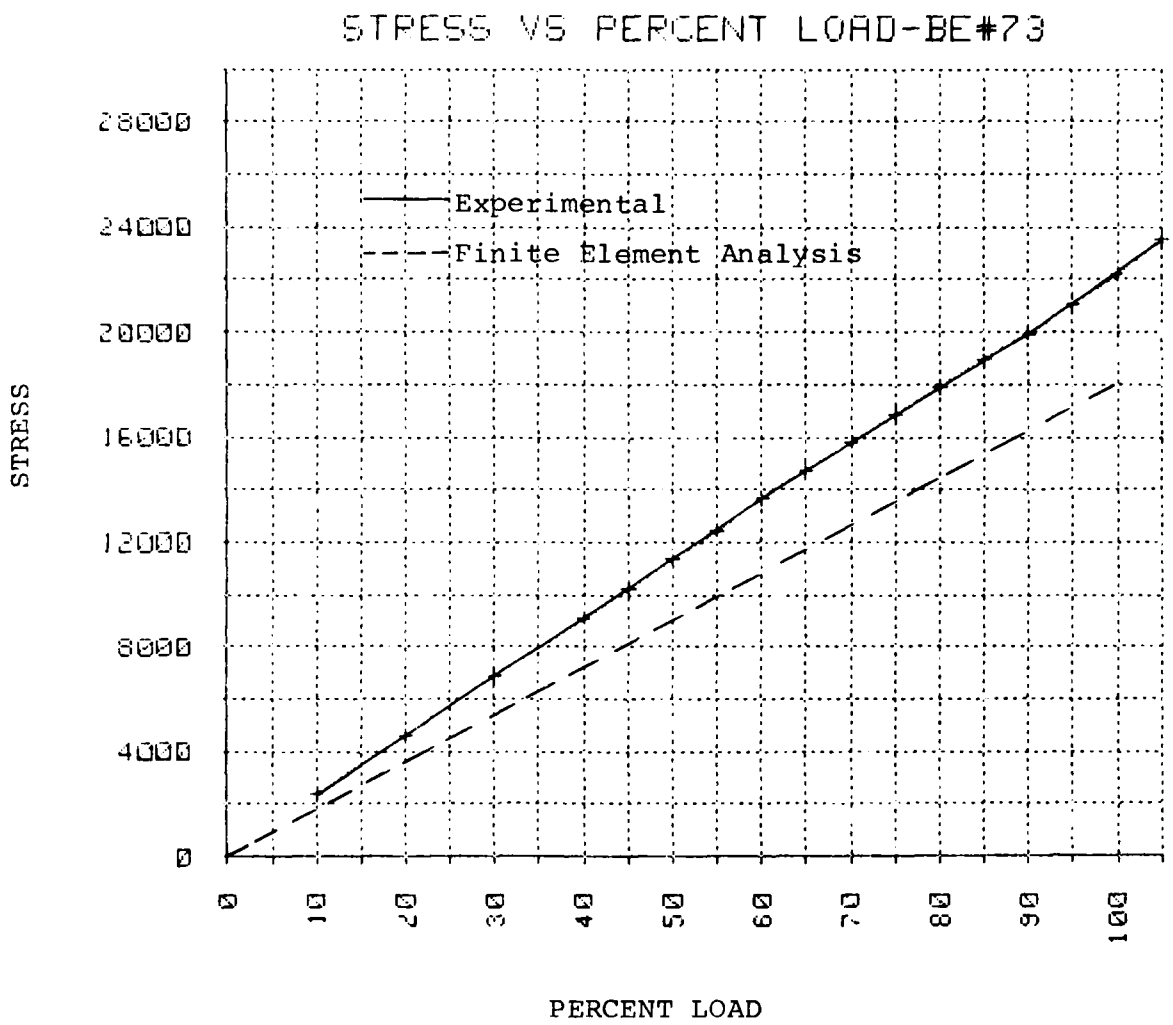

Figure 3.22ff. Axial Stress-Spar Cap Element 73.

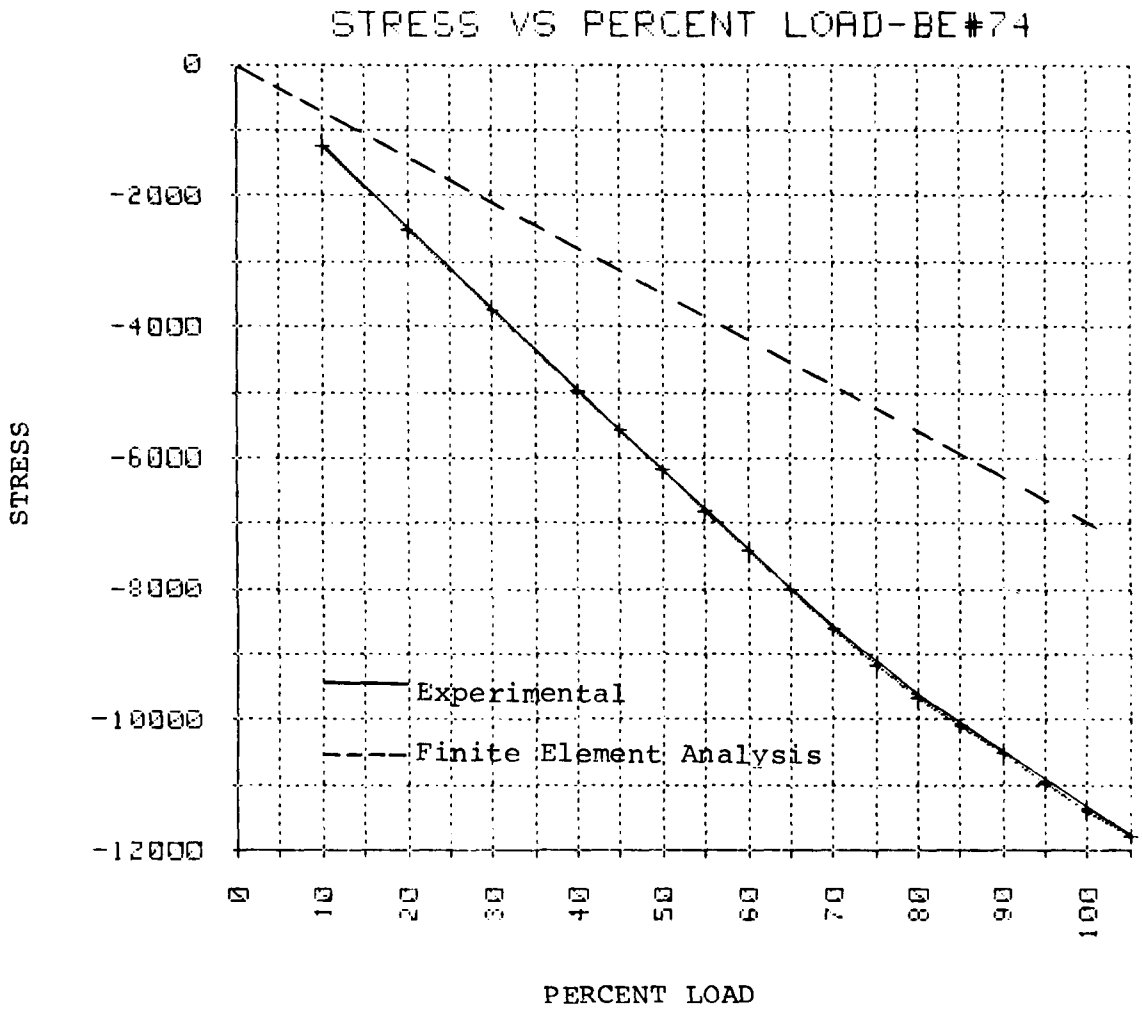

Figure 3.22gg. Axial Stress-Spar Cap Element 74.

The stresses in spar caps 35-40, and 69-74 (see Figure 3.21e) are considered in Figures 3.22v-gg. These results do not seem to have much of a pattern; some of the analytical vs. experimental comparisons (Bar elements 35 and 69, for example) are quite close. Other comparisons (Bar elements 36 and 70, for example) are fairly good for lower load levels. And still other comparisons are not good at all.

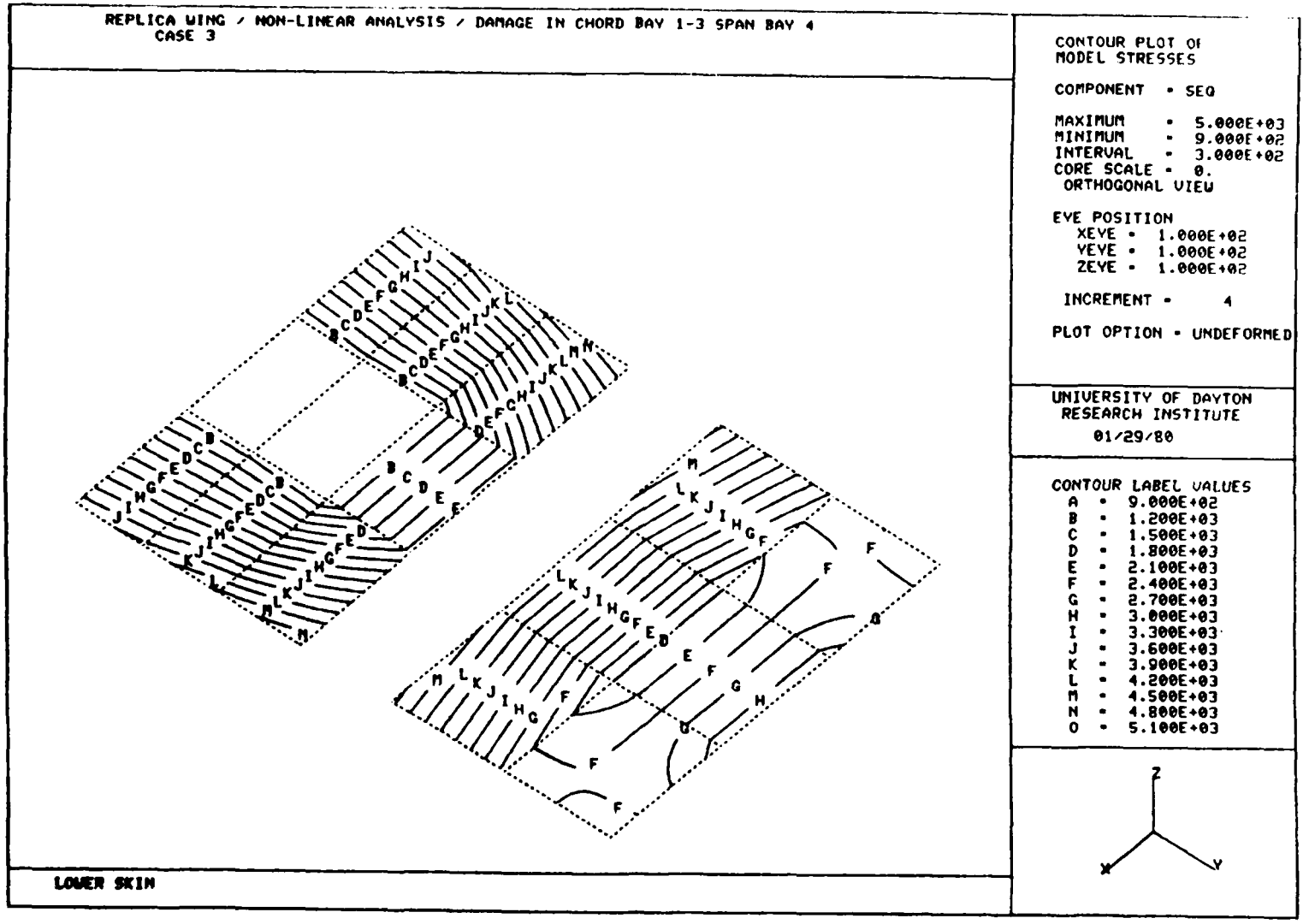

Figure 3.23a. Contours of Equivalent Stress - 20% Load.

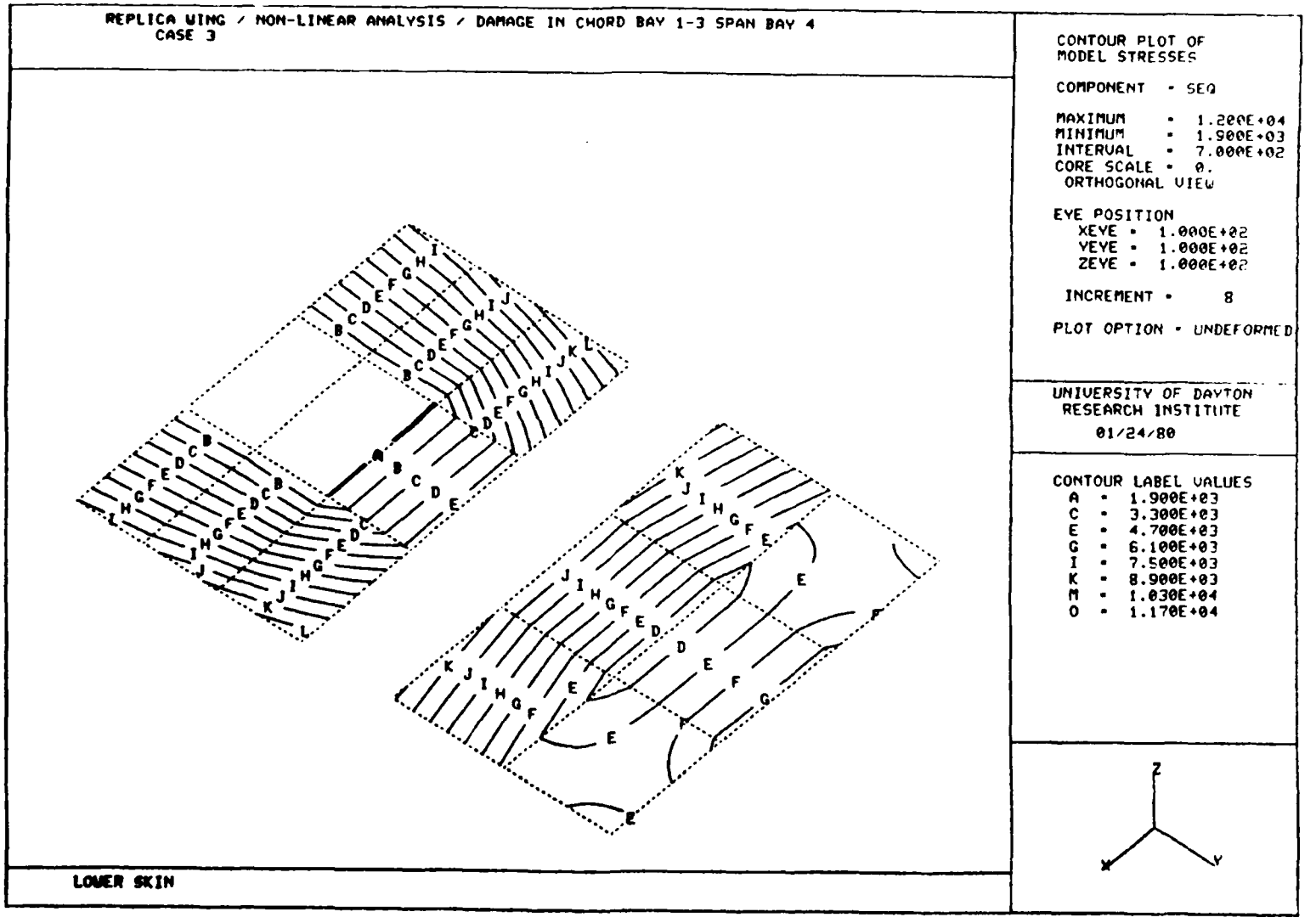

Figure 3.23b. Contours of Equivalent Stress - 40% Load.

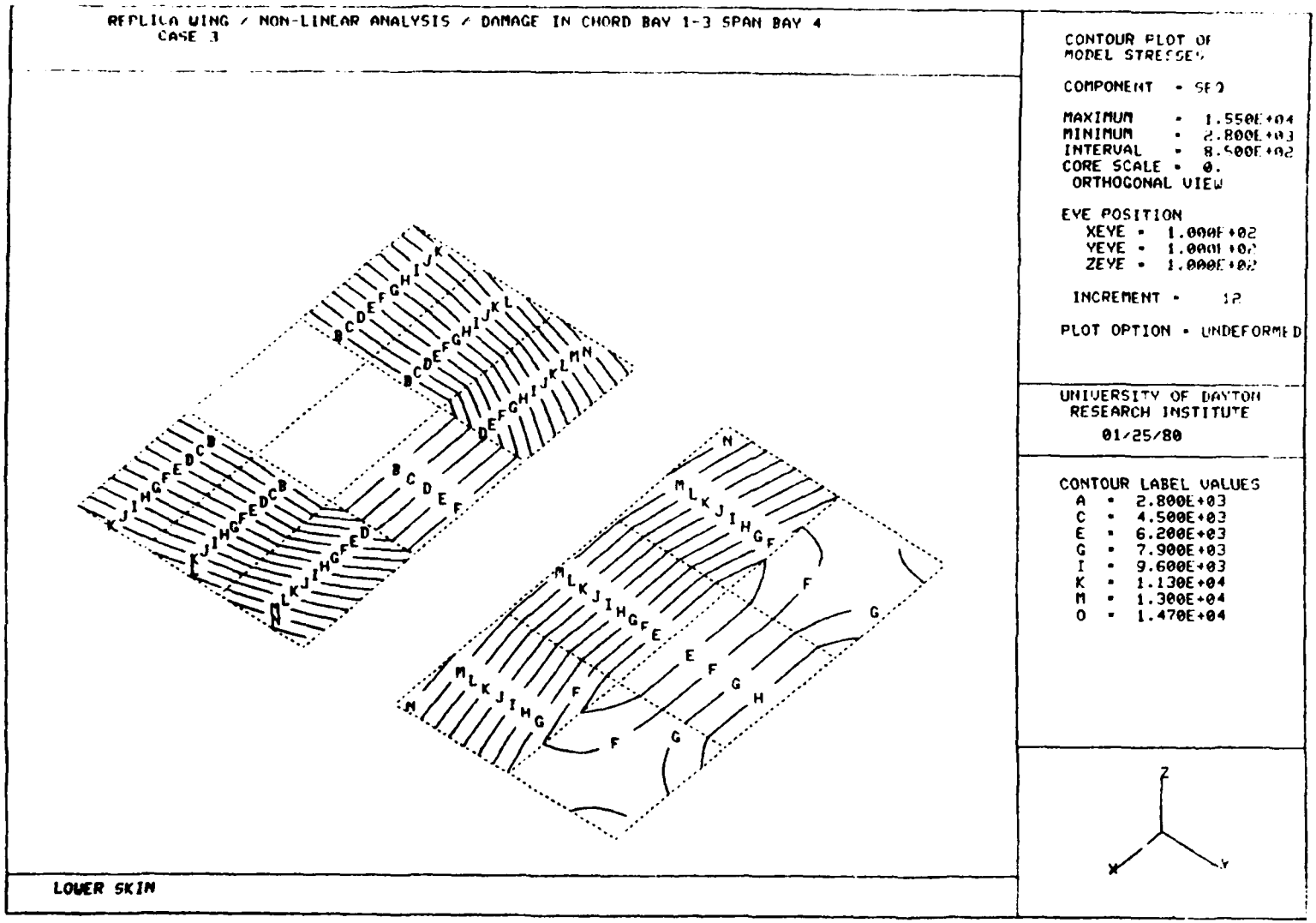

Figure 3.23c. Contours of Equivalent Stress - 60% Load.

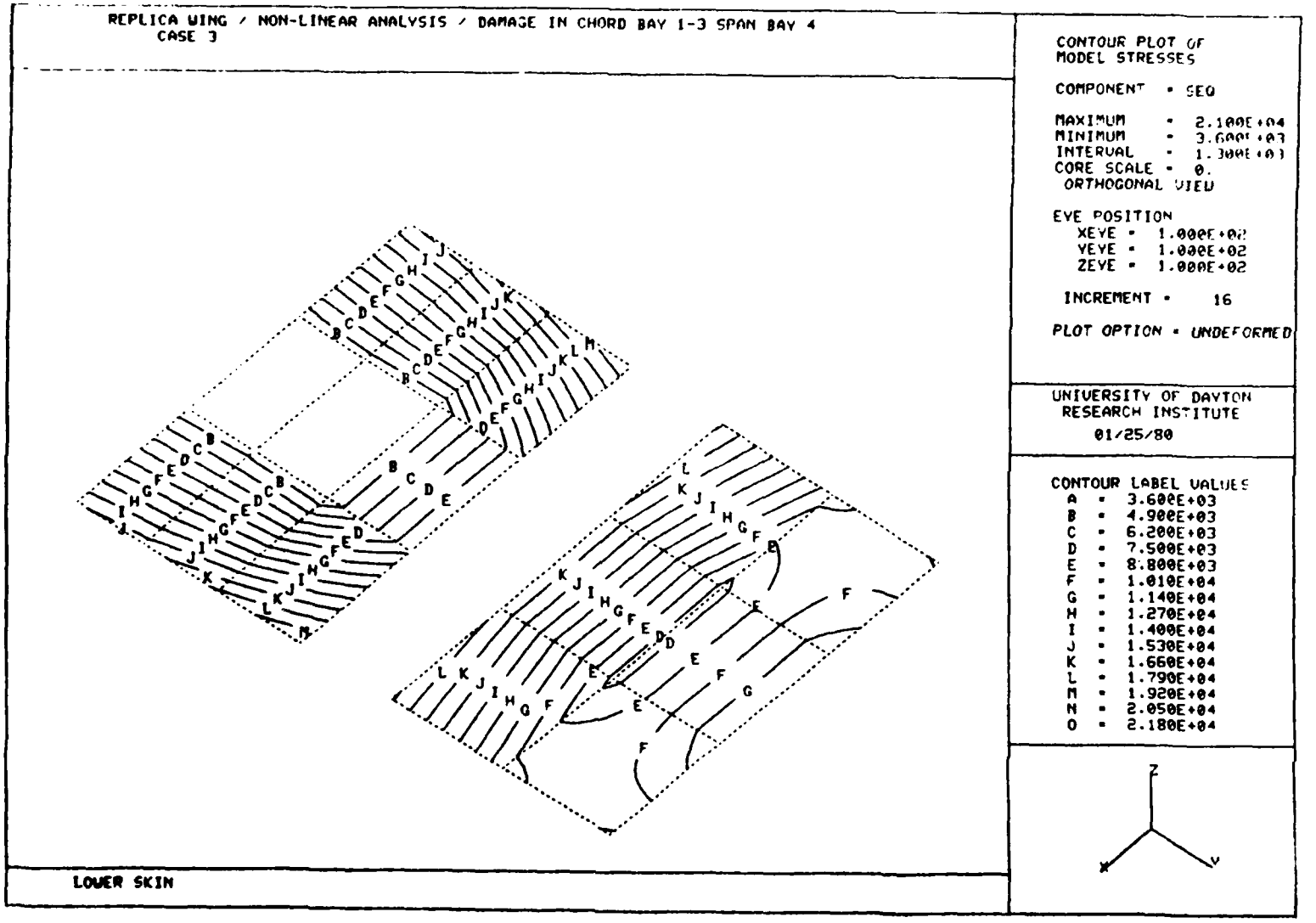

Figure 3.23d. Contours of Equivalent Stress - 80% Load.

SECTION 4
SUMMARY, CONCLUSIONS, AND RECOMMENDATIONS

An experimental test facility has been developed for performing realistic simulation of flight loads on sections of aircraft wing structures. The test facility is a self-contained flight loads simulation fixture consisting of a structure which applies loads to one end of a test specimen and supports the specimen at the other end, a hydraulic system which imposes loads through hydraulic actuators, and a control system to provide the test operator with a convenient means for controlling the application of the actuator loads during a test. The test facility was designed to operate within the confines of the Vertical Gunfire Facility at the Wright-Patterson Air Force Base. The test structure is self-reacting, and thus imposes no loads to the Vertical Gunfire Facility other than dead weight. The framework has been designed to be open in the area of the specimen so that the air flow and projectile impact capabilities of the existing facility are not interfered with. The operation of the test facility is performed through a control console located at a site remote from the physical test area. The operator can impose realistic flight loads (bending moment, shear, torque, etc.) to a test specimen by adjusting dials which control the load imposed on the load frame by hydraulic actuators. Proportional increases in the actuator loads can be controlled conveniently by the operator; this capability is useful for determining the residual strength of a damaged wing section, for example.

Experiments were performed on several replica test specimens, both undamaged and damaged, using the experimental test facility. On the basis of these tests, it is concluded that the experimental test facility does in fact provide the survivability/vulnerability engineer with a convenient means for imposing realistic flight loads on sections of aircraft structures.

In addition to the experimental test facility, an analytical technique was developed for predicting the internal load distributions of ballistically damaged, multiple load path aircraft wing structures. The analytical phase consisted of the modification of the three-dimensional nonlinear finite element program MAGNA to include membrane, bar, and shear panel elements, the development of a preprocessor to automatically generate the data for the finite element program given only an abbreviated set of data, and the development of a postprocessor to display graphically the results of the finite element program. At the suggestion of the Air Force, the analytical procedure was based on the use of simplified finite element models of wing structures consisting of two-dimensional membrane elements for the skins, two-dimensional shear panel elements for the spar and rib webs, and one-dimensional axial bar elements for the spar and rib caps. Using these elementary finite elements, a model of a wing structure is built using one element per bay. The use of the analytical procedure for predicting the response of aircraft wing sections (the same sections which are tested in the experimental facility) is carried out using three computer programs as shown in Figure 2.9. The programs are linked together by the creation of files; that is, the output of one program is used as input to the succeeding program.

The three parts of the analysis procedure (preprocessor, finite element program, and postprocessor) all operate as they were intended to operate. The preprocessor generates finite element models for undamaged and damaged wing structures. This is an interactive program which requires only a relatively small amount of data defined in terms convenient for the user. The primary limitation of the preprocessor is that it is restricted to generating finite element models using only bar, membrane, and shear panel elements as suggested by the Air Force. The MAGNA finite element program is a comprehensive finite element program specially developed to solve complex

nonlinear, static or dynamic structures problems. It has the capability of solving problems of a more general nature than those generated by the preprocessor. The postprocessor is a tool for presentation of the output of the finite element program in convenient graphical form such as undeformed and deformed geometry plots, and contour and relief plots of displacements, stresses and strains.

All of the tests performed with the experimental test facility were simulated with the analytical prediction tool. The comparison between the experimentally obtained and analytically predicted stresses in undamaged and slightly damaged replica test specimens were satisfactory, especially when the response was in the linear range. However, when a substantial amount of damage was present and/or when the response was nonlinear, the experimental and analytical results differed substantially. The University of Dayton thinks that the discrepancies in the results are due to the use of simplified bar/membrane/shear panel finite element models. This type of finite element model is generally adequate for undamaged wings because they act like box beams. However, the local response about a damaged area in a wing model cannot be adequately represented by such a simplified model.

On the basis of the results generated it can be concluded that the accurate experimental and analytical prediction of the stress distribution in damaged aircraft structures is feasible. However, certain refinements to the testing apparatus and to the analytical modeling procedure are recommended to improve the correlation between experimentally and analytically obtained data. The primary area for improvement to the testing apparatus is the method for attaching test specimens to the loading frame and to the reaction fixture. It is recommended that the attachment brackets be redesigned to prevent relative motion between the specimen, and the reaction and loading frames. This design change is necessary for improving the accuracy of the

displacements which are obtained experimentally. Every attempt should be made to measure accurate displacements, since displacements are the most accurate data predicted analytically by the finite element approach. It is also recommended that additional strains be recorded to obtain a more complete description of the stress state in a damaged test item, for comparison to analytically predicted data.

The primary area for improvements of the analytical prediction of the response of damaged wings is the method for finite element modeling. While the use of bars, membranes, and shear panels are certainly sufficient for representing the behavior of undamaged wings which respond essentially as box beams, the results obtained indicate that this approach does not produce accurately the stress response of damaged wings. Thus, it is recommended that a study be conducted to determine alternative modeling procedures for predicting damaged wing response.

REFERENCES

1. Roth, F. J., R. J. Dominic, and D. Bauer, "Structural Flight Loads Simulation Capability - Interim Technical Report - Load Fixture Design," UDRI-TR-77-40, University of Dayton, June 1977.

2. Bruner, T. S., M. P. Bouchard, M. J. Hecht, and F. K. Bogner, "Structural Flight Loads Simulation Capability - Structural Analysis Computer Program User's Manual," UDR-TR-80-73, University of Dayton, June 1980.

3. Fiscus, I. B., "Replica Test Specimen Design," UDR-TR-80-25, University of Dayton, January 1980.

4. Brockman, R. A., "MAGNA Computer Program User's Manual," UDR-TR-80-107, University of Dayton, November, 1980.

☆U.S.Government Printing Office: 1981 — 757-002/377

LMED

8